CHARACTERIZATION OF CLOUDWATER AND PRECIPITATION CHEMISTRY AND DEPOSITION AT ELEVATED SITES IN CENTRAL AND SOUTHERN CALIFORNIA

Thesis by

Jeffrey Lee Collett, Jr.

In Partial Fulfillment of the Requirements

for the Degree of

Doctor of Philosophy

California Institute of Technology

Pasadena, California

1989

(Submitted February 13, 1989)

Acknowledgments

Completion of this thesis would not have been possible without the support and assistance of a great many individuals. First, I would like to acknowledge the assistance of Bruce Daube. Without his expertise in designing the sophisticated sampling equipment used throughout all phases of this research, many of the reported results could not have been obtained. I also would like to thank Bruce, and my other colleagues, Bill Munger and Dieter Gunz, for their tireless efforts throughout thousands of hours of field work. This project simply could not have been completed without their assistance.

Thanks go to my thesis advisor, Professor Michael R. Hoffmann, for his continued support – intellectual, financial, and personal – over the years. I particularly would like to thank him for giving me the freedom to pursue this research as my own. Thanks also are due to the other members of my examination committee: Professor Jim Morgan, Professor Glen Cass, and Professor Fred Shair. Their insights have frequently guided my research efforts during my stay at Caltech.

I would like to acknowledge librarians Rayma Harrison and Gunilla Hastrup, not only for their technical assistance, but also for their constantly cheerful demeanor. Nancy Tomer also is acknowledged for her fine work in drafting many of the figures in this document. Thanks also are due to Sandy Brooks and Elaine Granger for their clerical assistance during the past four years.

The Federal Aviation Administration, the Veteran's Administration, the National Park Service, the California Air Resources Board, the Los Angeles County Fire Department, and the Carnegie Foundation all are gratefully acknowledged for granting access to the sampling stations used during this project. I particularly would like to thank the Research and Resource Management staffs at Sequoia National Park and the Resource Management staff at Yosemite National Park for

their assistance in conducting the Sierra cloudwater study.

I am grateful to the William and Flora Hewlett Foundation for providing a fellowship which supported my first year of study at Caltech. The California Air Resources Board also is gratefully acknowledged for financial support of my research.

Finally, I would like to thank all of the members of my family for their love and support throughout my academic endeavors. Most of all, I would like to thank Julie, my wife, for her love, patience, understanding, assistance, and support during the past three years. While there are many experiences at Caltech which I will remember fondly, meeting and marrying you, Julie, was by far the best. I love you.

Abstract

The chemical composition of cloudwater samples collected in the Sierra Nevada Mountains of central California between 1985 and 1988 was dominated by NH_4^+, NO_3^-, and SO_4^{2-}. The balance between these three species usually was responsible for determining the cloudwater pH, although inputs of formic and acetic acid also are believed to be important in this regard, particularly for relatively unpolluted samples. The pH of cloudwater sampled in Yosemite National Park, which ranged from 3.8 to 5.2, normally was lower than the pH of samples collected in Sequoia National Park (3.9 to 6.5). Cloudwater pH differences between the two Parks appear to be due to small differences in cloudwater concentrations of NH_4^+, NO_3^-, and SO_4^{2-}.

The composition of cloudwater in Sequoia National Park is determined primarily by the concentrations of precursor aerosol and soluble gases. Park aerosol concentrations were observed to increase during the approach of a cold front, producing higher pollutant concentrations in the clouds associated with the frontal activity than would be expected based on typical regional aerosol and gas concentrations.

Over 265 hours of cloud interception were observed, during a one–year period of continuous monitoring, at 1860 m elevation in Sequoia National Park. Most interception was observed at elevations above 1500 m – produced during the passage of convective clouds, associated with cold fronts, across the Sierra. Deposition of pollutants, including acids, to the forest canopy at elevations above 1500 m was estimated to be significant, relative to inputs from precipitation and dry deposition. Cloudwater interception may, in fact, be the dominant deposition mechanism for NH_4^+ and NO_3^-, particularly for isolated trees or ridgetop canopies where wind speeds are higher and cloudy air parcels can impact directly on foliar

surfaces.

A precipitation study, conducted in the South Coast Air Basin surrounding Los Angeles during the winter of 1987, illustrated the rapid scavenging of pollutants from the air column by falling raindrops. Results of a comparison of N(V) and S(VI) deposition during an extended precipitation event with the atmospheric loading of these species over the basin prior to the event suggested that both species were produced in the atmosphere during the rainstorm. Evidence was seen for in-cloud production of SO_4^{2-}, but not of NO_3^-.

Table of Contents

List of Figures

List of Tables

Thesis Overview and Summary

Overview

Interception of acidic cloudwater has been implicated as a possible contributor to the decline of forest stands both in North America and Europe. Plant injury in forests has been observed to increase at higher elevations where immersion in cloudwater is more frequent and other stress factors become important. In order to estimate the potential impact of acidic cloudwater deposition on forest communities, several issues must be addressed. Aside from the difficult questions concerning dose–response relationships between ambient cloudwater and members of the plant community, these issues include the frequency of cloud interception in the area of interest, the rate of cloudwater deposition to the plant surfaces, and the chemical composition of the deposited cloudwater. Contributions by cloudwater to acidic deposition also should be compared to contributions by precipitation and dry deposition.

The Sierra Nevada Mountains of California have extensive stands of conifers which may be sensitive to acidic cloudwater deposition. Emissions from the San Joaquin Valley and clouds associated with incoming frontal systems frequently pass through the region. Interception of cloudwater by the forest canopy may contribute significantly to regional deposition budgets for water, nutrients, and pollutants, including acids. In addition to cloud interception associated with the passage of frontal systems, two other mechanisms are thought to lead to the interception of fog and clouds in the region: (1) local formation of fog due to the rapid cooling of moist air produced during snow melt on sunny days, and (2) the lifting of dense winter "Tule" fogs, previously trapped near the floor of the San Joaquin Valley, due to a

reduction in atmospheric stability over the valley. These "Tule" fogs are often highly polluted, and their interception by Sierra vegetation may have important ecological consequences.

The initial chemical composition of cloudwater has been shown to be determined largely by the composition of the aerosol that serve as condensation nuclei and the ambient concentrations of soluble gases. The composition is altered as additional aerosol is scavenged and chemical reactions take place within the droplet. Therefore, in order to understand what influences cloudwater chemistry at a particular location, it is necessary to understand the processes that control local concentrations of aerosol and gases, particularly during the period immediately preceding cloud formation. These processes include emission rates, atmospheric reactions, transport routes, and deposition.

Concentrations of most inorganic aerosol and gas phase species in the southern and central Sierra Nevada Mountains of California are controlled primarily by meteorological conditions affecting transport from distant sources. Both the San Joaquin Valley and the San Francisco Bay area are thought to be important pollutant source regions affecting air quality in the central and southern Sierra. Local Sierra sources of species such as SO_2, NO_x, and NH_3 are relatively unimportant by comparison.

Meteorology within the San Joaquin Valley normally is dominated by the presence of high mountains that border the valley on three sides. Net air flow into the valley is generally from the northwest, except during the winter. Air masses exit the valley predominantly by passing over the Tehachapi Mountains located at the southeastern border of the valley. Afternoon upslope flows on both sides of the

valley, induced by preferential heating of the air along the mountain slopes, are thought to play a secondary role in transporting air out of the valley. The upslope flows form the primary mechanism for transport of air parcels from the valley floor up into the Sierra.

Temperature inversions in the air mass above the San Joaquin Valley floor are strongest in the winter but occur frequently throughout the year. The presence of the mountains surrounding the valley combines with an inversion to trap pollutants within the valley. The passage of frontal systems through the valley can serve to alleviate this condition by eliminating the temperature inversion, thus permitting pollutants to mix up to elevations where they may exit over the Tehachapi Mountains. Increased wind speeds often associated with the fronts also aid in the removal of valley pollutants. Frontal systems also may change the predominant direction of air flow within the valley from northwesterly to southerly, thereby altering the importance of various regional emissions to Sierra air quality.

Pollutant concentrations in the Sierra are affected significantly by the passage of cold fronts and often increase as a storm approaches. These increases may reflect an increase in the mixing height over the valley, a change in pollutant transport patterns, or some combination of these two factors. Increases in aerosol and gas concentrations with the advance of cold fronts may result in the production of cloudwater which is more polluted than might otherwise be expected, based on typical Sierra aerosol and gas concentrations. Interception of this polluted cloudwater by the forests on the slopes of the Sierra contributes to total pollutant deposition in the region.

The rate of cloudwater deposition to a forest canopy depends strongly on four

factors: (1) the liquid water content (LWC) of the fog or cloud, (2) the droplet size distribution, (3) the structure of the forest canopy, and (4) the ambient wind speed. Cumulative deposition over a specified period of time also depends on the frequency and duration of fog or cloud interception in that interval. The quantity of cloudwater deposited to the forest on a mountain slope may vary significantly with elevation, due to variations in the parameters governing the deposition process. Cloudwater deposition may increase with elevation, due to increases in average wind speeds and higher liquid water contents. The most important factor determining the elevational dependence of cloudwater deposition, however, is the elevational pattern of cloud interception. Different meteorological conditions may tend to favor cloud interception at different elevations. Convective clouds associated with frontal systems often have base elevations exceeding 1500 m; thus, these clouds will be intercepted most frequently at elevations above 1500 m. However, the lifting of "Tule" fogs from the floor of the San Joaquin Valley more likely will result in interception at lower elevations. Understanding elevational gradients in cloud interception is crucial to assessing the importance of cloudwater deposition for different regions in the Sierra Nevada Mountains.

Acid deposition is also a concern farther to the south in the South Coast Air Basin, surrounding Los Angeles. Much like the San Joaquin Valley, meteorology in the basin is dominated by the presence of high mountains on much of its border. Frequent temperature inversions and relatively low wind speeds combine to slow removal of pollutants by advection. During the winter, precipitation associated with frontal systems passing through the region serves to cleanse soluble pollutants from the atmosphere and to deposit them at the ground. Elevational patterns of wet deposition in the basin are affected by the relative importance of in-cloud and below-cloud scavenging processes. During periods when in-cloud scavenging

processes dominate, wet pollutant deposition in the mountains bordering the basin may exceed that observed on the basin floor, since rainwater concentrations may be similar at all elevations and precipitation amounts are generally higher in the mountains.

Following the onset of precipitation, changes in precipitation chemistry normally are apparent as pollutants are removed from the air column. If the precipitation persists, soluble pollutant concentrations may approach zero. Time–resolved data illustrating short–term changes in precipitation chemistry could provide information regarding the speed with which this scavenging process takes place. Comparisons of pre–storm aerosol and gas phase pollutant loadings in the atmosphere above the basin with cumulative wet deposition amounts during the storm also could provide information regarding the importance of pollutant replenishment mechanisms (i.e., emission, chemical production, and transport from other regions) during the storm. Since storm systems passing through Los Angeles generally have little or no contact with polluted air masses until they reach the basin, the buildup of pollutants following an extended basin–wide precipitation event also may provide clues regarding the rates at which these pollutants are emitted to, or chemically produced in, the local atmosphere.

Objectives

Several objectives formed the basis for the research that was conducted as a part of this thesis. These are listed below.

1. Identify those compounds which contribute significantly to the chemical composition of intercepted cloudwater in the Sierra Nevada Mountains of

central California. Interpret interactions between these chemicals as they affect properties of the cloudwater such as its pH.

2. Examine spatial and temporal variations in the chemical composition of the cloudwater. Analyze the variations to estimate the potential for acute vegetative damage due to cloudwater deposition in the region. Examine correlations between chemical species to help identify potential pollutant source types contributing to Sierra air quality during periods of cloud interception.

3. Investigate the relationship between Sierra cloudwater chemistry and the concentrations of precursor aerosol and gases. Examine the behavior of pollutant concentrations in the Sierra during the approach of frontal systems. Investigate the relationship between pollutant concentrations in the Sierra with those observed on the floor of the San Joaquin Valley.

4. Characterize the frequency of cloud interception in the Sierra as a function of elevation. Determine those elevations subjected to the largest quantities of deposited cloudwater.

5. Estimate the contributions of cloud interception to the deposition of water, nutrients, and pollutants to the vegetation canopy in the Sierra. Compare these inputs to those from precipitation and dry deposition.

6. Construct a conceptual model explaining the formation and deposition of cloudwater in the Sierra, with an emphasis on interpreting the chemical composition of the cloudwater.

7. Examine and test the feasibility of year–round operation of an automated cloudwater sampling network in a harsh mountain climate.

8. Compare the collection characteristics of the Caltech Active Strand Cloudwater Collector (used by several investigative groups around the world and in all recent Caltech cloudwater studies) with those of the Rotating Arm Collector (used in earlier Caltech investigations). Examine the chemical composition of samples collected by the two instruments in a side–by–side comparison to determine the compatibility of results obtained with the two samplers.

9. Investigate spatial and temporal variations in precipitation chemistry in the South Coast Air Basin. Evaluate the relative importance of in–cloud vs. below–cloud pollutant scavenging processes during precipitation. Assess the significance of these mechanisms in producing elevational gradients in wet deposition of pollutants.

10. Compare cumulative wet deposition of pollutants during an individual precipitation event in the South Coast Air Basin with total atmospheric loadings of these pollutants in the atmosphere over the basin prior to the storm. Use this comparison to evaluate the importance of pollutant production mechanisms during the storm.

Technical Plan

In order to achieve the objectives stated above, three investigative programs

were undertaken: (1) a side–by–side sampling comparison of the Caltech Active Strand Collector with the Rotating Arm Collector; (2) a multi–site study of precipitation chemistry in the South Coast Air Basin; and (3) an extensive study of cloudwater chemistry and the frequency of cloud interception in the Sierra Nevada Mountains of central California. These three programs are outlined briefly below.

During the summer of 1985, the Caltech Active Strand Collector (CASC) and the Rotating Arm Collector (RAC) were compared in a side–by–side study at an elevated coastal site bordering the Santa Barbara Channel. The comparison study, a complete description of which is provided in Chapter 6, was designed to provide for the simultaneous collection of cloudwater by the two instruments under a variety of conditions, including low and high cloud liquid water contents and highly polluted and relatively clean cloudwater. The collectors were compared with regard to their relative cloudwater collection rates and the compatibility of the chemical compositions of the collected cloudwater samples.

The precipitation study was conducted during the winter of 1987 and utilized five sampling stations (see Chapter 7). The stations were selected to represent both a "vertical" profile in the basin (Pasadena [elev. 200 m] – Henninger Flats [700 m] – Mt. Wilson [1700 m]) and an east–west horizontal transect (West Los Angeles – Pasadena – Riverside). Sub–event precipitation samples (i.e., discrete time–resolved samples from a single precipitation event) were collected automatically at each site using a refrigerated autosampler designed and built specifically for the project. Aerosol and gas samples also were collected at each site preceding, during, and following a number of storms.

Preliminary investigations of the chemical composition of intercepted

cloudwater in the Sierra Nevada Mountains were initiated in the fall of 1985 in Sequoia National Park. During this period, and during the spring of 1986, a number of cloud interception events were sampled at two sites in the Park, in order to ascertain the degree of cloudwater pollution in the region (see Chapter 1). Elevations of the sites were approximately 1500 and 1850 m. Samples were collected by manual operation of a CASC.

Following this preliminary sampling period, the scope of the Sierra project was increased significantly. Beginning in the summer of 1987 and extending through the fall of 1988, a total of fourteen cloudwater monitoring sites were operated in the Sierra (a complete description of this project is provided in Chapters 2 through 5). Elevations of the sites ranged from 820 to 2360 m. Eight of the stations were located in Sequoia National Park, while the remaining six were located in Yosemite National Park. All of the sites were equipped with an automated system which monitored the frequency of cloudwater interception and the rate of cloudwater deposition to a standard collector. In addition, the system measured wind speeds and precipitation.

Two sites also were equipped with a second system which automatically collected samples of cloudwater for chemical analysis. During the spring, summer, and fall, sub–event samples of cloudwater were collected and stored in a refrigerated environment. These samples were picked up at least once per week by a site operator. The system used to collect these samples included modified versions of the Caltech Active Strand Collector (CASC), cloudwater sensor, and fractionating autosampler used by this group in previous studies. During the winter, freezing temperatures necessitated the development of an entirely different collection system. This system incorporated a new cloudwater collector with

internally heated collection surfaces and an optical cloudwater sensor, used to determine when the collector should be activated.

Measurements of aerosol and gas concentrations during this study were made on an intensive basis at two sites in Sequoia National Park and one site in Visalia on the floor of the San Joaquin Valley. Intensive measurements also were utilized to investigate concentrations of unstable species,. including carbonyls, carboxylic acids, and peroxides, in Sierra cloudwater, and to examine elevational gradients in cloudwater chemistry and cloud liquid water content.

Summary of Findings

The cloudwater collector intercomparison illustrated the capacity of the CASC to collect samples at rates much higher than those exhibited by the RAC. Cloudwater was collected by the CASC at rates of up to 8.5 ml min^{-1}. The ratio of collection rates exhibited by the two instruments was close to the theoretically predicted ratio of 4.2:1 over a wide range of cloud liquid water contents (LWC); however, at low LWC, the ratio climbed rapidly above this value. Since the mass median droplet diameter typically decreases as LWC is decreased, the increase in the collection rate ratios was attributed to the differing collection efficiencies of the two collectors for small droplets.

Concentrations of Na^+, Cl^-, NO_3^- , SO_4^{2-}, NH_4^+, Ca^{2+}, and Mg^{2+} in samples collected simultaneously by the two instruments were compared by regressing the CASC sample concentrations on the RAC sample concentrations and comparing the slope of the fitted line to one. An instrumental variable technique was used for the regression, since an ordinary least squares fit would produce a bias in the estimate of

the slope due to the presence of random errors in both the independent and the dependent regression variables. Preferential collection of Na^+, Cl^-, and Ca^{2+} by the RAC, relative to the collection of these species by the CASC, was observed to occur with a confidence level greater than 95%. Preferential collection of Mg^{2+} by the RAC was observed to occur with a confidence level greater than 90%. The preferential collection also is believed to be due to the differing lower size cuts of the two samplers, since these ions, derived primarily from soil dust and sea spray, are expected to reside primarily in larger cloud droplets which make up a larger fraction of each RAC sample. No significant preferential collection by either collector was observed for NO_3^-, SO_4^{2-}, or NH_4^+. Based on the results of this study, cloudwater samples collected with the CASC are believed to be more representative of the overall chemical composition of the cloudwater than are samples collected by the RAC.

The South Coast Air Basin precipitation study (Chapter 7) provided an opportunity for the first field test of a refrigerated autosampler developed in our laboratory. The success achieved in using this instrument during this study led to its modification for use in several cloudwater studies, including the Sierra project. The fine time resolution in precipitation sampling obtained by using the autosampler allowed us to clearly demonstrate rapid scavenging of solutes during the initial stages of a precipitation event and rapid replenishment of solutes during pauses in the rain. The pH values of the sampled precipitation ranged from approximately 4 to 6, with Pasadena and Henninger Flats samples generally the most acidic. Precipitation samples from Riverside, which is near a large source of ammonia emissions, and West Los Angeles, which is located upwind of many of the basin's pollution sources during a storm, generally were found to have lower acidity.

Sulfate generally was the dominant anion in samples collected at West Los Angeles, near the coast. It also was found in slight excess over nitrate in precipitation samples from Riverside. While this result stands in sharp contrast to the strong dominance of nitrate in winter fogwater samples collected at Riverside, it is consistent with other precipitation data from the same area. Nitrate normally was found to be the dominant anion in samples collected at Pasadena, Henninger Flats, and Mt. Wilson, although not to the same extent that typically is observed in cloudwater collected at the same sites.

Two precipitation events were analyzed in detail. Data from the first event illustrated the importance of below–cloud scavenging processes. Much of the pollutant loading observed in rain collected on the basin floor during this event was shown to be scavenged by the precipitation as it fell through the lowest few hundred meters of the atmosphere. Despite the fact that most ion concentrations increased in the rain as it neared the basin floor, the precipitation pH was not greatly affected, indicating that the scavenged pollutants were, on average, essentially neutral. During the second event, below–cloud scavenging was not observed to be as important, and rainfall pollutant concentrations were more uniform with elevation. The flat rainfall concentration vs. elevation profile combined with increased levels of precipitation at Mt. Wilson to produce more wet pollutant deposition there during the second event than was observed at the other sites located on or near the basin floor. Since cumulative wet deposition at a site is a product of both the average concentration of a species in the precipitation and the total amount of precipitation falling at the site, and higher amounts of precipitation are normally observed at elevated sites in the basin, cumulative wet pollutant deposition at these sites frequently may exceed that observed on the basin floor.

Wet deposition of nitrate and sulfate during the second event was observed to significantly exceed what could be accounted for by washout of the pre–storm atmospheric burden of these species over the basin. Cumulative wet deposition of other ions during the storm was more closely correlated with their estimated pre–storm atmospheric burdens. Evidence of in–cloud production of sulfate was observed during this event, which may account for the extra sulfate deposition. No evidence was seen for in–cloud production of nitrate.

In order to develop an understanding of the role played by cloud interception in contributing to the deposition of water, nutrients, and pollutants in the Sierra, four separate processes must be examined. First, it is necessary to examine the relevant meteorological processes that produce clouds which may be intercepted by the mountains at the elevations of interest. Second, it is important to understand how pollutant transport mechanisms function in the region, particularly during periods immediately preceding cloud interception. Third, the processes which contribute to the chemical composition of the intercepted cloudwater, including scavenging of aerosols and gases, as well as chemical reactions within the cloud droplets, must be understood. Last, it is necessary to examine the values of parameters which govern the quantity of cloudwater deposited to the surface, including the frequency and duration of cloud interception, the cloud liquid water content, wind speeds during interception, and the structure of the vegetative canopy. The Sierra cloud interception study was designed to investigate all four of these processes, in order to facilitate development of a conceptual model of cloudwater deposition in the region. Major results of the study, described in Chapters 1 through 4, are summarized below.

Approximately 265 hours of cloud interception were observed at a site at

1856 m in Sequoia National Park, during a 12–month period of continuous monitoring. Peak interception periods occurred in November and April, while the lowest activity was observed during the summer months. Valid samples representing approximately 50% of the total interception time were collected at the site and analyzed to determine the concentrations of major ions.

The chemical composition of Sierra cloudwater is dominated by NO_3^-, SO_4^{2-}, and NH_4^+; however, large variations in the concentrations of these three species are observed, both between cloud interception events and within the course of a single event. The composition of the cloudwater appears to be determined largely by the composition of the precursor aerosol and gases. The balance between the cloudwater concentrations of NO_3^- and SO_4^{2-} vs. NH_4^+, at any given time, is largely responsible for determining the cloudwater pH; however, inputs of formic and acetic acid, which are found at significant concentration levels in Sierra cloudwater, also are believed to be important in this regard, particularly during periods when anthropogenic pollutant inputs are small. Intensive measurements of cloudwater chemistry revealed significant quantities of aqueous phase H_2O_2 in Sequoia National Park. Significant concentrations of carbonyls also were observed in Sequoia cloudwater. Carbonyl concentrations were dominated by formaldehyde and glyoxal.

The pH of the cloudwater samples collected in Sequoia National Park ranged from 3.9 to 6.5; samples collected in Yosemite National Park had pH values between 3.8 and 5.2. During periods of simultaneous collection, and on average, Yosemite samples were more acidic than Sequoia samples. The pH differential appears to be related to relatively small differences in the cloudwater concentrations of NO_3^-, SO_4^{2-}, and NH_4^+ at the two sites.

The technique of principal factor analysis was applied to data representing the chemical composition of 45 cloudwater samples, collected in Sequoia National Park during the fall of 1987, in order to statistically reveal potential ion sources contributing to the sample composition. Four important sources were hypothesized based on this analysis: (1) a source dominated by NO_3^-, SO_4^{2-}, and NH_4^+, reflecting anthropogenic inputs; (2) a source representing sea salt inputs of Na^+, Cl^-, and Mg^{2+}; (3) a soil dust source comprised of Ca^{2+}, K^+, and Mg^{2+}; and (4) an H^+ source, probably associated with organic acids, which were not routinely analyzed.

A comparison of aerosol and gas phase data collected simultaneously at Lower Kaweah (1856 m), Ash Mountain (550 m), and Visalia (90 m) indicated that the relative concentrations of species in the air masses at the upper two sites were fairly well correlated during the period studied, but considerable differences existed between the compositions at these two sites and the composition at Visalia. In addition, the air mass at Visalia exhibited considerable acid–neutralizing capacity, while air masses sampled in the Sierra were nearly neutral. These results indicate that the composition of air masses in Sequoia National Park can not be accounted for by a simple dilution of Visalia air masses during transport in the daily upslope flow. Higher relative concentrations of aerosol sulfate in the Park suggest that contributions from the southern San Joaquin Valley, where SO_2 emissions occur in conjunction with extensive oil–field activities, also may be important.

Pollutant transport routes within the San Joaquin Valley and in the adjacent Sierra are altered considerably preceding periods of cloud interception when frontal systems are moving through central California. Concentrations of aerosol pollutants were observed to increase in Sequoia National Park immediately preceding the arrival of a cold front. This increase appears to be related to both a breakdown in

the vertical stability of the atmosphere above the San Joaquin Valley and an increase in southerly flow aloft. Since regional cloudwater composition appears to be determined primarily by ambient aerosol and gas concentrations, increased aerosol concentration levels during the passage of a frontal system lead to the production of more polluted cloudwater in the Sierra than would be predicted based on average Sierra aerosol and gas concentrations.

Most Sierra cloud interception events are believed to result from the interception of convective clouds, associated with frontal activity; however, some evidence exists to suggest that dense winter "Tule" fogs, formed near the floor of the San Joaquin Valley, may intercept lower elevation sites in Sequoia National Park, when the atmosphere over the valley is destabilized. Interception of convective clouds is observed most frequently at sites above 1500 m elevation. Ridge–top sites, which often experienced the highest wind speeds, usually receive the greatest hydrological deposition fluxes from impacting cloudwater. Correlations of cloudwater deposition between sites in Sequoia National Park and similarly elevated sites in Yosemite National Park are often stronger than those between sites with differing elevations in a single Park.

Although the volume of water deposited to the canopy over the course of a year due to cloudwater interception is smaller than that due to precipitation, concentrations of NO_3^-, SO_4^{2-}, and NH_4^+ in the cloudwater at Lower Kaweah (elev. 1856 m) in Sequoia National Park are much higher than those typically observed in precipitation at the same site. Average concentrations of NH_4^+ and NO_3^- in cloudwater are more than ten times those observed in precipitation; cloudwater SO_4^{2-} concentrations are more than three times those observed in precipitation. Since the cloudwater concentrations are so much higher, even small inputs of

cloudwater can contribute relatively large quantities of these species to the ecosystem.

Estimates of annual deposition rates of major ions via cloudwater interception to the forest canopy in the vicinity of Lower Kaweah were calculated. The rates for NO_3^-, SO_4^{2-}, and NH_4^+ were calculated to be somewhat lower than were estimated based on preliminary measurements at the site, largely because wind speeds and cloud liquid water contents during interception turned out to be lower than previously assumed. The current deposition estimates are still significant, however, with regard to measured contributions from precipitation and estimated contributions from dry deposition. Cloudwater interception may, in fact, be the dominant deposition mechanism for NO_3^- and NH_4^+, particularly for isolated trees or ridge–top canopies where wind speeds are higher and cloudy air parcels can impact directly on foliar surfaces.

In summary, a common mechanism for pollutant deposition by cloudwater interception in the Sierra may be described conceptually as follows. The advance of a Pacific cold front from the north or northwest leads to a change in the predominant wind direction in the central valley of California from northwesterly to southerly, at least at some elevations. As the front crosses the valley, the atmosphere over the valley is destabilized, allowing pollutants previously trapped near the valley floor to mix up to higher elevations. These two meteorological changes act in combination to increase pollutant concentrations at elevations above 500 m in the region of Sequoia National Park. Ambient aerosol and soluble gases are scavenged efficiently by convective clouds associated with the frontal system, which begin to intercept the slopes of the Sierra, predominantly at elevations above 1500 m. Increased winds accompanying the convective activity enhance the

deposition of cloudwater to the vegetative canopy. Deposition of water and pollutants is most important for exposed conifers which serve as efficient natural cloudwater collectors; however, wet deposition of pollutants due to cloud interception is significant even for closed conifer canopies, also found predominantly at elevations above 1500 m.

Three automated cloudwater collection systems, designed and built at Caltech, were utilized successfully in the Sierra project (see Chapter 5). Each system was designed for a specific purpose. One system was used to collect sub–event samples of cloudwater for determination of temporal trends in cloudwater composition. A second system was utilized for the collection of super–cooled cloudwater droplets during the winter. The third system was utilized at several remote sites to monitor interception of cloudwater. The development and testing of each of these systems has greatly advanced the state of the art in automated cloudwater sampling technology and will facilitate the development of sampling networks for routine monitoring of fog and cloudwater composition, as well as for regional air quality model validation.

CHAPTER 1

CLOUDWATER CHEMISTRY IN SEQUOIA NATIONAL PARK

Atmospheric Environment

(in press)

Abstract

Interception of cloudwater by forests in the Sierra Nevada Mountains may contribute significantly to acid deposition in the region. Cloudwater sampled in Sequoia National Park had pH values ranging from 4.4 to 5.7. The advance of cold fronts into the Park appears to lead to higher aerosol and gas phase concentrations than are seen under normal mountain–valley circulations, producing higher cloudwater concentrations than might otherwise be expected. Estimates of annual deposition rates of NO_3^- , SO_4^{2-}, NH_4^+, and H^+ due to cloudwater impaction are comparable to those measured in precipitation.

Introduction

Interception of acidic cloudwater has been implicated as a possible contributor to the decline of forest stands both in North America and Europe (McLaughlin, 1985). Plant injury in forests has been observed to increase at higher elevations where immersion in cloudwater is more frequent and other stress factors become important (Johnson and Siccama, 1983). In order to estimate the potential impact of acidic cloudwater deposition on forest communities, several issues must be addressed. Aside from the difficult questions concerning dose–response relationships between ambient cloudwater and members of the plant community, these include the frequency of cloud impaction in the area of interest, the rate of cloudwater deposition to the plant surfaces, and the chemical composition of the deposited cloudwater. Contributions by cloudwater to acidic deposition should also be compared to contributions by precipitation and dry deposition.

Sequoia National Park (SNP), located in the southern Sierra Nevada Mountains of California, has extensive stands of conifers which may be sensitive to acidic cloudwater deposition. Emissions from the San Joaquin Valley and clouds associated with incoming frontal systems frequently pass through the Park (Smith et al., 1981). In order to assess the severity of the problem we have initiated an extensive study of cloudwater chemistry in SNP. Early results of this investigation, the first of its kind in the Sierra Nevada Mountains, are discussed below.

Site Description and Measurement Techniques

Sampling Sites

Cloudwater samples were collected at two sites in SNP during the fall of 1985 and the spring of 1986. The main collection site is situated on a granite outcrop (elev. 1856 m) at the Lower Kaweah Research Site below Giant Forest (Figure 1.1). The surrounding forest is mixed conifer. Several factors were considered in selecting this site for use in the study. First, the site is located at an elevation frequently observed to be impacted by clouds during the passage of storm systems. Second, the site was already in use as an air quality monitoring site and as an NADP rain collection site (Stohlgren and Parsons, 1987). Third, it is one of very few locations in the Park which provides open exposure to impacting clouds, has electric power, and is readily accessible. It should be mentioned, however, that the complex topography of the site makes interpretation of the exact meteorological situation corresponding to the observed cloudwater compositions difficult. As at most locations on the western slopes of the Sierras, the lifting of moist air as it passes over the mountains may lead to the production of orographic clouds which augment clouds present due to convective activity (Wallace and Hobbs, 1977). Despite this drawback, we feel that the Lower Kaweah research site is the best location presently available in the Park for conducting this type of study. The second site is located 3 km to the southwest at the Deer Ridge turnout on the General's Highway. The elevation of this site is approximately 1490 m. This site was selected as an alternate, to be used when temperatures at the Lower Kaweah site fell below freezing. Since no AC power is available at this site, the sampling equipment must be operated using a 12 V battery.

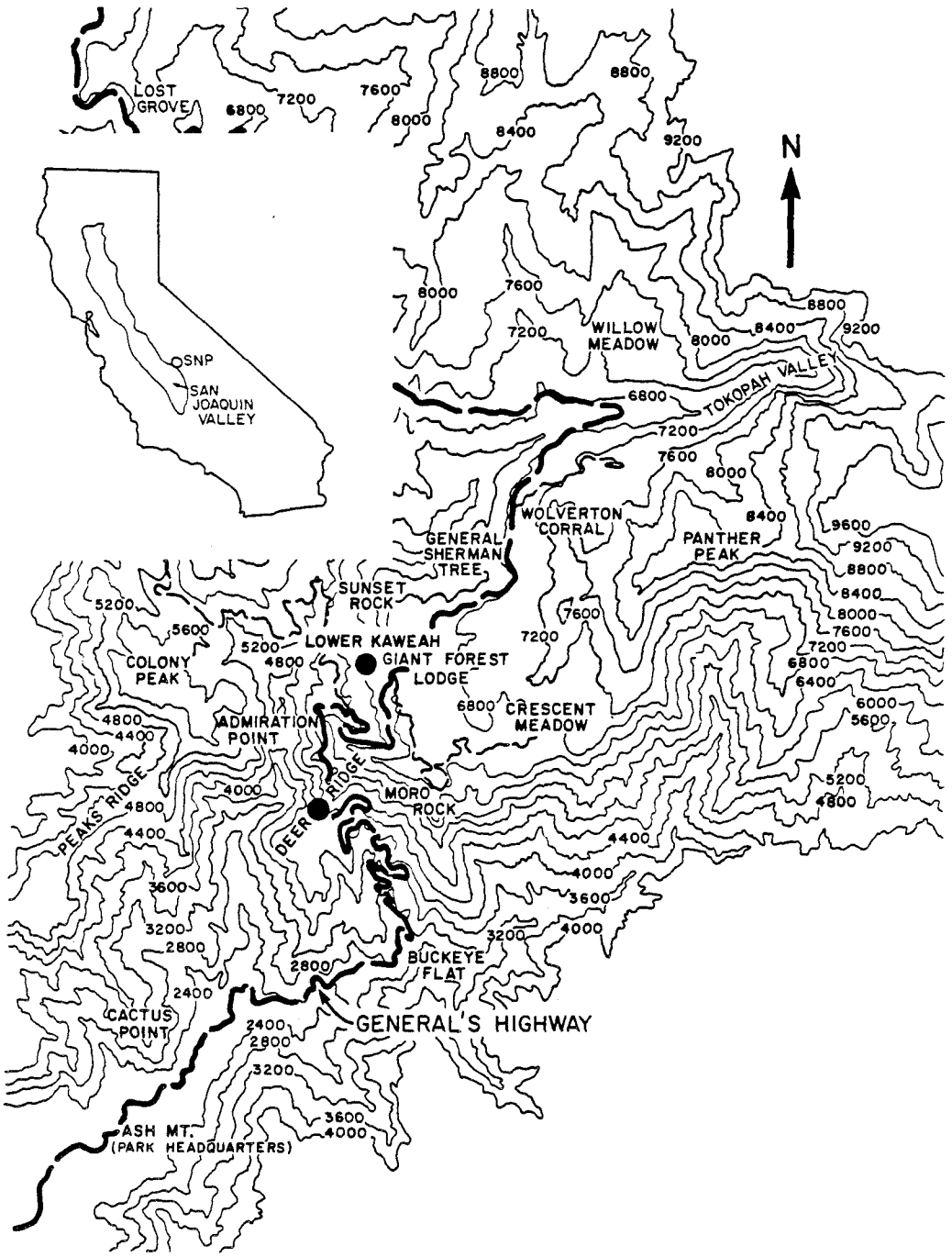

Figure 1.1. Map of Sequoia National Park showing the two sites used for cloudwater sampling. The inset shows the location of the Park relative to the San Joaquin Valley and the rest of California.

Measurement Techniques

Cloudwater samples were collected with the Caltech Active Strand Collector (CASC) depicted in Figure 1.2. The CASC (Daube et al., 1987a) is an improved version of the collectors described in detail elsewhere (Jacob et al., 1985a; Daube et al., 1987b). In addition to being used in Caltech cloudwater studies, more than twenty–five CASCs are currently in use by six other research groups. The CASC employs a fan to draw air across six angled banks of 510 μm teflon strands at a velocity of 9 m s^{-1}. Cloudwater droplets in the air parcel are collected on the strands by inertial impaction. The collected droplets run down the strands, aided by gravity and aerodynamic drag forces, through a teflon sample trough into a collection bottle. The 50% collection efficiency cutoff predicted from impaction theory corresponds to a droplet diameter of $\simeq$ 3.5 μm.

Data from a side–by–side comparison of the CASC with the Caltech Rotating Arm Collector (RAC) indicate that the instruments collect samples of coastal stratus with statistically indistinguishable concentrations of NO_3^-, SO_4^{2-}, H^+, and NH_4^+ (Hoffmann et al., 1988). The RAC (Jacob et al., 1984) was earlier found to collect representative samples in an intercomparison with samplers of five differing designs (Hering and Blumenthal, 1985). Differences in the sample concentrations of ions associated with soil dust and sea salt (Ca^{2+}, Mg^{2+}, Na^+, and Cl^-), however, were observed among the samples collected by different instruments in both intercomparison studies. Hering and Blumenthal attributed some of the discrepancies to contamination of the samples by soil dust kicked up in the study area. In the CASC–RAC study higher concentrations of Ca^{2+}, Mg^{2+}, Na^+, and Cl^- measured in RAC samples have been attributed to the failure of this instrument to efficiently collect droplets smaller than about 15 μm. A separate study (Munger,

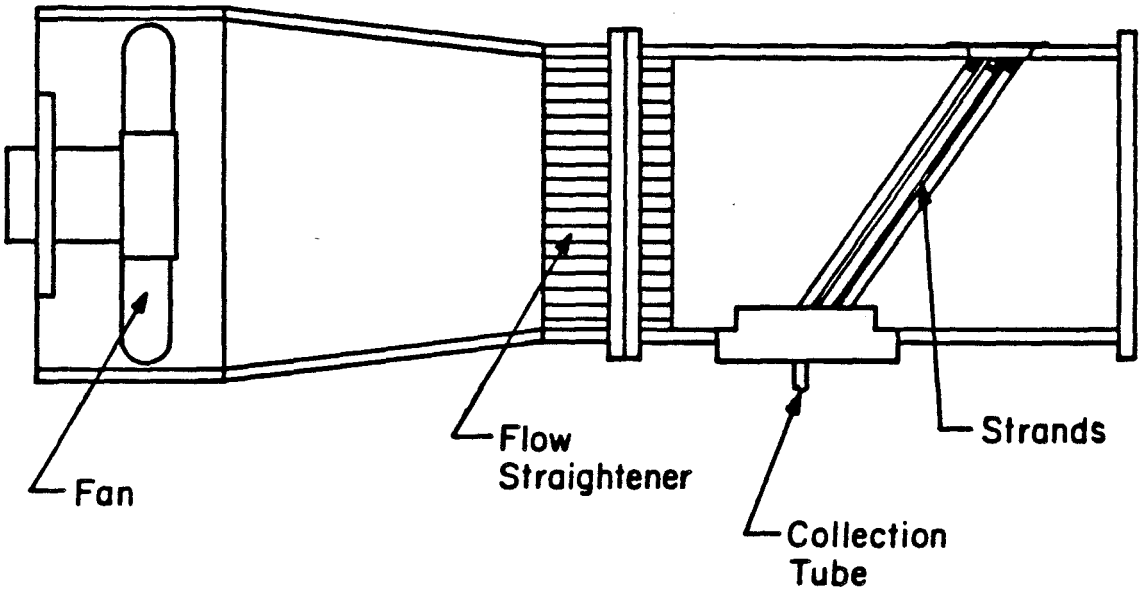

Figure 1.2. The Caltech Active Strand Collector (CASC). The length of the collector is 0.91 m (36 in.). Total sampled flow is 21.1 m^3/min.

1989) has indicated that ions associated with large aerosol, such as sea salt and soil dust, are found predominantly in the larger portion of the cloud droplet size spectrum in coastal stratus. Based on these results, we believe that the CASC provides a more representative sample of the chemical composition of the entire droplet spectrum than is provided by the RAC or other instruments with similarly low collection efficiencies for small droplets.

The major ions, Cl^-, SO_4^{2-}, and NO_3^-, were measured in our laboratory using a Dionex 2020i ion chromatograph with a Dionex AS–4 column and a bicarbonate–carbonate eluent. Na^+, Ca^{2+}, and Mg^{2+} concentrations were determined using a Varian Techtron AA6 atomic absorption spectrophotometer. NH_4^+ was measured by the phenol–hypochlorite method (Solorzano, 1967) using an Alpkem flow injection analyzer. Organic acids were preserved by adding chloroform (Keene et al., 1983) to an aliquot of the cloudwater sample immediately after collection and later analyzed by ion exclusion and normal ion chromatography run in parallel.

Aerosol and gas measurements were also made at the Lower Kaweah site using filter packs. Flow rates were controlled by critical orifices and verified with a calibrated flowmeter. Teflon filters (Gelman Zefluor, 1 μm pore size) were used to collect the aerosol for determination of major ions. An oxalic acid impregnated glass fiber backup filter was used to collect $NH_3(g)$. A nylon backup filter was used to collect $HNO_3(g)$. The nylon filters were extracted in the bicarbonate–carbonate eluent and the rest of the filters in distilled, deionized water on a reciprocating shaker. The extracts were then analyzed by the same methods that were used on the cloudwater samples.

Results and Discussion

A total of twelve cloudwater samples were collected during five cloud impaction events. All of the sampled events were associated with cold fronts approaching from the north or northwest. As mentioned above, cloud liquid water contents at the collection sites may have been enhanced by an orographic effect due to passage of the air masses over the Sierra. The first eleven samples were collected at the Lower Kaweah site. The last sample was collected on May 6, 1986, at the Deer Ridge site because temperatures at Lower Kaweah were near 0 $^{\circ}$C and the collected droplets froze on the strands of the CASC.

Cloudwater Composition

Table 1.1 summarizes the chemical composition of the samples. In Figure 1.3 the cloudwater loadings of NH_4^+, NO_3^-, and SO_4^{2-} are presented. (The cloudwater loading of a species is defined as the amount of that species present in cloudwater per unit volume of air. It is equivalent to the cloudwater concentration multiplied by the liquid water content of the cloud). Also listed in Table 1.1 are the estimated values of cloud liquid water content (LWC). These values are derived from the quotient of the sample collection rate with the product of the flow rate through the CASC (24.5 m^3/min.) and the theoretical collection efficiency of the CASC. The collection efficiency of the CASC is defined by the product of the overall strand collection efficiency (85% for a 10 μm droplet) and the percentage of air flowing through the collector that is sampled by the strands (86%).

Wide variations are seen in both the cloudwater concentrations and loadings of all the major species. The nitrate loading, for example, ranges from less than 1

Table 1.1. Chemical Composition of Sequoia Cloudwater

Date	Time	pH	Na^+	NH_4^+	Ca^{2+}	Mg^{2+}	Cl^-	NO_3^-	SO_4^{2-}	−/+	LWC
			←			μN			→		ml m^{-3}
10/21											
a	0927–1000	5.0	8	29	12	4	4	11	28	0.62	0.15
b	1000–1100	4.8	2	16	9	1	1	6	18	0.57	0.21
c	1100–1200	5.1	1	8	4	1	3	3	13	0.84	0.21
d	1200–1410	5.4	1	*	2	1	*	*	*	**	0.09
4/24											
a	1142–1305	5.0	680	1526	308	266	491	1140	665	0.82	0.03
b	1305–1405	4.8	157	594	58	47	129	354	269	0.86	0.16
c	1405–1505	4.8	231	900	72	66	192	537	396	0.88	0.04
5/03											
a	1200–1300	5.4	35	448	41	20	44	205	121	0.68	0.24
b	1300–1335	5.7	27	493	34	16	29	206	120	0.62	0.10
c	2015–2115	5.6	11	149	24	8	17	62	58	0.70	0.22
d	2115–2215	5.6	10	93	22	8	18	44	54	0.85	0.06
5/06											
a	1200–1250	4.4	44	132	18	***	55	94	83	1.00	0.22

* below 1 μN, ** concentrations too low to make accurate calculation, *** not measured, ion balance calculated for measured species.

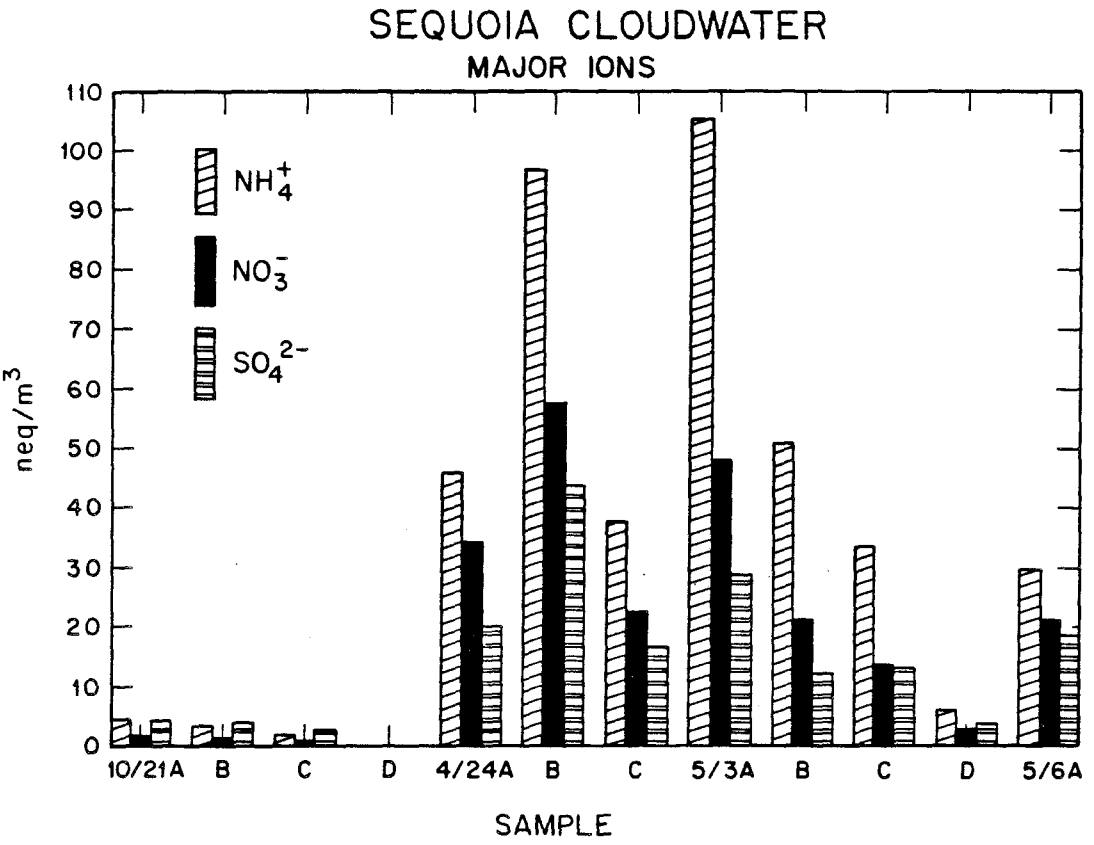

Figure 1.3. Cloudwater loadings of ammonium, nitrate, and sulfate in samples collected during the fall of 1985 and the spring of 1986 in Sequoia National Park.

neq m^{-3} up to about 60 neq m^{-3}. The ratio of NO_3^- to SO_4^{2-} varies from below 0.5 in the fall samples to more than 1.5 in some of the spring samples. The pH of the samples ranges from 4.4 to 5.7. The last sample, which is the most acidic, is not the sample with the highest ionic loading, indicating the importance of the ionic composition of the sample in determining its acidity.

The calculated inorganic ion balance for each sample (sum of measured inorganic anions/sum of measured cations) is shown in Table 1.1. For those samples with low ionic loadings it is not surprising to see this ratio differ significantly from 1.0 since relative analytical error increases near the detection limits. With the exception of the May 6 sample, however, there seems to be a consistent anion deficit, even for those samples with higher loadings. Upon collection of samples 4/24c, 5/03b, 5/03c, and 5/03d, a 2 ml aliquot of each sample was set aside and preserved with 50 μl of chloroform. Each aliquot was analyzed for the presence of formic acid, acetic acid, lactic acid, pyruvic acid, and propanoic acid. Table 1.2 lists the concentrations of the organic anions expected to be in each sample based on the measured concentrations of each acid and the pH of the samples as measured in the field. Also listed here are the ion balances for all measured species in the samples, organic and inorganic. In sample 5/03b the total of the concentrations of formate, acetate, lactate, and propionate is comparable to the nitrate concentration and is nearly twice the sulfate concentration. The concentrations in the other three samples are smaller, but still significant. Including these organic anions in the ion balances for the four samples changes them from 0.88, 0.62, 0.70, and 0.85, as listed in Table 1.1, to 0.95, 0.97, 0.97, and 1.10, respectively. These ratios are within the error of the analytical procedures.

Low molecular weight organic acids appear to be important contributors to

Table 1.2. Organic Anions in Sequoia Cloudwater

Sample	pH	Formate	Acetate	Pyruvate*	Lactate*	Propionate*	$-/+^{tot‡}$
		←		μN		→	
4/24							
c	4.8	68.5	13.8	10.4	0	5.2	0.95
5/03							
b	5.7	106.7	72.8	0	15.4	7.2	0.97
c	5.6	31.0	18.6	0	0	2.5	0.97
d	5.6	19.6	8.5	0	4.6	0	1.10

* Identification of this species is tentative.
‡ This column denotes the total ion balance including all measured species, organic and inorganic.

the overall chemical composition of SNP cloudwater. This observation is consistent with our previous results for San Joaquin Valley fog. Lower molecular weight organic acids have been shown to be important components of fog and cloudwater in the San Joaquin Valley below SNP (Jacob et al., 1986b) and in rainwater collected at remote as well as urban sites (Galloway et al., 1984; Kawamura and Kaplan, 1984). The solubility of low molecular weight carboxylic acids in water is enhanced by their dissociation to their respective conjugate bases (equation 1.2). Since most of the cloudwater samples had pH values above the pK_a values of the weak acids of interest, we expect that the organic acids will be effectively scavenged from the gas phase. When the pH of the cloudwater falls below the pK_a values of the organic acids, the solubility of these acids is correspondingly diminished.

(Eq'n. 1.1) $$HA_{(g)} \overset{H_a}{\rightleftharpoons} HA_{(aq)}$$

(Eq'n. 1.2) $$HA_{(aq)} \overset{K_a}{\rightleftharpoons} H^+_{(aq)} + A^-_{(aq)}$$

It is instructive to compare the cloudwater compositions observed in SNP with those measured at similar locations in other parts of the country. Average concentrations (and standard deviations) of NO_3^-, SO_4^{2-}, NH_4^+, and H^+ measured at two elevated sites in the northeastern U. S. (Whiteface Mountain, New York, and Mt. Moosilauke, New Hampshire) are listed in Table 1.3, along with the results of this study. Also listed here are results obtained at Laguna Peak, an elevated site located at the eastern end of California's Santa Barbara Channel. Average concentrations of H^+ measured in SNP cloudwater (11 μeq/l) were, on average, much lower than those observed at the other three sites (288 μeq/l at Mt. Moosilauke, 280 μeq/l at Whiteface Mountain, and 761 μeq/l at Laguna Peak).

Table 1.3. Comparison of Cloudwater Composition at Four Elevated Sites

Site	Elev.(m)	Date	Samples	NO_3^-	SO_4^{2-}	NH_4^+	H^+
				Average(Std. Dev.), μeq/l			
Sequoia N. P., CA [1]	1860	1985–86	12	132(206)	96(127)	237(310)	11(11)
Mt. Moosilauke, NH [2]	1220	1980–81	10	195(175)	342(234)	108(89)	288(193)
Whiteface Mt., NY [3]	1500	1976	28	110(52)	140(150)	89(61)	280(220)
Laguna Peak, CA [4]	450	1986	20	571(203)	462(197)	270(111)	761(339)

[1] This paper. Averages and standard deviations are weighted by the sample volumes.
[2] Lovett et al. (1982). Averages and standard deviations are not weighted by the sample volumes.
[3] Castillo et al. (1983). Data from non–precipitating stratiform. Averages and standard deviations are not weighted by the sample volumes.
[4] Munger (1989). Averages and standard deviations are weighted by the sample volumes.

These differences are correspondingly reflected by large differences in the typical cloudwater pH values measured at the sites. Cloudwater pH in SNP averaged about 5, while the two northeastern sites averaged about 3.5 and Laguna Peak averaged close to 3. Average concentrations of NO_3^- and SO_4^{2-} in SNP cloudwater (132 and 96 μeq/l, respectively) were much lower than those observed in Laguna Peak cloudwater (571 and 462 μeq/l), while concentrations of NH_4^+ were comparable (237 μeq/l in SNP and 270 μeq/l at Laguna Peak). The large excess of NO_3^- and SO_4^{2-} in the Laguna Peak cloudwater is balanced by the increased H^+, accounting for the difference in pH observed at the two sites.

Average concentrations of NO_3^- and SO_4^{2-} in cloudwater from Whiteface Mountain (110 and 140 μeq/l, respectively) were comparable to those in SNP cloudwater. The large difference in average cloudwater pH observed at these two sites is largely accounted for by lower inputs of base at Whiteface Mountain, where cloudwater concentrations of NH_4^+ averaged only 89 μeq/l, approximately one–third of the level observed in SNP cloudwater. The increased acidity observed at Mt. Moosilauke, relative to SNP, can be partially accounted for by the lower average cloudwater NH_4^+ concentration (108 μeq/l) observed there, but must also be partially attributed to a higher acid input. Cloudwater SO_4^{2-} concentrations at Mt. Moosilauke averaged 342 μeq/l. The average cloudwater NO_3^- concentration observed in Mt. Moosilauke cloudwater (195 μeq/l), however, was only slightly higher than that observed in samples from SNP.

Aerosol and Gas Phase Measurements

During the period May 1 to May 6, 1986, aerosol was continuously sampled at the Lower Kaweah site. The aerosol, collected generally in six–hour samples,

was analyzed for NO_3^- , SO_4^{2-} , Cl^-, NH_4^+ , Na^+, Ca^{2+}, and Mg^{2+}. In addition, simultaneous measurements of the gas phase concentrations of nitric acid and ammonia were made. Results obtained for the aerosol loadings of NO_3^- , SO_4^{2-}, NH_4^+, and Cl^- are shown in Figure 1.4. Under normal conditions upslope winds, that are caused by the heating of the air along the mountain slopes, should transport pollutants from the San Joaquin Valley to the Lower Kaweah site. Drainage flows, that begin as the sun sets and the air in contact with the slopes cools, bring cleaner air to the site and transport the aerosol back down into the valley. This pattern seems to be reflected in the data for May 4.

The data for the periods May 2–3 and May 5–6 show a distinctly different trend. In both periods aerosol loadings rose through the first day and continued to either rise or remain at elevated levels overnight and through some portion of the second day. A similar trend was observed in the gas phase concentrations. A cold front passed through the region during both periods. The arrows on Figure 1.4 show the approximate times at which clouds began to impact the cloud collection site at Lower Kaweah.

Figure 1.5 depicts the typical behavior of air masses during the passage of a cold front. The advancing denser cold air mass wedges its way under the warmer air mass. As the warm air mass is lifted and cooled, cloud formation and precipitation often result. Such a large scale lifting of a warm air mass previously in contact with the floor of the San Joaquin Valley could increase loadings of aerosol and gas phase species in the adjacent mountains. If the disturbance is large enough, the mountain–valley circulation may be overcome, resulting in a pattern of increased pollutant loadings at elevation until the front has passed. The data from May 2–3 and May 5–6 are consistent with this scenario.

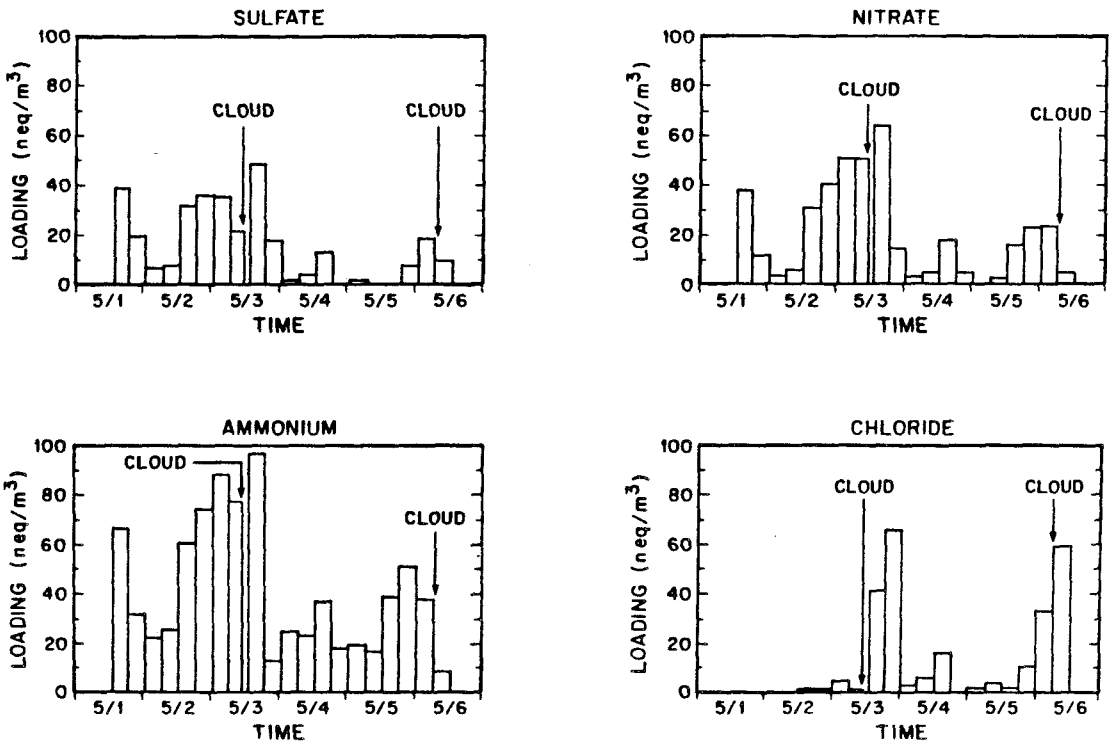

Figure 1.4. Aerosol Loadings of sulfate, nitrate, ammonium, and chloride measured at the Lower Kaweah research site in Sequoia National Park during the period 5/1–5/6/86. The arrows on the figures denote the times at which clouds were observed to begin impacting the hillside at the site.

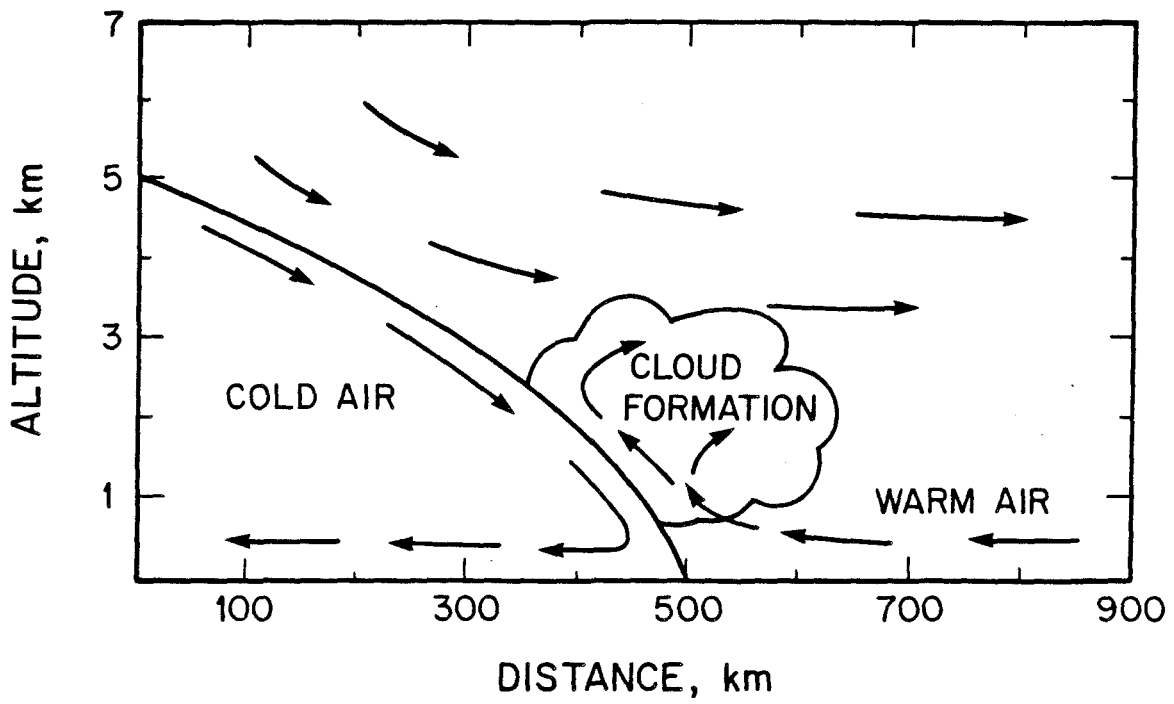

Figure 1.5. Typical behavior of warm and cold air masses during the advance of a cold front. In the figure the cold air mass is moving toward the right, wedging itself under the less dense warm air mass.

It has been shown previously (Jacob et al., 1985; 1986a,b; 1987) that cloudwater composition is in large part determined by the composition of the precursor aerosol and soluble gases. The possible coupling of peak gas phase and aerosol concentrations with the arrival of a front, as mentioned above, suggests that cloudwater loadings in Sequoia National Park or similar locations might be expected to be higher than would be predicted based on average gas phase and aerosol concentrations at the same location.

Cloudwater Deposition

The volume–weighted average concentrations of the 12 cloudwater samples collected in SNP during this study provide the best available estimate of the average cloudwater composition there. These can be used, along with estimates of the average cloudwater deposition rate and the annual average number of hours of cloudwater impaction, to estimate the cloudwater contribution to acidic deposition in the vicinity of Lower Kaweah. Lovett (1984) estimated cloudwater deposition rates to a subalpine balsam fir forest that varied linearly from 0.2 to 1.2 mm hr^{-1} for canopy top wind speeds of 2 to 10 m s^{-1}. The much taller forest in SNP should be expected to receive at least the same deposition rate under similar conditions. Selecting a moderate wind speed of 6 m s^{-1} yields a deposition rate of approximately 0.7 mm hr^{-1}. Data from a current study we are conducting indicates that 100 hours per year of cloud impaction at 2000 m in the Park is a conservative estimate. Annual deposition rates of H^+, NH_4^+, NO_3^-, and SO_4^{2-} calculated using the above information are summarized in Figure 1.6. Also depicted here are the annual average deposition rates for the same ions at the Lower Kaweah site contributed by precipitation (Stohlgren and Parsons, 1987). The estimated cloudwater deposition

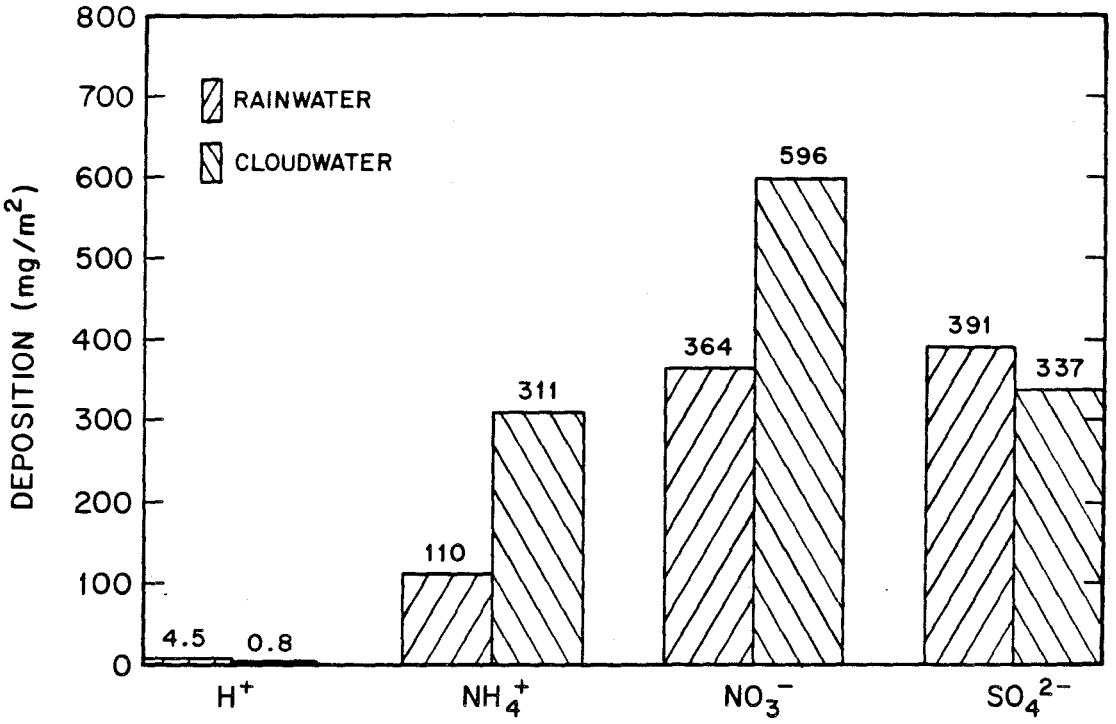

Figure 1.6. Annual deposition of major ions to the Lower Kaweah research site in Sequoia National Park by rainwater (measured, Stohlgren and Parsons, 1987) and cloudwater (estimated). Rainwater includes unknown contributions from snowfall. Estimates of cloudwater deposition are based on a cloudwater deposition rate of 0.7 mm/hr for 100 hr/yr (see the text for details). The average chemical composition of the cloudwater was taken as the volume–weighted average composition of the cloudwater sampled in the Park during the fall of 1985 and the spring of 1986.

rates of all four ions are comparable to the measured precipitation inputs. While the estimates of cloudwater contributions to deposition in the region are rough, an attempt has been made to keep them on the conservative side. The potential importance of this deposition mechanism therefore seems clear. Further investigation is needed to refine the estimates made above and to lead to an increased understanding of the relative contributions of the different pathways leading to acidic deposition in SNP.

Conclusions

Cloudwater was sampled during the fall of 1985 and the spring of 1986 in Sequoia National Park in the southern Sierra Nevada Mountains of California. Concentrations of major species in the cloudwater vary widely both within one cloudwater impaction event and from one event to another. The pH values of the samples range from 4.4 to 5.7. The most acidic sample was not the sample with the highest concentrations of NO_3^- and SO_4^{2-}; this result indicates the relative importance of the ionic composition of the sample as a primary determinant of acidity. Organic acids were found to be be important components of the chemical composition of the cloudwater in Sequoia National Park

A comparison of the chemical composition of the cloudwater in SNP with that collected at two elevated sites in the northeastern U. S. reveals that the SNP cloudwater is generally much less acidic. For one of the northeastern sites (Whiteface Mountain) this difference is largely due to smaller inputs of base, as evidenced by lower NH_4^+ cloudwater concentrations than were observed in SNP cloudwater. At the second northeastern site (Mt. Moosilauke) the levels of cloudwater NH_4^+ are similarly low, but at least part of the acidity is attributable to

larger acid inputs. At an elevated site along the southern California coast (Laguna Peak), cloudwater NH_4^+ concentrations were comparable to those observed in SNP. Higher concentrations of NO_3^- and SO_4^{2-} in Laguna Peak cloudwater, however, account for sample pH values averaging almost 1.5 units less than were observed in SNP.

The advance of cold fronts seems to lead to higher aerosol and gas phase loadings in the Park than would be seen under normal mountain–valley circulations, particularly during the night and morning hours. The arrival of these increased loadings prior to and during cloud impaction on the mountain slopes leads to higher cloudwater concentrations than would otherwise be expected. Estimates of annual deposition rates of NO_3^-, SO_4^{2-}, NH_4^+, and H^+ due to cloudwater impaction are comparable to those measured in precipitation.

Acknowledgments

We are grateful to the National Park Service, particularly the research staff at Sequoia National Park, for allowing us access to the sampling sites. This work was supported by a contract with the California Air Resources Board (Contract No. A4–075–32).

References

Castillo, R. A. and Jiusto, J. E. (1983) The pH and ionic composition of stratiform cloud water. *Atmos. Environ.* **17**, 1497–1505.

Daube, Jr., B. C., Flagan, R. C. and Hoffmann, M. R. (1987a) Active Cloudwater Collector. United States Patent No. 4,697,462.

Daube, Jr., B. C., Kimball, K. D., Lamar, P. A. and Weathers, K. C. (1987b) Two new ground–level cloud water sampler designs which reduce rain contamination. *Atmos. Environ.* **21**, 893–900.

Galloway, J. N., Likens, G. E., Keene, W. C. and Miller, J. M. (1982) The composition of precipitation in remote areas of the world. *J. Geophys. Res.* **87**, 8771–8786.

Hering, S. V. and Blumenthal, D. L. (1985) Fog sampler intercomparison study: Final Report, prepared for the Coordinating Research Council, 219 Perimeter Center Parkway, Atlanta, GA.

Hoffmann, M. R. (1988) Fog, cloud, and dew chemistry. Final Report to the California Air Resources Board, Contract No. A4–075–32.

Jacob, D. J., Wang, R. F. T. and Flagan, R. C. (1984) Fogwater collector design and characterization. *Envir. Sci. Technol.* **18**, 827–833.

Jacob, D. J., Waldman, J. M., Haghi, M., Hoffmann, M. R. and Flagan, R. C. (1985a) Instrument to collect fogwater for chemical analysis. *Rev. Sci. Instrum.* **56**, 1291–1293.

Jacob, D. J., Waldman, J. M., Munger, J. W. and Hoffmann, M. R. (1985b) Chemical composition of fogwater collected along the California coast. *Envir. Sci. Technol.* **19**, 730–736.

Jacob, D. J., Munger, J. W., Waldman, J. M. and Hoffmann. M. R. (1986a) The H_2SO_4–HNO_3–NH_3 system at high humidities and in fogs: 1. Spatial and temporal patterns in the San Joaquin Valley of California. *J. Geophys. Res.* **91**, 1073–1088.

Jacob, D. J., Waldman, J. M., Munger, J. W. and Hoffmann, M. R. (1986b) The H_2SO_4–HNO_3–NH_3 system at high humidities and in fogs: 2. Comparison of field data with thermodynamic calculations. *J. Geophys. Res.* **91**, 1089–1096.

Jacob, D. J., Shair, F. H., Waldman, J. M., Munger, J. W. and Hoffmann, M. R. (1987) Transport and oxidation of SO_2 in a stagnant foggy valley. *Atmos. Environ.* **21**, 1305–1314.

Johnson, A. H. and Siccama, T. G. (1983) Acid deposition and forest decline. *Envir. Sci. Technol.* **17**, 294A–305A.

Kawamura, K. and Kaplan, I. R. (1984) Capillary gas chromatography determination of volatile organic acids in rain and fog samples. *Anal. Chem.* **56**, 1616–1620.

Keene, W. C., Galloway, J. N. and Holden, J. D. (1983) Measurement of weak organic acidity in precipitation from remote areas of the world. *J. Geophys. Res.* **87**, 8771–8786.

Lovett, G. M., Reiners, W. A. and Olson, R. K. (1982) Cloud droplet deposition in subalpine balsam fir forests: Hydrological and chemical inputs. *Science* **218**, 1303–1304.

Lovett, G. M. (1984) Rates and mechanisms of cloud water deposition to a subalpine balsam fir forest. *Atmos. Environ.* **18**, 361–371.

McLaughlin, S. B. (1985) Effects of air pollution on forests: A critical review. *J. Air Poll. Control Assoc.* **35**, 512–534.

Munger, J. W. (1989) Ph. D. thesis, California Institute of Technology.

Smith, T. B., Lehrman, D. E., Reible, D. D. and Shair, F. H. (1981) The origin and fate of airborne pollutants within the San Joaquin Valley. Final Report to the California Air Resources Board, CARB–RR–81–15.

Solorzano, L. (1967) Determination of ammonia in natural waters by the phenol–hypochlorite method. *Limnol. Oceanogr.* **14**, 799–801.

Stohlgren, T. J. and Parsons, D. J. (1987) Variation of wet deposition chemistry in Sequoia National Park, California. *Atmos. Environ.* **21**, 1369–1374.

Wallace, J. M. and Hobbs, P. V. (1977) *Atmospheric Science: An Introductory Survey.* Academic Press, Inc., Orlando, FL.

CHAPTER 2

THE CHEMICAL COMPOSITION OF INTERCEPTED CLOUDWATER IN THE SIERRA NEVADA MOUNTAINS

Introduction

There is increasing recognition that deposition of cloudwater may significantly augment the deposition of acids, nutrients, and water by precipitation and dry deposition, particularly at elevated sites where immersion in clouds occurs frequently. This recognition stems largely from the recent issuance of several reports which address the frequency of cloud interception and/or the chemical composition of the intercepted cloudwater at a number of elevated locations, both in the U. S. (Lovett et al., 1982; Castillo et al., 1985; Waldman et al., 1985; Weathers et al., 1986, 1988; Mueller and Weatherford, 1988) and elsewhere (Dollard et al., 1983; Schemenauer, 1986; Schemenauer et al., 1987). In California, concern has been expressed about the potential damage acid deposition may inflict upon sensitive ecosystems in the Sierra Nevada Mountains. The deposition of acids by cloudwater interception in the Sierra has previously been estimated to be comparable to inputs from precipitation, based on preliminary measurements of cloudwater composition in Sequoia National Park (Chapter 1; Collett et al., 1989). Further study has since been undertaken to investigate more completely the frequency of cloud interception and the chemical composition of the impacting cloudwater in the Sierra. This chapter describes the results of this investigation.

Experimental Procedure

Two sites in the Sierra were chosen to serve as locations for monitoring the chemical composition of cloudwater. The first site, Lower Kaweah, is located at an elevation of 1856 m in Sequoia National Park. This site also was used for most of the preliminary measurements described in Chapter 1. Turtleback Dome (elev. 1590 m) in Yosemite National Park was selected as the second site. Both sites are

located in open areas and may readily be intercepted by approaching clouds. Both sites also are used for making a variety of other routine air quality measurements. There is very little traffic in the immediate vicinity of either site, although Highway 41 passes approximately 0.5 km from the Turtleback Dome site.

Beginning in September 1987, each site was equipped with an integrated cloudwater monitoring system. This system, described in detail in Chapter 5, included: (1) a Caltech Active Strand Cloudwater Collector (CASCC) to collect samples; (2) a cloudwater sensor to monitor the presence of clouds and activate and deactivate the CASCC; and (3) an autosampler to fractionate the samples collected by the CASCC to reveal temporal changes in cloudwater chemistry. Use of this system enables automated collection of cloudwater samples on a sub-event basis. The CASCC is automatically rinsed with distilled deionized water (D^2H_2O) before and after each event to ensure the cleanliness of the collection surfaces.

As described in Chapter 5, the integrated cloudwater system is not functional when ambient temperatures fall below 0 C, since the cloudwater droplets freeze on the collection surfaces in both the sensor and the CASCC. Operation of the autosampler during freezing conditions also poses considerable difficulty since collected sample may freeze in the autosampler distribution system. For these reasons, a separate winter cloudwater sampling system was developed and used at Lower Kaweah and Turtleback Dome from mid-January to mid-April of 1988. This system, described in Chapter 5, utilized a Caltech Heated Rod Cloudwater Collector (CHRCC). Stainless steel rods, which form the collection surfaces in this sampler, are internally heated, on a periodic basis, when temperatures fall below 4.5 C to melt accumulated frozen cloudwater (rime ice). A new optical cloudwater sensor was developed and used to monitor the presence of clouds during the winter

sampling period. The output signal from the sensor was monitored by a Campbell CR–10 programmable controller which was used to activate and deactivate the CHRCC, and to control the heating cycle.

The cloudwater monitoring sites were attended at least once per week by a site operator. The operator was responsible for picking up samples, replenishing the rinsewater reservoir, testing the operation of the equipment, and taking a blank to determine the cleanliness of the system. Samples were weighed by the operator and an aliquot was removed for determination of pH. The pH was measured using a pH meter with a combination electrode calibrated against pH 4 and 7 buffers. Finally, the samples were frozen and packed in a refrigerated shipping container, along with ice packs, and shipped to Caltech.

Upon arrival at Caltech, samples were allowed to warm to room temperature and the pH was measured again. Samples were then refrigerated at 4 C until further analysis could be completed. Concentrations of NO_3^-, SO_4^{2-}, and Cl^- were measured using a Dionex 2020i ion chromatograph equipped with an AS4 or AS4A column. A 2.8mM HCO_3^-/ 2.2 mM CO_3^{2-} solution was used as the eluent. Na^+, Ca^{2+}, Mg^{2+}, and K^+ concentrations were measured using a Varian Techtron AA6 atomic absorption spectrophotometer. An air/acetylene flame was used for Na^+ and K^+; N_2O/acetylene was used for Ca^{2+} and Mg^{2+} to minimize interferences. NH_4^+ was measured by the phenol–hypochlorite method (Solorzano, 1967) using an Alpkem flow injection analyzer.

Results and Discussion

Cloud Interception Frequency

Over 250 hours of cloudwater interception were observed at Lower Kaweah between September 1987 and August 1988. Figure 2.1 illustrates the number of hours of cloudwater interception observed during each of the twelve months of this period. The number of hours of interception is based primarily on data from the two cloudwater sensors. Data from early December were taken from a passive cloudwater collector located at the site (see Chapter 4). Periods when the integrated cloudwater monitoring system sensor data indicated interception durations less than 20 minutes were not included since the sensor reports a minimum of 15 minutes of interception each time it is activated.

The two peak months for cloudwater interception were November (74 hours) and April (63 hours). Approximately half of the interception in November was associated with a single storm system which immersed the site in clouds almost continuously for a day and a half. Most events were observed to be much shorter than this, typically on the order of a few hours. Smaller monthly interception amounts were observed in October (40 hours), January (25 hours), and May (32 hours). A few hours of interception were observed in each of the remaining months of the year, with the exception of September, during which no cloud interception was observed. Less precipitation fell in the Sierra during the period of the study than in most years. Since cloud interception at the site seems to be associated primarily with the passage of frontal systems, this suggests that cloud interception may have been somewhat below average for this period as well.

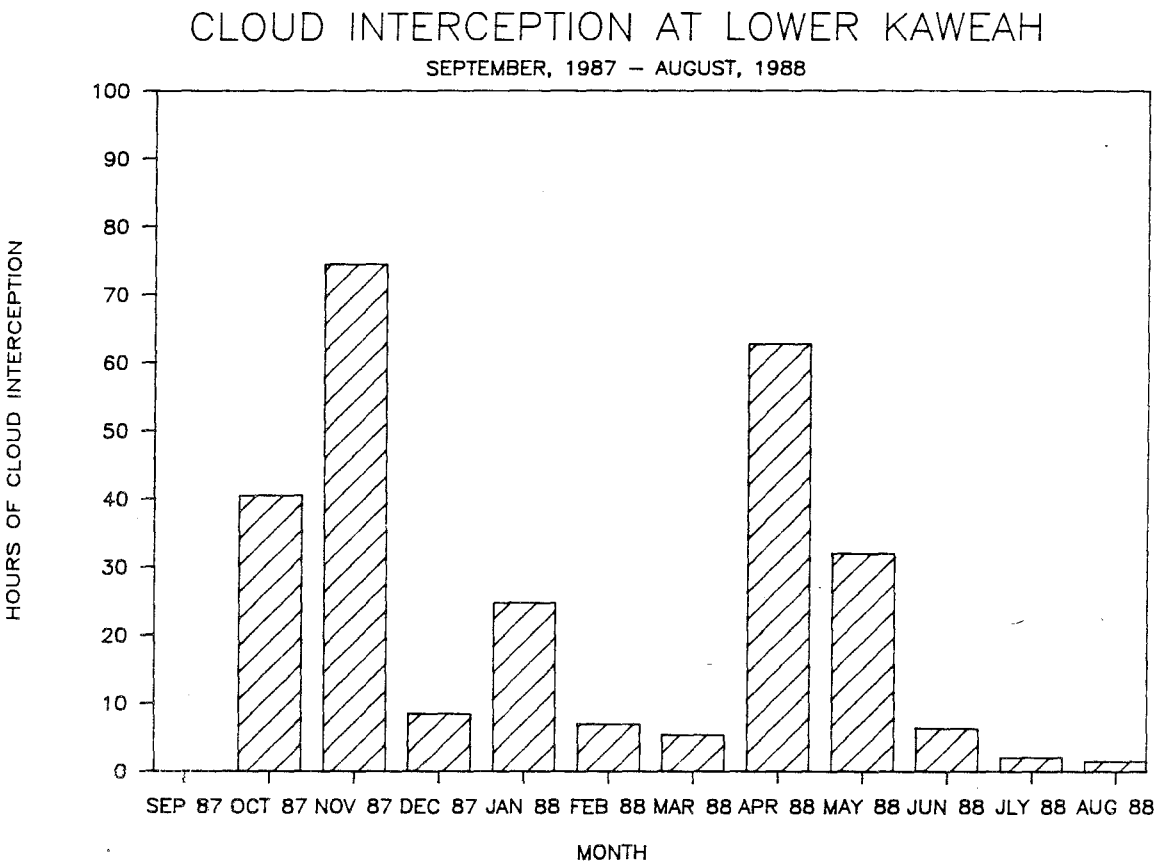

Figure 2.1. Number of hours of cloud interception observed at Lower Kaweah in Sequoia National Park for each month between September, 1987 and August, 1988.

The number of hours that Lower Kaweah was immersed in cloud during the study year is much less than has been estimated for some elevated sites in the Eastern U. S. and Canada. Reiners and Lang (1979) estimated that the fir zone (1220 to 1450 m) on the western slopes of the Green Mountains in Vermont is covered by clouds between 30 and 50% of the time. This estimate was based on an interpolation between visual observations of cloud interception at similar elevations at other northeastern U. S. locations. Schemenauer (1986) estimated that the summit of Roundtop Mountain (970 m) was immersed in clouds 44% of the time in 1985, based on the fraction of observation times at which clouds were seen at the summit. Observations were made twice daily.

Reliance on periodic visual observations introduces a great deal of uncertainty into estimates of cloud interception frequency. The interpretation of what constitutes cloud presence varies from one observer to another. In some reports fog is indicated anytime that visibility is reduced below a certain threshold, typically 1/8 or 1/4 mile. The thresholds for cloud observation by the two sensors in this study correspond to a visual range of less than 100 m. This lower visibility threshold provides a better indication of when cloudwater deposition to the forest canopy is likely to be important. Observers may also tend to indicate clouds are present if they are observed anywhere in the vicinity of the observation post, rather than solely when a single point is immersed in clouds. Furthermore, it is very difficult to know what occurs between observation times. If observations are made on a fixed time schedule, as is usually the case, a bias may be introduced if actual cloud presence is correlated with time of day. Aside from the differences in observation methods, it seems clear that the amount of cloud interception observed at Lower Kaweah is significantly lower than has been observed at some other locations.

Sampling Efficiency

Valid samples were obtained for approximately 50% of the 265 hours of cloudwater interception observed at Lower Kaweah. While we consider this sampling efficiency to be quite good for a study of this nature, it is possible to identify a number of reasons why the fraction of valid samples was not higher. Discussion of these reasons, which include the loss of sample at the beginning of each event during the collector rinse, exceedance of the finite sampling capacity of the autosampler, insufficient sample volume, problems associated with freezing temperatures, equipment malfunction, and human error, may aid the development of similar programs in the future.

While having an automated rinsing system was deemed necessary for obtaining valid samples of cloudwater using an automated sampling system, it does pose some limitations to sampling efficiency. Sample collected during the first 20 minutes of each event is discarded by the autosampler. This is done because the collection surfaces of the CASCC are rinsed with D^2H_2O at the beginning of each event; therefore, sample collected by the CASCC during the first few minutes of each event is diluted by rinsewater remaining on the collection strands. During short events, not collecting sample for the first 20 minutes will significantly reduce the fraction of interception time that is sampled.

The autosampler (Chapter 5), which contains 20 sample bottles, has a finite sampling capacity. While this capacity was designed to allow extended periods of cloudwater sampling by incorporating a sample distribution reservoir which saves only a portion of large samples, there were a few cases when that capacity was exceeded. An example was a 60-hour period between noon on October 31, 1987,

and midnight on November 2, 1987, when over 40 hours of cloudwater interception were observed. The problem of exceeding the autosampler capacity is exacerbated by periods of intermittent cloud interception. The autosampler is designed to store samples from different events separately. An event is considered finished when there is a break of approximately 30 minutes in cloud interception. Therefore, several short periods of cloud interception, separated by breaks of at least 30 minutes, can use up several of the bottles in the autosampler carousel, significantly reducing the capacity of the autosampler to sample more extended events that may occur afterward. This limitation is particularly important since a number of periods of brief cloud interception often occur in association with the arrival of clouds on the leading edge of a frontal system, while the arrival of the main cloud mass may produce extended interception periods later.

Samples smaller than 10 ml in volume were not considered valid. The reason for this is that cloudwater collected by the CASCC, as well as by most other cloudwater collectors, may contact a considerable amount of surface area in transit to the sample bottle. The smaller the sample, the greater the possibility that the sample composition will be affected significantly by even small quantities of residual rinsewater or contamination. Small samples, which have a higher surface area to volume ratio, are also more prone to evaporation problems during collection and storage than are large samples. Finally, samples smaller than 10 ml are more difficult to analyze accurately in the laboratory, because of the need to increase the volume by dilution to provide a sufficient quantity for analysis.

While winters are not extremely cold at 2000 m in the Sierra, freezing temperatures may occur throughout most of the year. Often the freezing temperatures are associated with the passage of a cold front – the same condition

which often produces cloudwater interception at Lower Kaweah. Deciding when to change from using the integrated cloudwater monitoring system to the winter collection system is difficult. Relatively warm temperatures during cloud interception in April of 1988 were followed by freezing temperatures during an event at the end of May. Use of the winter system reduces the amount of information that is obtained about the temporal variations in cloudwater composition, since only bulk cloudwater samples are obtained; use of the integrated cloudwater monitoring system permits freezing weather to halt operation, leaving gaps in the data base. We opted to use the winter system only during those months that we expected to be the coldest (January, February, and March), since the winter collector was previously untested and we were interested in obtaining data on temporal variations in cloudwater chemistry. As a consequence, there were several instances when freezing weather hampered operation, thereby reducing the total hours of valid cloudwater sample we obtained.

Overall, the performance of the collection systems was remarkably good, particularly considering that this was a pilot program employing a great deal of new and untested technology. There were relatively few cases of equipment failure or malfunction at Lower Kaweah, for either cloudwater monitoring system, throughout the course of the study. Those failures which did occur were often associated with pieces of equipment purchased from outside vendors and incorporated into the collection systems, and frequently were related to power loss and subsequent recovery. Equipment failure and malfunction led to very little down time at Sequoia.

More problems were encountered at Turtleback Dome in Yosemite. The most significant problem was a lightning strike which destroyed a National Park

Service transformer at the site. The loss of the transformer left the site without power for approximately six weeks in the fall of 1987. Unfortunately those six weeks comprised the most active autumn period of cloud interception. Several events were observed at Turtleback Dome during this period by the passive cloudwater monitoring system (see Chapter 4). As a consequence of the loss of power, no samples were collected for chemical analysis at Turtleback Dome during the fall of 1987. No samples were collected at Turtleback Dome during the winter either, due to malfunctions of the microprocessor in the controller which operated the winter collection system. These malfunctions, associated with poor electrical grounding through the AC power line, were remedied by wiring a direct line to the equipment; however, by the time the new line was installed, the limited number of interception events observed during the winter were over. Spring, summer, and fall sampling in 1988 were carried out at both Parks with relatively little equipment trouble.

Only a few samples failed to be collected or were compromised because of human error. The largest source of human error was associated with the high turnover rate of site operators in both Parks. This was particularly a problem in Sequoia National Park where six different people were responsible for operations at Lower Kaweah at different times during the 15–month study. The high turnover rate contributed to a lack of familiarity with equipment operation, which made it extremely difficult for the operators to deal with difficult or unusual situations that were not thoroughly documented in the procedure manual.

Cloudwater Composition

The pH of the cloudwater samples collected in Sequoia National Park ranged

from 3.9 to 6.5 (see Figure 2.2). Samples collected in the fall tended to be somewhat more acidic than those collected in the winter or spring. Inorganic compositions of the Sequoia cloudwater samples are presented in Tables 2.1 and 2.2. Blank concentrations of the measured species were generally near the analytical detection limits, throughout the course of the study, indicating that the collector rinsing procedure was keeping the system clean. Two things are readily apparent from the cloudwater composition data. First, the inorganic composition of the cloudwater is dominated by NO_3^-, SO_4^{2-}, and NH_4^+. Second, the sample pH is not highly correlated with the total ionic strength of the sample. The presence of naturally occurring formic and acetic acid, along with CO_2, will render the cloudwater somewhat acidic as these species partition into the aqueous phase. Significant concentrations of weak organic acids previously have been observed in Sequoia cloudwater (Collett et al., 1989; Chapters 1, 3). The cleanest samples of cloudwater (those with the lowest concentrations of measured ions) collected in Sequoia National Park were found to have pH values near 5. This is consistent with pH values observed in samples collected in remote areas of the world (Keene et al., 1983). Deviations from this pH regime are largely determined by the balance of inorganic acids and bases introduced into the sample. As indicated above, the most important inorganic species are SO_4^{2-} and NO_3^-, which represent acidic inputs to the cloudwater, and NH_4^+ which represents the dominant basic input. Samples with large excesses of NH_4^+, relative to the sum of NO_3^- and SO_4^{2-}, exhibit pH values greater than 5, while those with excesses of NO_3^- and SO_4^{2-} tend to be more acidic than the clean samples.

The volume–weighted average composition of the cloudwater samples collected at Lower Kaweah during different periods of the year is presented in Figure 2.3. Samples collected in the fall and spring were obtained using the

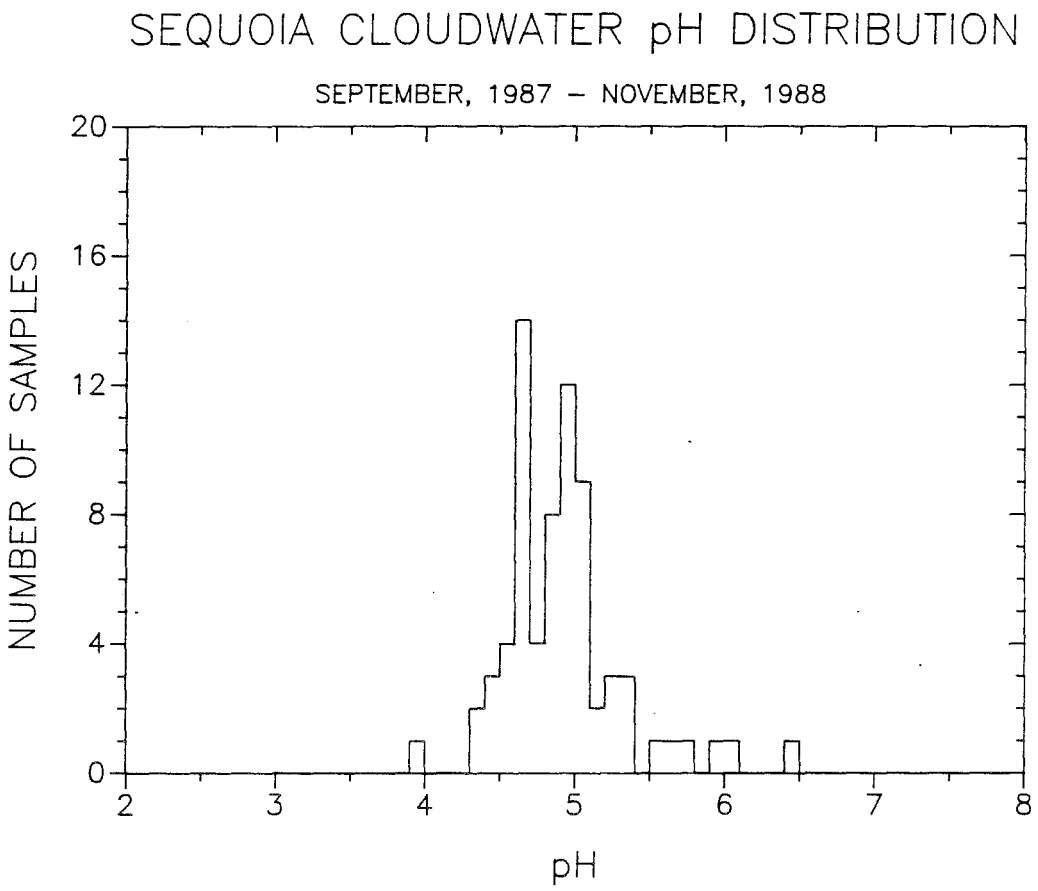

Figure 2.2. Distribution of sample pH values observed for cloudwater samples collected at Lower Kaweah in Sequoia National Park between September, 1987 and November, 1988.

Table 2.1. Chemical Composition of Sequoia Cloudwater CASCC Samples: 1987–88

Time	pH	Na^+	K^+	NH_4^+	Ca^{2+}	Mg^{2+}	Cl^-	NO_3^-	SO_4^{2-}
		←				μN			→
10/22/87									
1253–1324	4.95	3	4	57	6	1	6	41	17
1324–1416	4.87	1	2	29	3	1	2	23	11
1416–1603	5.14	13	13	33	13	4	18	35	18
2234–0015	5.13	5	4	7	8	1	6	16	8
10/24/87									
1423–1553	5.09	1	2	137	4	1	4	78	21
10/27/87									
1647–1741	4.90	2	6	93	5	1	11	49	21
10/28/87									
0724–0805	3.93	8	26	592	33	8	21	549	180
2112–2141	4.65	2	7	180	9	3	6	148	41
2258–0012	5.65	2	9	457	6	1	11	274	67
10/29/87									
0012–0141	6.04	1	3	270	3	2	6	152	36
0141–0608	5.09	0	1	43	3	1	0	32	9
0914–1035	4.70	1	7	79	6	2	7	56	27
1357–1504	4.44	3	12	234	9	4	12	174	67
1637–1920	4.67	1	7	202	7	1	9	128	47
10/31/87									
1414–1705	4.60	1	6	369	8	3	8	273	56
1705–1759	4.94	0	3	214	3	1	6	151	25
1759–1910	5.01	0	1	132	2	1	2	104	15
11/01/87									
0537–0627	4.86	0	3	99	2	1	2	78	13
0725–0829	4.82	0	4	99	4	1	4	78	15
0943–1050	4.70	0	2	83	2	0	2	68	11

Table 2.1 (Cont'd). Sequoia Cloudwater CASCC Samples: 1987–88

Time	pH	Na^+	K^+	NH_4^+	Ca^{2+}	Mg^{2+}	Cl^-	NO_3^-	SO_4^{2-}
		←				μN			→
11/01/87 (cont'd)									
1050–1218	4.75	0	1	62	1	0	2	55	7
1218–1339	5.35	0	0	44	1	0	1	33	4
1339–1457	4.72	0	1	47	2	0	2	43	6
1457–1628	4.96	0	1	32	1	0	0	25	5
1628–1831	4.57	0	3	225	2	1	7	163	33
1831–1950	4.94	0	2	145	1	1	5	98	21
1951–2109	4.62	0	3	284	2	1	11	196	40
11/02/87									
0135–0430	4.62	2	5	229	2	1	10	157	45
0430–0545	4.65	2	1	120	2	1	7	92	26
0545–0715	4.69	2	0	34	2	1	3	33	11
0715–0950	4.46	10	1	70	2	2	13	67	24
0950–1248	4.67	9	1	68	2	2	13	53	21
11/14/87									
1434–1523	4.36	15	8	441	7	6	37	365	93
1523–1558	4.80	5	2	180	2	2	20	137	37
1558–1639	4.93	3	1	122	2	2	12	93	25
1639–1720	4.98	3	0	106	1	1	11	81	21
1720–1812	4.96	2	1	112	2	1	10	85	22
1812–1906	4.94	1	0	97	2	1	9	74	18
1906–1959	4.98	0	0	75	1	1	6	59	15
1959–2126	4.70	1	1	114	2	1	14	92	24
11/17/87									
1110–1416	4.68	2	2	91	2	1	6	61	23
1416–1553	5.27	1	1	21	1	1	1	14	8
1553–1739	5.04	0	1	17	1	0	1	9	8
1739–1854	5.08	0	1	11	1	0	0	7	5
1854–2000	4.83	0	1	13	1	0	1	8	5
04/14/88									
0100–0156	5.07	19	4	613	20	7	18	265	136

Table 2.1 (Cont'd). Sequoia Cloudwater CASCC Samples: 1987–88

Time	pH	Na^+	K^+	NH_4^+	Ca^{2+}	Mg^{2+}	Cl^-	NO_3^-	SO_4^{2-}
		←				μN			→
04/28/88									
1020–1238	4.56	27	4	418	20	10	20	224	184
1238–1423	4.47	13	2	398	10	6	13	193	164
04/30/88									
0607–0754	4.69	5	1	115	8	3	2	62	60
05/17/88									
1206–1600	4.87	3	3	25	4	2	7	25	16
1600–1745	4.83	8	2	69	4	3	13	52	32
1745–2009	4.67	17	3	158	6	6	24	114	65
2009–2321	5.03	54	6	462	17	15	55	322	157
2321–0050	5.39	22	3	244	9	8	27	161	81
05/28/88									
2210–0108	6.49	63	8	45	72	13	12	22	70
06/05/88									
0441–0733	5.38	106	14	377	67	38	70	287	135
0928–1055	5.04	25	3	135	20	10	24	84	65
06/06/88									
0936–1036	5.55	187	14	338	70	50	167	235	127
08/25/88									
1603–1645	4.98	6	6	35	20	9	18	47	24
09/20/88									
1258–1714	4.90	64	15	652	117	38	59	311	187
1914–1951	5.22	2	2	11	10	4	4	16	7
09/21/88									
0516–0826	4.33	321	56	1611	295	117	162	1290	528
11/06/88									
1649–1733	4.74	36	22	1724	79	26	0	1008	141

Table 2.2. Chemical Composition of Sequoia Cloudwater CHRCC Samples: 1988

Time	pH	Na^+	K^+	NH_4^+	Ca^{2+}	Mg^{2+}	Cl^-	NO_3^-	SO_4^{2-}
		←				μN			→
1/30/88									
1422–1640	4.92	6	2	253	3	2	10	140	44
1/30–1/31/88									
4 Intervals	4.95	5	2	221	3	1	11	141	40
2/02/88									
1903–2212‡	5.08	15	6	1095	20	6	32	693	191
2/16/88									
1521–1813	4.56	20	8	1334	29	8	39	950	268
2/28/88									
2 Intervals	5.22	14	7	194	5	3	14	115	44
3/05–3/06/88									
2 Intervals	5.8	6	2	330	3	2	6	187	59
3/06/88									
1720–2109	6	5	1	167	2	2	4	79	26

‡ Cloud interception was not continuous during this period.

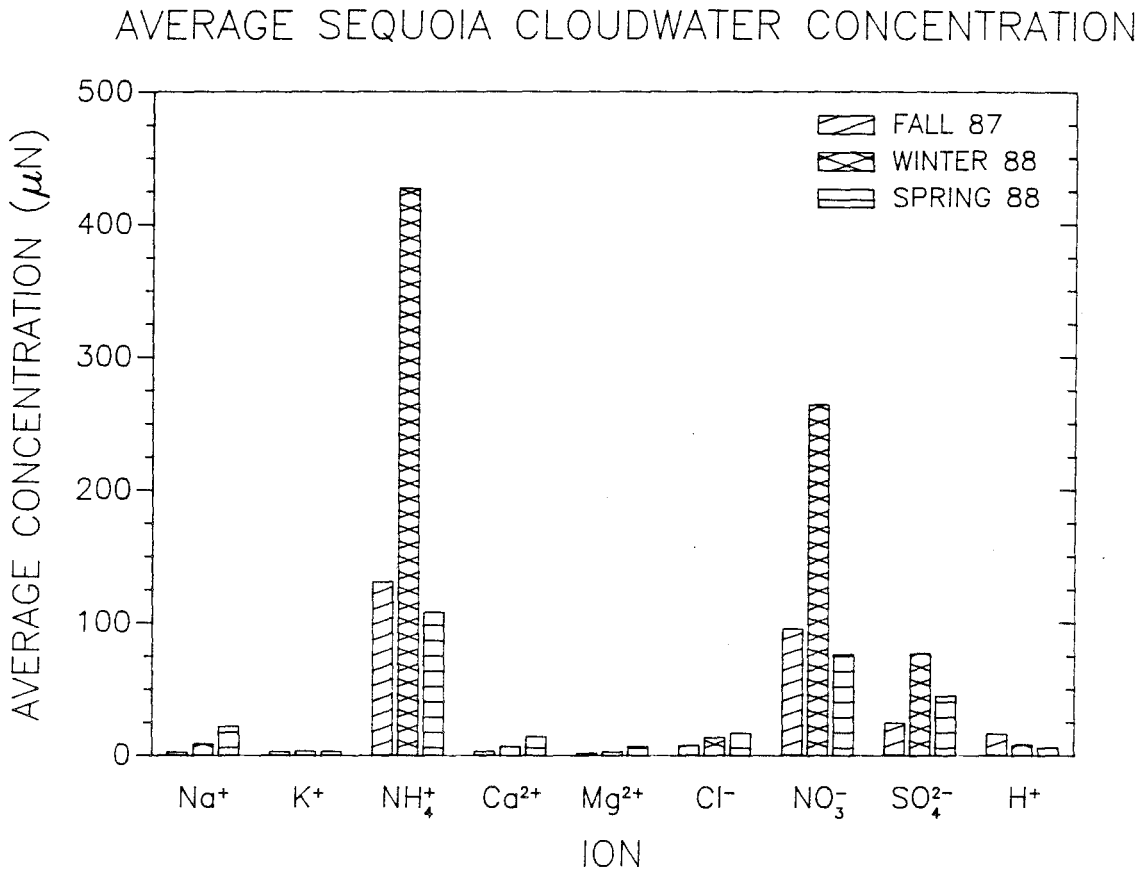

Figure 2.3. Seasonal comparison of volume–weighted average cloudwater compositions observed at Lower Kaweah in Sequoia National Park for the fall of 1987 and the winter and spring of 1988.

integrated cloudwater monitoring system; those collected in the winter were obtained with the winter collection system. Average cloudwater concentrations of the dominant species (NO_3^-, SO_4^{2-}, and NH_4^+) were highest during the winter, while fall and spring averages were more nearly equal. Since increased aerosol concentrations of these species at Lower Kaweah have been correlated with the breakdown of stable conditions in the atmosphere above the San Joaquin Valley (see Chapter 3), the higher concentrations observed in the winter may be associated with longer wintertime periods of stagnation in the valley, which allow a greater buildup of pollutants.

It is important to emphasize, however, that differences in the seasonal volume–weighted average concentrations of these species are no larger than many of the differences observed between events in a single season. There is also considerable variation observed within the course of a single event. An example of single–event variation is illustrated by the data from November 1–2, 1987. Concentrations of NO_3^-, SO_4^{2-}, NH_4^+, and H^+ observed in samples collected at Lower Kaweah during this event are depicted in Figure 2.4. Between approximately 1630 and 1830 PST on November 2, an increase of several hundred percent was observed in the concentrations of NO_3^-, SO_4^{2-}, and NH_4^+. The H^+ concentration in the cloudwater also was observed to increase by more than 100% during this period. The timing of the increases coincided with a cessation of rainfall observed at a nearby passive cloudwater monitoring station (Chapter 4).

Rain falling at lower elevations prior to 1630 may have scavenged a large fraction of the pollutants being transported up the slopes of the Sierra by the afternoon upslope breezes (Chapter 3) before they could be incorporated into the cloudwater at Lower Kaweah. When the rain stopped, the cloudwater loadings

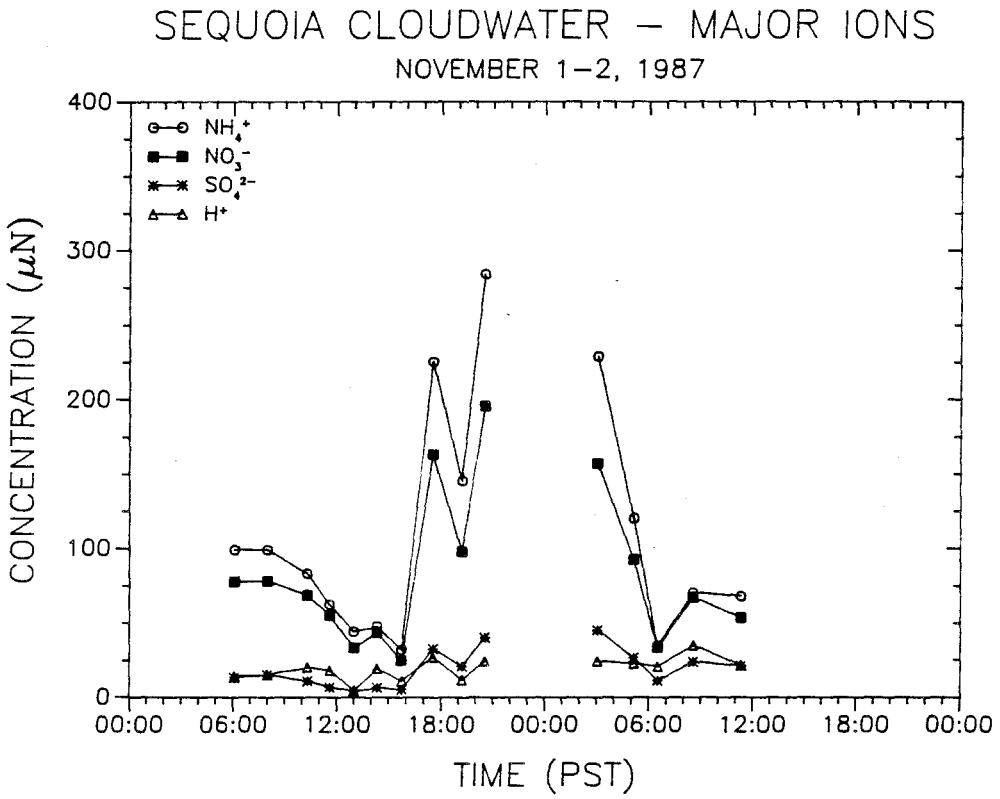

Figure 2.4. Cloudwater concentrations of major ions observed in samples collected at Lower Kaweah in Sequoia National Park on 1 and 2 November, 1987. Breaks in the lines represent significant breaks in cloud interception at the site.

observed at Lower Kaweah began to increase. A dip in the cloudwater concentrations around 1930 PST corresponded to a brief period of additional rainfall. Rainfall had also been observed intermittently beginning around 1100 PST and may explain the drop in cloudwater concentrations between 1030 and 1630.

No rainfall was observed prior to 1100 on November 1. A comparison of cloudwater concentrations prior to 1100 with those observed during non-precipitating conditions later in the day illustrates an increase of more than 100% for NO_3^-, SO_4^{2-}, and NH_4^+ through the afternoon. The concentration increases of these three species, all of which are found at high concentrations in aerosol near the valley floor, may have been associated with increased vertical mixing over the valley due to the arrival of the frontal system, or simply with transport up from the valley floor by the afternoon upslope breezes.

The technique of principal factor analysis (Harman, 1967) was applied to the cloudwater composition data set collected in Sequoia National Park during the fall of 1987. Principal factor analysis involves determining a small number of vectors, composed of combinations of different ions, which explain a large portion of the variance in the data set. The combinations of ions in the vectors may suggest sources of the cloudwater ions. A similar approach has been found useful for identifying potentially important sources in other studies (Knudson et al., 1977; Cahill et al., 1986).

The analysis utilized IMSL STAT/LIBRARY FORTRAN subroutines (IMSL, 1987) which were incorporated into a FORTRAN program. The first step was to derive the correlation matrix depicted in Table 2.3. The upper half of the matrix illustrates the complete set of ion correlations; the lower half depicts only

Table 2.3. Sequoia Cloud Composition Correlation Matrix Fall 1987

	Na^+	K^+	NH_4^+	Ca^{2+}	Mg^{2+}	Cl^-	NO_3^-	SO_4^{2-}	H^+
Na^+	1.00	0.48	0.29	0.45	0.74	0.82	0.37	0.44	0.41
K^+		1.00	0.67	0.95	0.84	0.53	0.73	0.84	0.74
NH_4^+			1.00	0.59	0.66	0.61	0.98	0.90	0.62
Ca^{2+}		0.95		1.00	0.84	0.44	0.70	0.82	0.79
Mg^{2+}	0.74	0.84		0.84	1.00	0.78	0.76	0.86	0.79
Cl^-	0.82				0.78	1.00	0.65	0.67	0.50
NO_3^-		0.73	0.98		0.76		1.00	0.95	0.76
SO_4^{2-}		0.84	0.90	0.82	0.86		0.95	1.00	0.85
H^+		0.74		0.79	0.79		0.76	0.85	1.00

Entries above the diagonal illustrate the entire correlation matrix. Only correlations greater than 0.7 are listed in the lower half of the matrix.

those correlations greater than 0.7. The data illustrate that there is a large degree of correlation between many of the measured ion concentrations. It is interesting to note that there are no negative correlations between any of the ions. The combination of these two factors indicates that most ion concentrations tend to rise and fall as a group in this data set. This trend is consistent with two major processes thought to control the cloudwater concentrations at Lower Kaweah. Increases in the mixing height over the San Joaquin Valley, as discussed in Chapter 3, are likely to lead to simultaneous increases in most, if not all, of the major inorganic species concentrations observed at Lower Kaweah. Alternatively, washout by rainfall will reduce ambient concentrations of the inorganic species.

The correlation matrix was diagonalized to yield nine eigenvectors and their respective eigenvalues. The four most important eigenvectors, explaining 99% of the total variance in the data, are listed in Table 2.4. The corresponding eigenvalues also are listed here. The percent of total variance in the original data set spanned by each of the eigenvectors is given by the quotient of the eigenvalue corresponding to that vector divided by the sum of the eigenvalues (Knudson et al., 1977). The variances explained by each of the four eigenvectors listed in Table 2.4 are 76%, 12%, 8%, and 3%, arranged in order of decreasing eigenvalue. The value of each factor loading in an eigenvector indicates the importance of that factor's contribution to the composition of the vector. The first eigenvector contains significant contributions from almost all of the measured ions and may be considered to represent the total dissolved ion concentration. A similar pattern was observed in the factor loadings for the principal eigenvector explaining spatial variations in the composition of Puget Sound rainfall (Knudson et al., 1977). The fact that such a vector explains the majority of the variance in the data set from this study might have been foreseen based on the high degree of interspecies

Table 2.4. Sequoia Cloud Composition Eigenvectors Fall 1987

Eigenvalue*	6.55	1.07	0.73	0.26
% Variance‡	76	12	8	3
Na^+ Loading	0.61	0.71	–0.03	–0.01
K^+ Loading	0.89	–0.10	–0.31	–0.23
NH_4^+ Loading	0.84	–0.30	0.44	–0.12
Ca^{2+} Loading	0.87	–0.15	–0.43	–0.12
Mg^{2+} Loading	0.94	0.23	–0.13	0.02
Cl^- Loading	0.76	0.51	0.30	0.01
NO_3^- Loading	0.91	–0.26	0.31	0.01
SO_4^{2-} Loading	0.97	–0.19	0.09	0.04
H^+ Loading	0.85	–0.16	–0.20	0.41

* Values of the remaining five eigenvalues are all less than 0.03

‡ The percent of the variance present in the original data set accounted for by each vector.

correlation observed in the correlation matrix.

By rotating the vectors in space, it is possible to simplify the vector structures to aid interpretation of source contributions. One useful technique is the varimax rotation which maximizes the variance contained within each vector (Harman, 1967). The effect of this rotation is to force component contributions either toward one or zero. The rotated vectors obtained by transforming the four eigenvectors in Table 2.4 by the varimax rotation are listed in Table 2.5. The percent of variance explained by each vector is listed in the table as well. Like the eigenvectors, these four vectors together explain 99% of the total variance in the original data set; however, the contributions made by three of the four rotated vectors, unlike those of the eigenvectors, are comparable.

The first rotated vector contains large contributions from NH_4^+, NO_3^-, and SO_4^{2-}, with smaller contributions from the remaining ions. The composition of this vector suggests that aerosol containing NH_4^+, NO_3^-, and SO_4^{2-} contributes significantly to the composition of the cloudwater in Sequoia National Park. The vector may also include contributions from gas phase NH_3 and HNO_3, which readily equilibrate to NH_4^+ and NO_3^- upon dissolution in cloudwater. As discussed in Chapter 3, all of these species are found at high concentrations near the floor of the San Joaquin Valley and are transported by daytime upslope winds into the adjoining Sierra. The dominance of the NO_3^- loading over the SO_4^{2-} loading in the rotated vector indicates that this source component is probably dominated by NH_4^+ and NO_3^- with smaller inputs of SO_4^{2-}.

The second rotated vector is dominated by inputs from Na^+, Cl^-, and Mg^{2+}. This composition suggests that there is a strong contribution to variance in the

Table 2.5. Sequoia Cloud Composition Rotated Vectors Fall 1987

% Variance‡	34	25	30	10
Na^+ Loading	0.05	0.90	–0.26	0.09
K^+ Loading	0.40	0.26	–0.84	0.13
NH_4^+ Loading	0.94	0.18	–0.27	0.09
Ca^{2+} Loading	0.32	0.20	–0.88	–0.25
Mg^{2+} Loading	0.39	0.60	–0.59	0.30
Cl^- Loading	0.44	0.83	–0.13	0.11
NO_3^- Loading	0.87	0.23	–0.35	0.25
SO_4^{2-} Loading	0.73	0.28	–0.51	0.36
H^+ Loading	0.41	0.21	–0.51	0.69

‡ The percent of the variance present in the original data set accounted for by each vector.

cloudwater composition associated with inputs of sea salt which contains large concentrations of these ions. A third important source is suggested by the composition of the third vector which includes large contributions from Ca^{2+}, K^{+}, and Mg^{2+}. These ions are representative of inputs of soil dust.

The combination of these three vectors accounts for 89% of the variance in the inorganic composition of the samples studied. The fourth vector accounts for most of the remaining variance. The only significant contribution to this vector comes from H^{+}. Small contributions from NO_3^- and SO_4^{2-} are also seen, suggesting that some of the H^{+} may be associated with inputs of HNO_3 and H_2SO_4. Since the loadings of these species are so small (equivalent only to that from Mg^{2+}), however, a more reasonable hypothesis of the H^{+} source might be weak carboxylic acids. Formic and acetic acid, as indicated above, often make important contributions to the acidity of the cloudwater at Lower Kaweah, particularly during periods with little anthropogenic input. Since these species undergo rapid biological degradation in unpreserved samples (see Chapter 1), they are not routinely analyzed and their cloudwater concentrations were not available to be included in this statistical analysis.

There is no strong evidence, based upon this principal factor analysis, indicating that different anthropogenic source regions were operative in contributing to variations of Sequoia cloudwater concentrations of NO_3^-, SO_4^{2-}, and NH_4^+ during different events in the fall of 1987. Rather, the analysis suggests that there was a single dominant source of these three species, represented by the first rotated vector. It is possible, however, that the hypothesized source represents a mixture of inputs from areas throughout the San Joaquin Valley and perhaps even the San Francisco Bay area. It is also possible that the regional signatures of NO_3^-, SO_4^{2-}, and NH_4^+ are

not sufficiently different to allow them to be separated out by this analysis with only 45 samples. Since the variance in the high NH_4^+ concentrations observed in the cloudwater samples are explained so well by the first rotated vector, however, it seems that the hypothesized source is probably associated with the large emissions of NH_3 characteristic of the central and southern San Joaquin Valley.

The inorganic chemical composition of the cloudwater collected at Turtleback Dome in Yosemite National Park is listed in Table 2.6. Cloudwater samples collected at this site tended to be more acidic than those collected at Lower Kaweah during the spring of 1988. Figure 2.5 depicts the distribution of sample pH values observed at each site during this period. Sequoia samples had pH values between 4.4 and 6.5; samples at Yosemite had pH values between 3.8 and 5.2. Some of the difference in the distributions may be due to some storms producing interception events only at one Park or the other; however, samples collected on April 28 and 30 at Turtleback Dome were observed to be more acidic than those collected simultaneously at Lower Kaweah.

Volume–weighted average cloudwater concentrations of NO_3^- and NH_4^+ were observed to be quite similar in the two Parks during the spring. This is illustrated in Figure 2.6. The higher level of free acidity in the Yosemite cloudwater is also apparent from this figure. At least part of the increase appears, on an average basis, to come from higher inputs of SO_4^{2-} in Yosemite. Differences in inputs of formic and acetic acid may also contribute to increased acidity of the Yosemite cloudwater. An increase in sample pH was often observed between the time that samples were collected and measured in Yosemite and the time that the pH measurement was repeated a few days later in Pasadena. This increase was more prevalent among higher pH samples, suggesting that the rise may have resulted

Table 2.6. Chemical Composition of Yosemite Cloudwater CASCC Samples: 1988

Time	pH	Na^+	K^+	NH_4^+	Ca^{2+}	Mg^{2+}	Cl^-	NO_3^-	SO_4^{2-}
		←				μN			→
04/14/88									
1745–1921	4.66	5	2	10	8	3	5	16	13
1921–2031	4.90	2	1	5	3	2	0	6	4
2031–2115	5.05	7	2	4	6	2	5	8	6
04/15/88									
1054–2155	4.48	1	1	14	4	1	0	20	9
04/16/88									
1530–1908	4.41	4	14	83	6	2	14	62	31
04/23/88									
1435–1736	4.59	9	5	126	23	8	8	50	115
1736–1922	4.69	4	3	96	15	5	3	34	73
1922–2039	4.77	2	1	64	9	3	1	26	49
2039–2202	4.66	2	2	69	10	3	1	32	53
04/28/88									
1027–1130	4.00	16	4	447	20	9	9	245	197
1130–1221	3.96	12	2	325	11	6	9	227	173
1221–1323	3.96	8	2	330	7	4	8	205	170
1323–1417	3.88	9	2	379	8	4	10	236	204
04/30/88									
0126–0339	4.08	51	5	189	33	20	23	237	134
0409–0506	4.37	25	3	87	18	11	14	105	64
0506–0600	4.34	23	2	74	15	9	16	87	54
0600–0655	4.54	19	1	56	9	7	17	59	41
0655–0820	4.32	32	2	93	12	10	30	95	74
0956–1002	4.92	6	1	16	4	2	7	14	9
1353–1407	5.13	5	1	10	4	2	5	10	7
05/12/88									
2302–2354	4.52	12	3	115	14	8	5	67	54
2354–0031	4.43	8	2	91	11	5	6	81	68

Table 2.6 (Cont'd). Yosemite Cloudwater CASCC Samples: 1988

Time	pH	Na^+	K^+	NH_4^+	Ca^{2+}	Mg^{2+}	Cl^-	NO_3^-	SO_4^{2-}
		←				μN			→
05/13/88									
0031–0148	4.25	6	1	104	8	3	4	92	76
0148–0236	3.89	19	5	252	22	12	16	230	186
05/17/88									
0243–0321	4.69	6	2	48	9	4	3	30	41
0421–0533	4.99	2	1	17	3	2	1	15	14
0616–0809	4.73	4	1	35	5	2	2	25	33
0809–0854	4.45	5	1	51	7	3	4	36	45
05/28/88									
1923–2003	4.95	1	2	62	5	2	11	33	23
2010–2150	5.08	0	1	20	5	0	4	15	9
2150–0007	5.08	1	0	13	1	1	5	10	9
05/29/88									
0125–0225	4.30	67	3	72	8	17	79	52	83
1041–1130	4.99	4	0	15	1	1	13	10	7
11/13/88									
0904–1109	4.68	13	9	32	35	13	19	58	27
1645–1802	5.04	4	1	20	4	2	4	10	8
1802–1945	5.15	1	1	8	2	2	0	5	1
1945–2036	5.26	0	0	3	0	0	9	3	1
11/14/88									
1326–1426	5.10	8	1	5	4	3	9	5	2
11/16/88									
1725–1930	4.61	1	2	9	4	2	1	6	10
1930–2054	4.75	1	1	7	2	1	0	5	7
2054–2240	4.75	4	1	13	2	2	4	13	7
2240–2358	4.28	30	3	56	6	7	33	65	35
11/23/88									
0621–0952	4.87	5	4	9	4	NA	4	10	4

NA denotes not available

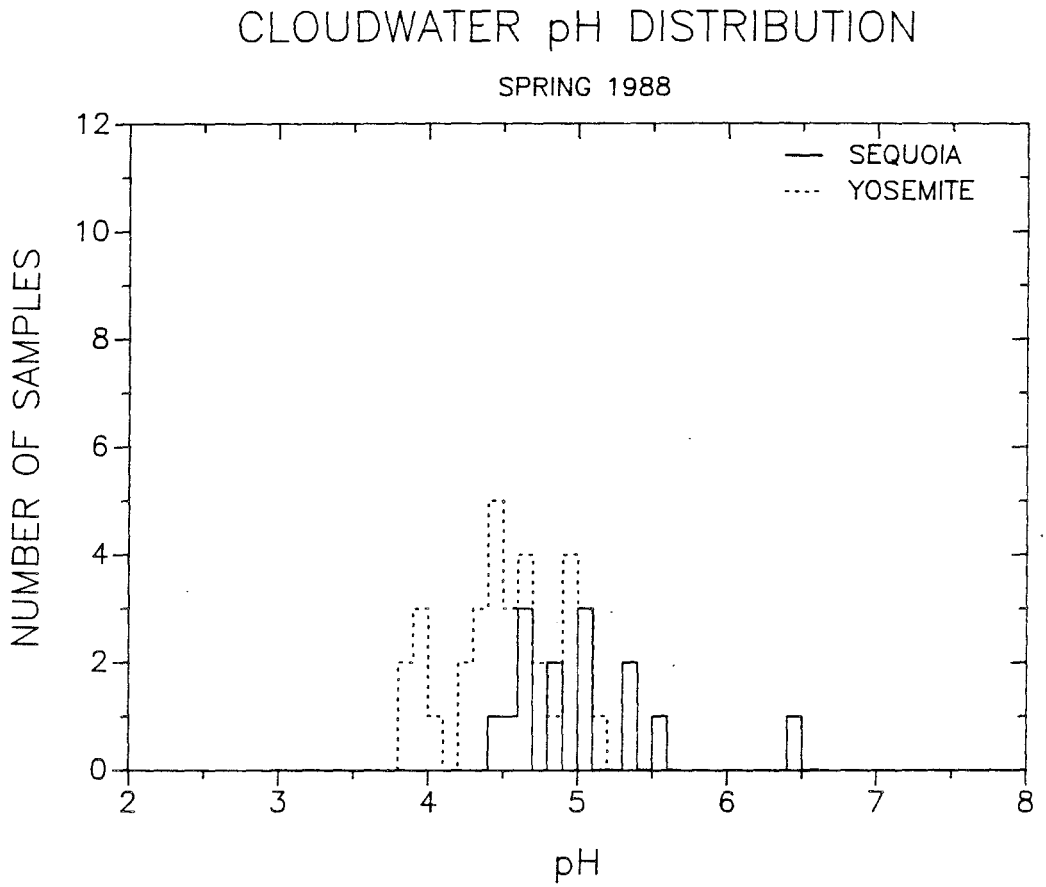

Figure 2.5. Comparison of pH values observed in samples collected at Lower Kaweah in Sequoia National Park and at Turtleback Dome in Yosemite National Park during the spring of 1988.

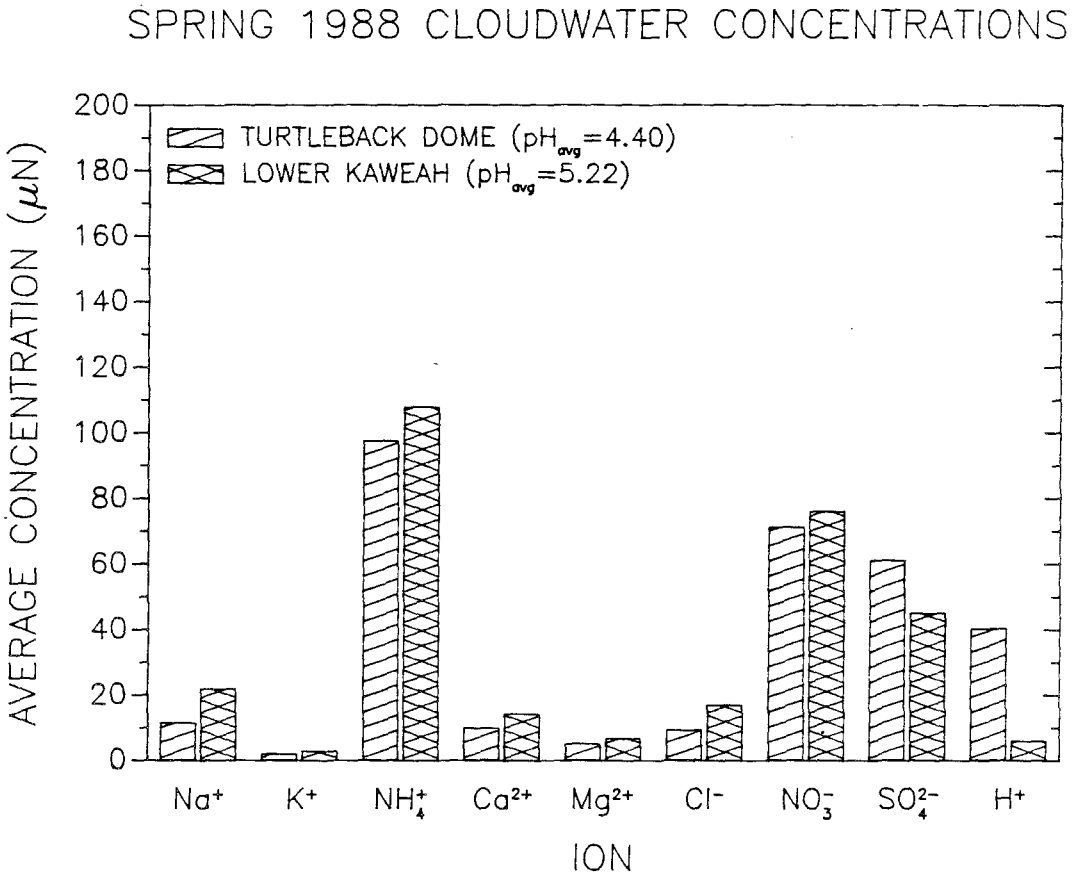

Figure 2.6. Volume–weighted average concentrations of major ions measured in samples collected at Lower Kaweah in Sequoia National Park and at Turtleback Dome in Yosemite National Park during the spring of 1988.

from microbial degradation of lower molecular weight organic acids, such as formic and acetic acid, in the samples. The rise in the pH of precipitation samples has previously been used to estimate sample concentrations of carboxylic acids (Keene and Galloway, 1984). While this evidence, along with the prevalence of formate and acetate in Sequoia cloudwater, suggests that organic acids are probably present at some level in Yosemite cloudwater, no direct determinations are available to evaluate the importance of their contribution to cloudwater acidity at Turtleback Dome.

A comparison of the cloudwater concentrations observed at Turtleback Dome and Lower Kaweah on April 28, 1988 is presented in Figure 2.7. Once again the higher free acidity in the Yosemite cloudwater is evident, with the average pH slightly less than 4.0, compared to a pH of 4.5 at Sequoia. In this case, the higher H^+ concentration appears to be largely compensated for by a lower concentration of NH_4^+ and higher concentrations of NO_3^- and SO_4^{2-} at Yosemite. It is worth noting that relatively small percentage changes in the amounts of mineral acids and bases in the cloudwater, as observed in this example, can dramatically change the pH.

We previously have pointed out the role of ammonia in limiting the acidification of cloudwater in Sequoia National Park (Chapter 1; Collett et al., 1989). The neutralization of cloudwater acidity by ammonia is largely responsible for maintaining the pH of Sequoia cloudwater above levels commonly seen at elevated sites in the eastern U. S. In the absence of ammonia inputs to the cloudwater sampled on November 28, pH values would have dropped below 3.3 at Yosemite, provided other inputs remained constant. Sample pH values at Sequoia on February 16, 1988, could have fallen as low as pH 2.9 in the absence of neutralization by ammonia. Without the high degree of neutralization by ammonia,

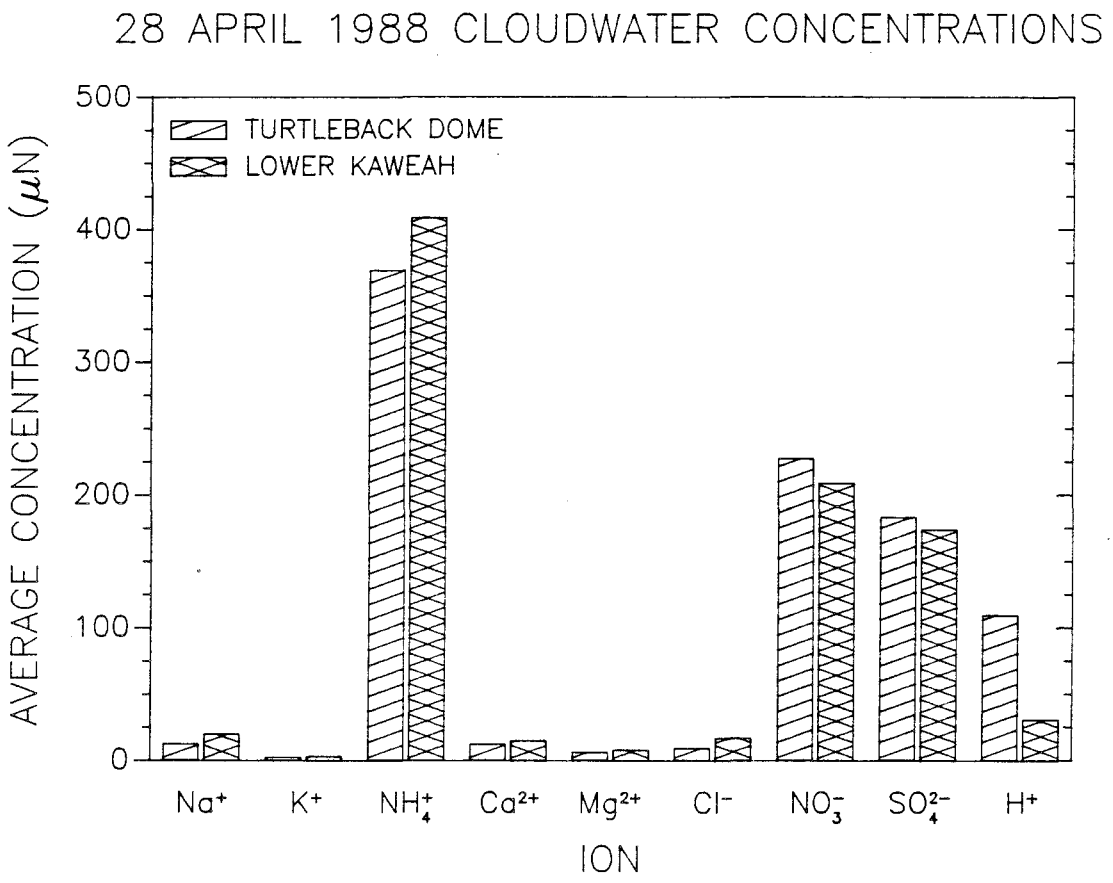

Figure 2.7. Volume–weighted average concentrations of major ions measured in samples collected simultaneously at Lower Kaweah in Sequoia National Park and at Turtleback Dome in Yosemite National Park on 28 April, 1988.

cloudwater in the Sierra might regularly have pH values well below 4.0.

The role of neutralization by ammonia has also been addressed with regard to the composition of fogwater sampled on the floor of the San Joaquin Valley (Jacob et al., 1986), where the balance of local emissions of NH_3 vs. NO_x and SO_2 often determines fogwater acidity. While considerably more mixing of valley emissions occurs before they are transported up the slopes of the Sierra, the comparison between Sequoia and Yosemite cloudwater illustrates that regional differences in cloudwater acidity, associated with relatively small differences in local balances of acids and bases, are important in the Sierra as well.

While the presence of ammonia serves to reduce the free acidity of Sierra cloudwater, and nitrogen in the form of NH_3 or NH_4^+ is an important plant nutrient, the atmospheric deposition of large quantities of NH_4^+ may have deleterious effects upon the Sierra ecosystem. Nitrification of NH_4^+ in the soil is known to produce nitric acid (van Breemen et al., 1982), leading to acidification of the soil column. The uptake of NH_4^+ by the roots of plants is usually accompanied by oxidation and release of hydrogen ions or organic acids (Nihlgard, 1985), which will also contribute to soil column acidification. Other problems associated with excess nitrogen deposition include increased susceptibility to frost, biological enemies, and other air pollutants; excess nitrogen deposition may also create a distorted mineral balance in the environment surrounding a plant, which may lead to deficiencies of magnesium, potassium, phosphorus, molybdenum, and boron, all of which are needed to assimilate nitrogen and synthesize proteins in plant cells (Nihlgard, 1985).

While concentrations of the inorganic species observed in the cloudwater appear to be insufficient to cause acute damage to vegetation, the concentrations of

these species actually present at the vegetative surfaces, during and following periods of cloudwater interception, may be greater than those observed in the collected cloudwater samples. The chemical composition of cloudwater droplets collected along the California coast has been observed to vary with droplet size within a single cloud parcel (Hoffmann, 1988; Munger et al., 1989). Similar observations recently have been made indirectly by Noone et al. (1988) as well. Smaller cloud droplets in the coastal clouds were observed both to be more acidic than larger droplets and more concentrated in NO_3^-, SO_4^{2-}, and NH_4^+. Larger droplets were observed to be more concentrated in species associated with soil dust and sea salt: Na^+, Ca^{2+}, and Mg^{2+}. If such differences exist in the cloudwater in the Sierra, a more detailed picture of the chemical composition of individual droplets is needed to assess the potential for vegetative damage. Droplets deposited on vegetative surfaces also may interact with previously deposited material. Such material could include particles and gases deposited via dry deposition mechanisms or residues of evaporated cloudwater droplets or rain drops. The interaction of the freshly deposited droplets with these previously deposited materials could lead to the exposure of the plant surfaces to higher concentrations of acids and other species than are found in the cloudwater alone. Finally, evaporation of deposited cloudwater, either in subsaturated conditions during an interception event or following an event, will lead to increases in the aqueous concentrations present at the plant surface. The potential importance of this mechanism has been outlined by Unsworth (1984).

Clearly there is a strong possibility that the aqueous concentrations present at vegetative surfaces may, at times, significantly exceed those present in bulk samples of cloudwater. More work is needed to evaluate the importance of concentration enrichment to determine the potential for acute vegetative damage in

the Sierra. Another issue of concern is the cumulative deposition of chemical species to the forest ecosystem. The role of cloudwater interception in contributing to this process is evaluated in the following section.

Cloudwater Deposition

Significant quantities of NO_3^-, SO_4^{2-}, H^+, and NH_4^+ are deposited at Lower Kaweah by precipitation (Stohlgren and Parsons, 1987). Dry deposition is also expected to contribute significantly to the total deposition of these species in the region, particularly during the long dry periods in the summer when pollutants are seldom scavenged by cloud processes or rainfall (Cahill et al., 1986; Bytnerowicz and Olszyk, 1988). We previously suggested that the deposition of NO_3^-, SO_4^{2-}, H^+, and NH_4^+ via cloudwater interception at Lower Kaweah may be comparable to amounts introduced by precipitation (Collett et al., 1989; Chapter 1). Although the volume of water deposited to the canopy over the course of a year due to cloudwater interception is smaller than that due to precipitation, concentrations of NO_3^-, SO_4^{2-}, and NH_4^+ in the cloudwater at Lower Kaweah are much higher than those typically observed in precipitation at the same site. Figure 2.8 illustrates this difference. Average concentrations of NH_4^+ and NO_3^- in cloudwater are more than ten times those observed in precipitation; cloudwater SO_4^{2-} concentrations are more than three times those observed in precipitation. Since the cloudwater concentrations are so much higher, even small inputs of cloudwater can contribute relatively large quantities of these species to the ecosystem. Our original estimates of cloudwater deposition values were based on a limited set of cloudwater composition data collected during the fall of 1985 and the spring of 1986. Given the considerable body of data that has been collected in the current study, it is now possible to refine the initial estimates, and to compare them with the precipitation deposition data

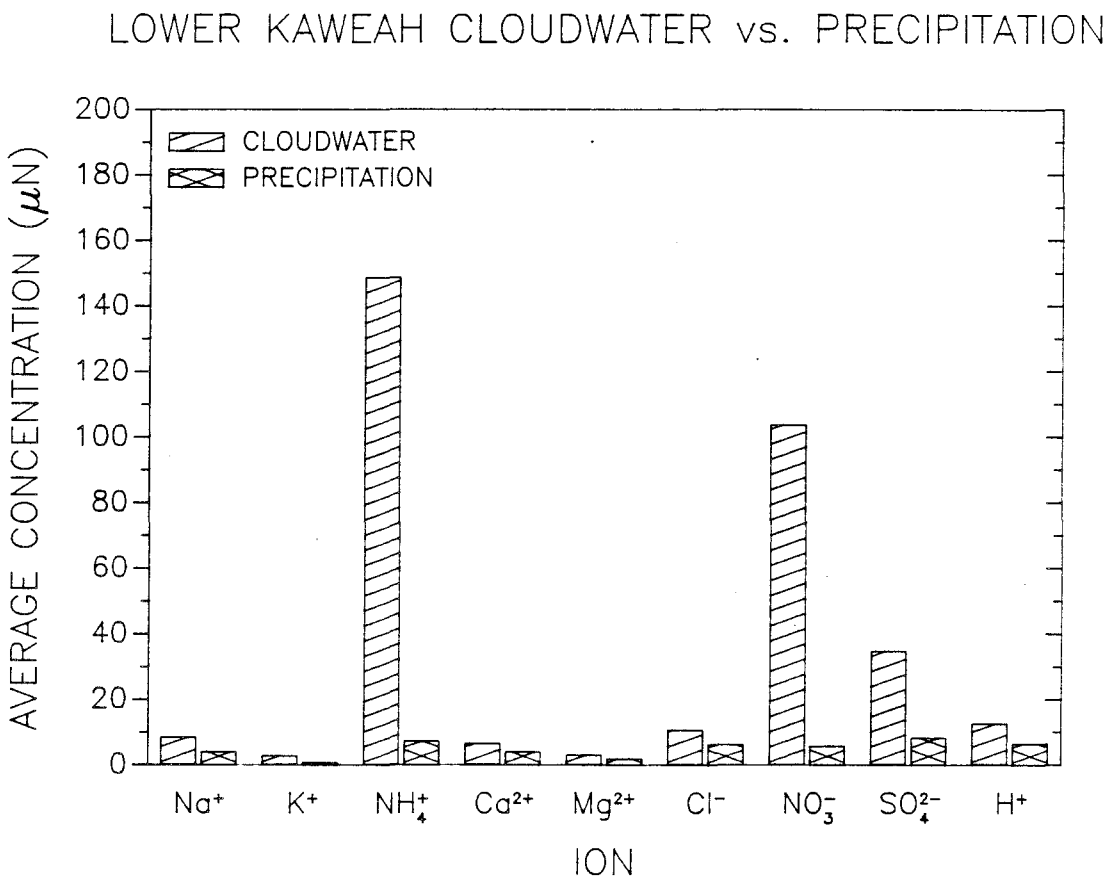

Figure 2.8. Comparison of volume–weighted average cloudwater concentrations observed at Lower Kaweah in Sequoia National Park between September, 1987 and August, 1988 (this study) with volume–weighted average concentrations observed in precipitation at the same site between 1981 and 1984 (Stohlgren and Parsons, 1987).

and with dry deposition data recently collected in Sequoia National Park.

In order to determine the flux of a given species to the surface (or vegetation canopy) via cloudwater deposition, two parameters must be established. First, it is necessary to identify the gross flux of cloudwater to the surface. Second, the average cloudwater concentration of the species of interest must be known. The product of the gross cloudwater flux and the average cloudwater concentration of the species yields the flux of interest. The data gathered in this study enable us to identify the average cloudwater composition with reasonable confidence for the period studied. Estimating the total quantity of cloudwater deposited to the canopy is more difficult.

The deposition rate of cloudwater to the canopy is largely controlled by the wind speed, the aerodynamic structure of the canopy, the droplet size distribution, and the cloud liquid water content (Lovett and Reiners, 1986). Several authors have utilized a variety of approaches to determine the deposition of cloudwater to a vegetation canopy. These approaches have included measurements of throughfall beneath the canopy during periods of cloudwater deposition (Yosida, 1953; Azevedo and Morgan, 1974; Olson et al., 1981; Dasch, 1988), micrometeorological methods (Dollard et al., 1983), and modeling (Lovett, 1984; Unsworth, 1984). Lovett's model design is analogous to Ohm's law for DC electrical circuits. The flux of droplets to the canopy is determined by the ratio of a potential gradient to a resistance. The gradient consists of the droplet concentration difference between the air above the canopy and the vegetation surface. The resistance is composed of two portions: the resistance to turbulent transfer of the droplets down through the canopy and the resistance to droplet transport through the boundary layer to the plant surface. The model predicts cloudwater deposition rates, in a closed canopy of

10.5 m balsam fir, varying nearly linearly from 0.2 to 1.1 mm hr^{-1} for canopy–top wind speeds of 2 to 10 m s^{-1}, a liquid water content of 0.4 g m^{-3}, and a modal droplet diameter of 10 μm (Lovett, 1984). Local deposition fluxes along gaps in the forest canopy are expected to be higher due to increased penetration of droplet–laden air parcels from above the canopy into the gaps (Lovett and Reiners, 1986).

Some reports of cloudwater deposition, estimated from throughfall measurements, have indicated deposition rates comparable to those predicted by Lovett (1984). Yosida (1953) reported droplet deposition rates of approximately 0.5 mm hr^{-1} in a coastal forest intercepted by dense fog. Azevedo and Morgan (1974) measured fog drip beneath a large redwood in northern California at rates as high as 4 cm day^{-1} over a two–day period (implying an average deposition rate greater than 1.6 mm hr^{-1}) and rates up to 4.6 cm day^{-1} (0.8 mm hr^{-1}) under other trees located at a ridge top. Dasch (1988) reported deposition rates averaging 0.3 mm hr^{-1} to a single exposed tree on the summit of Clingmans Peak, North Carolina, but only 0.03 mm hr^{-1} in a dense spruce–fir forest located just below the summit. The lower value was substantially below what Dasch predicted using Lovett's model, adapted for local conditions.

Given the discrepancy present in the literature over the validity of Lovett's (1984) model estimates, and the uncertainty associated with adapting the model to other forest canopies, it is difficult to assess what deposition rates should be assumed for the canopy at Lower Kaweah. The presence of large gaps in the canopy there suggests that, as was observed in the studies where the trees were more greatly exposed, Lovett's model estimates are probably not too high, and may underestimate actual local deposition rates. Since many of the trees in the vicinity

of Lower Kaweah, including Giant Sequoias, are much taller than those modeled by Lovett (1984), we are further inclined to believe that the model deposition estimates, adjusted for local wind speeds and liquid water contents, will be on the conservative side for Lower Kaweah.

Wind speeds measured at Lower Kaweah during periods of cloud interception typically were observed to be on the order of 3 m s^{-1}; values of cloud LWC typically were observed to be approximately 0.15 g m^{-3}. Lovett's (1984) model predicts a gross cloudwater deposition rate of approximately 0.3 mm hr^{-1} for a 3 m s^{-1} wind speed and a liquid water content (LWC) of 0.4 g m^{-3} for the balsam fir canopy he modeled. Scaling the model prediction for the lower values of LWC observed at Lower Kaweah yields an estimated deposition rate of approximately 0.12 mm hr^{-1}, implying that the 265 hours of cloud interception observed there should have deposited approximately 31 mm of cloudwater during the period from September 1987 to August 1988.

The annual cloudwater deposition of ions to the forest canopy at Lower Kaweah can be estimated by combining the amount of cloudwater deposited with the volume weighted average ion concentrations in the deposited cloudwater. Figure 2.9 illustrates the results of this calculation for NO_3^- (199 mg m^{-2}), SO_4^{2-} (52 mg m^{-2}), NH_4^+ (84 mg m^{-2}), and H^+ (0.4 mg m^{-2}). These estimates are substantially less than were previously predicted (596, 337, 311 and 0.8 mg m^{-2} for NO_3^-, SO_4^{2-}, NH_4^+ and H^+, respectively), based on preliminary observations of cloudwater composition from Sequoia National Park (Collett et al., 1989). The current estimates are lower largely because wind speeds during interception and values of cloud LWC turned out to be smaller than expected. The revised cloudwater deposition estimates, however, are still significant compared to precipitation inputs.

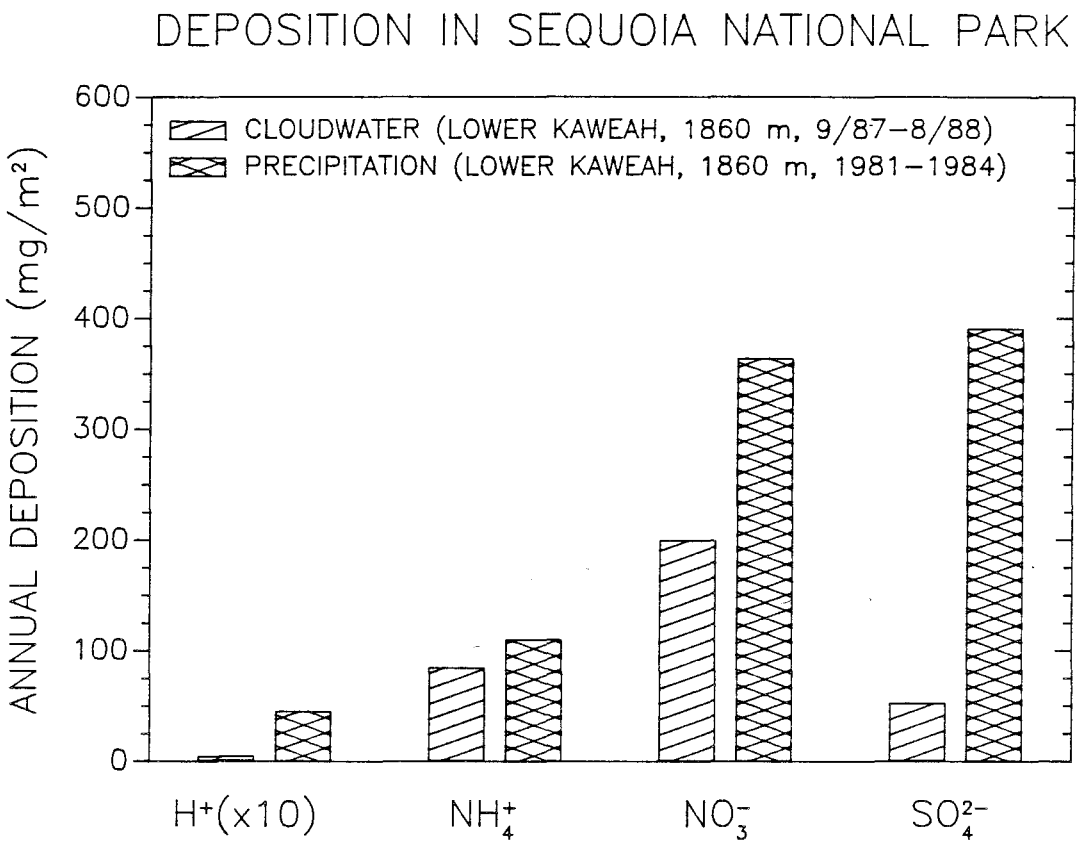

Figure 2.9. Annual deposition of major ions at Lower Kaweah in Sequoia National Park by precipitation (measured, Stohlgren and Parsons, 1987) and cloudwater interception (estimated). Estimates of ion deposition via cloudwater interception assume a hydrological deposition rate of 0.12 mm cloudwater hr^{-1}. See the text for details.

This is particularly true for NO_3^- and NH_4^+. For purposes of comparison, estimates of the annual deposition of the four species in precipitation also have been included in Figure 2.9. Precipitation deposition estimates were taken from Stohlgren and Parsons (1987) and are based on weekly samples collected at Lower Kaweah between 1981 and 1984. Annual deposition of NH_4^+ is slightly higher in precipitation (110 mg m^{-2}) than is predicted in cloudwater; NO_3^- deposition (364 mg m^{-2}) is 82% higher; SO_4^{2-} deposition (391 mg m^{-2}) and H^+ deposition (4.5 mg m^{-2}) are factors of seven and eleven higher, respectively, in precipitation. Since the cloudwater deposition estimates are calculated for a closed canopy, however, local cloudwater fluxes of these species to single trees, to trees near the edge of the canopy, or to trees on a ridgetop may be several times higher than predicted here, due to greater cloudwater hydrologic deposition rates observed in such regions (Lovett and Reiners, 1986; Dasch, 1988). Cloudwater hydrological deposition rates to a passive cloudwater collector located on a nearby ridgetop, in fact, were observed to exceed 4.0 mm hr^{-1} (see Chapter 4), compared to the model estimate of 0.12 mm hr^{-1} used here; rates of cloudwater deposition to a passive cloudwater collector located in Yosemite National Park have been observed to exceed 20 mm hr^{-1}, during periods of high wind (Chapter 4).

Dry deposition also is an important contributor to the deposition of pollutants in the Sierra. Bytnerowicz and Olszyk (1988) reported rates of dry deposition of NO_3^-, SO_4^{2-}, NH_4^+, and H^+ to natural and surrogate surfaces at Emerald Lake, a high elevation (2740 m) lake in Sequoia National Park, during three separate periods in the summer of 1987. Average deposition rates reported for Teflon coated branches of lodgepole pine, western white pine, and Coulter pine correspond to approximately 282, 73, 56, and 0.5 mg m^{-2} y^{-1} for NO_3^-, SO_4^{2-}, NH_4^+, and H^+, respectively, assuming similar deposition rates throughout the year. Since

concentrations of these species generally average higher in the summer when rainfall is infrequent, these rates should be considered as upper limits to actual annual rates of dry deposition at Emerald Lake. These "upper limits" are quite comparable to the annual deposition rate estimates for the same species due to cloud interception at Lower Kaweah. Unfortunately, there is a lack of data representing actual dry deposition measurements at other sites on the western slopes of the Sierra (Bytnerowicz and Olszyk, 1988). Cahill et al. (1986) observed that summer concentrations of SO_4^{2-} at Lower Kaweah were approximately twice the levels observed at Emerald Lake, suggesting that summertime dry deposition of SO_4^{2-} at Lower Kaweah is probably higher than at Emerald Lake. Similar differences in concentrations and deposition rates are likely for the other species as well. Even if summertime rates of dry deposition at Lower Kaweah are twice those observed at Emerald Lake, however, annual deposition rates are not likely to greatly exceed the "upper limits" established for Emerald Lake, suggesting that dry deposition and cloud interception are both important contributors to total deposition in the region.

While considerable uncertainty remains in the estimates of ionic deposition due to cloudwater interception at Lower Kaweah, it seems clear that this deposition mechanism is important, and may even dominate the deposition of NO_3^- and NH_4^+ to exposed trees and ridge–top canopies. Stohlgren and Parsons (1987) observed annual variations in deposition of NO_3^-, SO_4^{2-}, and NH_4^+ in precipitation in excess of 100%. Similar variations are probable in cloudwater deposition. Longer term monitoring of the cloudwater composition in the region, as well as the frequency and duration of cloudwater interception, is needed to determine the importance of annual variations in cloudwater deposition. Field measurements of hydrologic deposition rates to the forest canopy during cloud interception also would aid the establishment of more accurate water and ion flux estimates. Finally, there is a

need to measure rates of dry deposition to the forest canopy in the region of Lower Kaweah, so that the relative importance of the three deposition pathways (precipitation, cloud interception, and dry deposition) may be established. Since annual dry deposition fluxes are probably negatively correlated with the deposition fluxes associated with precipitation and cloud interception, it is desirable to measure contributions from all three deposition pathways concurrently.

Conclusions

Cloudwater intercepting the slopes of the Sierra was sampled at two locations between September of 1987 and November of 1988. One site was located at 1856 m in Sequoia National Park while the second site was located at 1590 m in Yosemite National Park. Automated cloudwater sampling systems were used to collect the samples. The time during which clouds were observed to intercept the mountain slopes at the Sequoia site totaled 265 hours for the 12–month period between September 1987 and August 1988. Peak interception periods occurred in November and April, while the lowest activity was observed during the summer months. Valid samples representing approximately 50% of the total interception time were collected at the Sequoia site and analyzed to determine the concentrations of major ions.

The chemical composition of the sampled cloudwater in both Parks was dominated by NO_3^-, SO_4^{2-}, and NH_4^+. The balance between the cloudwater concentrations of NO_3^- and SO_4^{2-} vs. NH_4^+ was largely responsible for determining the cloudwater pH, although inputs of formic and acetic acid are also believed to be important in this regard, particularly for less polluted samples. The pH of the cloudwater samples collected at the Sequoia site ranged from 3.9 to 6.5; samples

collected in Yosemite had pH values between 3.8 and 5.2. During periods of simultaneous collection, and on average, Yosemite samples were more acidic than Sequoia samples. The pH differential appears to be related to relatively small differences in the cloudwater concentrations of NO_3^-, SO_4^{2-}, and NH_4^+ at the two sites. The role of cloudwater acidity neutralization by inputs of ammonia was clearly observed. In the absence of large ammonia inputs, sample pH values in the Sierra may fall below 3.0.

The technique of principal factor analysis was applied to data representing the chemical composition of 45 cloudwater samples, collected in Sequoia National Park during the fall of 1987, in order to statistically reveal potential ion sources contributing to the sample composition. Four important sources were hypothesized based on this analysis: (1) a source dominated by NO_3^-, SO_4^{2-}, and NH_4^+, reflecting anthropogenic inputs; (2) a source representing sea salt inputs of Na^+, Cl^-, and Mg^{2+}; (3) a soil dust source comprised by Ca^{2+}, K^+, and Mg^{2+}; and (4) an H^+ source, probably associated with organic acids which were not routinely analyzed.

Estimates of annual deposition rates of major ions via cloudwater interception to the forest canopy at the Sequoia site were calculated. The rates for NO_3^-, SO_4^{2-}, and NH_4^+ were calculated to be somewhat lower than previously were estimated for the same site, largely because wind speeds and cloud liquid water contents during interception turned out to be lower than previously assumed. The current deposition estimates are still significant, however, with regard to measured contributions from precipitation and estimated contributions from dry deposition. Cloudwater interception may, in fact, be the dominant deposition mechanism for NO_3^- and NH_4^+, particularly for isolated trees or ridgetop canopies where wind speeds are higher and cloudy air parcels can impact directly on foliar surfaces.

Acknowledgments

We are grateful to the National Park Service for granting us access to the sampling sites in both Yosemite and Sequoia National Parks. We also would like to acknowledge the assistance of the Research and Resource Management staffs at Sequoia National Park and the Resource Management staff at Yosemite National Park. Several members of these staffs, including Dave Parsons, Tom Stohlgren, Annie Esperanza, and Diane Ewell of Sequoia National Park, and Teri Grosse, Charisse Sydoriak, Carol Moses, and Theresa Dunn of Yosemite National Park, made important contributions to the success of this project. Several people served as site operators during the course of the project: Bob Stanley, Tom Suk, Louis Andaloro, Paul Schlitt, Diane Ewell, and Meg Heim at Sequoia National Park, and Jan Cauthorn, Antonina Hines, and Theresa Dunn at Yosemite National Park. This project would not have been possible without their dedicated efforts. Our colleagues J. William Munger and Dieter Gunz also deserve recognition for their assistance in the field and laboratory and for numerous helpful discussions. This work was funded by the California Air Resources Board (CARB contract #A6−185−32).

References

Azevedo, J. and Morgan, D. L. (1974) Fog precipitation in coastal California forests. *Ecology* **55**, 1135–1141.

Bytnerowicz, A. and Olszyk, D. M. (1988) Measurement of atmospheric dry deposition at Emerald Lake in Sequoia National Park. Final Report to California Air Resources Board, Sacramento, CA.

Cahill, T. A., Annegarn, H., Ewell, D. and Feeney, P. J. (1986) Particulate monitoring for acid deposition research at Sequoia National Park California. Final report to California Air Resources Board, Sacramento, CA.

Castillo, R. A., Kadlecek, J. and McLaren, S. (1985) Selected Whiteface Mountain cloud water concentrations summers 1981 and 1982. *Water, Air, Soil Pollut.* **24**, 323–328.

Collett, J., Jr., Daube, B., Jr., Munger, J. W. and Hoffmann, M. R. (1989) Cloudwater chemistry in Sequoia National Park. *Atmos. Environ.*, in press.

Dasch, J. M. (1988) Hydrological and chemical inputs to fir trees from rain and clouds during a 1–month study at Clingmans Peak, NC. *Atmos. Environ.* **22**, 2255–2262.

Dollard, G. J., Unsworth, M. H. and Harve, M. J. (1983) Pollutant transfer in upland regions by occult precipitation. *Nature* **302**, 241–243.

Harman, H. H. (1967) *Modern Factor Analysis*, 2nd Ed., Univ. of Chicago Press, Chicago, 474 p.

Hoffmann, M. R. (1988) Fog, cloud, and dew chemistry. Final report to California Air Resources Board, Sacramento, CA.

International Mathematical and Statistical Libraries (1987) *STAT/LIBRARY – FORTRAN Subroutines for Statistical Analysis*, IMSL, Houston, TX.

Jacob, D. J., Munger, J. W., Waldman, J. M. and Hoffmann, M. R. (1986) The H_2SO_4–HNO_3–NH_3 system at high humidities and in fogs: I. Spatial and temporal patterns in the San Joaquin Valley of California. *J. Geophys. Res.* **91**, 1073–1088.

Keene, W. C. and Galloway, J. N. (1984) Organic acidity in precipitation of North America. *Atmos. Environ.* **18**, 2491–2497.

Keene, W. C., Galloway, J. N. and Holden, J. D. (1983) Measurement of weak organic acidity in precipitation from remote areas of the world. *J. Geophys. Res.* 88, 5122–5130.

Knudson, E. J., Duewer, D. L., Christian, G. L. and Larson, T. V. (1977) Application of factor analysis to the study of rain in the Puget Sound region. In *Chemometrics, Theory and Applications* (ed. B. R. Kowalski). ACS Symposium Series 52, Washington, D. C., 80–116.

Lovett, G. M. (1984) Rates and mechanisms of cloud water deposition to a subalpine balsam fir forest. *Atmos. Environ.* **18**, 361–371.

Lovett, G. M., Reiners, W. A. and Olson, R. K. (1982) Cloud droplet deposition in subalpine balsam fir forests: hydrological and chemical inputs. *Science* 218, 1303–1304.

Lovett, G. M. and Reiners, W. A. (1986) Canopy structure and cloud water deposition in subalpine coniferous forests. *Tellus* **38B**, 319–327.

Mueller, S. F. and Weatherford, F. P. (1988) Chemical deposition to a high elevation red spruce forest. *Water, Air,* and *Soil Pollut.* **38**, 345–363.

Munger, J. W., Collett, Jr., J., Daube, Jr., B. and Hoffmann, M. R. (1989) Chemival composition of coastal stratus clouds: dependence on droplet size and distance from the coast. submitted to *Atmos. Environ.*

Nihlgard, B. (1985) The ammonium hypothesis – an additional explanation to the forest dieback in Europe. *Ambio* **14**, 2–8.

Noone, K. J., Charlson, R. J., Covert, D. S., Ogren, J. A. and Heintzenberg, J. (1988) Cloud droplets: solute concentration is size dependent. *J. Geophys. Res.* **93**, 9477–9482.

Olson, R. K., Reiners, W. A., Cronan, C. S. and Lang, G. E. (1981) The chemistry and flux of throughfall and stemflow in subalpine balsam fir forests. *Holarctic Ecol.* **4**, 291–300.

Reiners, W. A. and Lang, G. E. (1979) Vegetational patterns and processes in the balsam fir zone, White Mountains, New Hampshire. *Ecology* **60**, 403–417.

Schemenauer, R. S. (1986) Acidic deposition to forests: the 1985 Chemistry of High Elevation Fog (CHEF) project. *Atmos. Ocean* **24**, 303–328.

Schemenauer, R. S., Cereceda, P. and Carvajal, N. (1987) Measurements of fog water deposition and their relationships to terrain features. *J. Climate Appl. Meteorol.* **26**, 1285–1291.

Solorzano, L. (1967) Determination of ammonia in natural waters by the phenol–hypochlorite method. *Limnol. Oceanogr.* **14**, 799–801.

Stohlgren, T. J. and Parsons, D. J. (1987) Variation of wet deposition chemistry in Sequoia National Park, California. *Atmos. Environ.* **21**, 1369–1374.

Unsworth, M. H. (1984) Evaporation from forests in cloud enhances the effects of acid deposition. *Nature* **312**, 262–264.

van Breemen, N., Burrough, P. A., Velthorst, E. J., van Dobben, H. F., de Wit, T., Ridder, T. B. and Reijnders, H. F. R. (1982) Soil acidification from atmospheric ammonium sulphate in forest canopy throughfall. *Nature* **299**, 548–550.

Waldman, J. M., Munger, J. W., Jacob, D. J. and Hoffmann, M. R. (1985) Chemical characterization of stratus cloudwater and its role as a vector for pollutant deposition in a Los Angeles pine forest. *Tellus* **37B**, 91–108.

Weathers, K. C., Likens, G. E., Bormann, F. H., Eaton, J. S., Bowden, V. B., Andersen, J. L., Cass, D. A., Galloway, J. N., Keene, W. C., Kimball, K. D., Huth, P. and Smiley, D. (1986) A regional acidic cloud/fog water event in the eastern United States. *Nature* **319**, 657–658.

Weathers, K. C., Likens, G. E., Bormann, F. H., Bicknell, S. H., Bormann, B. T., Daube, Jr., B. C., Eaton, J. S., Galloway, J. N., Keene, W. C., Kimball, K. D., McDowell, W. H., Siccama, T. G., Smiley, D. and Tarrant, R. A. (1988) Cloudwater chemistry from ten sites in North America. *Environ. Sci. Technol.* **22**, 1018–1026.

Yosida, Z. (1953) General survey of the studies on fog–preventing forest. In *Studies on Fogs in Relation to Fog–preventing Forest* (ed. T. Hori). Tanne Trading Co., Sapporo, Japan, 1–23.

CHAPTER 3

INTENSIVE STUDIES OF SIERRA CLOUDWATER CHEMISTRY AND ITS RELATIONSHIP TO PRECURSOR AEROSOL AND GAS CONCENTRATIONS

Introduction

The initial chemical composition of cloudwater has been shown to be determined largely by the composition of the aerosol that serve as condensation nuclei and the ambient concentrations of soluble gases (Jacob et al., 1985, 1986, a, b, 1987). The composition is altered as additional aerosol is scavenged and chemical reactions take place within the droplet. In order to understand what influences cloudwater chemistry at a particular location, therefore, it is necessary to understand the processes that control local concentrations of aerosol and gases, particularly during the period immediately preceding cloud formation. These processes include emission rates, atmospheric reactions, transport routes, and deposition.

Concentrations of most inorganic aerosol and gas phase species in the southern and central Sierra Nevada Mountains of California are controlled primarily by meteorological conditions affecting transport from distant sources. Figure 3.1 illustrates the location of the Sierra relative to the population centers of central California. Both the San Joaquin Valley and the San Francisco Bay area are thought to be important pollutant source regions affecting air quality in the central and southern Sierra. Local Sierra sources of species such as SO_2, NO_x, and NH_3 are relatively unimportant by comparison.

A conceptual model of transport within the San Joaquin Valley has been described by Smith et al. (1981). Meteorology is normally dominated by the presence of high mountains that border the valley on three sides. Net air flow into the valley is from the northwest for all months except January and February. Mass continuity requires the existence of a compensating flow out of the valley. The most

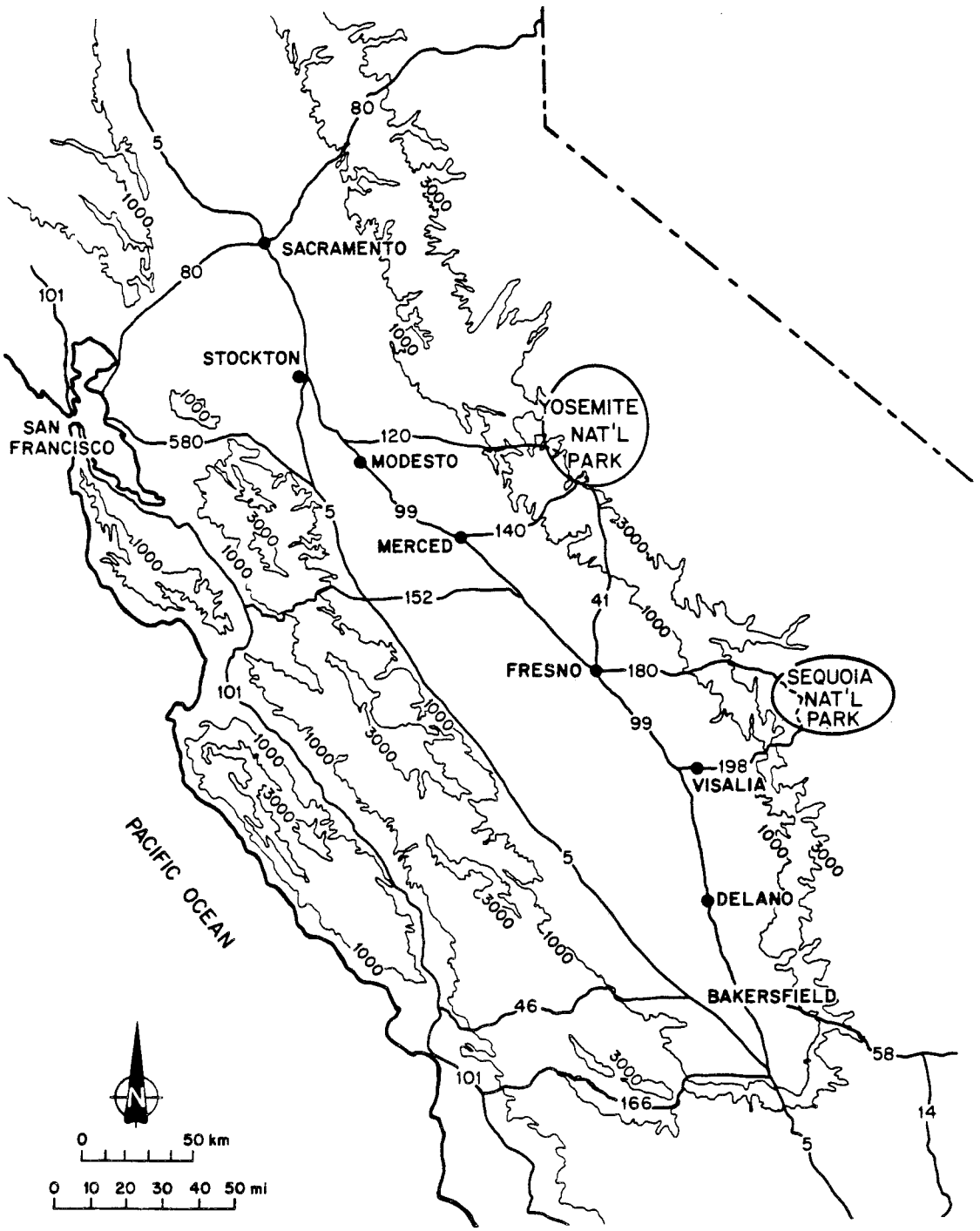

Figure 3.1. Map of central California indicating the location of Sequoia National Park relative to the major population centers. Also indicated are major highways in the region. Contours are included for the 1000 and 3000 foot levels to illustrate the general topography of the region.

effective exit transport mechanism is thought to be a continuation of the northwesterly flow over the Tehachapi Mountains at the southeastern end of the valley. Afternoon upslope flows on both sides of the valley, induced by preferential heating of the air along the mountain slopes, are thought to play a secondary role in transporting air out of the valley. The upslope flows form the primary mechanism for transport of air parcels from the Valley floor up into the slopes of the Sierra.

Temperature inversions in the air mass above the San Joaquin Valley floor are strongest in the winter, but occur frequently throughout the year (Smith et al., 1981). The presence of the mountains surrounding the valley combines with an inversion to trap pollutants within the valley. The passage of frontal systems through the valley can serve to alleviate this condition by eliminating the temperature inversion, thus permitting pollutants to mix up to elevations where they may exit over the Tehachapi Mountains. Increased wind speeds often associated with the fronts also aid in the removal of valley pollutants. Frontal systems may also change the direction of predominant air flow within the valley from northwesterly to southerly, thereby altering the importance of various regional emissions to Sierra air quality.

Past studies have indicated that pollutant concentrations at Lower Kaweah (elev. 6240 feet) in Sequoia National Park (see Figure 3.1) are significantly affected by the passage of cold fronts. Collett et al. (1989) observed increasing concentrations of aerosols and gases as a cold front approached (see also Chapter 1). It was speculated that the increases were due, at least in part, to increases in vertical mixing within the valley. Cahill et al. (1986) observed a similar trend for concentrations of fine particle sulfur, attributing the increase to synoptic scale changes accompanying the cold front which led to increased southerly air flow from

the Bakersfield area. Large quantities of SO_2 are released to the atmosphere in conjunction with oil field activities in the vicinity of Bakersfield.

Increases in aerosol and gas concentrations with the advance of cold fronts may significantly affect the chemical composition of the cloudwater produced in the storm system. The mechanism by which these increases occur (e.g. increased vertical mixing, increased southerly flow, or both) may affect the balance between different species (e.g. NO_3^- vs. SO_4^{2-}, or acids vs. bases) in the air mass and in the cloudwater, since different pollutant source regions have different emission signatures.

This chapter describes the results of a study to investigate more completely the behavior of aerosol and gas concentrations at Lower Kaweah in conjunction with the advance of a cold front through the region, and how those concentrations were reflected in the chemistry of the cloudwater associated with the front. The study also was designed to examine the composition of cloudwater collected simultaneously at two different elevations. The results of that investigation are described here as well, including a discussion of concentrations of organic acids, carbonyls, S(IV), and H_2O_2 in the cloudwater.

Experimental Procedure

In order to investigate spatial and temporal variations of aerosol and gas concentrations during the study, three sampling stations were established: Visalia (elev. 300 feet), Ash Mountain (1800 feet), and Lower Kaweah (6240 feet). Aerosol and gas phase samples were collected using a filter pack technique. Teflon filters (Gelman Zefluor, 1 μm pore size) were used to collect aerosol for determination of

major ions. A pair of oxalic acid impregnated quartz fiber backup filters was used to collect NH_3. A nylon filter was used to collect HNO_3. Each of the stations was equipped with two automated aerosol collectors (see Figure 3.2) to enable simultaneous collection of samples at all three sites. Each collector can hold up to three sets of filter packs at one time and features a programmable timer to enable automated sampling during three separate time periods. Flow rates through the filter packs (10.8 l min^{-1}) are controlled by critical orifices.

Consecutive six-hour samples were collected continuously at the three sites during the period from 0100 PST on April 26, 1988 to 1300 PST on April 29, 1988, except for the morning of April 28, when the schedule was altered at Lower Kaweah due to the presence of intercepting clouds. Filters were picked up from Visalia and Ash Mountain between 1100 and 1300 PST daily. Those at Lower Kaweah were retrieved at least twice daily. Retrieved filters were placed individually in covered petri dishes and stored in sealed plastic bags at 4 C until analyzed. The quartz filters were extracted in distilled deionized water (D^2H_2O); the Teflon filters were wetted with ethanol and extracted in D^2H_2O; the nylon filters were extracted in a bicarbonate/carbonate solution. Filter extracts were analyzed by the methods described below for the analysis of cloudwater samples.

Cloudwater samples were collected with two Caltech Active Strand Cloudwater Collectors (CASCC). A complete description of the CASCC (Daube et al., 1987) is given in Chapter 5. One CASCC was co-located at the Lower Kaweah research site with the regular automated cloudwater sampling system (see Chapter 2) and the automated aerosol collector. This CASCC, equipped with a rain-excluding inlet, was powered by a 12 V power supply. The second CASCC was operated using a 12 V deep cycle marine battery, enabling a second sampling

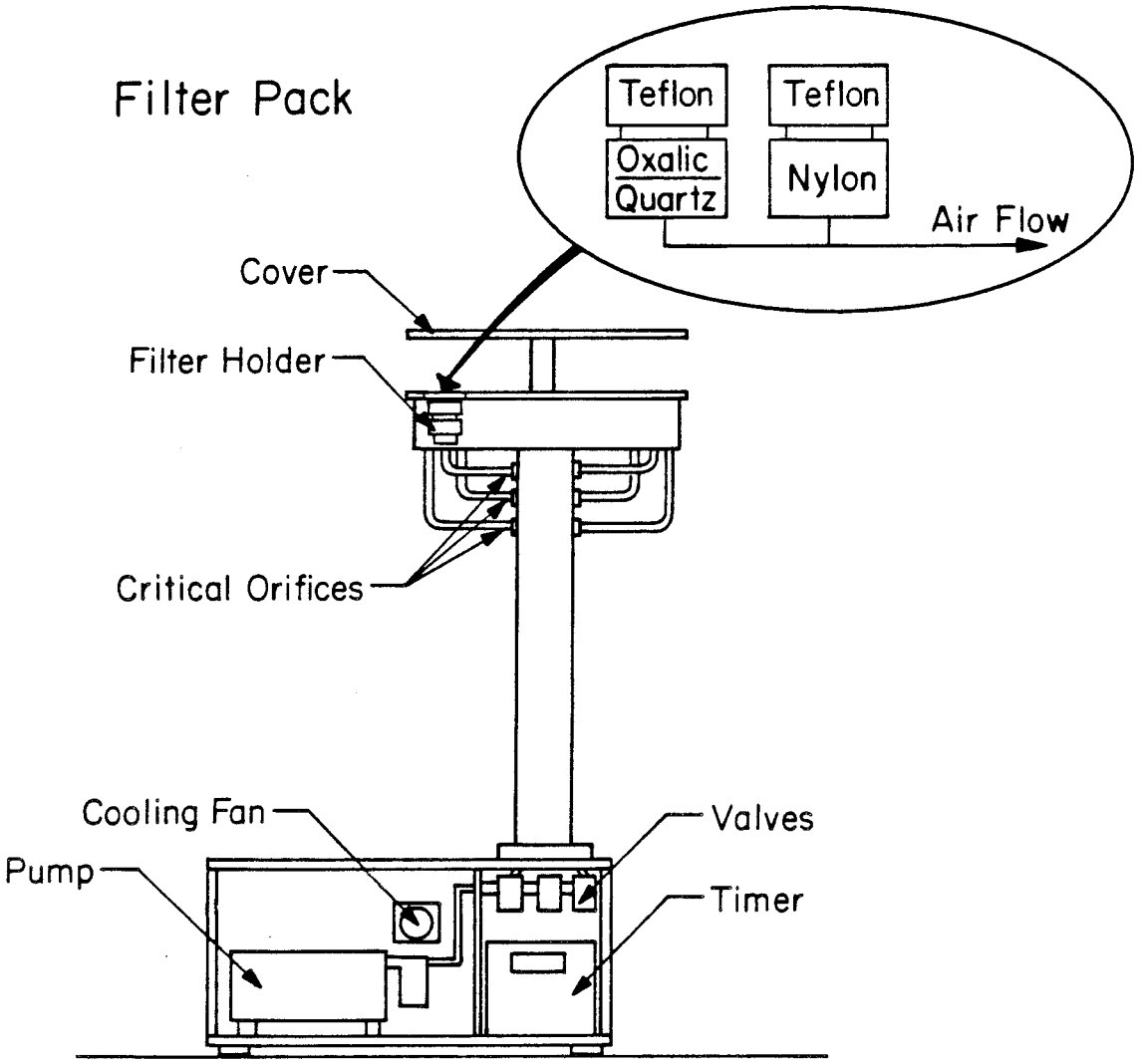

Figure 3.2. The automated aerosol and gas sampler used in the study. Air is sampled using a filter pack method described in the text.

location to be selected during a cloud interception event without power requirement restrictions. The site selected is located at approximately 6450 feet elevation near Moro Rock, 1.5 miles southeast of Lower Kaweah. The second CASCC was operated without a rain–excluding inlet. Samplers at both sites were operated manually. Samples were collected over half–hour intervals.

Cloudwater samples were weighed immediately after collection to determine their volume. An aliquot of each sample was removed to determine sample pH. A Radiometer PHM80 Standard pH meter with a GK2320C semi–micro combination electrode calibrated with pH 4 and 7 buffers was used to measure the pH. Small aliquots of sample also were removed and treated to stabilize reactive species. S(IV) was stabilized as the hydroxymethanesulfonate by adding buffered CH_2O (Dasgupta et al., 1980). CH_2O was reacted with NH_4^+–acetylacetone (Nash, 1953) to form 3,5–dihydro–1,4–dihydrolutidine (DDL), which is stable for several weeks (Reitz, 1980). A buffered solution of p–OH phenylacetic acid (POPA) and peroxidase was used to preserve peroxides (Lazrus et al., 1985) by formation of the dimer. Carboxylic acids were preserved by addition of chloroform (Keene et al., 1984). Carbonyls were derivatized with 2,4–dinitro–phenylhydrazine (DNPH) in acidic solution (Grosjean and Wright, 1983). Samples and aliquots were stored at 4 C until analysis.

The major ions, Cl^-, NO_3^-, and SO_4^{2-}, were measured in our laboratory using a Dionex 2020i ion chromatograph with a Dionex AS–4A column and a 2.8 mM HCO_3^-/ 2.2 mM CO_3^{2-} eluent. Na^+, Ca^{2+}, Mg^{2+}, and K^+ concentrations were measured using a Varian Techtron AA6 atomic absorption spectrophotometer. An air/acetylene flame was used for Na^+ and K^+; N_2O/acetylene was used for Ca^{2+} and Mg^{2+} to minimize interferences. NH_4^+ was measured by the phenol–hypochlorite

method (Solorzano, 1967) using an Alpkem flow injection analyzer.

The stabilized CH_2O was measured by absorption at 412 nm, after addition of I_2 to accelerate the decomposition of sulfonates (Smith and Erhardt, 1975). S(IV) was analyzed by the pararosaniline method (Dasgupta, 1981). This method was adapted for flow injection analysis. Peroxide was measured by the fluorescence of the POPA dimer (Lazrus et al., 1985). This method is sensitive to both H_2O_2 and some organic peroxides; however, the significantly lower Henry's Law coefficients of CH_3OOH and peroxoacetic acid suggest that they will not be found at significant concentrations in cloudwater (Lazrus et al., 1985). Carboxylic acids were measured using ion exclusion chromatography. A Dionex ICE−AS1 column was employed with dilute HCl as the eluent.

The dinitrophenylhydrazone derivatives of carbonyls were extracted three times in 60/40 (v/v) hexane/dichloromethane after adding cyclohexanone 2,4−dinitrophenylhydrazone (Aldrich) as an internal standard. The organic fraction was washed with D^2H_2O to remove excess acid and unreacted DNPH, and then evaporated to dryness under a stream of N_2. The extracted and dried hydrazones were refrigerated until analysis. Previous work has shown that the derivatives are stable during storage (Munger et al., 1989). Immediately before analysis the residue was dissolved in tetrahydrofuran (THF). The derivatized carbonyls were separated by HPLC on a C18 column (Alltech Spherisorb ODS−2), using 45/27.5/27.5 (v/v/v) H_2O/CH_3CN/THF as the mobile phase. Aldehydes and ketones were determined by absorbance at 365 nm; each analysis was repeated at 430 nm to determine the dicarbonyls, which absorb at a higher wavelength. Standards were prepared from carbonyl hydrazones that were previously synthesized and purified.

Results and Discussion

Aerosol and Gases

The dominant species observed in the aerosol at Visalia, Ash Mountain, and Lower Kaweah were NO_3^-, SO_4^{2-}, and NH_4^+ (see Table 3.1). Smaller concentrations of Na^+, K^+, Ca^{2+}, Mg^{2+}, and Cl^- also were observed. No attempt was made to measure organic aerosol in this study. By comparing the ratio of NH_4^+ to the sum of NO_3^- and SO_4^{2-}, the relative neutrality of the aerosol, with respect to the dominant species, may be examined. The results of this calculation, presented in Figure 3.3, indicate that the aerosol at all three sampling locations was essentially neutral during the period studied.

Figure 3.4 presents the results for a similar acid–base balance that has been expanded to include gas phase concentrations of NH_3 and HNO_3. When these gas phase concentrations are included, the air mass at Visalia is seen to be consistently basic, due to large inputs of NH_3. Excess acid neutralizing capacity at Visalia, in the form of NH_3, has been observed in past investigations (Jacob et al., 1986); during the same study, fogwater formed in the region was found to consistently have a very high pH (range: 5.5–7.2), due to the high NH_3 inputs. The high density of cattle feed lots surrounding Visalia (see Figure 3.5) are most likely the predominant source of NH_3 for the region. The air masses sampled at both Ash Mountain and Lower Kaweah were found to be considerably less basic than those observed at Visalia during the study period. However, samples from both sites were observed to be somewhat basic, with those from Ash Mountain more basic than Lower Kaweah samples.

Table 3.1. Aerosol and Gas Composition

Date	Time	Na^+	NH_4^+	Ca^{2+}	Mg^{2+}	Cl^-	NO_3^-	SO_4^{2-}	NH_3	HNO_3
		←			neq m^{-3}			→	← nmole m^{-3}	→
LOWER KAWEAH										
4/26	0100–0700	0.0	18.0	9.8	3.0	0.8	5.1	13.4	42.8	4.1
4/26	0700–1300	0.0	12.7	7.1	4.5	0.0	5.4	10.3	22.2	0.0
4/26	1300–1900	0.0	35.3	8.5	3.0	0.0	11.2	30.6	66.5	17.1
4/27	0100–0700	0.0	30.7	16.1	4.5	0.5	9.1	26.2	10.7	2.2
4/27	0700–1300	0.0	24.4	6.9	3.0	0.0	8.6	12.3	43.3	9.1
4/27	1300–1900	0.0	73.7	6.4	3.6	0.0	32.0	35.8	61.1	17.0
4/27	1900–0100	0.0	66.5	7.8	4.5	0.5	16.8	47.8	18.9	4.6
4/28	0100–0700	0.0	70.5	6.4	2.1	0.0	21.2	50.4	8.6	2.1
4/28	0700–1130	1.5	98.1	8.6	3.9	0.3	54.4	40.5	37.9	3.4
4/28	1530–1900	0.0	166.3	6.2	3.5	3.3	88.4	78.9	15.7	1.1
4/28	1900–0100	0.0	93.8	9.1	4.1	0.0	36.3	44.2	12.2	1.0
4/29	0100–0700	0.0	39.3	7.8	3.0	0.0	9.0	32.9	6.3	0.3
4/29	0700–1300	0.3	101.6	7.7	4.5	0.0	38.8	64.0	21.2	3.5
ASH MOUNTAIN										
4/26	0100–0700	0.0	51.6	4.2	4.5	0.0	6.6	18.8	67.3	1.7
4/26	0700–1300	0.0	47.2	13.2	4.0	0.8	12.2	38.6	159.3	23.7
4/26	1300–1900	0.0	103.5	11.8	5.5	0.0	30.3	72.0	320.9	37.2
4/26	1900–0100	0.0	63.3	8.5	2.4	0.0	9.5	52.2	115.9	13.2
4/27	0100–0700	0.0	40.1	12.6	3.5	0.0	8.6	30.3	48.5	6.0
4/27	0700–1300	0.0	37.2	11.2	2.1	0.0	9.3	23.7	95.3	22.5
4/27	1300–1900	0.0	88.7	13.2	5.5	8.2	21.3	61.2	266.1	67.9
4/27	1900–0100	0.0	64.6	12.0	5.5	8.4	20.3	47.8	132.1	12.5
4/28	0100–0700	0.0	64.6	9.9	5.5	1.0	17.5	49.9	59.8	5.4
4/28	0700–1300	10.7	126.1	12.6	9.1	12.0	76.8	69.2	112.3	14.4
4/28	1300–1900	20.0	194.5	16.7	9.1	0.0	109.6	108.8	76.5	37.3
4/28	1900–0100	6.6	141.5	5.7	5.5	0.0	41.8	101.6	45.9	9.4
4/29	0100–0700	0.0	98.1	5.0	4.5	14.0	21.6	83.3	39.0	6.2
4/29	0700–1300	1.9	100.8	6.8	4.5	0.0	28.4	88.7	109.4	39.1
VISALIA										
4/26	0100–0700	0.0	293.0	28.5	8.1	4.8	124.9	100.1	685.6	7.8
4/26	0700–1300	2.8	335.3	34.9	9.6	2.4	246.3	101.1	934.8	47.6
4/26	1300–1900	0.0	163.1	24.4	6.6	0.0	80.9	76.4	940.2	135.2
4/26	1900–0100	0.0	229.2	56.8	12.1	3.2	125.0	91.3	1200.5	19.9
4/27	0100–0700	0.0	181.3	46.4	7.6	0.6	69.2	86.4	527.4	12.9
4/27	0700–1300	0.0	318.4	59.5	11.6	0.0	212.2	121.7	863.8	101.5
4/27	1300–1900	1.2	152.5	33.3	9.1	0.5	63.9	87.2	840.4	157.4
4/27	1900–0100	22.2	96.1	38.1	13.1	4.8	58.1	72.3	916.8	13.5
4/28	0100–0700	19.9	186.0	25.7	15.0	6.7	85.0	87.7	839.9	5.9
4/28	0700–1300	21.2	233.0	43.6	12.6	10.7	178.1	79.0	549.0	26.5
4/28	1300–1900	15.8	175.0	33.3	11.1	0.1	98.5	97.7	398.8	106.9
4/28	1900–0100	15.2	294.2	34.7	13.1	5.0	192.5	116.3	500.4	27.6
4/29	0100–0700	9.3	256.8	22.4	10.0	3.3	131.9	89.2	605.1	8.1
4/29	0700–1300	7.1	183.3	65.1	12.6	2.1	149.8	78.4	670.4	86.0

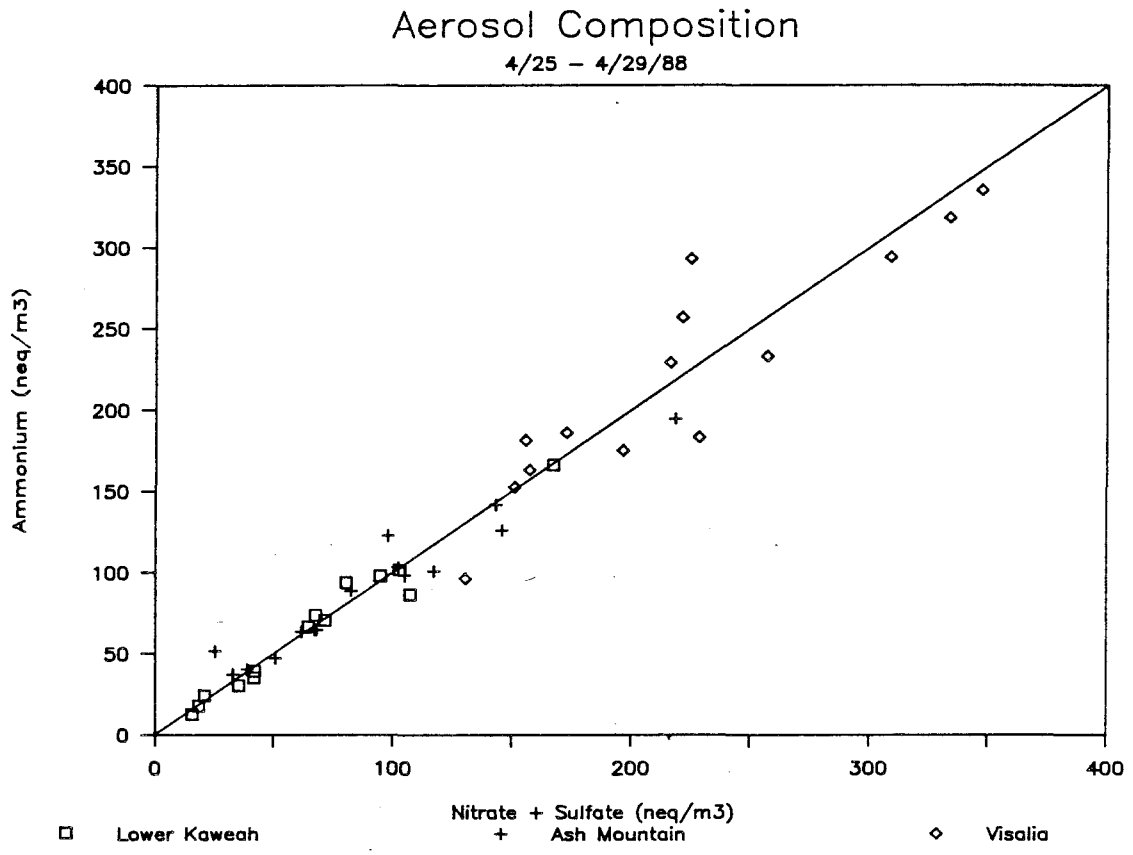

Figure 3.3. Balance of ammonium with nitrate and sulfate (all in neq m^{-3}) in aerosol samples collected at Visalia, Ash Mountain, and Lower Kaweah between April 25 and April 29, 1988.

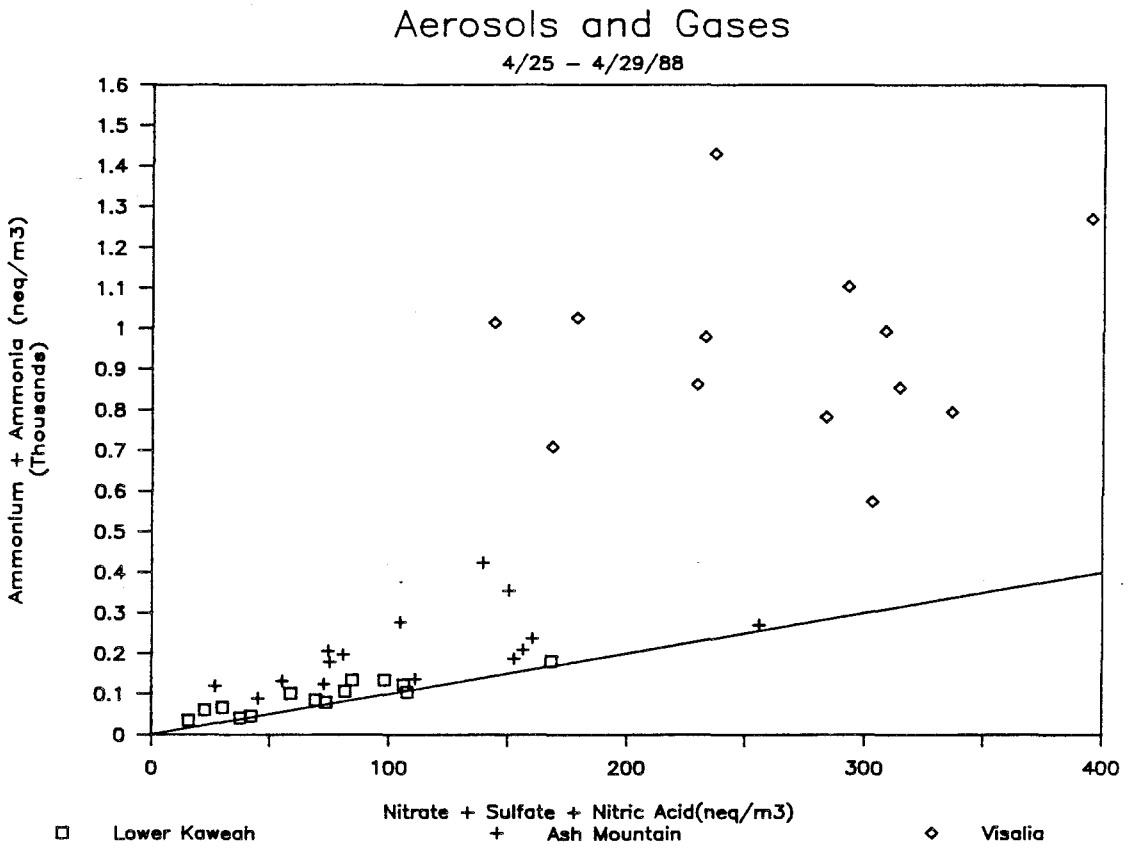

Figure 3.4. Balance of ammonium (neq m^{-3}) plus ammonia (nmole m^{-3}) with nitrate (neq m^{-3}), sulfate (neq m^{-3}), and nitric acid (nmole m^{-3}) in aerosol and gas samples collected at Visalia, Ash Mountain, and Lower Kaweah between April 25 and April 29, 1988.

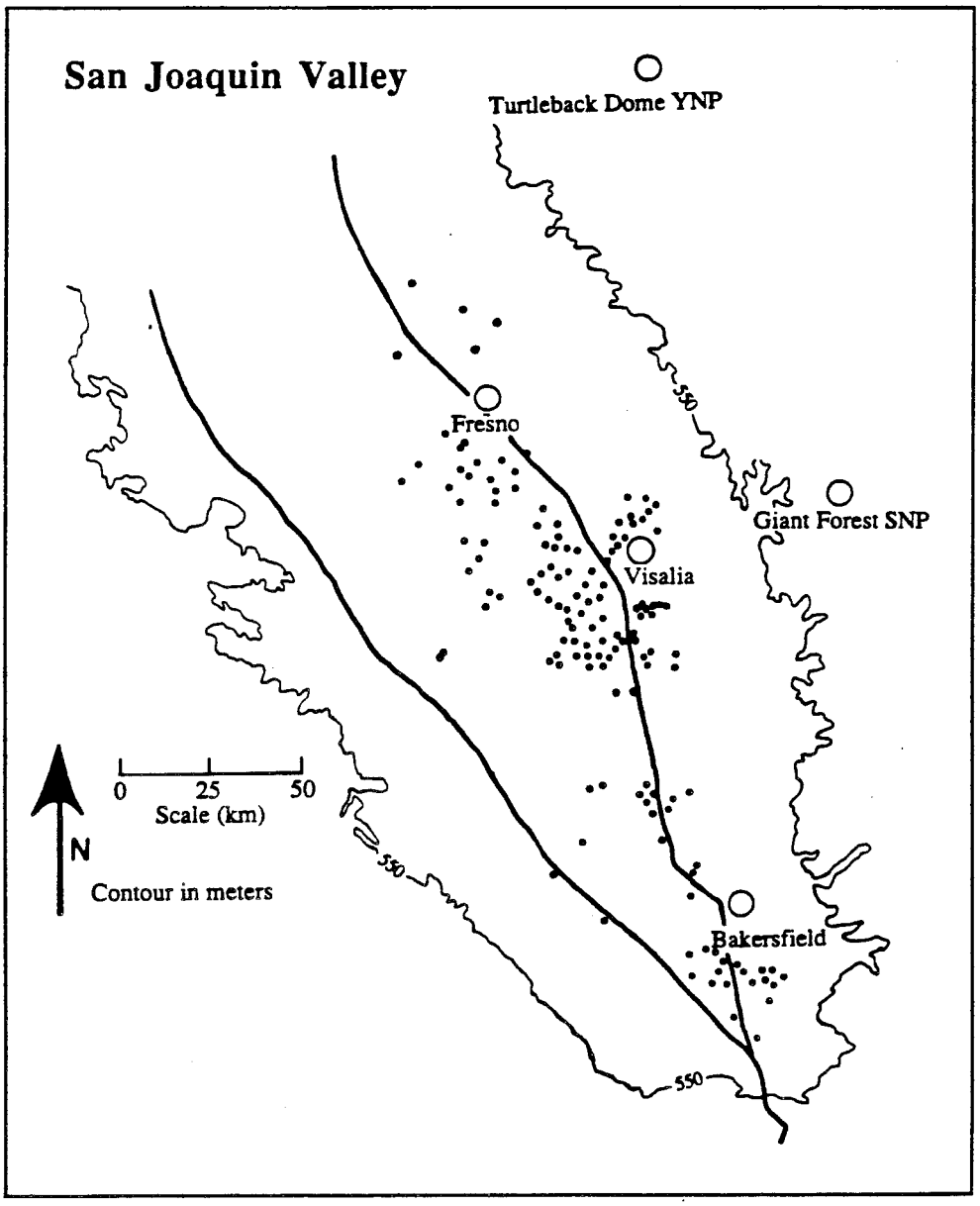

Figure 3.5. Map of the San Joaquin Valley illustrating some of the major ammonia emissions sources for the region. The black circles represent confined feeding operations.

Excess base in samples collected at Visalia exceeded excess base in samples at Ash Mountain on both an absolute basis and a relative basis (see Figure 3.6). The same is true of the comparison between Ash Mountain and Lower Kaweah, for those samples collected during the first two–thirds of the study period. The samples collected after sunrise on April 28, however, had essentially equivalent ratios of base to acid. The difference in base/acid ratios between sampling locations is one indication that the air mass observed at the upper site, in each comparison, is not simply a diluted version of the air mass observed at the lower site. Either some other change is taking place as air is transported from Visalia to Ash Mountain to Lower Kaweah on the upslope breezes (e.g., preferential deposition of gas phase NH_3, or gas phase production of SO_4^{2-} or NO_3^-), or the air masses sampled at the upper two sites have at least some contribution from other source regions.

Examination of the ratio of N(V) to S(VI) also indicates that a simple dilution of air from the Visalia area, as it is transported in the upslope flow, does not account for the air mass compositions observed at the upper two sites (see Figure 3.7). The N(V)/S(VI) ratio was calculated as the sum of gas phase HNO_3 (nmole m^{-3}) and aerosol NO_3^- (neq m^{-3}), divided by aerosol SO_4^{2-} (neq m^{-3}). The measured ratios at Ash Mountain and Lower Kaweah were quite similar during most of the sampling periods, typically hovering around one–half during the night and morning hours, when downslope winds predominate. During the daylight hours, the ratio often was observed to lie closer to one. The N(V)/S(VI) ratio at Visalia, meanwhile, was never observed to fall significantly below one and was often found to approach three. The observations at Visalia, like those at the other two sites, also indicated that the ratio shifted toward a predominance of N(V) during the daytime hours.

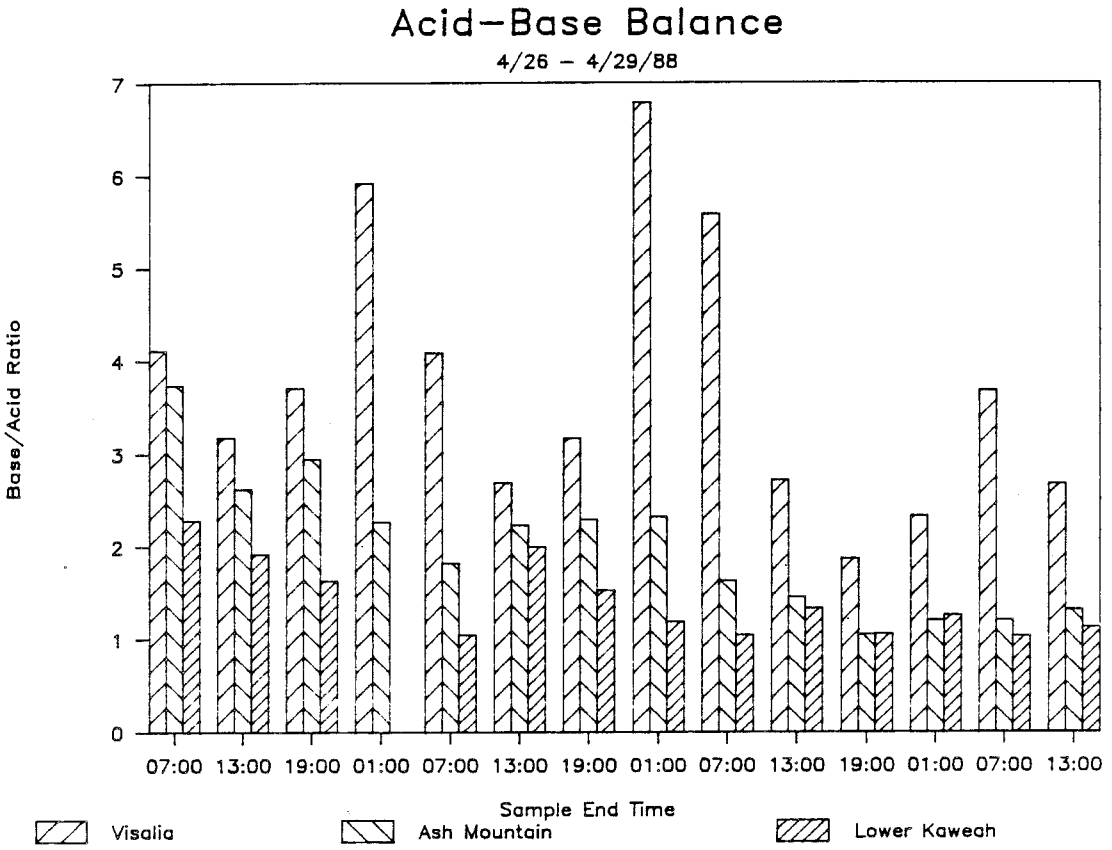

Figure 3.6. Acid–base balance as a function of time in the air masses sampled at Visalia, Ash Mountain, and Lower Kaweah between April 26 and April 29, 1988. Species included are nitrate, nitric acid, sulfate, ammonium, and ammonia. Nitrate, sulfate, and ammonium contributions were calculated as neq m^{-3}; ammonia and nitric acid contributions were calculated as nmole m^{-3}.

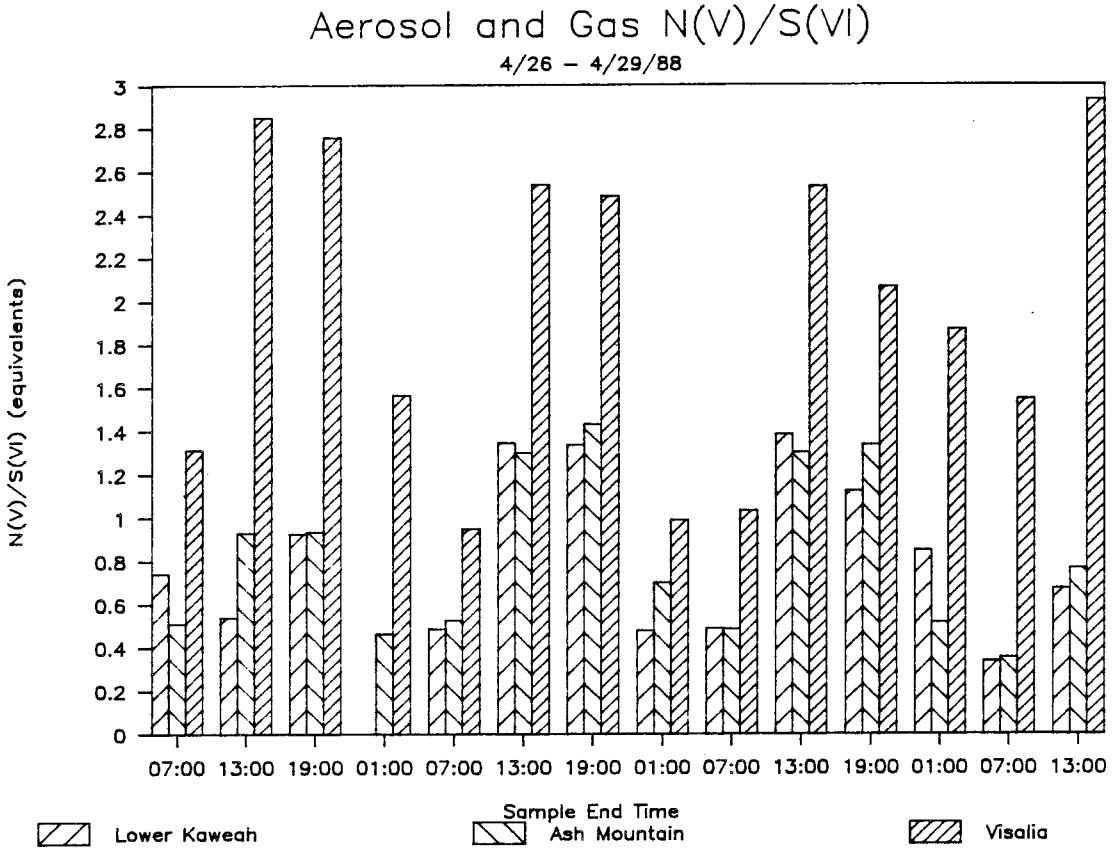

Figure 3.7. Ratios of N(V) to S(VI) in the air masses sampled at Visalia, Ash Mountain, and Lower Kaweah between April 26 and April 29, 1988. Species included are nitrate, nitric acid, and sulfate. Nitrate and sulfate contributions were calculated as neq m^{-3}; nitric acid contributions were calculated as nmole m^{-3}.

Surface winds at Visalia typically blew out of the northwest during the daytime and out of the southeast at night, throughout the study period (see Figure 3.8). Southerly winds have been observed at night on numerous occasions along the eastern edge of the San Joaquin Valley (Smith et al., 1981) and are believed to be the result of terrain-blocking of the predominant northwesterly flow at the valley's southern boundary. Increased vertical stability at night prevents the flow from exiting over the Tehachapi Mountains and forces it to return northward along the eastern valley boundary, establishing what has come to be known as the Fresno eddy. Since large emissions of SO_2 occur in the southern San Joaquin Valley due to extensive oil field activity, a shift to southerly winds at night might be expected to result in an enrichment of SO_4^{2-} in night time aerosol at locations farther north, including Visalia. Concentrations of aerosol SO_4^{2-} at Visalia, however, were observed to be relatively constant over the study period (see Figure 3.9) and exhibited no strong correlation with either wind direction or time of day.

The changes in the ratio of N(V) to S(VI) at Visalia are actually the result of daytime increases in both aerosol NO_3^- concentrations and HNO_3 concentrations. Concentrations of these species are depicted in Figure 3.10. These increases are most likely due to photochemical oxidation of NO_x emitted from morning traffic, both locally and in the larger cities located to the north.

An examination of the concentration vs. time profiles for the major aerosol species measured at Lower Kaweah reveals a substantial increase in concentrations on April 28, compared to the levels seen during the preceding two days. This is illustrated in Figures 3.11 through 3.13 for NO_3^-, SO_4^{2-}, and NH_4^+. A similar pattern is apparent in the concentration profiles of these three species at Ash Mountain as well. Perhaps most notable is that concentrations of NO_3^-, SO_4^{2-}, and NH_4^+ in the

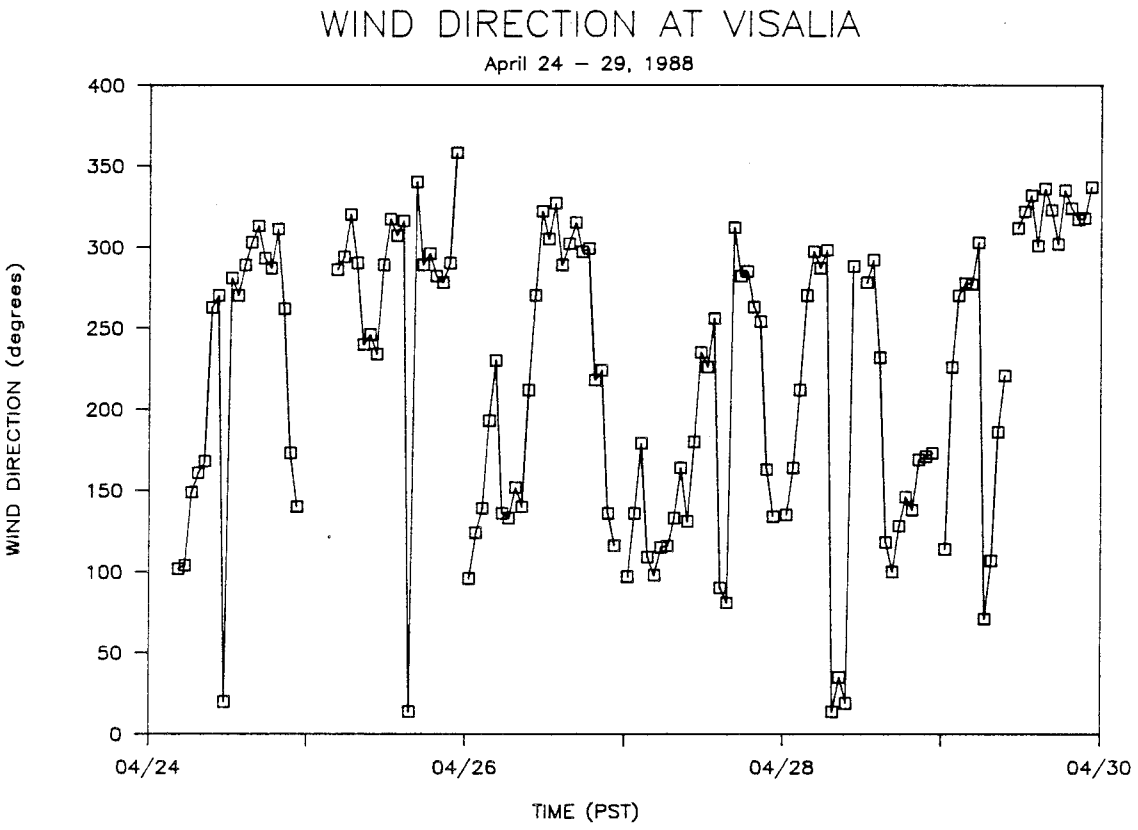

Figure 3.8. Half–hour averages of wind direction at Visalia between April 24 and April 30, 1988. Breaks in the line indicate missing data.

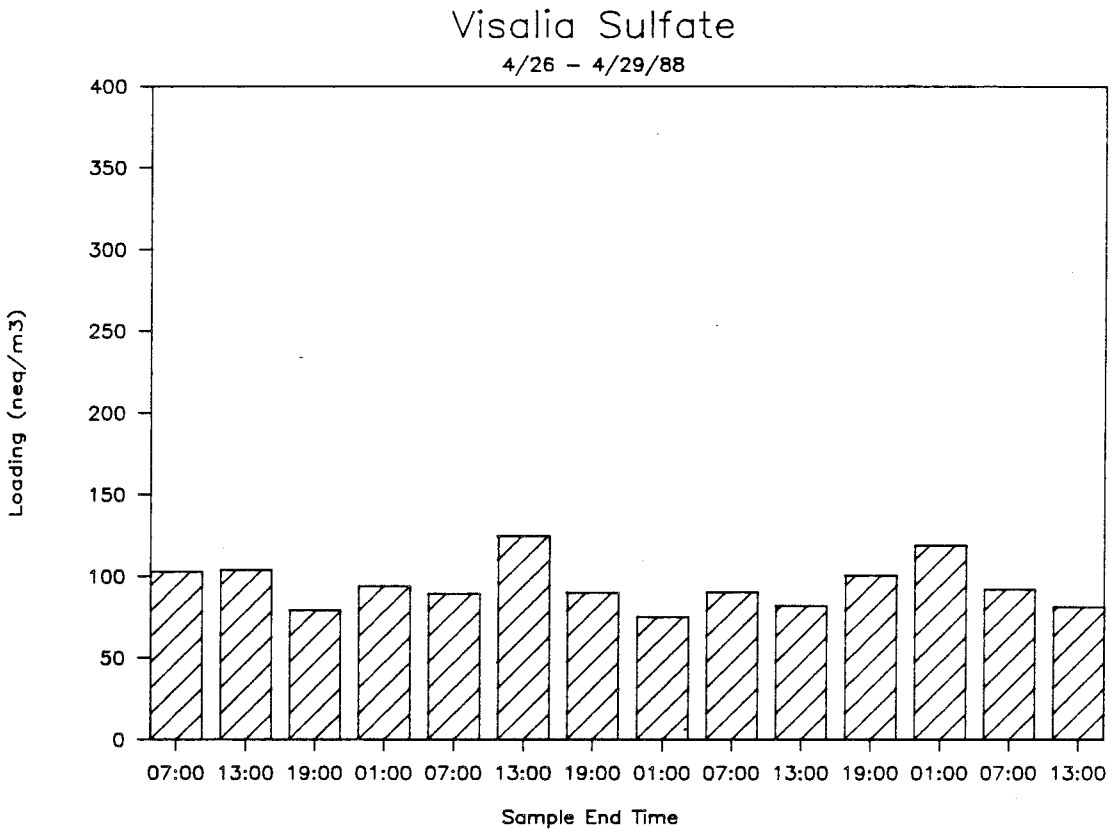

Figure 3.9. Aerosol loading of sulfate at Visalia between April 26 and April 29, 1988.

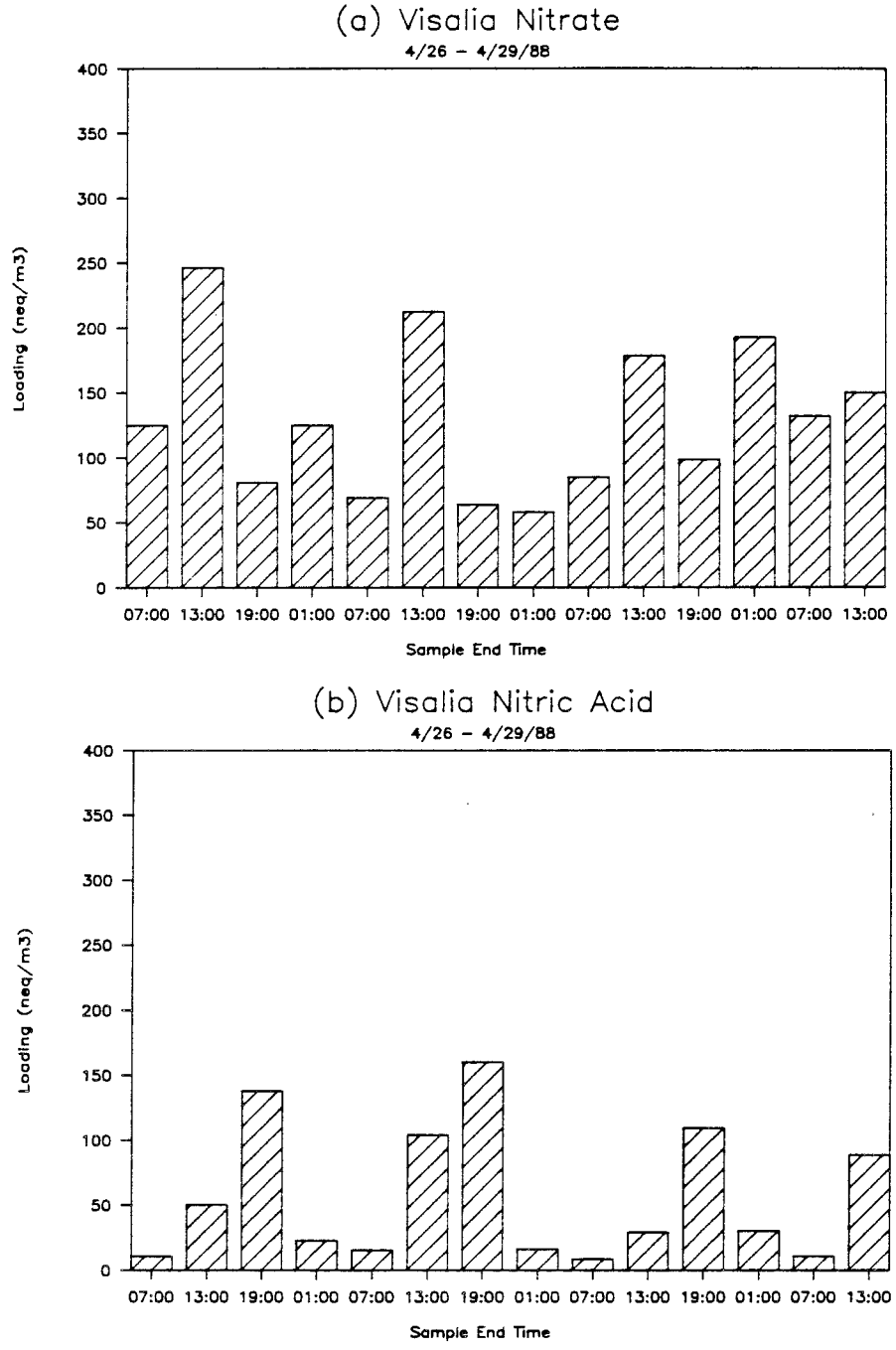

Figure 3.10. (a) Aerosol loading of nitrate at Visalia between April 26 and April 29, 1988. (b) Gas phase loading of nitric acid at Visalia between April 26 and April 29, 1988.

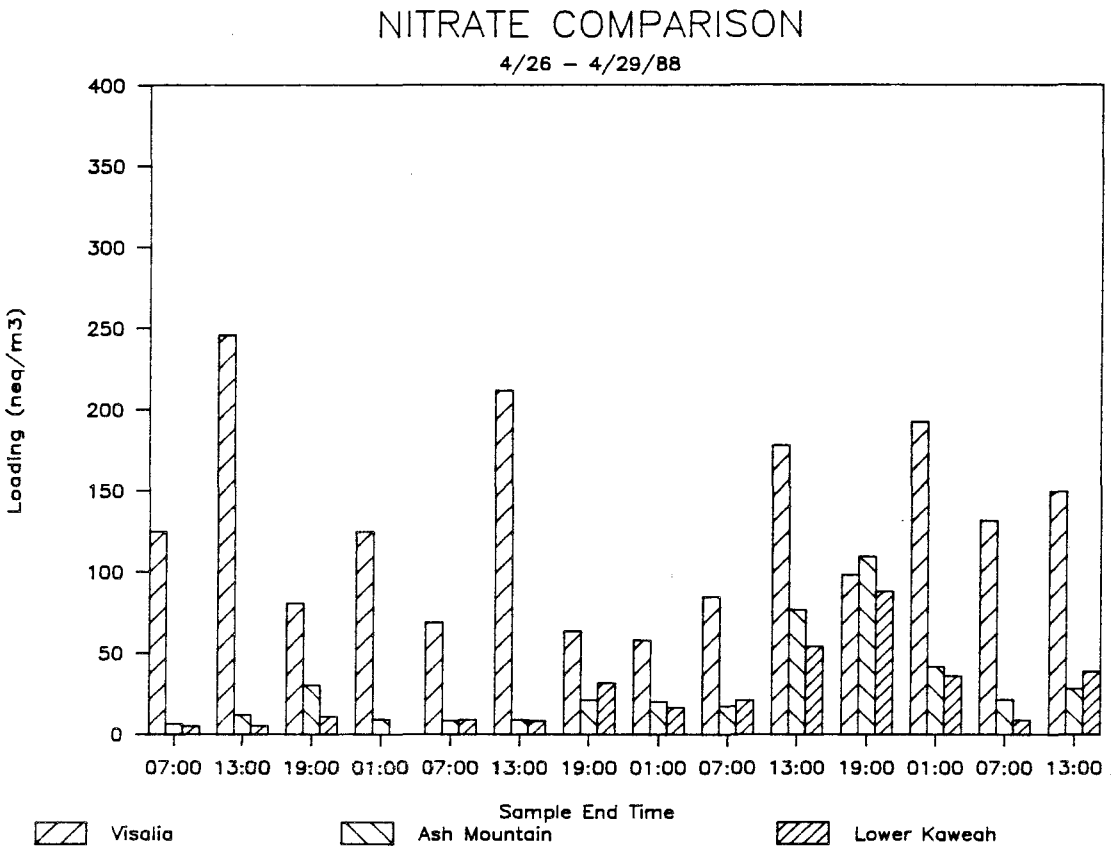

Figure 3.11. Comparison of aerosol nitrate loadings at Visalia, Ash Mountain, and Lower Kaweah between April 26 and April 29, 1988.

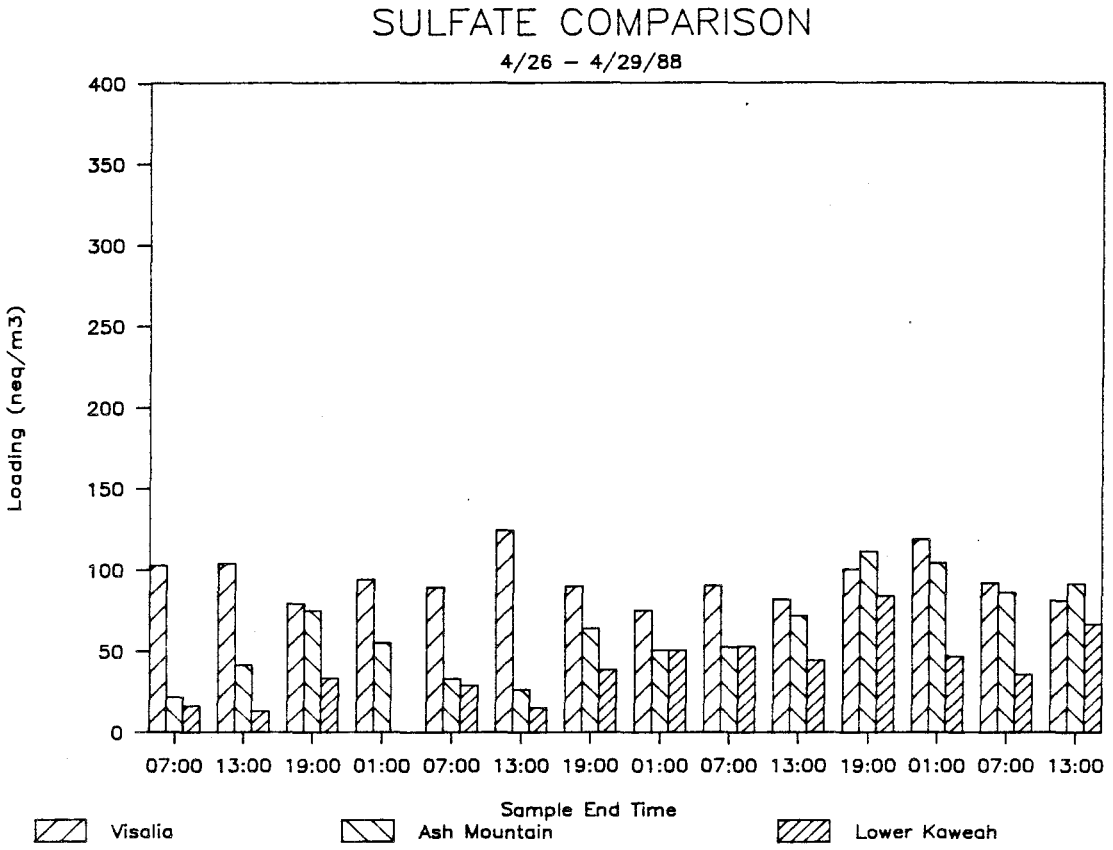

Figure 3.12. Comparison of aerosol sulfate loadings at Visalia, Ash Mountain, and Lower Kaweah between April 26 and April 29, 1988.

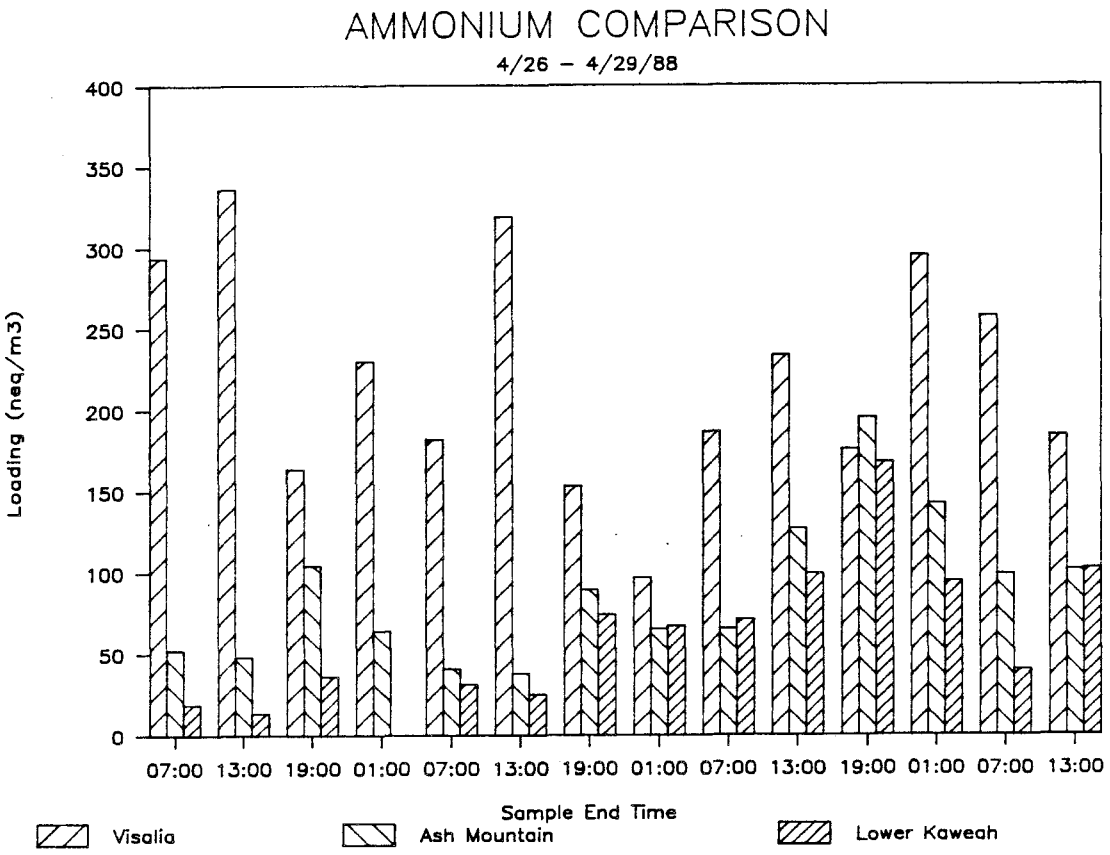

Figure 3.13. Comparison of aerosol ammonium loadings at Visalia, Ash Mountain, and Lower Kaweah between April 26 and April 29, 1988.

aerosol were consistently higher at Visalia than at the other two sites, until the afternoon of April 28. During that sampling period, concentrations of all three species essentially were equivalent at the three locations, possibly indicating that the air mass over the valley had become well mixed up to at least 6,000 feet.

At 1000 PDT on the morning of April 28, clouds were sighted below Lower Kaweah with an upper boundary of approximately 4,500 feet. These clouds, associated with the approach of a slow–moving cold front, gradually rose over the next few hours, enveloping the two cloudwater sampling locations. The approach of the frontal system appeared to increase mixing in the atmosphere above the valley floor. Vertical temperature profiles measured in the atmosphere over both Bakersfield and Fresno (Figure 3.14) indicated a substantial reduction in early morning stability on April 28, relative to the previous two days. These observations are consistent with the hypothesis that a decrease in atmospheric stability over the valley enabled pollutants, previously trapped near the valley floor, to mix up to higher elevations, consequently increasing pollutant loadings observed at both Ash Mountain and Lower Kaweah.

Gas phase concentrations of both NH_3 and HNO_3 at Lower Kaweah and Ash Mountain on the afternoon of April 28, however, were much lower than those observed at Visalia (see Figures 3.15 and 3.16). In fact, unlike the aerosol concentrations, they did not increase substantially above peak afternoon levels observed earlier in the week. This is not sufficient evidence, however, to conclude that these species were not mixed from the valley floor up to Lower Kaweah. Gas phase concentrations of both species are controlled by equilibrium with an aerosol phase. The equilibrium strongly depends on temperature and relative humidity. The high temperature observed on April 28 in Visalia was 27 C (NOAA, 1988a),

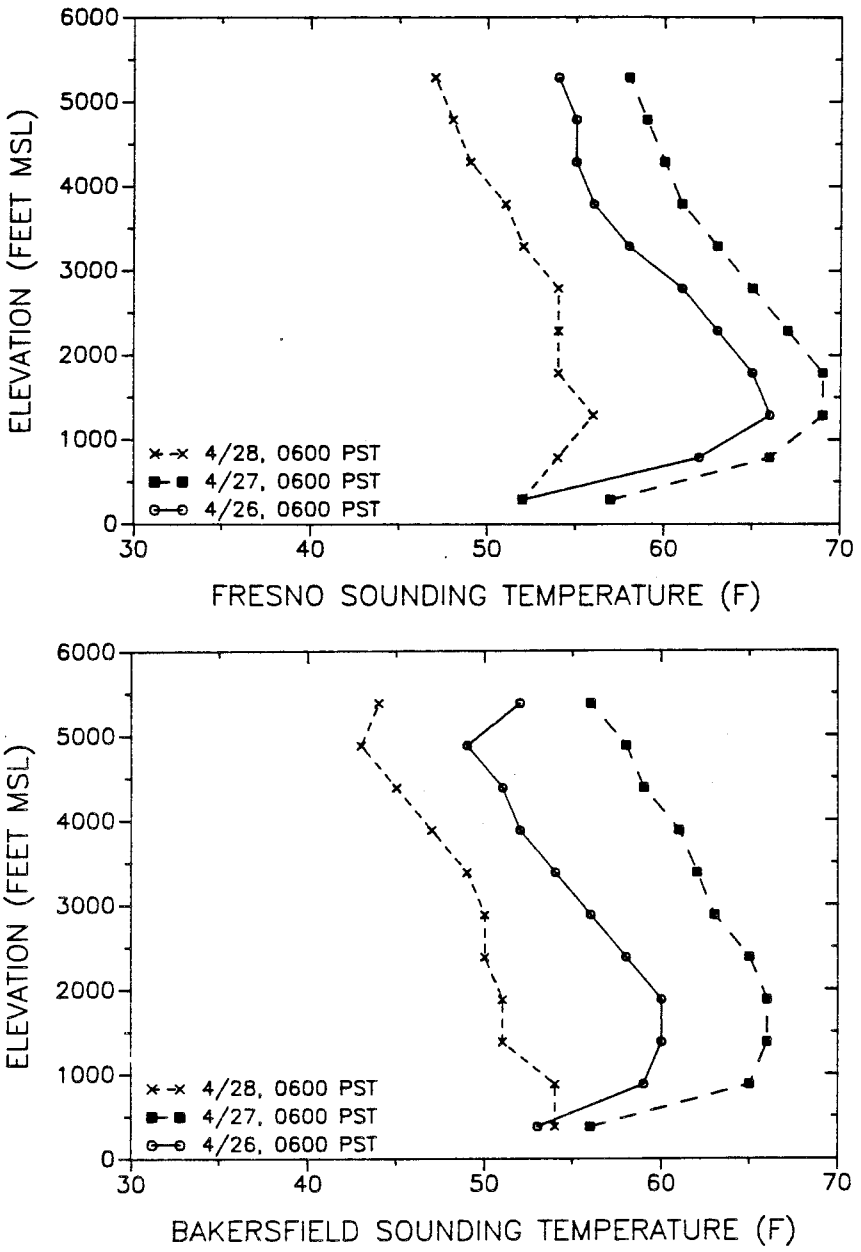

Figure 3.14. Vertical temperature profiles measured at Fresno and Bakersfield at 0600 PST on the mornings of April 26, 27, and 28, 1988.

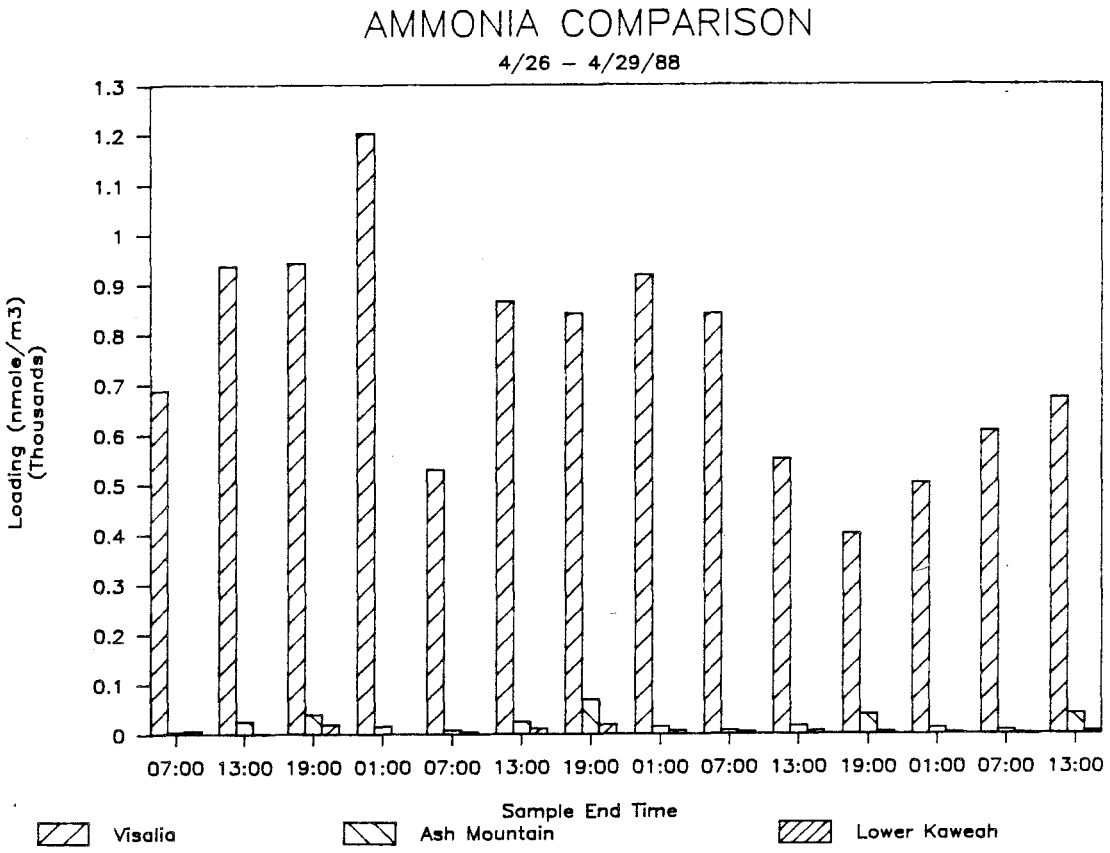

Figure 3.15. Comparison of gas phase ammonia loadings at Visalia, Ash Mountain, and Lower Kaweah between April 26 and April 29, 1988.

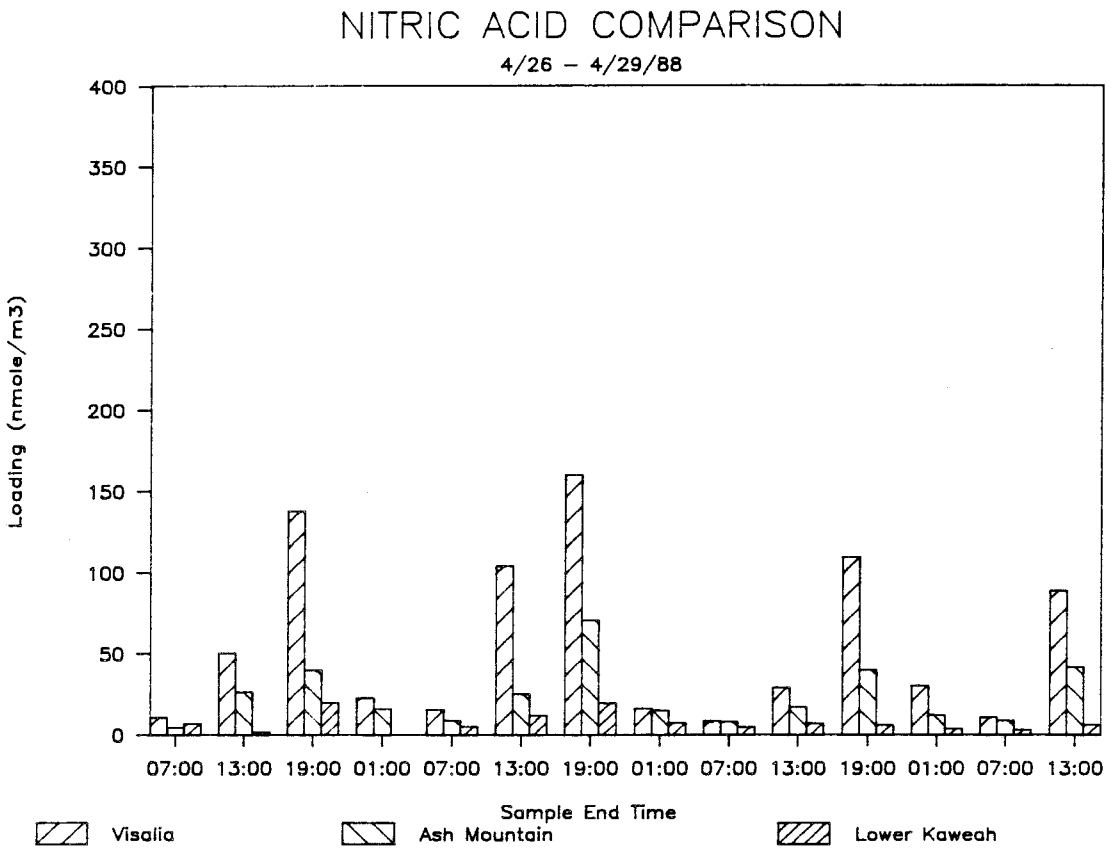

Figure 3.16. Comparison of gas phase nitric acid loadings at Visalia, Ash Mountain, and Lower Kaweah between April 26 and April 29, 1988.

and relative humidities along the length of the valley ranged from 45 to 55% during the afternoon and early evening (NOAA, 1988b, c). Based on these observations, along with the aerosol and gas phase data from Visalia, equilibrium predictions for the H_2SO_4–NH_3–HNO_3 system indicate that 72% of the NH_3 and 58% of the HNO_3 should have resided in the gas phase (Pilinis and Seinfeld, 1987). The observations indicated 70% and 53%, respectively, resided in the gas phase – in good agreement with the equilibrium predictions. At Lower Kaweah afternoon temperatures were approximately 5 C; relative humidities exceeded the deliquescence point of NH_4NO_3 ($\simeq$ 74% at 278 K; Seinfeld, 1986) throughout the afternoon. Equilibrium calculations, utilizing these conditions and the observed aerosol and gas phase concentrations at the site, predict that 11% of the NH_3 and 6% of the HNO_3 should reside in the gas phase. The observations are once again in good agreement with these predictions: 11% NH_3 and 7% HNO_3. The large differences in NH_3 and HNO_3 concentrations between Visalia and Lower Kaweah are not surprising in view of these circumstances.

Variations in the HNO_3–NH_3 system aerosol–gas partition coefficients, as a function of temperature and relative humidity, imply that intersite comparisons of gas phase concentrations of NH_3 and HNO_3, or aerosol concentrations of NH_4^+ and NO_3^-, are not very meaningful under conditions experienced in this study. Given the large differences in temperature and relative humidity between the sampling locations, it is better to compare total concentrations of N(–III), given by the sum of NH_3 and NH_4^+, and N(V), given by the sum of HNO_3 and NO_3^-. Figure 3.17 illustrates the concentration vs. time profiles of N(V) for the three sites. While N(V) concentrations are seen to peak on the afternoon of April 28, as was observed for NO_3^- aerosol concentrations, differences in concentrations are maintained between the three sites. N(–III) concentrations at Lower Kaweah also are observed

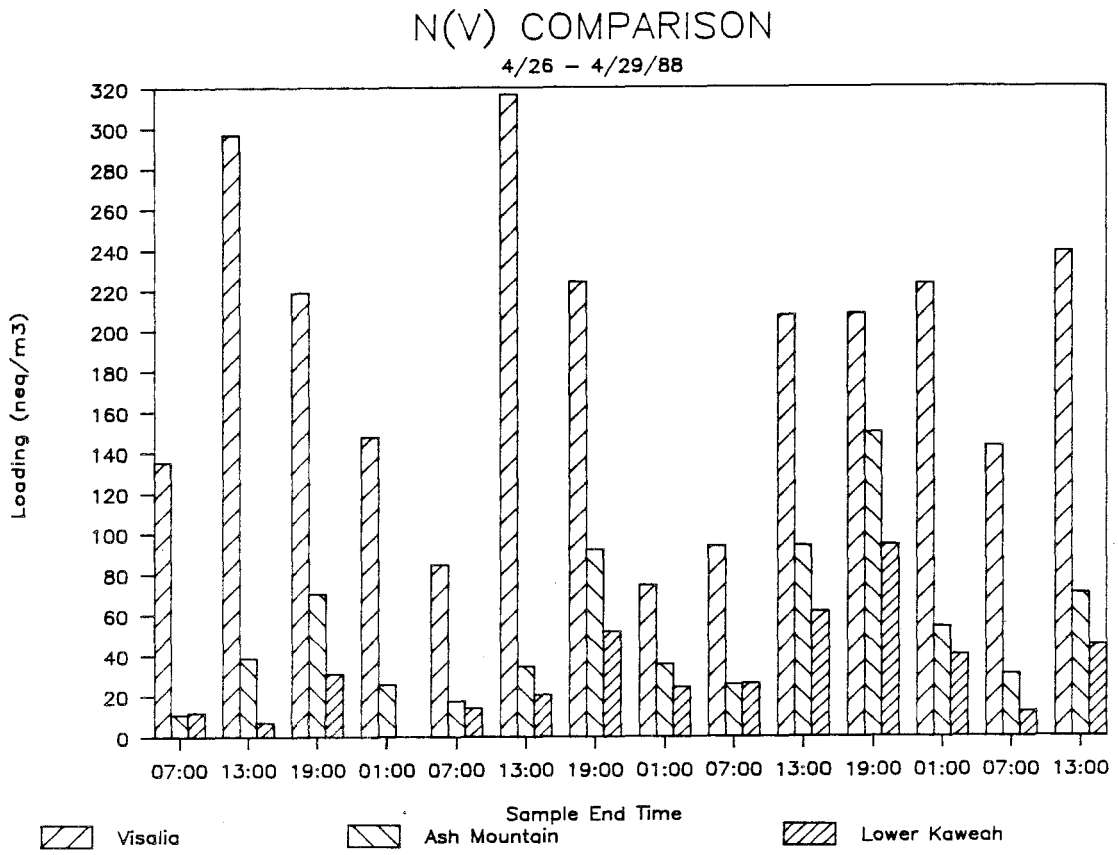

Figure 3.17. Comparison of total N(V) loadings in the air masses sampled at Visalia, Ash Mountain, and Lower Kaweah between April 26 and April 29, 1988. N(V) includes aerosol nitrate (neq m^{-3}) and gas phase nitric acid (nmole m^{-3}).

to peak during the same period (see Figure 3.18), although the increase above levels seen earlier in the week is not as great as was observed in the case of N(V). Similar to N(V) concentrations, N(–III) concentrations maintain an elevational gradient, with Visalia exhibiting the highest concentrations. Concentration differences between the three sites, however, are significantly reduced for both N(V) and N(–III) on the afternoon of April 28.

While the vertical N(V) and N(–III) concentration profiles indicate that the air over the valley was not well–mixed to 6,000 feet, the observed decrease in atmospheric stability on April 28 still may have contributed significantly to the rise in pollutant levels observed both at Ash Mountain and Lower Kaweah. Both the velocity of the upslope flow, and the flow depth, have been found to increase with distance upward along the slope (Smith et al., 1981). These increases were attributed to contributions of heat and buoyancy by the sunlit slope to the flow. Increasing depth and velocity increase the total flux in the upslope flow, requiring entrainment of additional air from above the valley floor. Since the air in higher elevation layers is generally cleaner than air near the valley floor, the concentration of pollutants within the slope flow should decrease with elevation. A decrease in vertical stability above the valley floor, which allows pollutants previously trapped near the surface to mix up to higher elevations, will increase the concentrations of pollutants in the "dilution" air, preventing pollutant concentration levels in the upslope flow from decreasing as rapidly.

It is important to examine the behavior of wind patterns in the valley during this period to evaluate their potential for influencing pollutant levels at Lower Kaweah. Winds at Lower Kaweah typically follow a very predictable pattern (upslope flow during the day, downslope flow at night), driven by slope heating

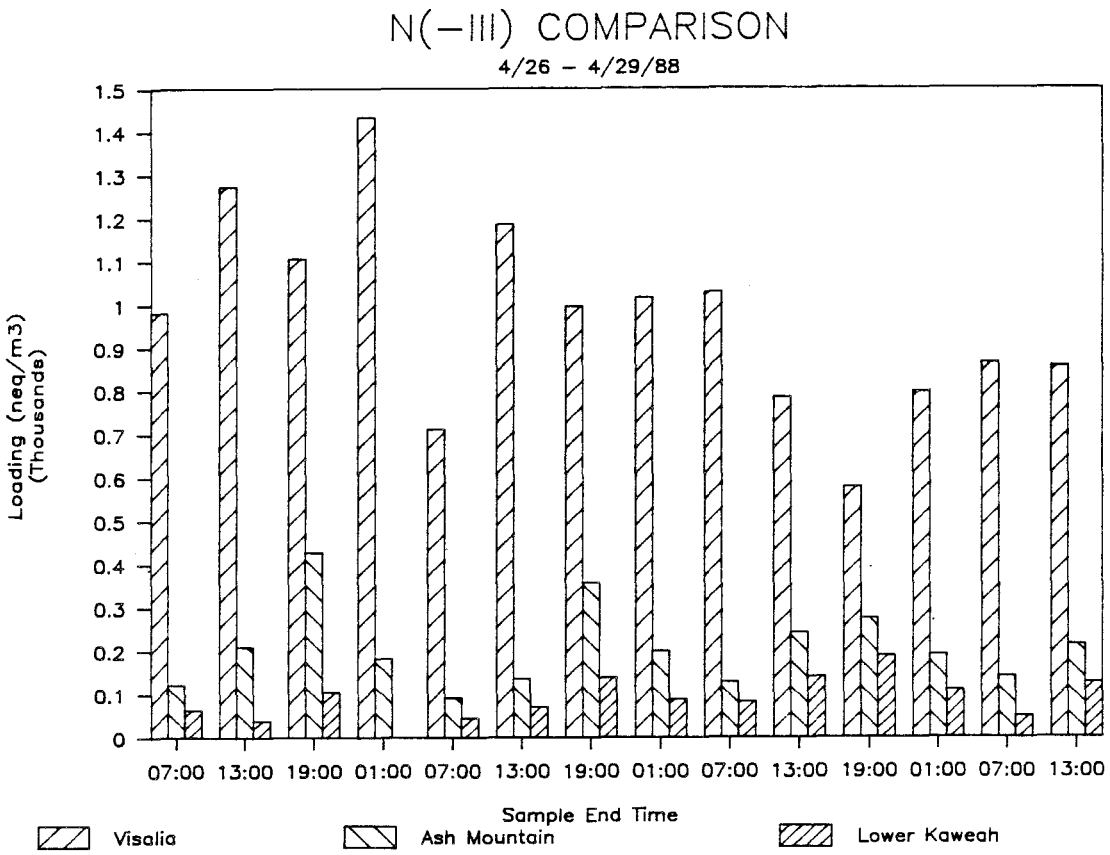

Figure 3.18. Comparison of total N(–III) loadings in the air masses sampled at Visalia, Ash Mountain, and Lower Kaweah between April 26 and April 29, 1988. N(–III) includes aerosol ammonium (neq m^{-3}) and gas phase ammonia (nmole m^{-3}).

effects. On at least one occasion, a break in this pattern has been observed, leading to continued upslope flow, even at night. This breakdown was observed in association with the passage of a strong frontal system. Disruption of the upslope–downslope flow pattern could account for increased pollutant loadings at elevated sites, particularly during the night and early morning, as was observed in past work (Collett et al., 1989). During this study, however, no significant breakdown was observed in the diurnal upslope–downslope flow pattern (see Figure 3.19). In fact, a slight decrease in the velocity of the daytime upslope flow was observed at Lower Kaweah, probably due to reduced solar heating of the slopes in the presence of cloud cover.

As indicated previously, increases in fine particle sulfur concentrations at Lower Kaweah have been observed in conjunction with the approach of a cold front (Cahill et al., 1986). The increase, observed at night during downslope flow conditions, was attributed to generation of southerly winds by the frontal system. In the current study, an increase in aerosol SO_4^{2-} was observed as the cold front approached. In this case, however, the April 28 rise in SO_4^{2-} concentrations was observed predominantly during upslope flow. Surface level winds at Visalia (Figure 3.8) blew from the south for a relatively short period of time on the morning of April 28. A much more extended southerly surface flow pattern was observed the previous morning. Vertical wind profiles measured in the atmosphere above Fresno on the mornings of April 26, 27, and 28 are depicted in Figure 3.20. These data also indicate that southerly flow was much more predominant at most elevations on April 27 than on April 28. Despite these observations, concentrations of SO_4^{2-} measured at Lower Kaweah were higher on April 28 than on April 27. This suggests that the increase in aerosol SO_4^{2-} observed in this study is not attributable predominantly to increased southerly flow from Bakersfield and the southern San

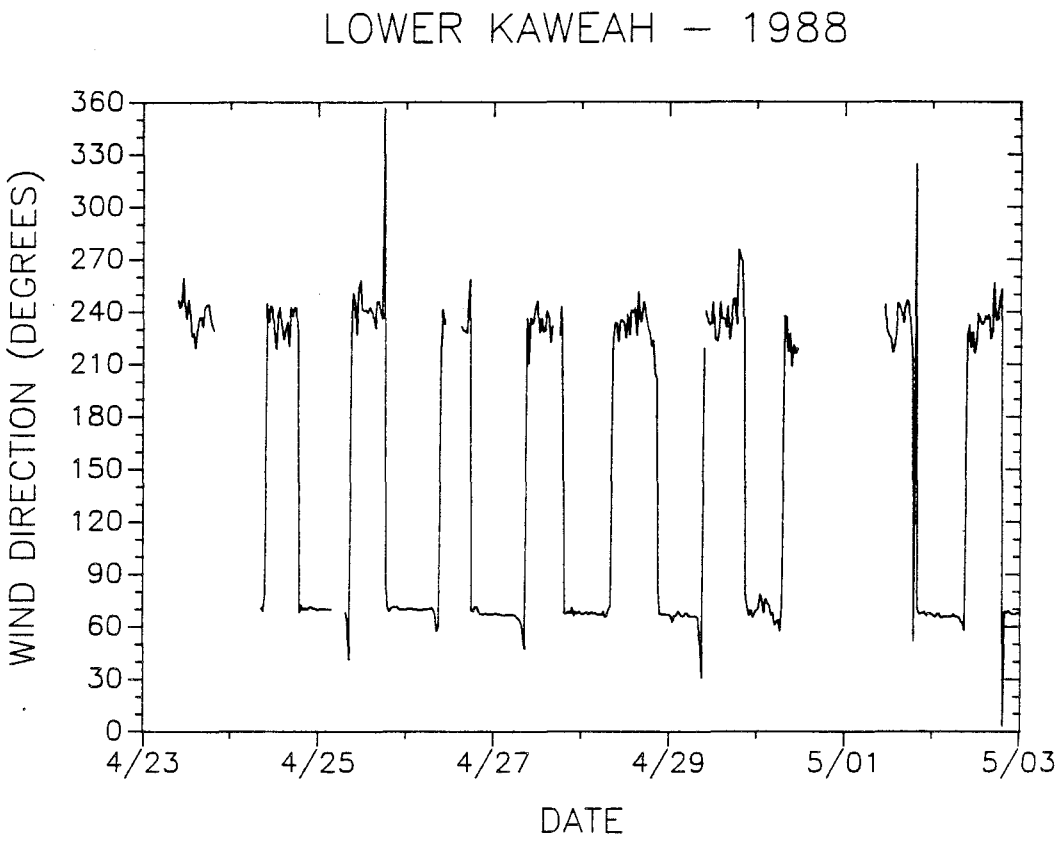

Figure 3.19. Wind direction at Lower Kaweah during the study period.

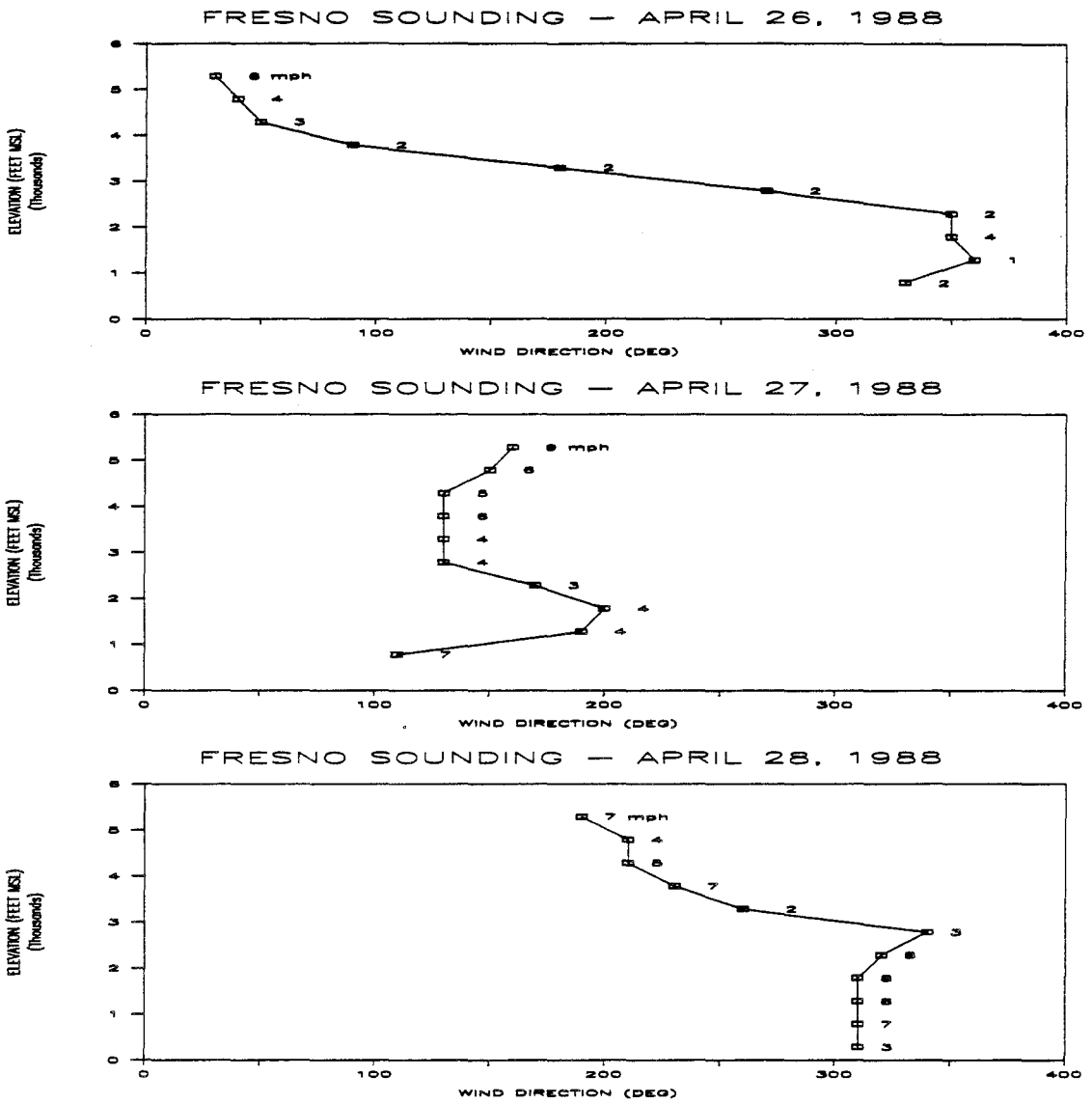

Figure 3.20. Vertical profiles of wind speed and direction measured at Fresno at 0600 PST on the mornings of April 26, 27, and 28, 1988.

Joaquin Valley. Increased vertical mixing at Bakersfield, observed on the morning of April 28 (see Figure 3.14), however, may have allowed pollutants to mix up higher in the atmosphere than they could earlier in the study. Since upper level winds in the valley were still blowing from the south (see Figure 3.20), the increased mixing may have allowed southern San Joaquin Valley emissions to be transported more readily to Lower Kaweah.

Based on the preceding observations, it appears that, at least for the study period in question, the reduction in vertical stability, associated with the approach of the front, was the most important factor contributing to the rise in pollutant levels observed at Lower Kaweah and Ash Mountain. During the passage of a stronger frontal system, changes in wind direction (reflected either by a breakdown of the upslope–downslope flow at Lower Kaweah, or a strong increase in southerly flow) may play a more important role.

Cloudwater

Clouds began intercepting the hillside at Lower Kaweah at approximately 1100 PDT on April 28. By 1230 they had become dense enough to sample, and collection commenced. The battery powered CASCC was put into operation near Moro Rock at 1130, with the first sample collected from 1145 to 1200. Cloudwater was sampled continuously, in half–hour samples, until 1500 at Lower Kaweah, when the cloud base rose above the site, and until 1600 at Moro Rock, when the clouds dissipated. No rain was observed during the event. Concentrations of major inorganic ions, observed in the cloudwater samples collected at the two sites, are shown in Table 3.2. Concentrations of species observed in a blank taken by rinsing the collection surfaces of the CASCC at Moro Rock prior to sample collection also

Table 3.2. Chemical Composition of Sequoia Cloudwater

Time	pH	Na^+	K^+	NH_4^+	Ca^{2+}	Mg^{2+}	Cl^-	NO_3^-	SO_4^{2-}	LWC
		←				μN			→	ml m^{-3}
LOWER KAWEAH										
1230–1300	4.62	27	3	411	18	9	16	216	184	0.25
1300–1330	4.64	20	2	399	14	7	17	199	175	0.20
1330–1400	4.54	15	2	398	9	6	30	200	175	0.19
1400–1430	4.48	14	1	425	9	5	16	211	177	0.19
1430–1500	4.36	16	3	523	11	7	20	273	231	0.08
MORO ROCK										
1145–1200	4.75	29	NA	345	18	9	NA	175	144	0.23
1200–1230	4.70	22	12	345	11	7	23	164	144	0.26
1230–1300	4.69	17	3	303	8	5	13	154	135	0.37
1300–1330	4.64	19	2	346	9	6	14	183	150	0.28
1330–1400	4.61	21	2	386	10	7	15	211	164	0.27
1400–1430	4.48	19	1	358	9	6	13	207	156	0.28
1430–1500	4.44	20	2	385	12	7	5	191	142	0.31
1500–1530	4.38	18	2	389	10	7	5	209	157	0.21
1530–1600	4.34	35	3	584	18	12	14	336	236	0.15
BLANK		1	1	4	2	1	1	2	2	

NA denotes not available.
The blank concentration has been subtracted from the sample concentration for each species.

are listed here. Blank concentrations of all species but K^+ were negligible with respect to the concentrations observed in the cloudwater samples. The background concentration of 1 μN K^+ was significant only because such low concentrations were observed in the cloudwater (2–13 μN).

The pH of the cloudwater dropped continuously over the sampling period at both sites (Figure 3.21), falling from 4.75 to 4.34 at Moro Rock, and from 4.62 to 4.36 at Lower Kaweah. Comparison of cloudwater pH for those samples collected simultaneously at the two sites reveals that cloudwater sampled at Lower Kaweah had comparable, or slightly higher free acidity than cloudwater at Moro Rock. The pH levels observed during this event were somewhat lower than those typically observed during the spring at Lower Kaweah (see Chapter 2). The drop in pH at both sites (corresponding to an 82% increase in H^+ at Lower Kaweah and a 157% increase at Moro Rock) coincided with a decrease in the cloudwater ratio of NH_4^+ to the sum of NO_3^- and SO_4^{2-}.

The composition of the cloudwater collected at both sites was dominated by concentrations of NO_3^-, SO_4^{2-}, and NH_4^+. These ions were observed to be the dominant contributors in all of the samples collected at Lower Kaweah (see Chapter 2). NO_3^- and SO_4^{2-} concentrations represent the major inorganic contributions to atmospheric acidity provided by HNO_3 and H_2SO_4. NH_4^+ concentrations are indicative of the major inorganic contribution to neutralization of atmospheric acidity by NH_3. Concentrations of all three species are plotted in Figures 3.22 and 3.23 for samples collected at Lower Kaweah and Moro Rock, respectively. Concentrations at both sites were observed to rise toward the end of the sampling period. The rise in concentrations corresponded to an increase in visibility, and a decrease in the collection rate of the CASCC, at each site. Since the collection rate

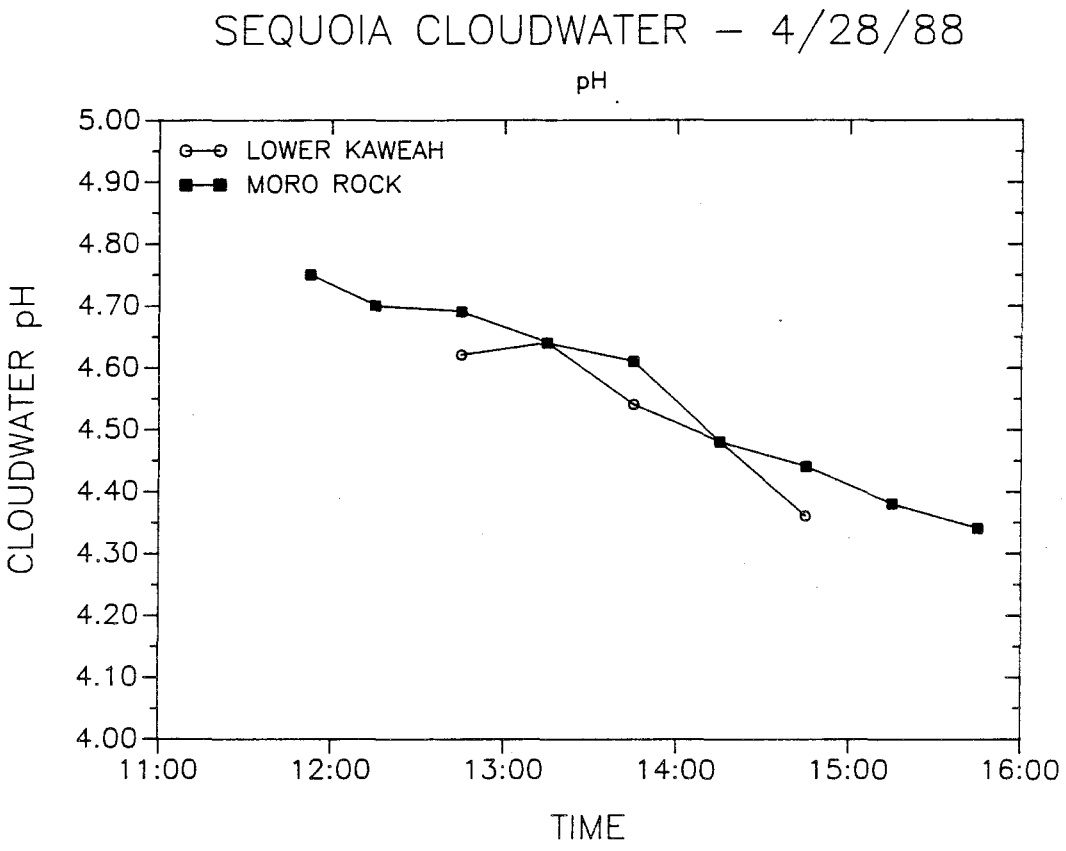

Figure 3.21. pH of the cloudwater samples collected at Lower Kaweah and Moro Rock on April 28, 1988.

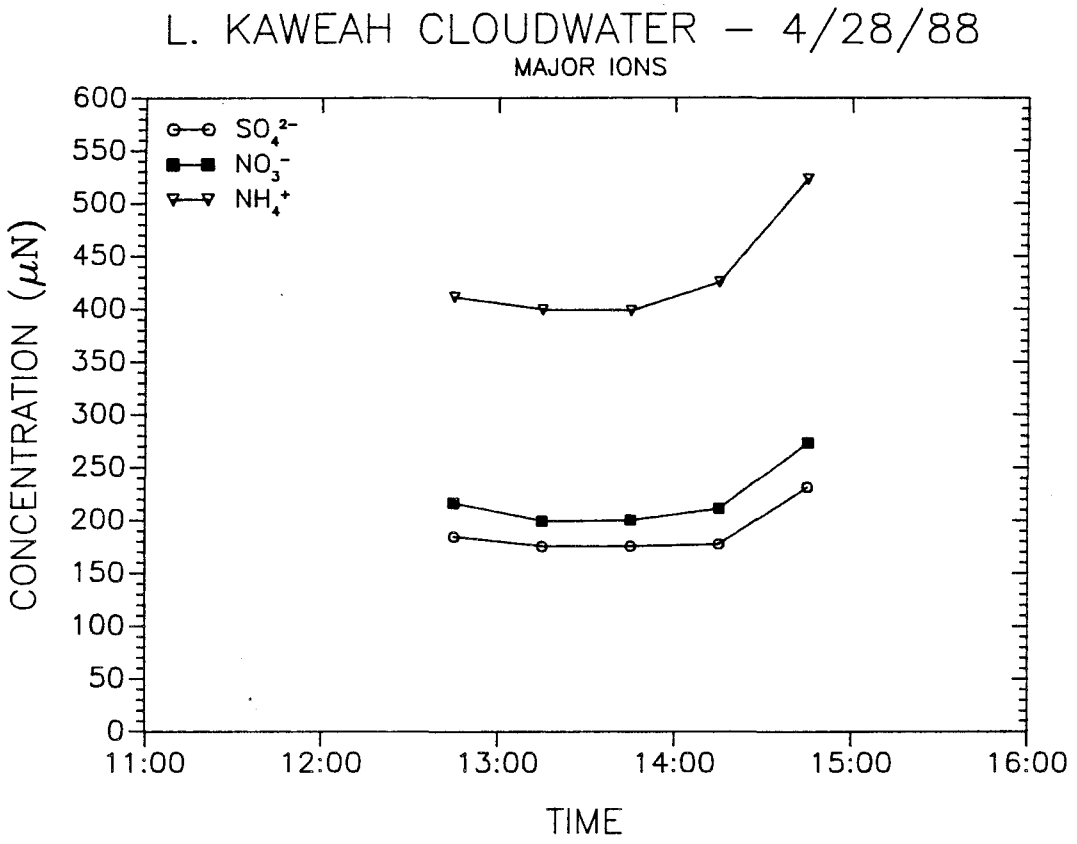

Figure 3.22. Concentrations of nitrate, sulfate, and ammonium in cloudwater samples collected at Lower Kaweah on April 28, 1988.

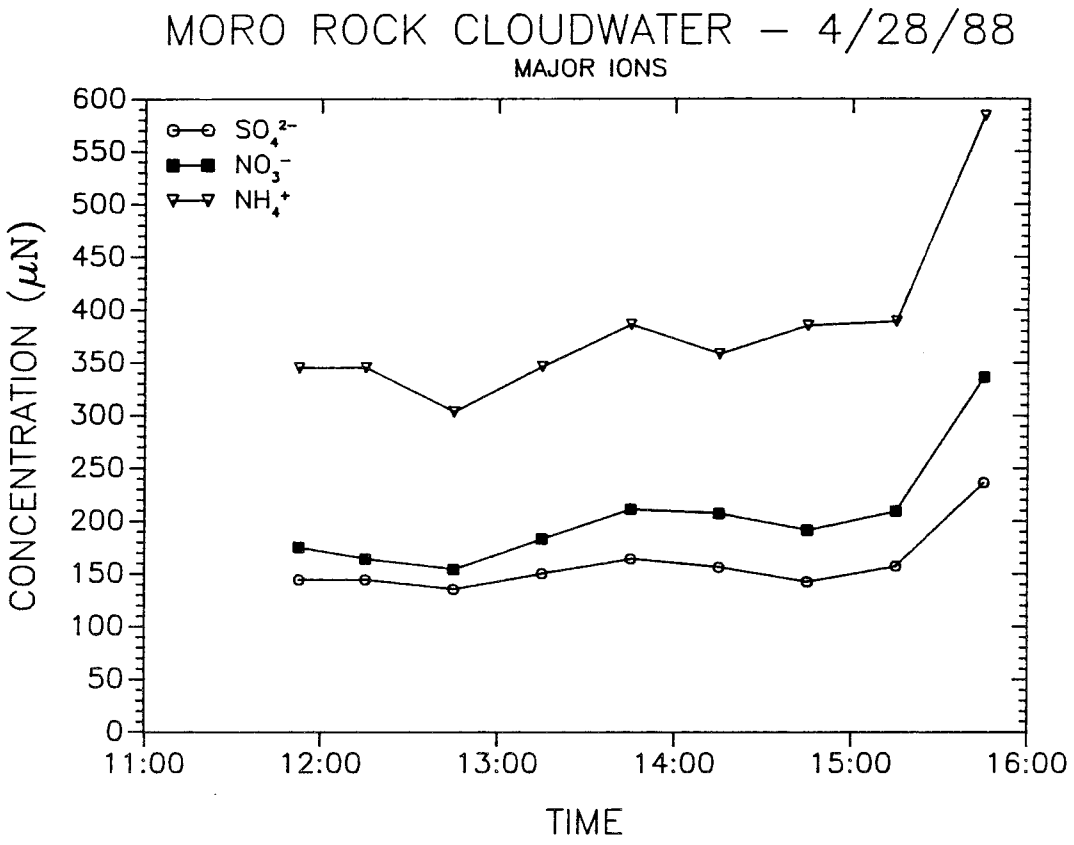

Figure 3.23. Concentrations of nitrate, sulfate, and ammonium in cloudwater samples collected at Moro Rock on April 28, 1988.

of the CASCC depends on the liquid water content (LWC) of the clouds being sampled (see Chapter 5), it is possible that a decrease in cloud LWC may have been the cause of the concentration increases. This seems particularly likely since the concentrations at the two sites did not increase simultaneously, despite the fact that the sites are located relatively close to one another.

Calculated values of the cloud LWC, based on the theoretical collection efficiency of the CASCC and the observed cloudwater collection rate, are listed in Table 3.2. The performance of the two CASCCs used in the study differed slightly because of the use of a rain–excluding inlet on the Lower Kaweah collector. Corrections have been made to the estimates of LWC for each collector, utilizing laboratory measurements of the velocity across the impaction surface in the two collector configurations. Calculated values of LWC are averages over the length of each sample collection period. They range from 0.08 to 0.25 ml H_2O m^{-3} air at Lower Kaweah and from 0.15 to 0.37 ml H_2O m^{-3} air at Moro Rock.

By multiplying the cloudwater concentration of a species by the LWC, it is possible to obtain an estimate of the loading of that cloudwater species in the air mass sampled. Units of cloudwater loading are concentration per volume of air. Cloudwater loadings of NO_3^-, SO_4^{2-}, and NH_4^+ are presented in Figures 3.24 through 3.26. The loadings are fairly constant during the middle of the sampling period at both sites. Some fluctuations are apparent, however, near the beginning and the end of the event. These fluctuations appear to be correlated with changes in LWC. During periods of higher LWC, the cloudwater loadings of the three species increase; when LWC drops, the cloudwater loadings generally drop. This trend suggests that scavenging of N(V), S(VI), and N(–III) from the aerosol and gas phases may have been more efficient at higher LWC. Loadings observed at Moro Rock were

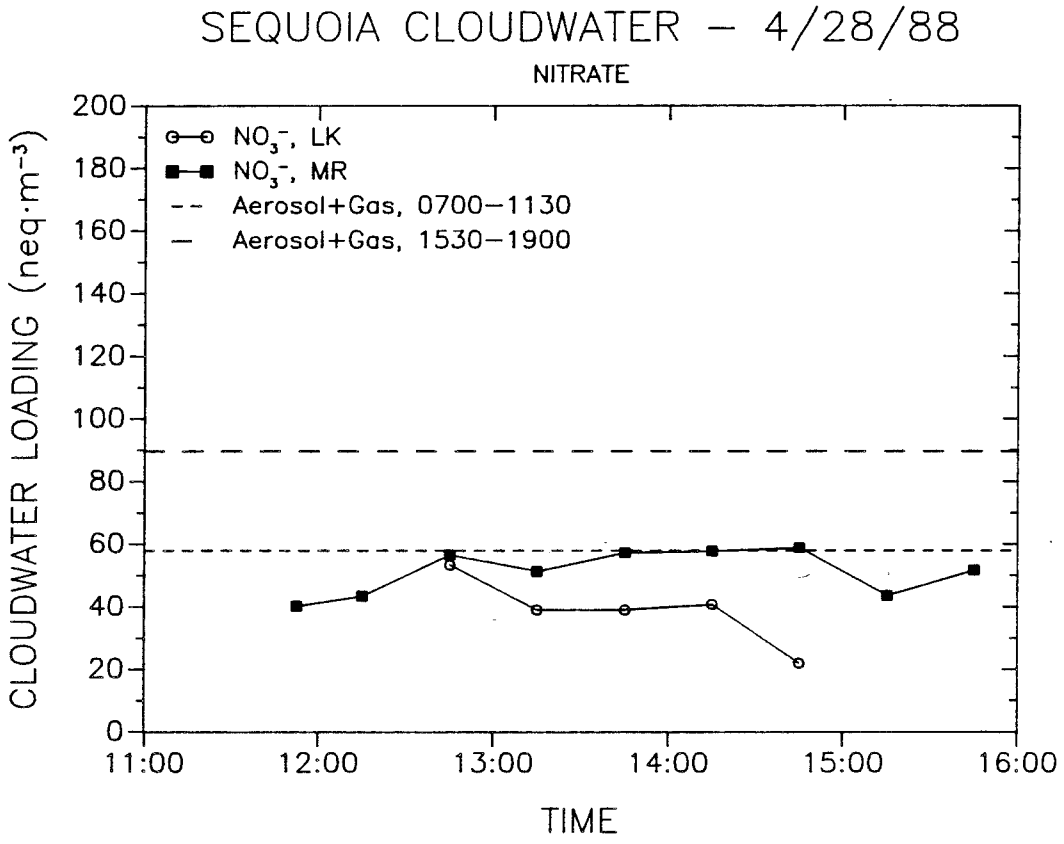

Figure 3.24. Cloudwater loadings of nitrate (neq m^{-3}) at Lower Kaweah and Moro Rock on April 28, 1988. The loading for each period is calculated based on the collection rate of the CASCC and the sample nitrate concentration. Total N(V) loadings observed in the air mass at Lower Kaweah prior to and following the cloud interception event are included for reference.

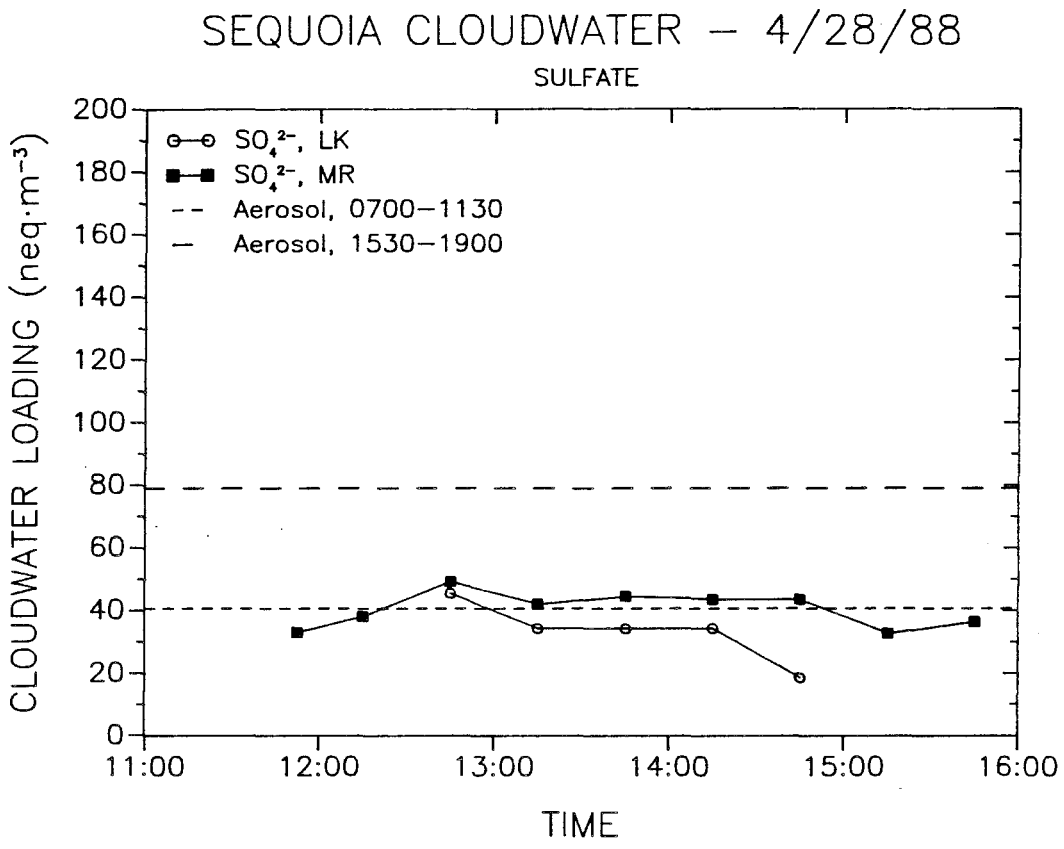

Figure 3.25. Cloudwater loadings of sulfate (neq m^{-3}) at Lower Kaweah and Moro Rock on April 28, 1988. The loading for each period is calculated based on the collection rate of the CASCC and the sample nitrate concentration. Aerosol sulfate loadings observed in the air mass at Lower Kaweah prior to and following the cloud interception event are included for reference.

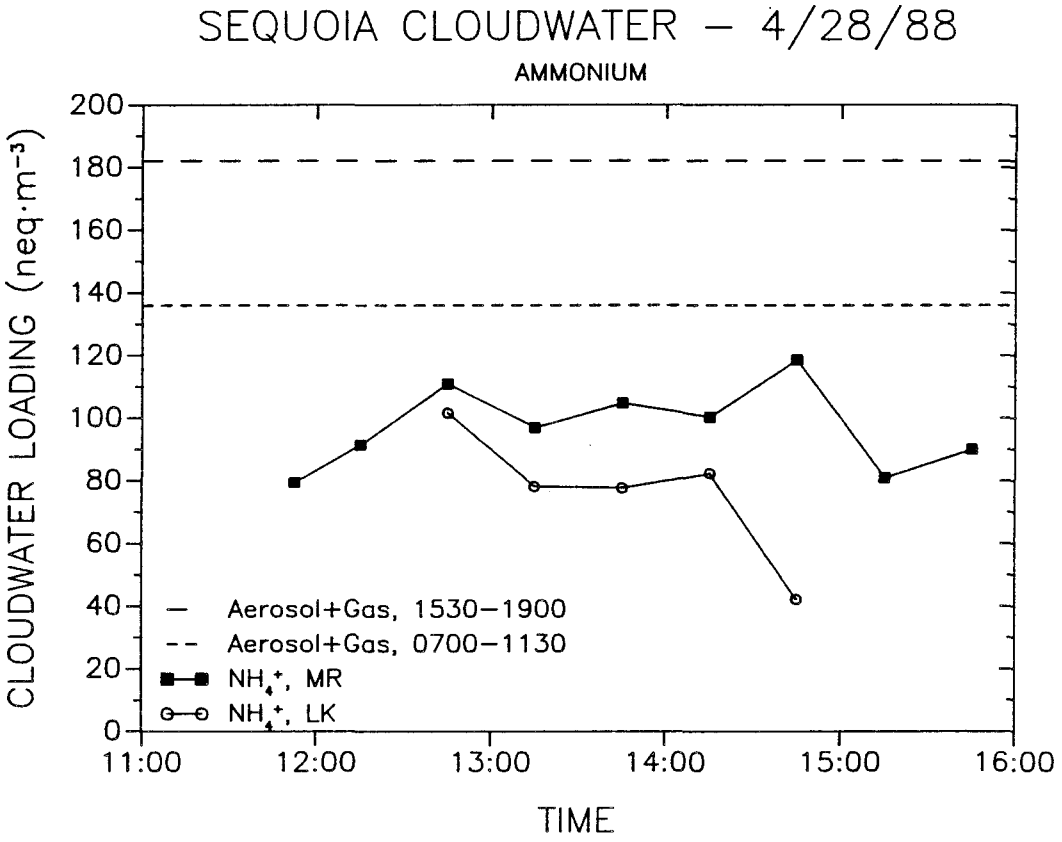

Figure 3.26. Cloudwater loadings of ammonium (neq m^{-3}) at Lower Kaweah and Moro Rock on April 28, 1988. The loading for each period is calculated based on the collection rate of the CASCC and the sample nitrate concentration. Total N(–III) loadings observed in the air mass at Lower Kaweah prior to and following the cloud interception event are included for reference.

somewhat higher than those at Lower Kaweah. Since observed LWC values were also higher at Moro Rock, the differences in cloudwater loadings at the two sites are consistent with the hypothesis that higher LWC was responsible for more efficient scavenging by the cloudwater.

It is not unreasonable to expect that scavenging of small aerosol particles, which contain much of the NH_4^+, NO_3^-, and SO_4^{2-} (Seinfeld, 1986), will be affected by changes in LWC. Variations in LWC observed during the event were most likely the product of changes in supersaturation of the air mass (increased supersaturation leading to increased LWC). At a given supersaturation, there is a critical minimum size for aerosol nucleation. Aerosol smaller than this size, about 0.1 μm for typical cloud conditions (Mason, 1971), are scavenged through impaction and diffusion processes, which are less efficient than nucleation. As supersaturation in the cloud is increased, the critical size for nucleation is decreased, and small aerosol is scavenged with increased efficiency. This can lead to an increase in cloudwater loadings of those species contained in the small aerosol. Scavenging of NH_3 and HNO_3 from the gas phase is quite efficient at the pH values observed during this event and probably was not affected significantly by the changes in LWC.

It is important to point out that the observed changes in cloudwater loadings of NO_3^-, SO_4^{2-}, and NH_4^+ may have been due to causes other than variations in aerosol scavenging efficiency. The values of LWC are calculated using the cloudwater collection rate of the CASCC, assuming a collection efficiency that is independent of LWC. Past observations have revealed that clouds with higher LWC typically have a higher mass median droplet diameter (Best, 1951). Since the collection efficiency of the CASCC is greater for larger droplets, this implies that cloudwater in higher LWC clouds should be collected more efficiently. The error

associated with neglecting this effect introduces a bias into the estimates of LWC and, hence, cloudwater loadings. At higher LWC, the loadings tend to be overestimated; at lower LWC, they are underestimated. The magnitude of this error, however, is less than 5% over the range of LWC observed in the study, assuming that the droplet size distribution being sampled was not highly unusual. The fluctuations in cloudwater loadings significantly exceeded 5%.

Intermittent sampling of clear air parcels tends to reduce the half–hour average values of LWC and therefore leads to underestimation of values of cloudwater loading in the cloudy parcels of interest. Such a situation can occur when the clouds being sampled become "patchy," with interspersed volumes of cloudy and clear air, and is common at the upper and lower boundaries of a cloud. Visual observations during the study indicated that this phenomenon may have been important during the last half–hour of sampling at Lower Kaweah, when the lower cloud boundary was approaching the elevation of the site, but not during any other periods. No periods of "patchiness" were observed while sampling at Moro Rock. Lower estimates of LWC at Moro Rock toward the end of the sampling period, however, may partially be due to a decrease in the sampling efficiency of the CASCC, as the battery voltage dropped. The fan which draws the air through the CASCC was observed to slow somewhat during the final sampling period. The possible effects of patchiness at Lower Kaweah, and dropping battery voltage at Moro Rock are limited primarily to the final half–hour sample at each site and do not affect the hypothesis of variations in aerosol scavenging efficiency during the rest of the sampling period.

Another potential explanation of the observed variations in values of cloudwater loading of the major species lies in the possibility that aerosol and gas

phase concentrations of these species, entering the bottom of the cloud in the upslope flow, may not have been constant. Indeed, data presented above illustrate that these concentrations vary considerably throughout the course of a day. However, the likelihood of the half–hour average concentrations varying by 20% from one period to the next, with no consistent trend, seems small given the regularity of the upslope flow in the region and the distance from emission sources. In addition, it seems more than mere coincidence that the variations in cloudwater loading are correlated so well with cloud LWC. Nevertheless, in the absence of short term aerosol and gas phase measurements, it is not possible to rule out variations in clear air loadings of these species as a source of variation in cloudwater loadings.

Total atmospheric loadings of N(V), S(VI), and N(–III), respectively, measured prior to and following the cloud interception event, are illustrated in Figures 3.24 through 3.26, along with the values of each species' cloudwater loading. (Measurements made during the cloud interception event have not been included due to uneven deposition of cloudwater droplets on the filter surfaces. The irregular pattern of deposition, associated with the orientation of the filters relative to the wind direction during periods of moderate to high wind speed, is a common problem in such environments.) Comparison of the cloudwater loading of all three major species with these clear air loadings suggests that a large fraction of each species was incorporated into the cloudwater. Once again, in the absence of reliable short term aerosol and gas measurements during the sampling period, it is not possible to calculate accurate scavenging ratios.

Measurements of peroxide concentrations in cloudwater at the two sites ranged from 15 to 47 μM, with those at Lower Kaweah consistently higher than

those at Moro Rock (see Table 3.3). As indicated previously, these concentrations are believed to represent primarily H_2O_2. Cloudwater loadings of H_2O_2 are presented in Figure 3.27. During the first hour and a half of sampling, the loading was observed to increase substantially. H_2O_2 loadings drop off, toward the end of the sampling period, at both sites. These drops, however, may be due largely to biases in the estimate of LWC toward the end of the event at each site, as discussed above. The high Henry's Law coefficient for H_2O_2, 1.4 x 10^5 M atm^{-1} at 293 K (Yoshizumi et al., 1984), indicates that H_2O_2 will be scavenged almost entirely from the gas phase. Cloudwater loadings of H_2O_2, therefore, are good indicators of the total concentration of H_2O_2 in the air mass. This implies that the increases in the total amount of H_2O_2 in the cloudwater, during the first portion of sampling, may reflect increases in gas phase concentrations of H_2O_2 entering the bottom of the cloud. Gas phase H_2O_2 concentrations have been shown to be positively correlated with photolysis rates under slightly polluted conditions (Stockwell, 1986), so an increase at midday should be expected. It also is possible that aqueous phase production of H_2O_2 contributed to the increase, although gas phase production typically is thought to dominate, particularly at the pH range observed in the current study (McElroy, 1986).

Aqueous phase oxidation of S(IV) to S(VI) by dissolved H_2O_2 is the dominant pathway for production of SO_4^{2-} in cloudwater at pH values below 5 (Jacob and Hoffmann, 1983), as long as H_2O_2 is available. Cloudwater concentrations of S(IV) at Lower Kaweah and Moro Rock, listed in Table 3.3, were not observed to be higher than 6 μM in any of the samples. Given that Lower Kaweah was located near cloud base, this indicates that in-cloud production of SO_4^{2-} was probably not important during this event.

Table 3.3. H_2O_2 and S(IV) in Sequoia Cloudwater

Site	Time	pH	H_2O_2	S(IV)
			← μM →	
LK	1230–1300	4.62	26	6
LK	1300–1330	4.64	36	6
LK	1330–1400	4.54	35	6
LK	1400–1430	4.48	37	<4
LK	1430–1500	4.36	47	<4
MR	1145–1200	4.75	16	<4
MR	1200–1230	4.70	15	6
MR	1230–1300	4.69	16	<4
MR	1300–1330	4.64	22	<4
MR	1330–1400	4.61	22	<4
MR	1400–1430	4.48	23	6
MR	1430–1500	4.44	23	<4
MR	1500–1530	4.38	27	<4
MR	1530–1600	4.34	30	<4
	BLANK		0	<4

LK denotes Lower Kaweah. MR denotes Moro Rock.
S(IV) concentrations <4 μM were not detected.

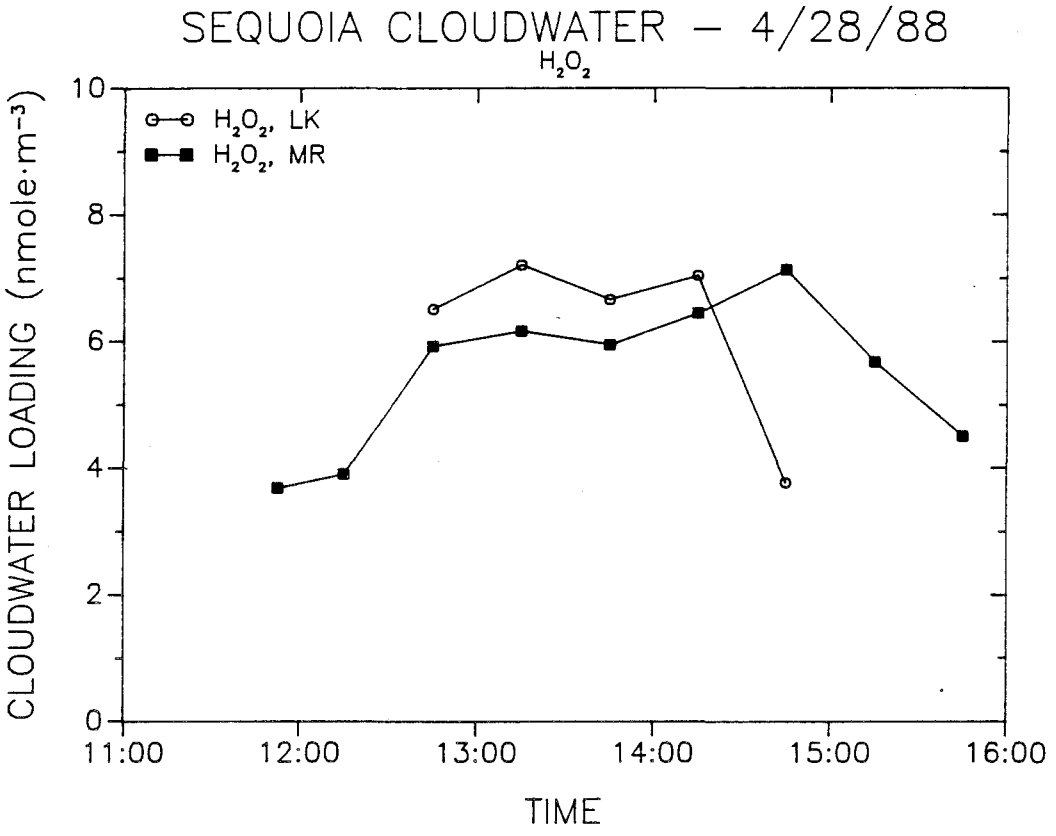

Figure 3.27. Cloudwater loadings of H_2O_2 (nmole m^{-3}) at Lower Kaweah and Moro Rock on April 28, 1988. The loading for each period is calculated based on the collection rate of the CASCC and the sample H_2O_2 concentration.

Carboxylic acids, found in remote as well as urban areas (Keene et al., 1983), have both natural and anthropogenic sources. These include automotive exhaust, burning of biomass, and atmospheric oxidation of hydrocarbons (Talbot et al., 1988). Oxidation of isoprene, a natural hydrocarbon emitted from vegetation, may be a particularly important source of formic acid (Jacob and Wofsy, 1988), especially in a region like Sequoia National Park. Ratios of formate to acetate in fogwater samples previously collected on the floor of the San Joaquin Valley varied considerably (Munger et al., 1989), depending on sampling location. Samples collected in Visalia exhibited acetate concentrations in excess of formate concentrations, while samples from other locations often were more concentrated in formate. Cloudwater samples collected previously at Lower Kaweah were found to be enriched in formate, relative to acetate (Collett et al., 1989).

Short chain carboxylic acids were found to contribute significantly to the composition of the cloudwater sampled in this study. Formic acid was the predominant carboxylic acid in all of the samples. Concentrations of formic acid ranged from 22 to 24 μM; acetic acid concentrations ranged from 6 to 9 μM; and pyruvic acid concentrations ranged from 1 to 5 μM. Differences between the concentrations of each of the species observed at the two sites are not statistically significant.

Concentrations of the conjugate bases (formate, acetate, and pyruvate) are listed in Table 3.4. These were calculated using the measured pH of each sample and the acid dissociation constant for each acid, adjusted for the ambient temperature. Due to the low pK_a values of formic and pyruvic acid, both of these species exist almost entirely in the deprotonated form in the pH range observed. Since the pH of the cloudwater was near the pK_a of acetic acid, approximately half

Table 3.4. Carboxylic Acids in Sequoia Cloudwater

Site	Time	pH	Formate	Acetate	Pyruvate*	% H^+	−/+
			←	μN	→		
LK	1230–1300	4.62	30.1	3.8	3.9	157.5	0.92
LK	1300–1330	4.64	30.2	4.0	3.0	162.5	0.91
LK	1330–1400	4.54	25.8	3.0	3.7	112.6	0.95
LK	1400–1430	4.48	24.4	2.7	4.0	93.9	0.89
LK	1430–1500	4.36	23.5	2.0	4.7	69.3	0.91
MR	1145–1200	4.75	28.6	3.9	2.8	198.1	NA
MR	1200–1230	4.70	26.5	3.4	2.6	162.9	0.87
MR	1230–1300	4.69	24.2	3.5	1.2	141.7	0.92
MR	1300–1330	4.64	24.6	3.1	2.1	129.9	0.92
MR	1330–1400	4.61	25.5	3.0	2.1	124.4	0.93
MR	1400–1430	4.48	20.4	2.2	1.8	73.6	0.93
MR	1430–1500	4.44	18.2	1.9	1.7	60.0	0.78
MR	1500–1530	4.38	19.8	1.9	1.8	56.2	0.84
MR	1530–1600	4.34	23.9	1.9	2.1	60.8	0.87
	BLANK		0	0	0		

LK denotes Lower Kaweah; MR denotes Moro Rock.
* Identification of this species is tentative.
% H^+ denotes the maximum contribution of the carboxylate anions to free acidity.
−/+ denotes the total ion balance including all measured species, organic and inorganic.
NA denotes not available.

the acetic acid should exist in the samples as acetate.

The sum of the concentrations of formate, acetate, and pyruvate in each sample can be compared to the H^+ concentration to estimate the maximum possible contribution of these weak acids to free acidity in the cloudwater. Results of this comparison, listed in Table 3.4, indicate that carboxylate concentrations measured about 200% of the H^+ concentration at the start of the event and fell to about 60% of the H^+ concentration by the end of the event. The maximum contribution of formate, acetate, and pyruvate to free acidity in these samples, therefore, dropped from 100% to 60% over the course of the event. This is a maximum contribution because the free acidity measured in the samples cannot be apportioned between the weak carboxylic acids and the strong mineral acids. In cloudwater from Sequoia National Park, in particular, much of the acidity introduced by these species is neutralized by NH_3, either in precursor aerosol or in the cloud droplets. Typically, H^+ concentrations are only a small fraction of NH_4^+ concentrations in samples collected in the region (Collett et al., 1989; Chapters 1 and 2).

A variety of carbonyl and dicarbonyl compounds are found in the atmosphere. A review of their chemistry has been provided recently by Finalyson–Pitts and Pitts (1986). Primary sources of carbonyl compounds include emissions from animal excretions, forest fires, and incomplete combustion processes (Carlier et al., 1986). While emission as primary compounds is common, the bulk of the total concentrations of these species in the atmosphere is believed to come from secondary sources. Formaldehyde, frequently observed at significant levels in fog and cloudwater (Munger et al., 1989), is a product of the oxidation of naturally occurring hydrocarbons including isoprene, while acetaldehyde is formed from the oxidation of amines, propene, and 2–butene (Finlayson–Pitts and Pitts, 1986).

Benzaldehyde, glyoxal, and methylglyoxal are formed from the oxidation of simple aromatic hydrocarbons such as toluene (Carlier et al., 1986, Finlayson–Pitts and Pitts, 1986), produced in engine exhaust. Glyoxal and methylglyoxal have been found, along with formaldehyde, at significant concentrations in fog samples collected in the mountains surrounding Los Angeles (Steinberg and Kaplan, 1984).

Concentrations of carbonyl and dicarbonyl compounds observed in the cloudwater samples collected at Moro Rock and Lower Kaweah are indicated in Table 3.5. During most periods, formaldehyde was the dominant species, with concentrations ranging from 8 to 14 μM – much lower than previously observed on the valley floor (6 to 498 μM; Munger et al., 1989). Second in importance was glyoxal, measured at concentrations between 5 and 13 μM. Smaller concentrations of acetaldehyde, methylglyoxal, and benzaldehyde also were observed. A peak with retention time matching the retention time of propanal in the standards was observed in most of the samples, but not in the blank. The peak was not definitely identified as a propanal peak, however, and may represent a combination of responses from three–carbon species in the samples. The area of these peaks indicated concentrations as high as 5 μM in some of the samples, based on the propanal response in the standards. These concentrations are surprisingly high in view of the low solubility of these species in water, indicating that equilibrium gas phase concentrations must have been much higher than would normally be expected.

Glyoxal and methylglyoxal concentrations were at least two times less than those reported for fog by Steinberg and Kaplan (1984), although acetaldehyde concentrations were comparable. Benzaldehyde was only observed toward the end of the sampling period, at both sites, suggesting that it may have been associated

Table 3.5. Carbonyls in Sequoia Cloudwater

Site	Time	Form	Acet	Glyox	Mglyox	Benz
		←		μM		→
LK	1230–1300	14.1	2.8	9.7	2.2	0.0
LK	1300–1330	12.2	2.2	10.6	2.2	0.0
LK	1330–1400	10.5	1.9	7.2	1.6	0.0
LK	1400–1430	11.5	2.1	9.8	1.9	0.8
LK	1430–1500	10.3	2.8	13.1	2.5	0.6
MR	1145–1200	10.6	1.1	5.9	1.4	0.0
MR	1200–1230	10.2	1.0	5.5	1.3	0.0
MR	1230–1300	11.2	1.1	7.7	1.5	0.0
MR	1300–1330	10.6	0.5	4.7	1.2	0.0
MR	1330–1400	9.0	0.2	6.5	1.3	0.0
MR	1400–1430	7.9	0.5	4.4	0.9	0.0
MR	1430–1500	8.7	0.9	5.4	1.1	0.0
MR	1500–1530	7.8	0.9	5.8	1.3	0.1
MR	1530–1600	11.6	1.9	9.6	1.9	0.4
	BLANK	2.7	1.0	1.2	0.0	0.0

LK denotes Lower Kaweah; MR denotes Moro Rock.
Form denotes formaldehyde; Acet denotes acetaldehyde; Glyox denotes glyoxal; Mglyox denotes methylglyoxal; Benz denotes benzaldehyde.
The blank concentration has been subtracted from the sample concentration for each species.

with emissions from morning traffic in the valley below, which require a few hours to be transported by the upslope flow to the elevation of the sampling sites.

Conclusions

Measurements of major inorganic aerosol species are presented for three sites in central California during a four day period in April, 1988. Measurements were made at Visalia (elev. 300 feet), Ash Mountain (1800 feet) and Lower Kaweah (6240 feet). Concentrations of NH_3 and HNO_3 also were measured at these locations. Aerosol compositions were nearly neutral at all locations, however, large concentrations of NH_3 at Visalia contributed significantly to the alkalinity of the total air mass there. Concentrations of all major species were observed to decrease from Visalia to Ash Mountain to Lower Kaweah, during most of the sampling periods. Ratios of N(V) to S(VI) at Ash Mountain and Lower Kaweah were markedly different than those observed at Visalia, suggesting that at least some contribution to air quality at the higher elevations must come from another source area.

Concentrations at Ash Mountain and Lower Kaweah exhibited diurnal fluctuations, with peaks in the late afternoon, consistent with the transport of pollutants from San Joaquin Valley sources by daytime upslope winds. Concentrations of most of these species reached a maximum at Ash Mountain and Lower Kaweah on April 28, increasing as a weak cold front approached. Concentrations at Visalia were somewhat lower on April 28 than earlier in the week. A reduction in atmospheric stability above the valley on April 28, associated with the approach of the storm system, appears to have contributed to the increased concentrations observed at the upper two sites by allowing pollutants previously

trapped near the valley floor to mix up to higher elevations. Upper level wind data indicate that at least part of the air mass sampled at Lower Kaweah and Ash Mountain on April 28 may have passed over the southern San Joaquin Valley.

Clouds began intercepting the hillside at Lower Kaweah at approximately 1100 PDT on April 28. Five cloudwater samples were collected at Lower Kaweah, while nine were obtained at a second site 1.5 miles southeast and 200 feet higher in elevation (Moro Rock). The pH of the cloudwater at both sites was observed to fall throughout the course of the event, dropping as low as 4.34. NO_3^-, SO_4^{2-}, and NH_4^+ were the major inorganic species observed in the cloudwater. The cloudwater pH drop coincided with an increase in the ratio of NH_4^+ to the sum of NO_3^- and SO_4^{2-}.

The clouds sampled at Moro Rock were denser than those sampled at Lower Kaweah. Concentrations of major ions were correspondingly lower at Moro Rock. The clouds appeared to scavenge a large fraction of the aerosol NO_3^-, SO_4^{2-}, and NH_4^+, as well as the gas phase HNO_3 and NH_3. Total loadings of NO_3^-, SO_4^{2-}, and NH_4^+ in the cloudwater were positively correlated with cloud liquid water content, suggesting that scavenging efficiencies for these particles may have been similarly correlated. Short term aerosol and gas measurements needed to confirm this hypothesis are not available.

H_2O_2 was observed at significant concentrations in the cloudwater, ranging from 15 to 47 μM. S(IV) concentrations were $\leq$ 6 μM in all samples, even near cloud base, indicating that aqueous phase production of SO_4^{2-} was probably not important during this event. Significant concentrations of formic and acetic acids were observed. Carbonyl concentrations in the cloudwater were dominated by formaldehyde and glyoxal.

Acknowledgments

We are grateful to the National Park Service, particularly the research staff at Sequoia National Park, for granting us access to sites within the Park. We gratefully acknowledge the California Air Resources Board for providing access to the sampling site in Visalia and for providing financial support for this project (CARB contract #A6–185–32).

References

Best, A. C. (1951) Drop–size distribution in cloud and fog. Q. Jl. R. met. Soc. 77, 418–426.

Cahill, T. A., Annegarn, H., Ewell, D. and Feeney, P. J. (1986) Particulate monitoring for acid deposition research at Sequoia National Park California. Final report to California Air Resources Board, Sacramento, CA.

Carlier, P., Hannachi, H. and Mouvier, G. (1986) The Chemistry of carbonyl compounds in the atmosphere – A Review. *Atmos. Environ.* **20**, 2079–2099.

Collett, J., Jr., Daube, B., Jr., Munger, J. W. and Hoffmann, M. R. (1989) Cloudwater chemistry in Sequoia National Park. *Atmos. Environ.*, in press.

Daube, B. C., Jr., Flagan, R. C. and Hoffmann, M. R. (1987) *Active Cloudwater Collector.* United States Patent # 4,697,462, Oct. 6, 1987.

Dasgupta, P. K., DeCesare, K. and Ullrey, J. C. (1980) Determination of atmospheric sulfur dioxide without tetrachloromercurate (II) and the mechanism of the Schiff reaction. *Anal. Chem.* **52**, 1912–1922.

Dong, S. and Dasgupta, P. K. (1987) Fast flourimetric flow injection analysis of formaldehyde in atmospheric water. *Environ. Sci. Technol.* **21**, 581–588.

Finlayson–Pitts, B. J. and Pitts, J. N., Jr. (1986) *Atmospheric Chemistry: Fundamentals and Experimental Techniques.* John Wiley, New York, 1098 p.

Graedel, T. E., Hawkins, D. T. and Claxton, L. D. (1986) *Atmospheric chemical compounds: Sources, occurrence, and bioassay.* Academic Press, New York.

Grosjean, D. (1982) Formaldehyde and other carbonyls in Los Angeles ambient air. *Environ. Sci. Technol.* **16**, 254–262.

Grosjean, D. and Wright, B. (1983) Carbonyls in urban fog, ice fog, and cloudwater

and rainwater. *Atmos. Environ.* **17**, 2093–2096.

Jacob, D. J. and Hoffmann, M. R. (1983) A dynamic model for the production of H^+, NO_3^-, and SO_4^{2-} in urban fog. *J. Geophys. Res.*, **88**, 6611–6621.

Jacob, D. J., Waldman, J. M., Munger, J. W. and Hoffmann, M. R. (1985) Chemical composition of fogwater collected along the California coast. *Envir. Sci. Technol.* **19**, 730–736.

Jacob, D. J., Munger, J. W., Waldman, J. M. and Hoffmann, M. R. (1986a) The H_2SO_4–HNO_3–NH_3 system at high humidities and in fogs: I. Spatial and temporal patterns in the San Joaquin Valley of California. *J. Geophys. Res.* **91**, 1073–1088.

Jacob, D. J., Waldman, J. M., Munger, J. W. and Hoffmann, M. R. (1986a) The H_2SO_4–HNO_3–NH_3 system at high humidities and in fogs: II. Comparison of field data with thermodynamic calculations. *J. Geophys. Res.* **91**, 1089–1096.

Jacob, D. J., Shair, F. H., Waldman, J. M., Munger, J. W. and Hoffmann, M. R. (1987) Transport and oxidation of SO_2 in a stagnant foggy valley. *Atmos. Environ.* **21**, 1305–1314.

Jacob, D. J. and Wofsy, S. C. (1988) Photochemical production of carboxylic acids in a clean continental atmosphere, in *Acid Deposition Processes at High Elevation Sites*, edited by H. M. Dunsworth, D. Reidel, Hingham, Mass. (in press).

Kawamura, K., Ng, L. L. and Kaplan, I. R. (1985) Determination of organic acids (C_1–C_{10}) in the atmosphere, motor exhausts, and engine oils, *Environ, Sci. Technol.* **19**, 1082–1086.

Kawamura, K. and Kaplan, I. R. (1984) Capillary gas chromatography determination of volatile organic acids in rain and fog samples. *Anal. Chem.* **56**, 1616–1620.

Keene, W. C. and Galloway, J. N. (1984) Organic acidity in precipitation of North America. *Atmos. Environ.* **18**, 2491–2497.

Keene, W. C. and Galloway, J. N. (1986) Considerations regarding sources for formic and acetic acids in the troposphere. *J. Geophys. Res.* **91**, 14466–14474.

Keene, W. C., Galloway, J. N. and Holden, J. D. (1983) Measurement of weak organic acidity in precipitation from remote areas of the world. *J. Geophys. Res.* 88, 5122–5130.

Lazrus, A., Kok, G. L., Gitlin, S. N., Lind, J. A. and McLaren, S. E. (1985) Automated fluorometric method for hydrogen peroxide in atmospheric precipitation. *Anal. Chem.* **57**, 917–922.

Mason, B. J. (1971) *The Physics of Clouds*, 2nd Ed., Oxford University Press, London.

McElroy, W. J. (1986) Sources of hydrogen peroxide in cloud water. *Atmos. Environ.* **20**, 427–438.

Munger, J. W., Collett, J., Jr., Daube, B. D., Jr. and Hoffmann, M. R. (1989) Carboxylic acids and carbonyl compounds in southern California clouds and fogs. *Tellus*, in press.

Nash, T. (1953) The colorimetric estimation of formaldehyde by means of the Hantszch reaction. *Biochem. J.* **55**, 416–421.

National Oceanic and Atmospheric Administration (1988a) California climatological data, April 1988, **92**, No. 4, 52 p.

National Oceanic and Atmospheric Administration (1988b) Local climatological data – Bakersfield, CA, April 1988, available from the National Climatic Data Center, Asheville, NC, 4 p.

National Oceanic and Atmospheric Administration (1988c) Local climatological data – Fresno, CA, April 1988, available from the National Climatic Data Center, Asheville, NC, 4 p.

Pilinis, C. and Seinfeld, J. H. (1987) Continued development of a general equilibrium model for inorganic multicomponent atmospheric aerosols. *Atmos. Environ.* **21**, 2453–2466.

Reitz, E. B. (1980) The stabilization of small concentrations of formaldehyde in aqueous solutions. *Analyt. Lett.* **13**, 1073–1084.

Seinfeld, J. H. (1986) *Atmospheric Chemistry and Physics of Air Pollution,* John Wiley. New York, 738 pp.

Smith, R. V. and Erhardt, P. W. (1975) Nash determination for formaldehyde in the presence of bisulfite. *Anal. Chem.* **47**, 2462–2454.

Smith, T. B., Lehrman, D. E., Reible, D. D. and Shair, F. H. (1981) The origin and fate of airborne pollutants within the San Joaquin Valley. Final Report to California Air Resources Board, Sacramento, CA.

Solorzano, L. (1967) Determination of ammonia in natural waters by the phenol–hypochlorite method. *Limnol. Oceanogr.* **14**, 799–801.

Steinberg, S. and Kaplan, I. R. (1984) The determination of low molecular weight aldehydes in rain, fog, and mist by reversed phase liquid chromatography of the 2,4–dinitrophenyl hydrazone derivatives. *Intern. J. Environ. Anal. Chem.* **18**, 253–266.

Stockwell, W. R. (1986) A homogeneous gas phase mechanism for use in a regional acid deposition model. *Atmos. Environ.* **20**, 1615–1632.

Talbot, R. W., Beecher, K. M., Harriss, R. C. and Cofer, W. R., III. (1988) Atmospheric geochemistry of formic and acetic acids at a mid–latitude temperate site. *J. Geophys. Res.* **93**, 1638–1652.

Yoshizumi, K., Aoki, K., Nouchi, I., Okita, T., Kobayashi, T., Kamakura, S. and Tajima, M. (1984) Measurements of the concentration in rainwater and of the Henry's law constant of hydrogen peroxide. *Atmos. Environ.* **18**, 395–401.

CHAPTER 4

SPATIAL AND TEMPORAL VARIATIONS IN PRECIPITATION AND CLOUD INTERCEPTION IN THE SIERRA NEVADA MOUNTAINS OF CENTRAL CALIFORNIA

Introduction

Interception of fog and clouds by forests has been shown to remove significant quantities of water, nutrients, and pollutants from the atmosphere. This is particularly true for forests growing near the ocean, or on mountain slopes, which are frequently immersed in fog or clouds. Kerfoot (1968) and Schemenauer (1986) have reviewed several studies undertaken to examine this phenomenon. In some cases, intercepted cloudwater has been estimated to deposit as much water as rainfall deposits. Kerfoot (1968) cites several instances where interception of cloudwater is believed to supply the water necessary for the survival of certain plant varieties in otherwise inhospitable habitats.

The rate of cloudwater deposition depends strongly on four factors: (1) the liquid water content (LWC) of the fog or cloud, (2) the droplet size distribution, (3) the structure of the forest canopy, and (4) the ambient wind speed (Lovett and Reiners, 1986). Cumulative deposition over a specified period of time also depends on the frequency and duration of fog or cloud interception in that interval.

The quantity of cloudwater deposited to the forest on a mountain slope may vary significantly with elevation, due to variations in the parameters governing the deposition process. Cloudwater deposition may increase with elevation, due to increases in average wind speeds and higher liquid water contents. The most important factor determining the elevational dependence of cloudwater deposition, however, is the elevational pattern of cloud interception. Different meteorological conditions may tend to favor cloud interception at different elevations. The upper boundary of coastal stratus clouds, for example, may be limited to 500 to 1000 m elevation by the presence of a strong temperature inversion. Cloud interception in

this environment will occur primarily at elevations at or below the predominant inversion height. Alternatively, convective clouds associated with frontal systems often have base elevations exceeding 1500 m; thus, these clouds will be intercepted most frequently at higher elevations. Schemenauer et al. (1987) found that deposition rates of cloudwater to passive cloudwater collectors located on a coastal mountain in Chile were maximal at 700 m and decreased at higher elevations. While this pattern presumably reflects a prevalence of cloud interception at 700 m elevation, their monitoring system did not actually collect information regarding the frequency or duration of interception, which could support or refute this hypothesis.

In the southern and central Sierra Nevada Mountains of California, interception of cloudwater by the forest canopy is believed to contribute significantly to regional deposition budgets for water, nutrients, and pollutants (Chapters 1, 2; Collett et al., 1989). Three mechanisms are thought to lead to the interception of fog and clouds in the region: (1) the passage of frontal systems, which often leads to interception of convective clouds by the mountain slopes; (2) local formation of fog due to the rapid cooling of moist air produced during snow melt on sunny days; and (3) the lifting of dense "Tule" fogs previously trapped near the floor of the San Joaquin Valley (Jacob et al., 1986), due to a reduction in atmospheric stability over the valley. In conjunction with a study of the chemical composition of intercepted cloudwater in the Sierra (Chapter 2), a field program was initiated to evaluate the frequency and duration of cloudwater interception, as a function of elevation, in Sequoia and Yosemite National Parks. The results of this investigation, which are essential for determining which elevations in the Sierra are likely to be affected by the deposition of cloudwater, are described in this chapter.

Experimental Procedure

Monitoring Sites

Fourteen Sierra sites were selected to serve as cloudwater monitoring stations throughout the course of the study, which lasted from September, 1987 until November, 1988. Eight of the sites, referred to as SQ1 through SQ8, were located in Sequoia National Park (Figure 4.1); six, YO1 through YO6, were located in Yosemite National Park (Figure 4.2). The chemical composition of intercepted cloudwater was monitored at sites YO3 and SQ5 (see Chapter 2). Sites were generally located in open areas where ambient clouds could intercept the site directly, although two stations (SQ4 and YO1) were situated in sparse woodland. Sites were selected so that an elevational gradient was represented in each Park; sites also were chosen to represent roughly the same range of elevations in the two Parks, in order to facilitate regional comparisons. Several factors prevented the selection of entirely comparable sites. Sites generally could not be highly visible to Park visitors, could not be located in designated wilderness areas, and had to be accessible by foot. Figures 4.3 and 4.4 illustrate the elevations of the chosen sites in Sequoia and Yosemite National Parks, respectively. The elevational gradient represented in Sequoia National Park stretched from 820 to 2360 m; site elevations in Yosemite National Park ranged from 1220 to 2300 m.

Equipment

Intercepted cloudwater was collected at each site using a passive cloudwater monitoring system, described in detail in Chapter 5. This system included a passive cloudwater collector, which utilized ambient winds to collect cloudwater droplets by

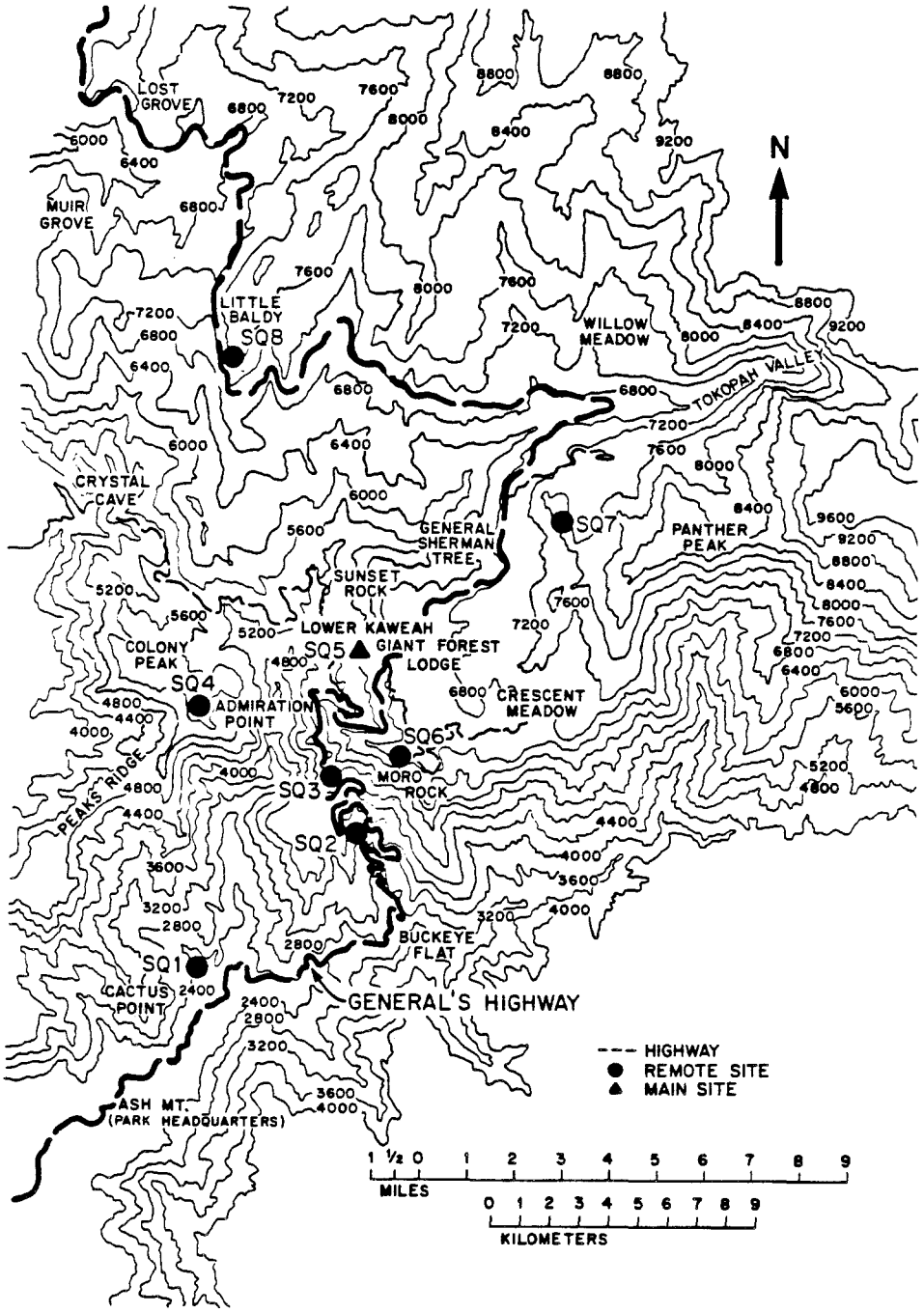

Figure 4.1. Map of Sequoia National Park indicating the locations of the cloudwater monitoring sites, labeled as remote and main sites. SQ5, labeled as a main site, also was utilized to collect cloudwater samples for chemical analysis (see Chapter 2). Contours are labeled in feet.

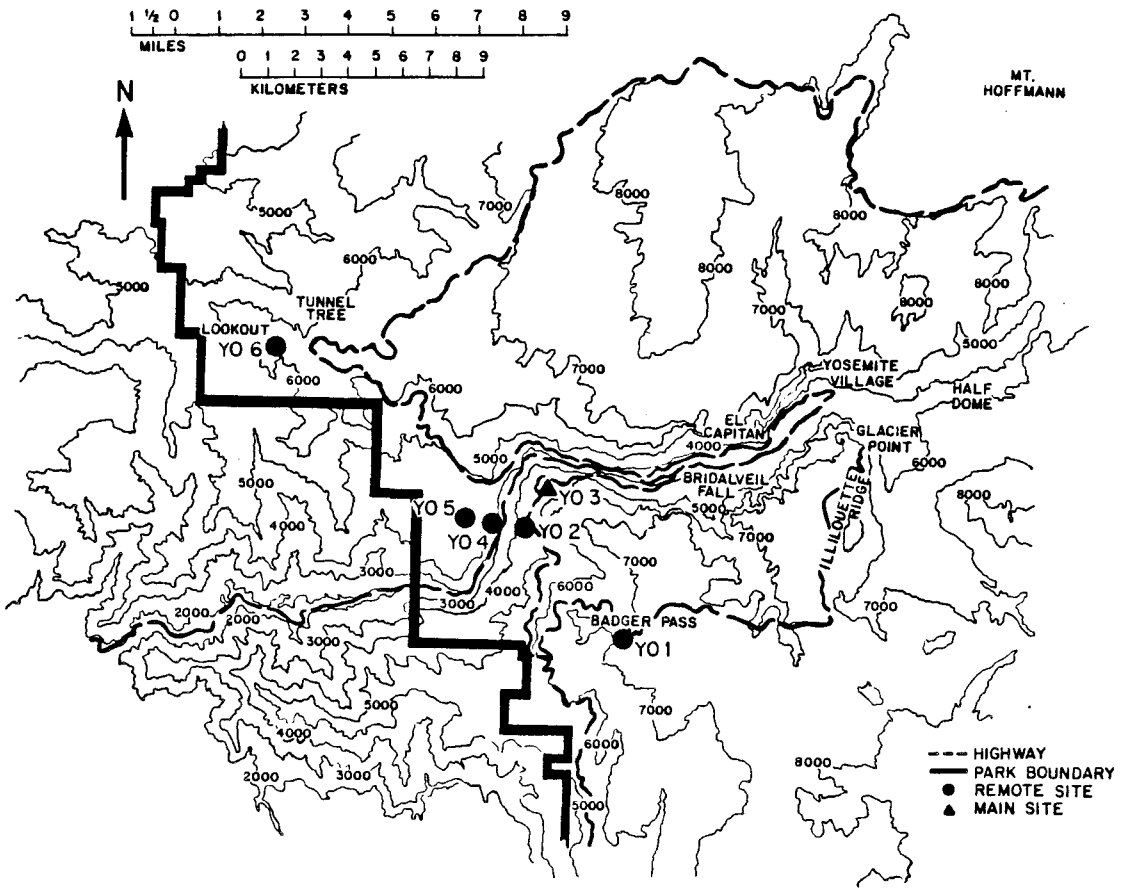

Figure 4.2. Map of Yosemite National Park indicating the locations of the cloudwater monitoring sites, labeled as remote and main sites. YO3, labeled as a main site, also was utilized to collect cloudwater samples for chemical analysis (see Chapter 2). Contours are labeled in feet.

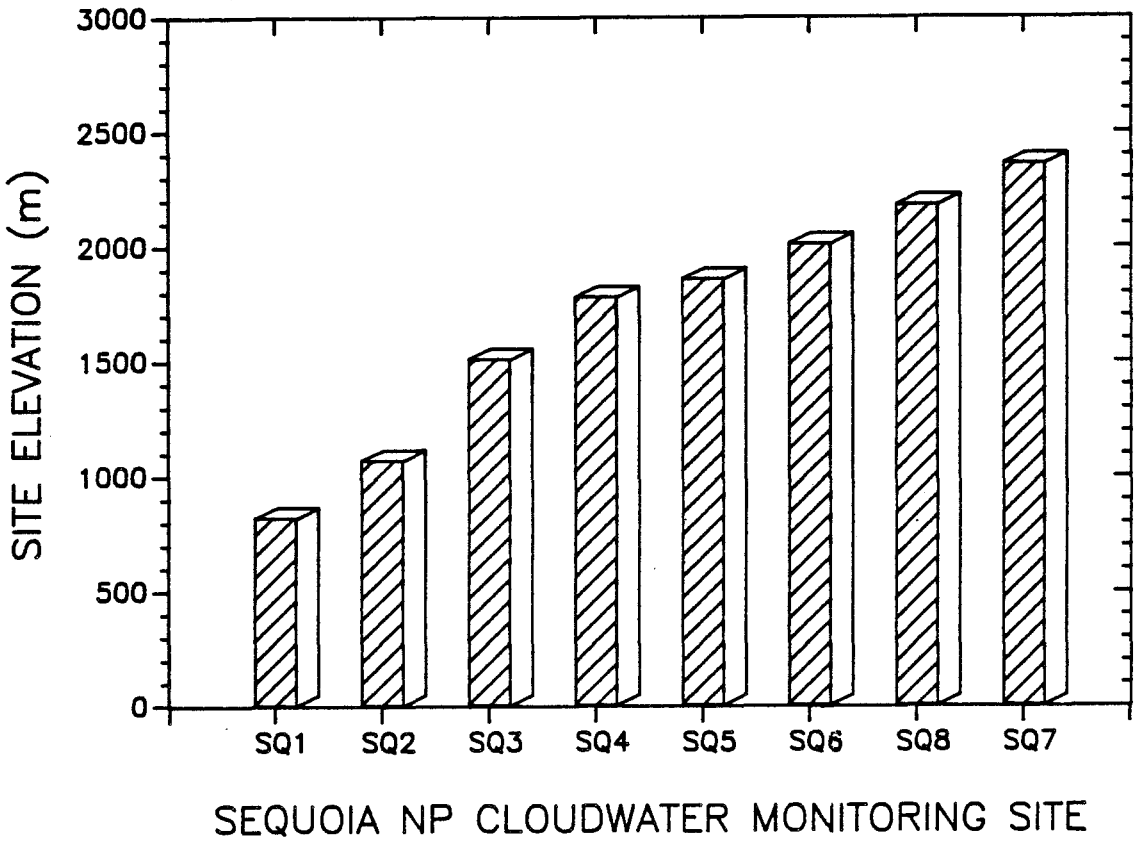

Figure 4.3. Elevations of the cloudwater monitoring sites in Sequoia National Park.

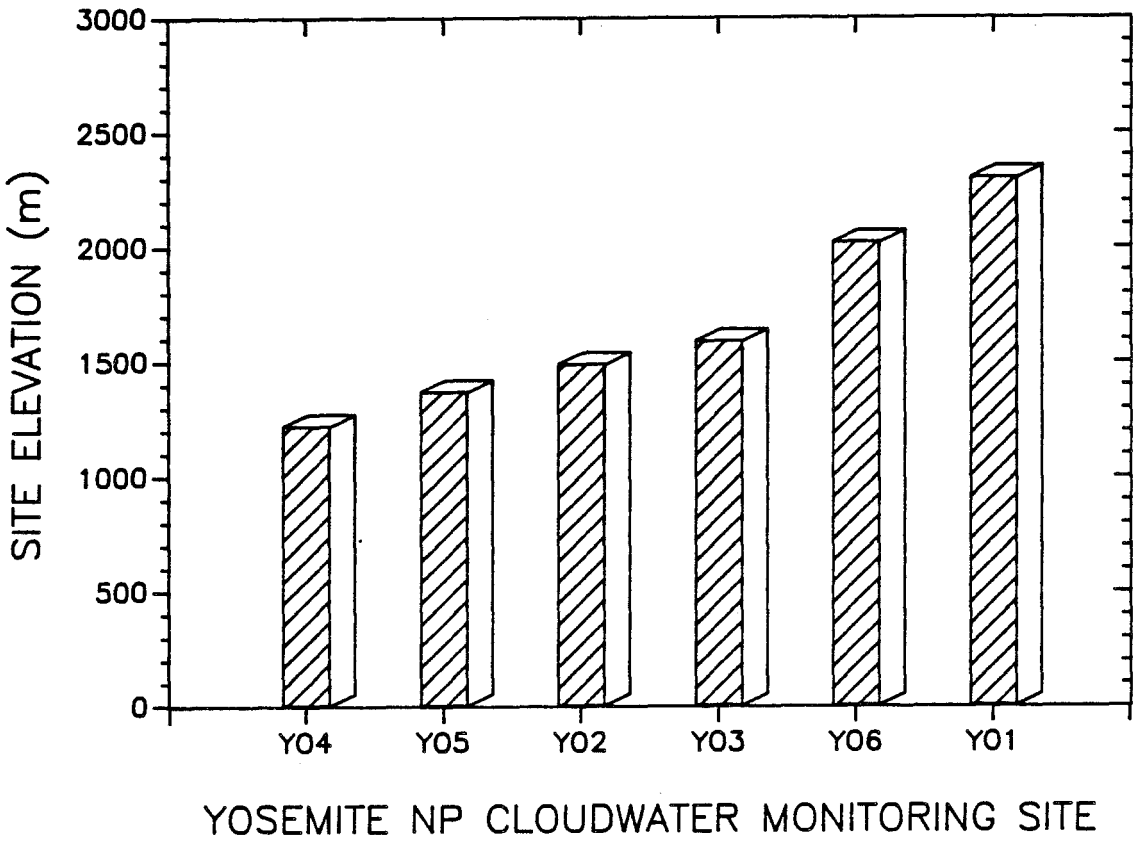

Figure 4.4. Elevations of the cloudwater monitoring sites in Yosemite National Park.

inertial impaction. Use of a passive collector, rather than an active collector, served to minimize power requirements (all power had to be supplied from batteries carried in to each site), and to provide a good record of only those interception periods when ambient winds were high enough to produce significant rates of cloudwater deposition to the forest canopy. The monitoring system also includes a tipping cup gauge which measures the volume of cloudwater collected, an anemometer which measures ambient wind speeds during interception, a tipping cup rain gauge which measures rainfall at the site, a data–logging system, and two 6 V batteries which supply all power used at the site.

Sites were serviced monthly. Data was transferred from the data–logger to an NEC Multispeed portable computer carried to each site. After transferring the data, the monitoring system was checked to make sure that the equipment was functioning properly, and the batteries were replaced. In the event of damage to the equipment or equipment malfunction, an attempt was made to remedy the problem at the site. When this was not possible, due to extensive damage or an unanticipated malfunction, site operations had to be discontinued, or at least curtailed, until the next visit. The most common problems encountered were failure of components in the data–logging system, bugs in the data–logging software, and equipment damage by curious black bears.

The tipping cup gauges used to measure collected volumes of rainfall and intercepted cloudwater were identical. The gauges tip every time 8.7 ml of water are collected, corresponding to 0.26 mm of rainfall for the rain gauge and 0.46 mm of intercepted cloudwater for the passive cloudwater collector. Predicting actual rates of cloudwater deposition to the nearby forest canopy, based on observed rates of deposition to the passive cloudwater collector, is difficult because the structure of

the canopy is largely unknown. Furthermore, the structure varies considerably from one location to another. Dasch (1988) and Lovett (1984) modeled cloudwater deposition to two eastern U.S. fir stands with total surface area indexes (SAI) of 6 and 7, respectively (SAI is defined as the ratio of the total surface area of a canopy component to the corresponding plan area). Trees studied in both areas were approximately 10 m high. Taller trees in the Sierra probably have greater values of SAI. The SAI of the passive cloudwater collector is 11.8, suggesting that deposition rates to this instrument are probably roughly comparable to cloudwater deposition rates experienced by the larger exposed conifers in the Sierra. Deposition rates to trees within a closed canopy will be considerably lower because of reduced wind speeds within the canopy and removal of droplets by trees located upwind.

Data Processing

The data record from each site includes a log of the number of tips recorded by each tipping cup counter (rain and cloudwater) during the monitoring period, and the time at which each tip occurred. Five minute average wind speeds were also recorded during all periods of precipitation or cloud interception. The design of the data–logging system limited observations to a single output at a time (tipping cup gauges or anemometer). In order to accommodate this restriction, the data–logger program contained a loop which alternately monitored the status of each input. The time required to execute this loop depends on the wind speed, since a wind speed measurement subroutine in the loop monitors one full period of the sinusoidal output of the anemometer, the length of which is inversely proportional to the anemometer's rotational velocity. If the length of the period exceeds a predetermined time, corresponding to a wind speed of approximately 0.5 m s^{-1}, execution of the subroutine is terminated. In order not to miss any pulses generated

by tips of the rain or cloudwater gauges, which might occur while the wind speed subroutine is executed, the data logging circuitry lengthens the duration of the incoming pulses. Initially the pulses were lengthened to approximately one second. Longer pulses were not used, so that the chance of obtaining overlapping responses from the two gauges would be reduced. At low wind speeds ($\leq$ 1 m s^{-1}), however, execution of the wind speed subroutine requires slightly longer than one second, consequently, rain or cloudwater tips occurring right at the beginning of the subroutine go undetected under these conditions. We estimate, based on field experiments, that the percentage of tips missed during low wind speeds is approximately 10% using this system. Because of the prevalence of low wind speeds observed during cloud interception and rainfall during the fall of 1987, the system was modified for the spring sampling period by lengthening the pulse duration. While this modification resulted in a few cases of overlapping responses from the two gauges, it eliminated the problem of underestimating rainfall and cloud interception at low wind speeds.

As indicated in Chapter 5, data collected by the data-logger was stored as compactly as possible to reduce the memory requirements. Data collected from the data-loggers was first processed by a BASIC program which converted the compact data to a form which was more readily analyzed. The transformed data was then imported into a spreadsheet file for further processing. Since the passive cloudwater collector is an efficient collector of rain as well as intercepted cloudwater, the tips of the cloudwater gauge had to be partitioned into two groups: those due to rainfall and those due to cloudwater. Partitioning was possible only because of the simultaneous collection of rainfall data at each site. Experiments designed to compare the relative responses to rainfall exhibited by the cloudwater collector and the rain gauge indicated essentially equivalent responses at wind speeds between 1.5

and 3 m s^{-1}; however, preferential collection of rainfall by the rain gauge was observed at lower wind speeds (see Chapter 5). Similar patterns were observed in Sierra field data during periods of rainfall without simultaneous cloud interception; consequently, tips of the cloudwater gauge, observed during rainfall, were removed from the Sierra site records, on a one–to–one correspondence with observed tips of the rain gauge. This method of eliminating the rain response of the cloudwater gauge is believed to provide a slightly conservative estimate of the overall quantity of intercepted cloudwater.

Results and Discussion

Cloudwater interception was monitored at the fourteen Sierra monitoring stations from September, 1987 through October, 1988, although some of the sites were not in use during the entire period. Approximately half of the sites were removed during the winter months because freezing of the intercepted cloudwater on the collection strands of the passive cloudwater collector would prevent measurement of the volume collected, and could lead to strand breakage. Snowfall collected by both the rain gauge and the cloudwater collector also creates data interpretation difficulties. Some of the lower elevation sites were left in place through the winter, however, to test winter operation of the system and to obtain a record of cloud interception at lower elevations during this period. One of the sites in Yosemite, YO1, was accidentally damaged when it was removed by untrained personnel in November of 1987. In addition to the equipment damage, data collected by this station during late October and early November was lost as well. This station was not used following this incident.

Figures 4.5 through 4.9 illustrate the record of rainfall and cloudwater

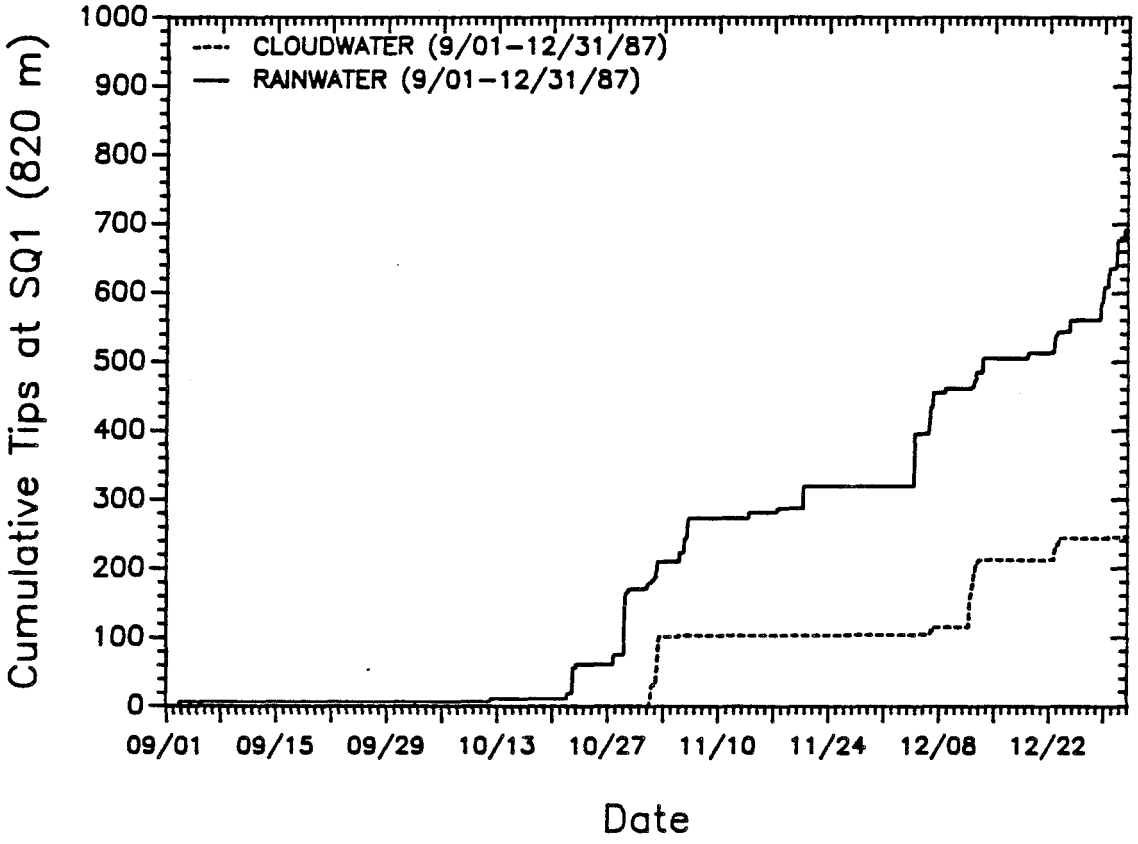

Figure 4.5. Precipitation and cloudwater deposition at SQ1 (elev. 820 m) during the fall of 1987. Each tip of the rain gauge corresponds to 0.26 mm of precipitation; each tip of the cloudwater gauge corresponds to 0.46 mm of deposited cloudwater.

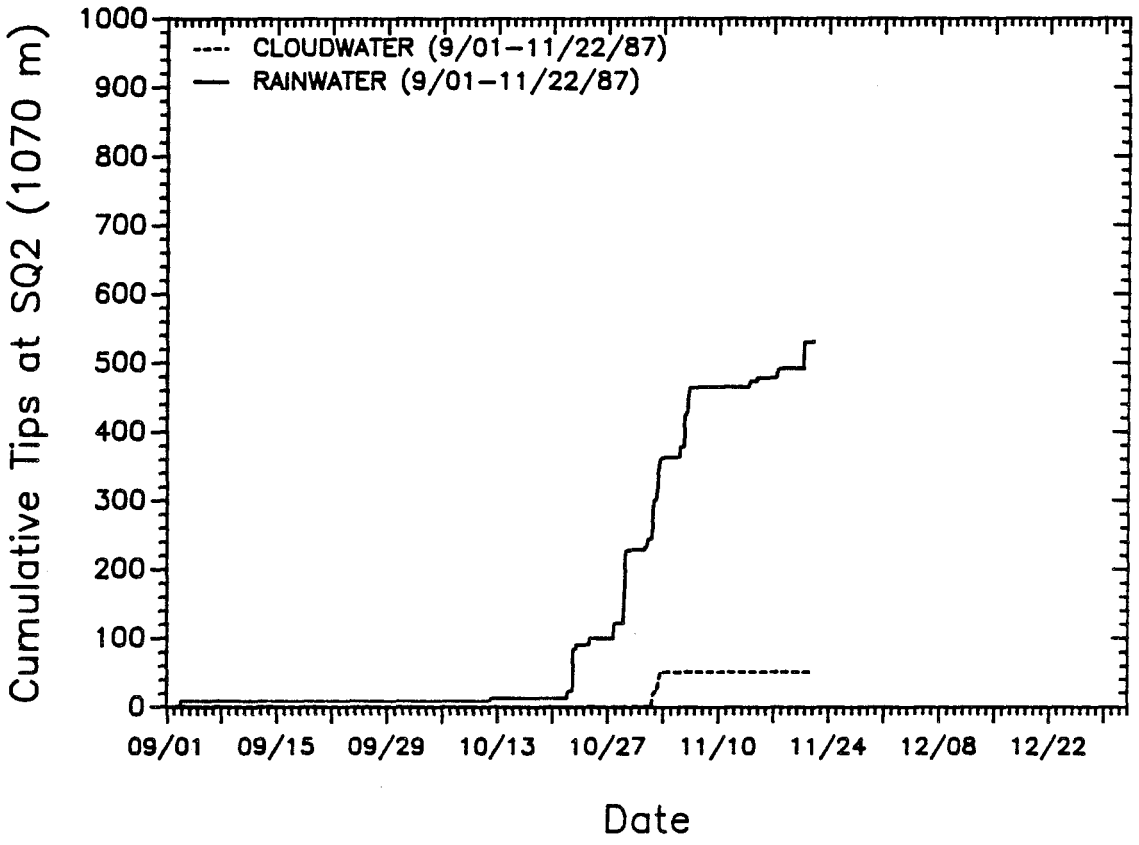

Figure 4.6. Precipitation and cloudwater deposition at SQ2 (elev. 1070 m) during the fall of 1987. Each tip of the rain gauge corresponds to 0.26 mm of precipitation; each tip of the cloudwater gauge corresponds to 0.46 mm of deposited cloudwater.

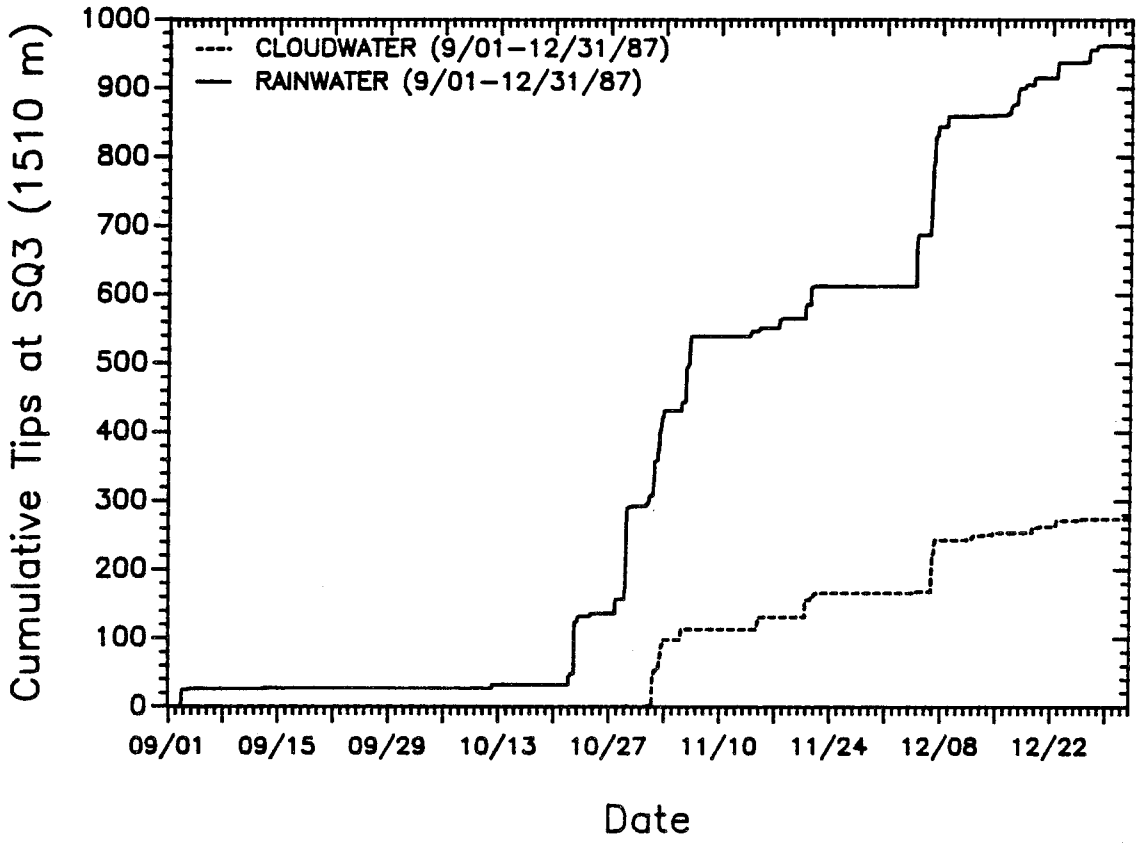

Figure 4.7. Precipitation and cloudwater deposition at SQ3 (elev. 1510 m) during the fall of 1987. Each tip of the rain gauge corresponds to 0.26 mm of precipitation; each tip of the cloudwater gauge corresponds to 0.46 mm of deposited cloudwater.

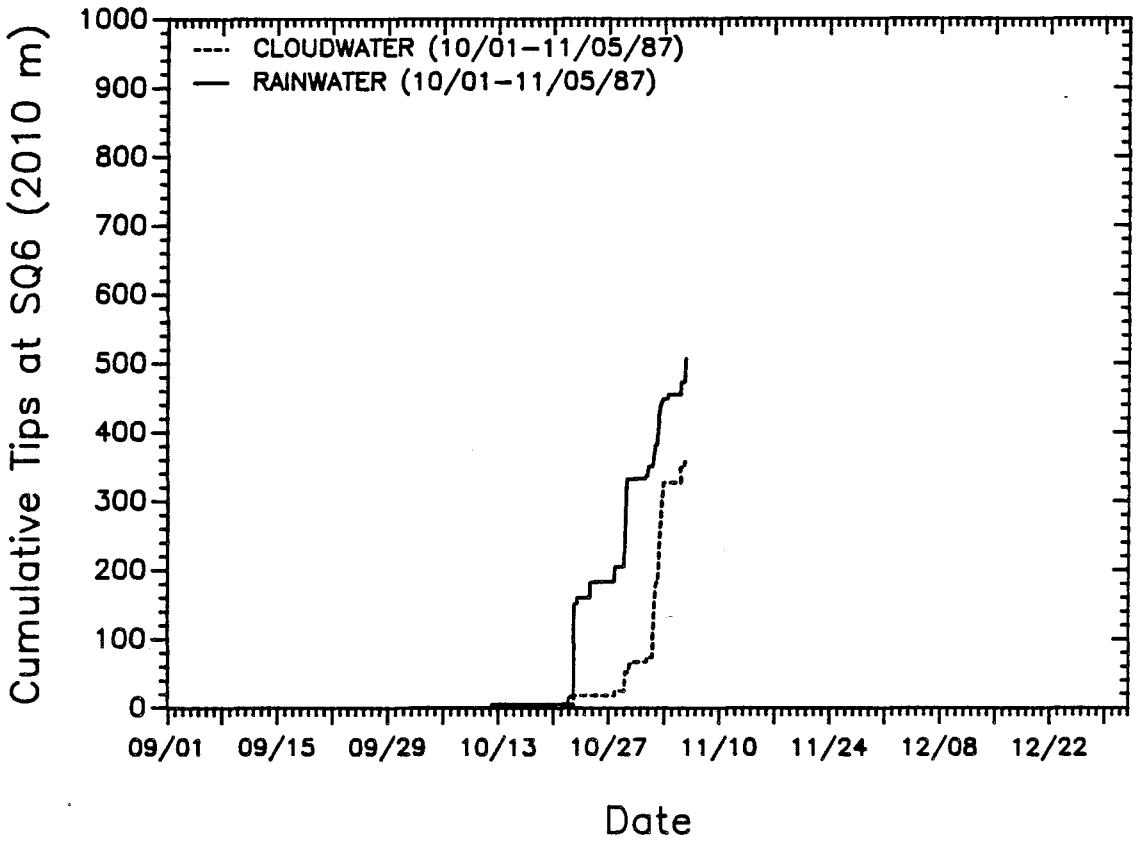

Figure 4.8. Precipitation and cloudwater deposition at SQ6 (elev. 2010 m) during the fall of 1987. Each tip of the rain gauge corresponds to 0.26 mm of precipitation; each tip of the cloudwater gauge corresponds to 0.46 mm of deposited cloudwater.

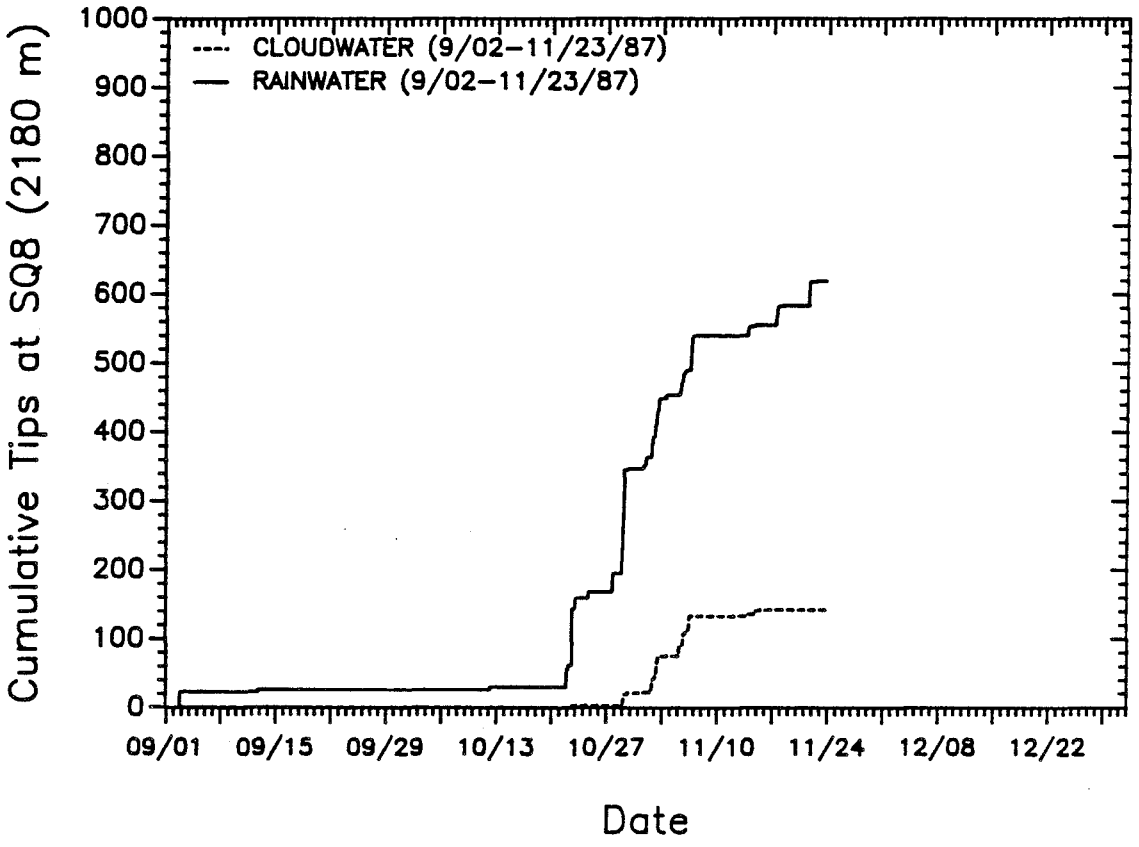

Figure 4.9. Precipitation and cloudwater deposition at SQ8 (elev. 2180 m) during the fall of 1987. Each tip of the rain gauge corresponds to 0.26 mm of precipitation; each tip of the cloudwater gauge corresponds to 0.46 mm of deposited cloudwater.

deposition for sites SQ1, SQ2, SQ3, SQ6, and SQ8, respectively, from September through mid–November of 1987 (records for some of the sites extend through December). The ordinate in each plot depicts the number of tips by each gauge at the given site; the abscissa represents time. Precipitation contributions to the cloudwater collector record have already been subtracted. Little activity in the way of precipitation or cloud interception was observed before late October, but late October and early November comprised the most active period of cloud interception observed during the study. Rainfall collected at all five sites exceeded the amount of deposited cloudwater, on an absolute basis. Typically the ratio of rainfall collected to cloudwater collected was on the order of three or four during this period, although at SQ6 the ratio was only slightly higher than one. SQ6 (elev. 2010 m) is located on a fairly open ridge top and at least part of the increased cloudwater deposition at this site is attributable to higher wind speeds observed during cloud interception. We also can compare the hydrological inputs of rainfall and cloud interception per square meter of surface area covered by each collector. Recalling that each tip of the rain gauge corresponds to 0.26 mm of rainfall, while each tip of the cloudwater gauge corresponds to nearly twice as much deposited cloudwater (0.46 mm), it is clear that cloudwater interception is an important phenomenon at these sites. On the basis of deposition per unit area, it seems likely that the input of cloudwater to exposed conifers near SQ6 exceeded the input from rainfall during this period. Since the roots of each tree have access to rainfall deposited in some undefined region beyond this area, however, exact apportionment of the hydrological deposition to the tree is not possible.

It is instructive to examine rates of cloudwater deposition to the passive collectors during individual events, to assess the magnitude of deposition rates observed. Deposition rates during the fall of 1987 typically were observed to be the

largest at SQ6. During a 2.5–hour period on the evening of October 28, 1987, cloudwater was deposited to the collector at SQ6 at an average rate of 4.0 mm hr^{-1}; a rate of 1.2 mm hr^{-1} was observed during a 4–hour period the following day. Cloudwater deposition rates at SQ6, during an extended interception event on November 1, averaged 4.3 mm hr^{-1} over an 11–hour period. Wind speeds ranged from 1 to 3 m s^{-1} during this period. High deposition rates also were observed at other monitoring stations. During an overlapping 7–hour period on November 1, cloudwater deposition to the collector at SQ3 (1510 m) averaged 3.1 mm hr^{-1}. These deposition rates are somewhat greater than reported for deposition to an exposed redwood in northern California (1.6 mm hr^{-1}; Azevedo and Morgan, 1974), and much higher than reported for cloudwater deposition to a single exposed 10 m fir tree on the summit of Clingmans Peak in North Carolina (0.3 mm hr^{-1}; Dasch, 1988). The surface area index of the tree studied by Dasch (1988) was estimated to be approximately half that of our collector, suggesting that larger cloudwater deposition rates experienced by the collector in this study probably are indicative of substantially higher deposition rates to exposed conifers near the sites as well.

Cloudwater concentrations of NO_3^- and NH_4^+ are typically an order of magnitude or more higher in Sequoia National Park (SNP) than SNP precipitation concentrations of these same species (see Chapter 2). Therefore, it is likely that the deposition of these species to exposed conifers near SQ3, SQ6, and SQ8, via cloud interception, exceeded that due to precipitation during the fall of 1987; deposition of SO_4^{2-} probably also was dominated by cloudwater interception, at least at SQ6, since SO_4^{2-} concentrations average more than three times higher in SNP cloudwater than in SNP precipitation (Chapter 2). Cloudwater deposition rates to trees located in closed canopies in the region are probably significantly lower than the rates hypothesized here for exposed trees (Lovett and Reiners, 1986; Dasch, 1988);

consequently, pollutant deposition to closed canopies may be dominated by rainfall or dry deposition.

Rainfall amounts at SQ2, SQ3, SQ6, and SQ8, from September through mid–November of 1987, were quite comparable (130–160 mm), while the lowest elevation site, SQ1, experienced considerably less rainfall (80 mm). Rainfall was generally observed simultaneously at most of the sites; amounts were just smaller at lower elevation (see Figures 4.5 through 4.9). A comparison of the cloudwater interception records illustrated in these figures reveals that cloud interception events, in contrast to rainfall, often occurred only at the higher elevation sites. This is a reflection of the fact that most of the intercepted clouds were associated with frontal systems approaching from the north or northwest, with cloud bases often located above 1500 m elevation.

Rainfall and cloudwater interception data for the fall of 1987 are presented for Yosemite National Park (YNP) sites YO2, YO3, YO4, and YO6 in Figures 4.10 through 4.13, respectively. Rainfall at YO2, YO4, and YO6 was comparable to that observed at the higher elevation SNP sites during the period ending in mid–November. Data for YO3 is missing for much of this period because of data–logger failure. Cloudwater deposition at YO2 (1490 m) and YO4 (1220 m) was fairly low during this period, somewhat less than was observed at the lowest elevation SNP site: SQ1 (820 m). YO2 and YO4 are situated on the slopes of the Merced River canyon. The canyon, which has a north–south orientation in this region, is relatively narrow, preventing most frontal system clouds, advancing from the west or northwest, from dropping into the canyon interior where these two sites are located. Cloudwater deposition at YO6 (2020 m) was greater than that observed at all but one of the Sequoia sites: SQ6. The timing of the interception

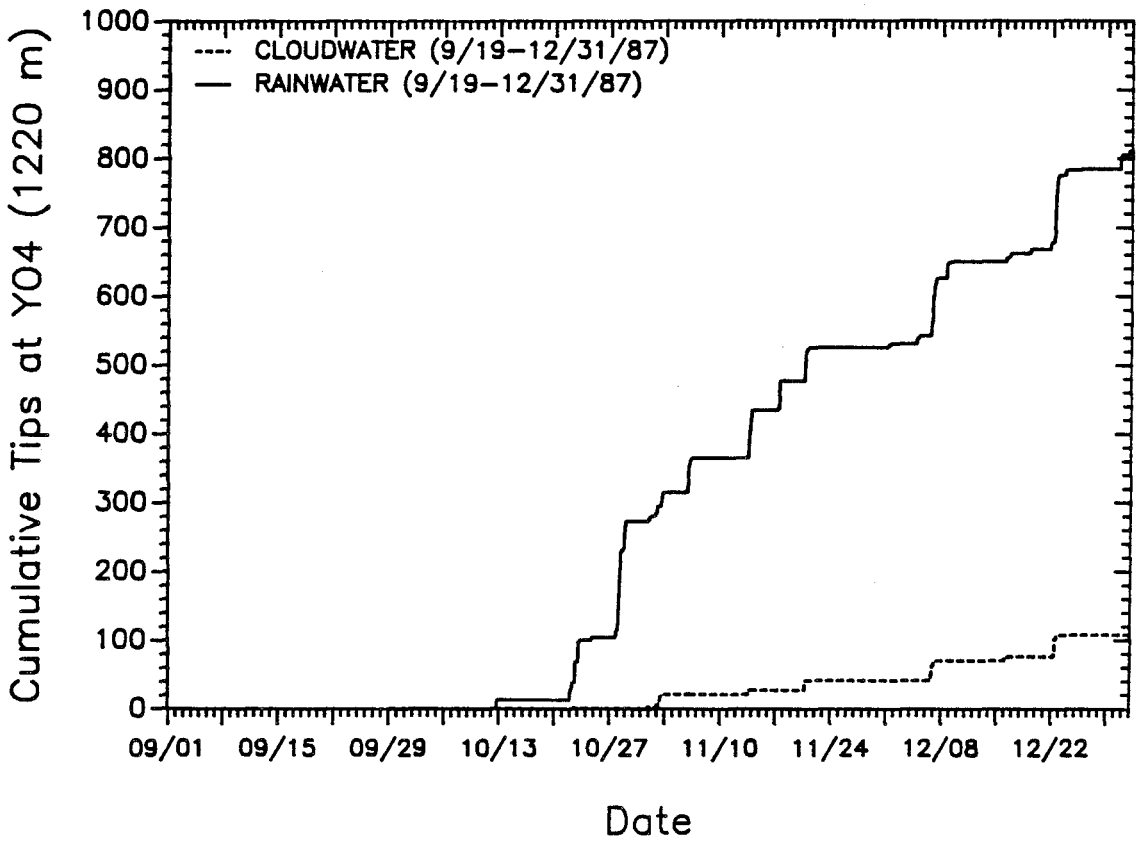

Figure 4.10. Precipitation and cloudwater deposition at YO2 (elev. 1490 m) during the fall of 1987. Each tip of the rain gauge corresponds to 0.26 mm of precipitation; each tip of the cloudwater gauge corresponds to 0.46 mm of deposited cloudwater.

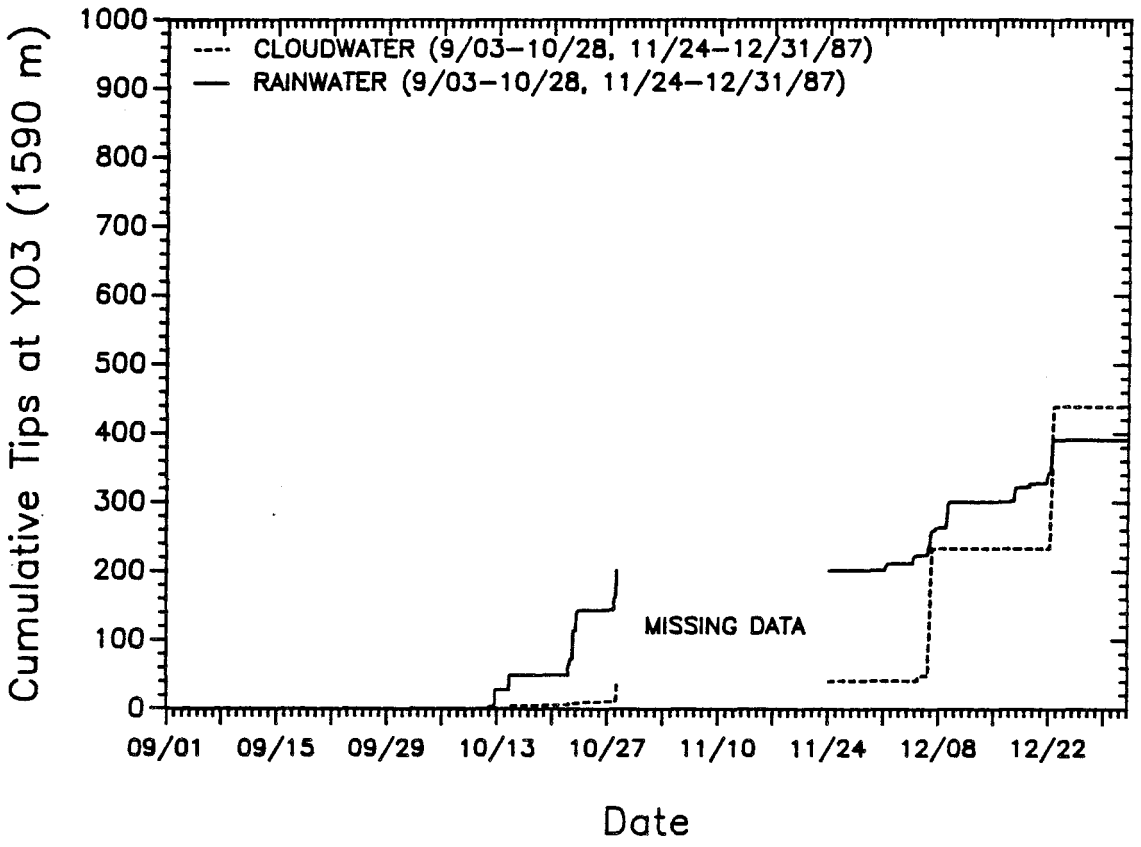

Figure 4.11. Precipitation and cloudwater deposition at YO3 (elev. 1590 m) during the fall of 1987. Each tip of the rain gauge corresponds to 0.26 mm of precipitation; each tip of the cloudwater gauge corresponds to 0.46 mm of deposited cloudwater.

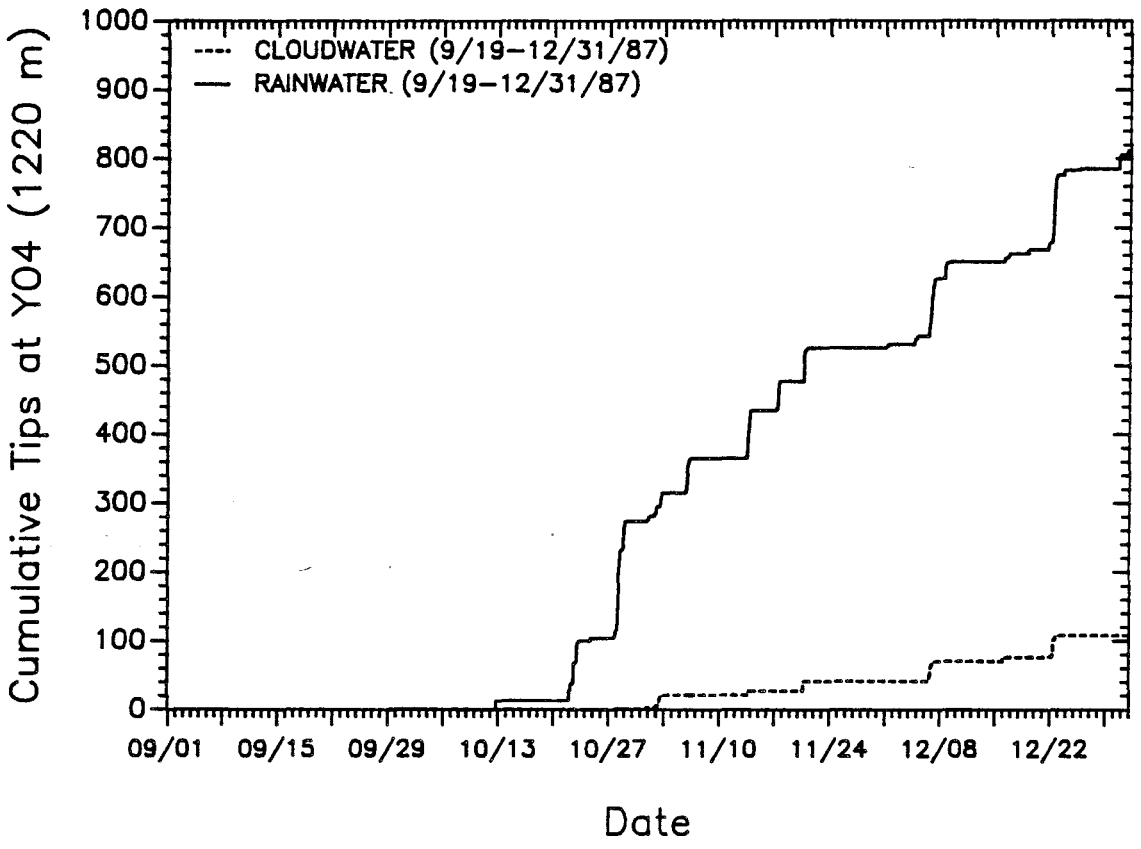

Figure 4.12. Precipitation and cloudwater deposition at YO4 (elev. 1220 m) during the fall of 1987. Each tip of the rain gauge corresponds to 0.26 mm of precipitation; each tip of the cloudwater gauge corresponds to 0.46 mm of deposited cloudwater.

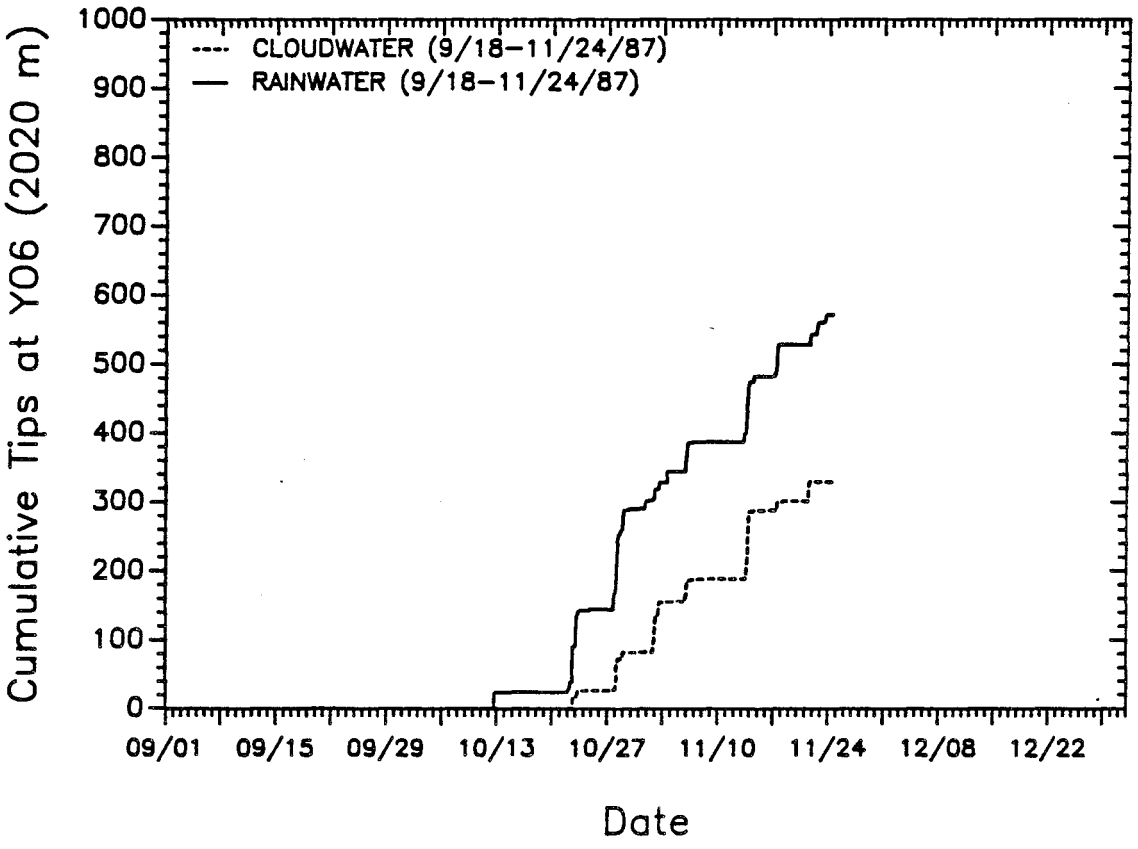

Figure 4.13. Precipitation and cloudwater deposition at YO6 (elev. 2020 m) during the fall of 1987. Each tip of the rain gauge corresponds to 0.26 mm of precipitation; each tip of the cloudwater gauge corresponds to 0.46 mm of deposited cloudwater.

events at YO6 also agreed quite well with that at both SQ6 and SQ8, which are located at 2010 m and 2180 m, respectively. YO6 is situated just below the summit of a fairly open hillside, and, like SQ6 and SQ8, has good exposure to the west.

Several cold fronts crossed the Sierra Nevada Mountains during the month of December, depositing a substantial amount of snow. Nevertheless, there were several cloud interception events at lower elevations that we were able to successfully monitor during this period. Data collected at sites SQ1 and SQ3, from late November through the end of 1987, are depicted in Figures 4.5 and 4.7. Rainfall during this period represents the sum of actual rainfall and snowmelt in the rain gauge. While cloudwater interception events during this period generally were witnessed simultaneously by both sites, the volume of cloudwater collected differed significantly between the two sites for a given event. Cloudwater interception on the late morning of December 22, for example, was much greater at SQ1 (820 m) than at SQ3 (1510 m). This interception event followed a period of dense fog in the southern San Joaquin Valley, which had persisted through most of December 21 and into the morning of December 22 (NOAA, 1987). Since much greater interception activity was observed at the lower site (SQ1) on December 22, it seems likely that the cloud interception was the result of lifting of the fog layer previously trapped near the valley floor. This observation indicates a need to monitor the chemical composition of cloudwater during the winter at lower elevation sites (500 to 1000 m) in SNP, since southern San Joaquin Valley fogs have been shown to be heavily polluted (Jacob et al., 1986).

Figures 4.10 through 4.12 display the observations made at sites YO2, YO3, and YO4, from late November through the end of December, 1987. The measured rainfall and cloudwater deposition patterns at YO2 and YO4 were quite similar.

Approximately 80 mm of rain and melted snow was measured at both sites during this period. Fifty percent more rain was measured at YO3; cloudwater deposition at YO3 was three times the levels observed at YO2 and YO4, despite the close proximity of these three sites (see Figure 4.2). Wind speeds at YO3 typically were observed to be much higher than at YO2 and YO4, providing a more conducive environment for high rates of cloudwater deposition. In addition, YO3 is situated on top of a granite dome, and is completely exposed to convective clouds approaching from almost any direction, whereas YO2 and YO4 are shielded somewhat by the walls of the Merced River canyon.

Major events involving both rainfall and cloudwater impaction were observed in both Parks on December 6 and December 22, 1987. In fact, there generally seems to be a high degree of correlation between periods of cloud interception and precipitation in the two Parks. In several cases, correlations between deposition rates at a given elevation in SNP and those at a similar elevation in YNP are much stronger than those between sites at different elevations in a single Park. This is not terribly surprising, given that much of the cloudwater deposition is due to interception of convective clouds associated with the passage of frontal systems across the Sierra. Often the cloud base in such systems lies above the elevations of several of the lower sampling sites, as observed previously, but the horizontal extent of the system may reach for several hundred kilometers, easily covering the 150 km between the two Parks. Nevertheless, there are many occasions when clouds are observed at one Park, but not at the other, particularly when the passing frontal system is centered in extreme northern or extreme southern California.

Data collection during the winter was greatly complicated by the presence of snow and rime ice. Since no temperature record was available at the sites, it is

difficult to ascertain whether tips of the two gauges during this period were due to cloud interception, rain, hail, or melting snow. In addition several problems were experienced with the data–loggers during this period. For this reason, only those data collected in December have been presented from the winter sampling period; however, as indicated in Chapter 2, relatively little cloud interception activity was observed during January, February, or March.

Data collected at the thirteen Sierra cloudwater monitoring sites (SQ1 through SQ8 and YO2 through YO6) between early May and late August, 1988 are presented in Figures 4.14 through 4.26 (little activity was recorded between the end of August and early November, when the stations were removed). While several rain events were observed over the course of the spring and summer, only two major cloud interception events were observed during this period. These occurred on May 17 and May 28, and were observed at almost all of the monitoring stations.

Amounts of cloudwater deposited in these two events generally were larger at the higher elevation sites, as was observed to be the case in most of the previous interception events. Total cloudwater deposition at SNP, in the two events, was dominated by contributions on May 17, while cloudwater deposition at YNP was generally greater in the May 28 event. Volumes of cloudwater collected at several of the sites in these two events were relatively large compared to the seasonal total precipitation. At YO3, in fact, the volume of cloudwater collected on May 28 exceeded the total volume of precipitation collected between early May and the end of October, underscoring the importance of cloudwater deposition in the Sierra. Rates of cloudwater deposition to the collector, during a 5–hour period on the evening of May 28, averaged more than 24 mm hr^{-1}. Wind speeds observed at the site during this period averaged approximately 10 m s^{-1}. A remarkably high

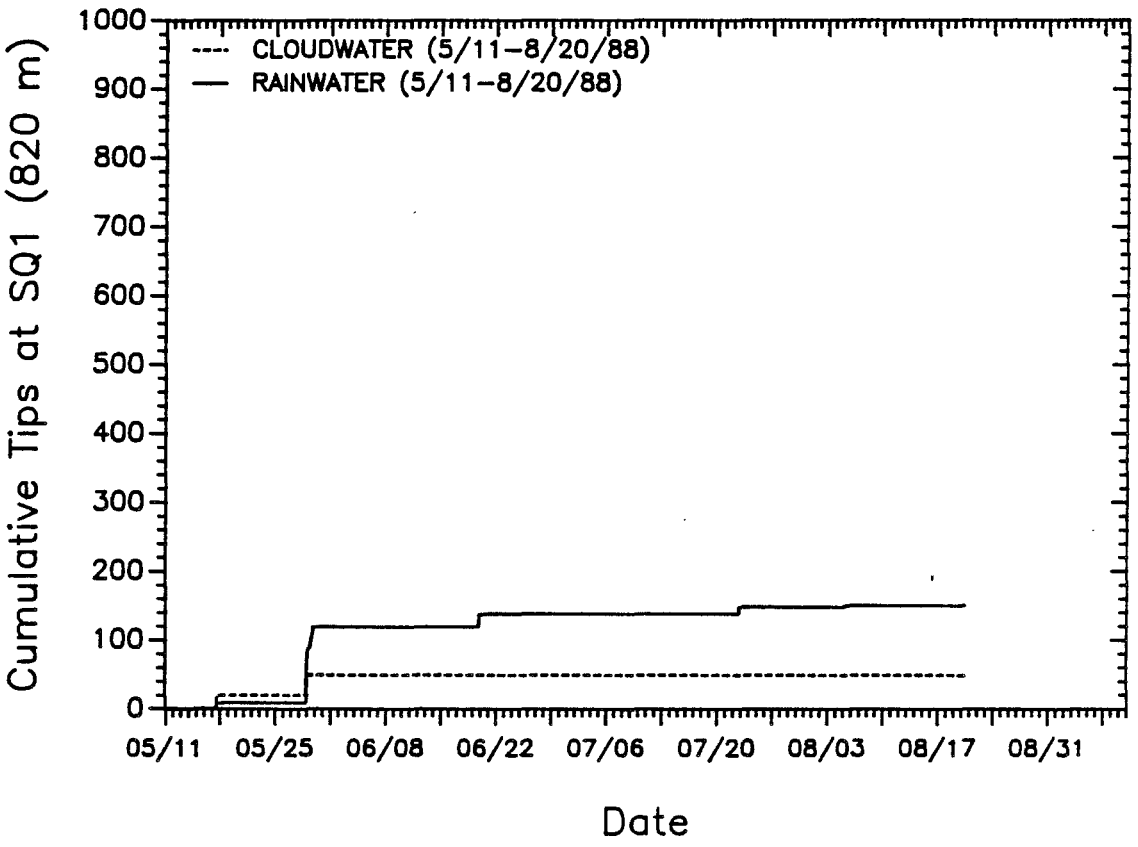

Figure 4.14. Precipitation and cloudwater deposition at SQ1 (elev. 820 m) during the spring and summer of 1988. Each tip of the rain gauge corresponds to 0.26 mm of precipitation; each tip of the cloudwater gauge corresponds to 0.46 mm of deposited cloudwater.

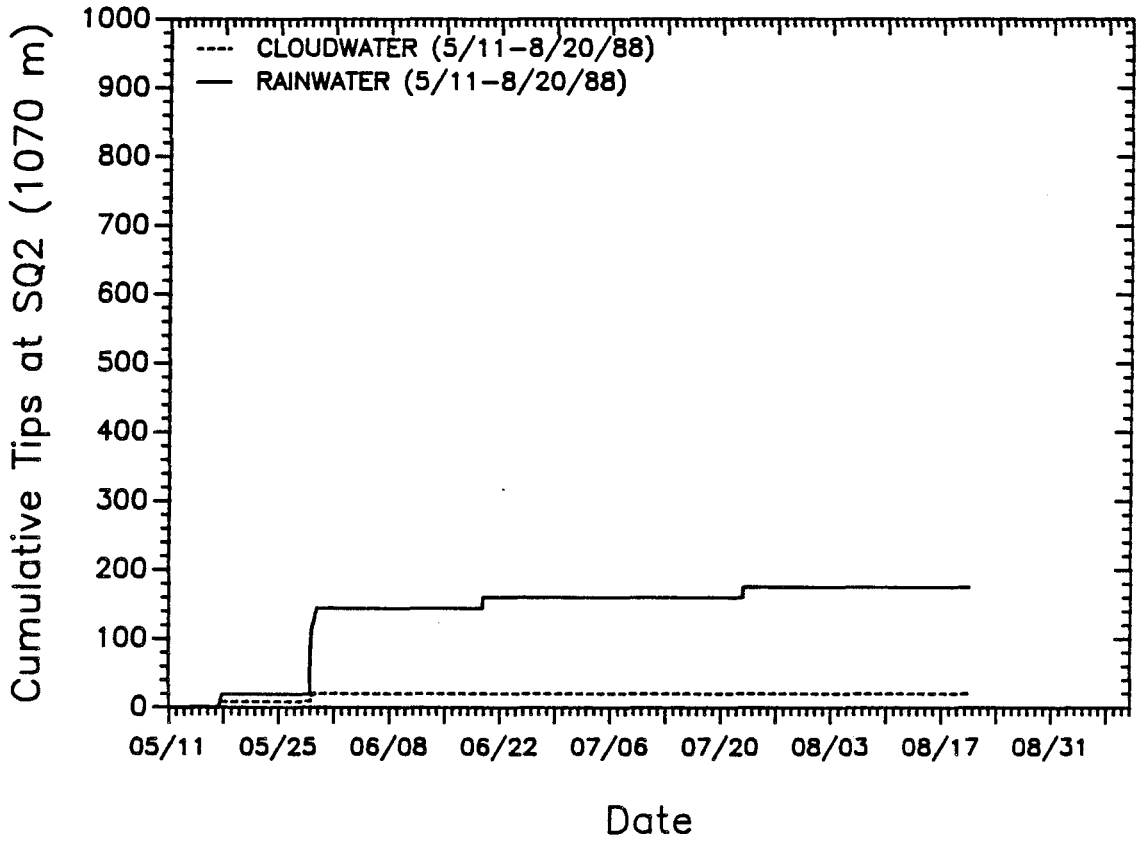

Figure 4.15. Precipitation and cloudwater deposition at SQ2 (elev. 1070 m) during the spring and summer of 1988. Each tip of the rain gauge corresponds to 0.26 mm of precipitation; each tip of the cloudwater gauge corresponds to 0.46 mm of deposited cloudwater.

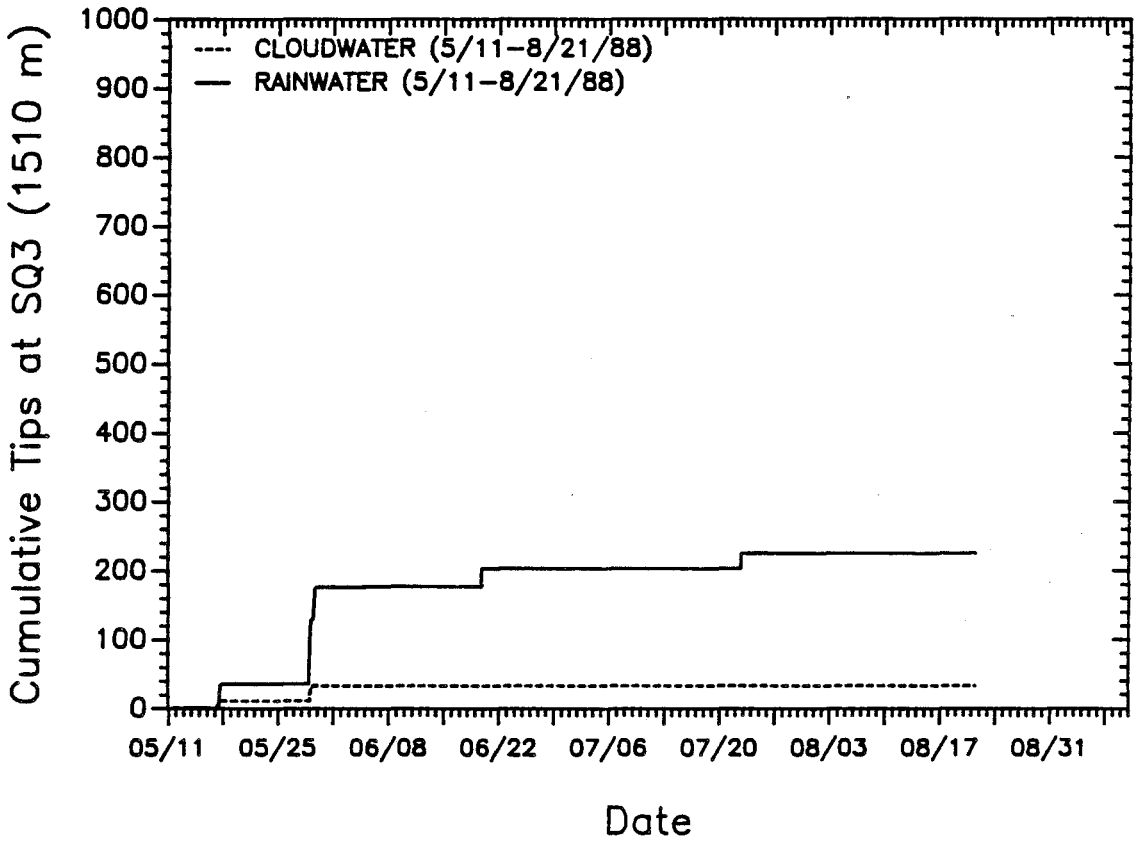

Figure 4.16. Precipitation and cloudwater deposition at SQ3 (elev. 1510 m) during the spring and summer of 1988. Each tip of the rain gauge corresponds to 0.26 mm of precipitation; each tip of the cloudwater gauge corresponds to 0.46 mm of deposited cloudwater.

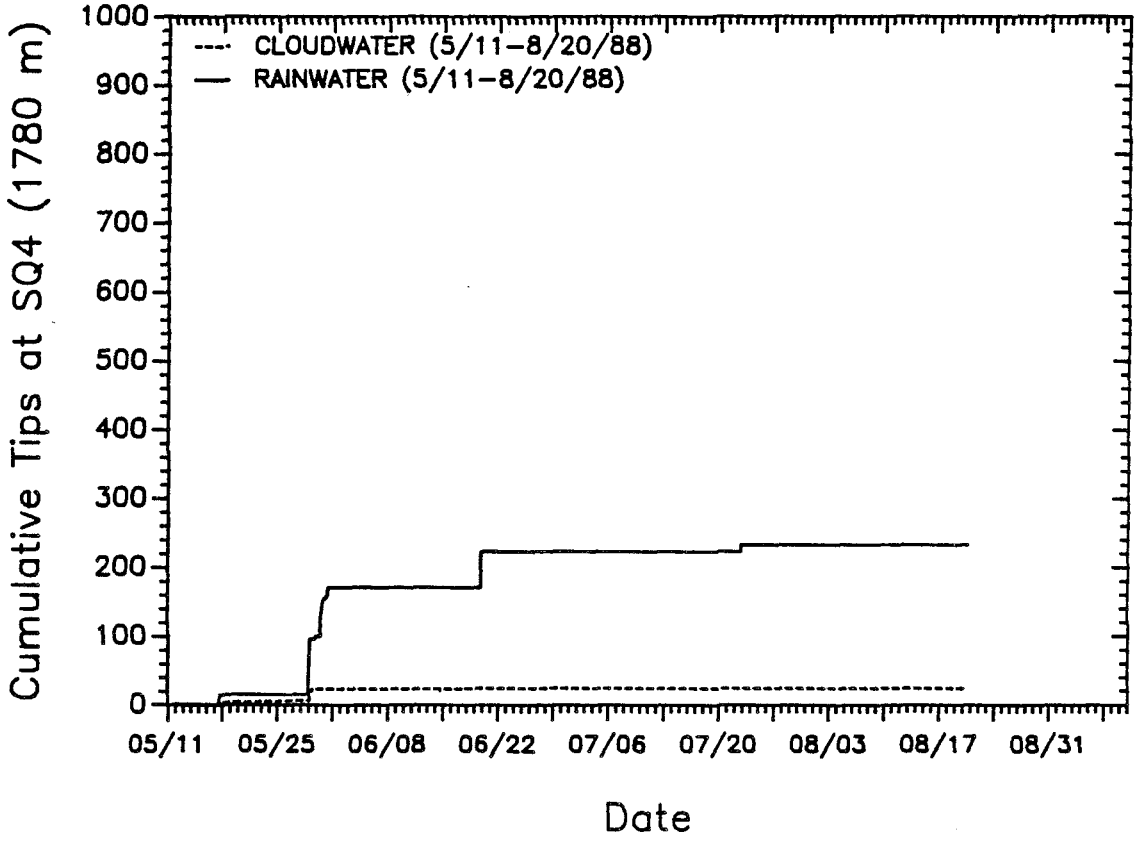

Figure 4.17. Precipitation and cloudwater deposition at SQ4 (elev. 1780 m) during the spring and summer of 1988. Each tip of the rain gauge corresponds to 0.26 mm of precipitation; each tip of the cloudwater gauge corresponds to 0.46 mm of deposited cloudwater.

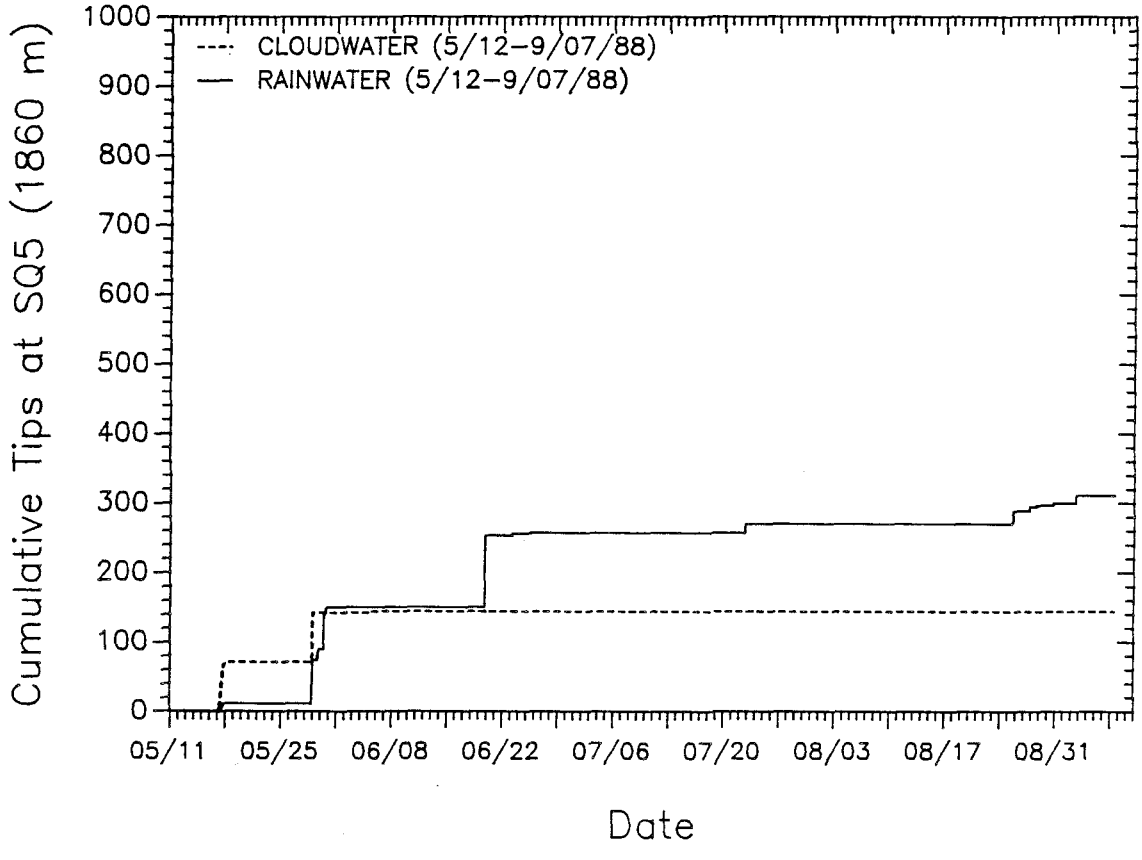

Figure 4.18. Precipitation and cloudwater deposition at SQ5 (elev. 1860 m) during the spring and summer of 1988. Each tip of the rain gauge corresponds to 0.26 mm of precipitation; each tip of the cloudwater gauge corresponds to 0.46 mm of deposited cloudwater.

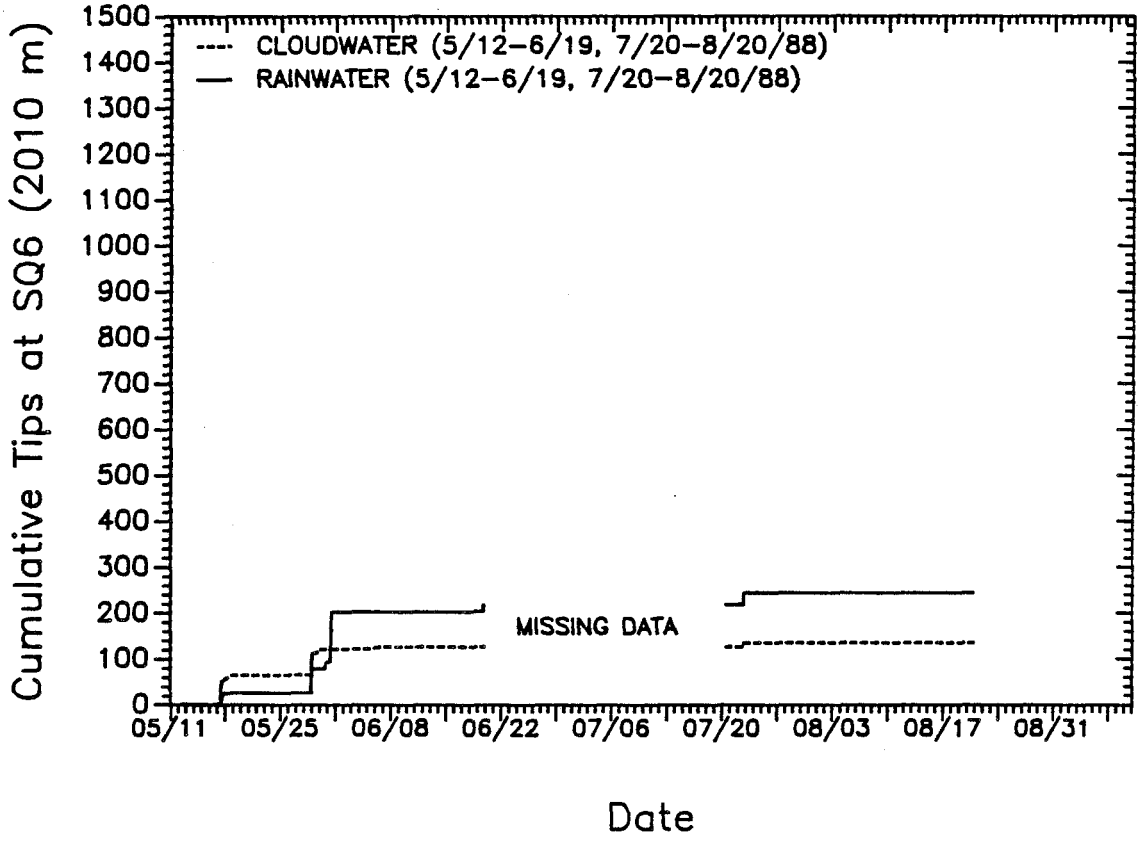

Figure 4.19. Precipitation and cloudwater deposition at SQ6 (elev. 2010 m) during the spring and summer of 1988. Each tip of the rain gauge corresponds to 0.26 mm of precipitation; each tip of the cloudwater gauge corresponds to 0.46 mm of deposited cloudwater.

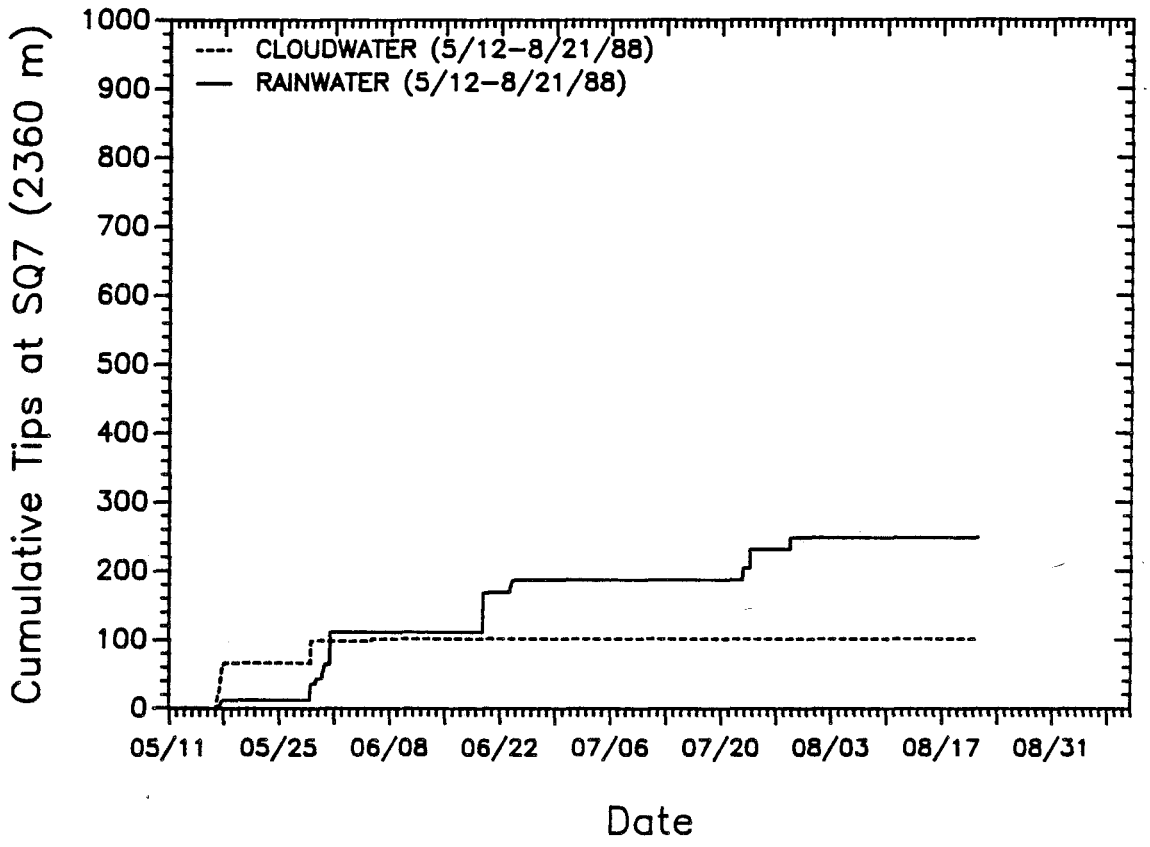

Figure 4.20. Precipitation and cloudwater deposition at SQ7 (elev. 2360 m) during the spring and summer of 1988. Each tip of the rain gauge corresponds to 0.26 mm of precipitation; each tip of the cloudwater gauge corresponds to 0.46 mm of deposited cloudwater.

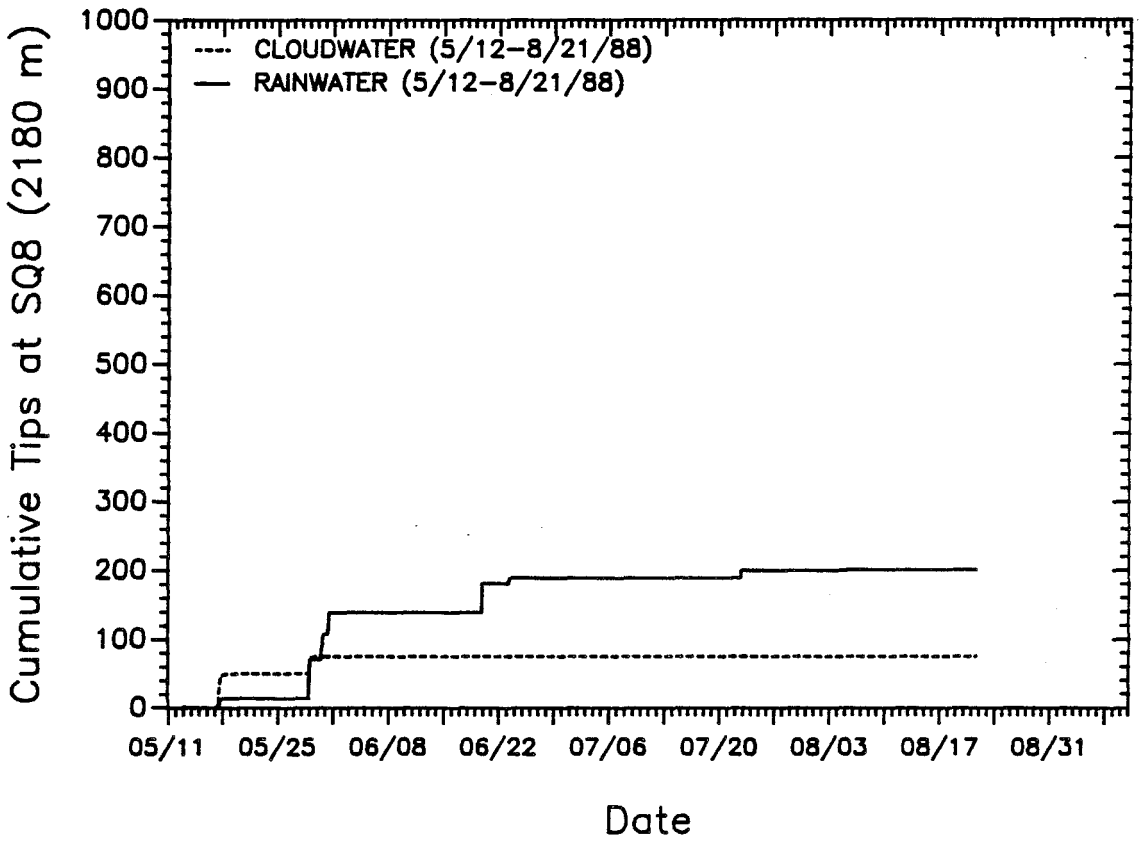

Figure 4.21. Precipitation and cloudwater deposition at SQ8 (elev. 2180 m) during the spring and summer of 1988. Each tip of the rain gauge corresponds to 0.26 mm of precipitation; each tip of the cloudwater gauge corresponds to 0.46 mm of deposited cloudwater.

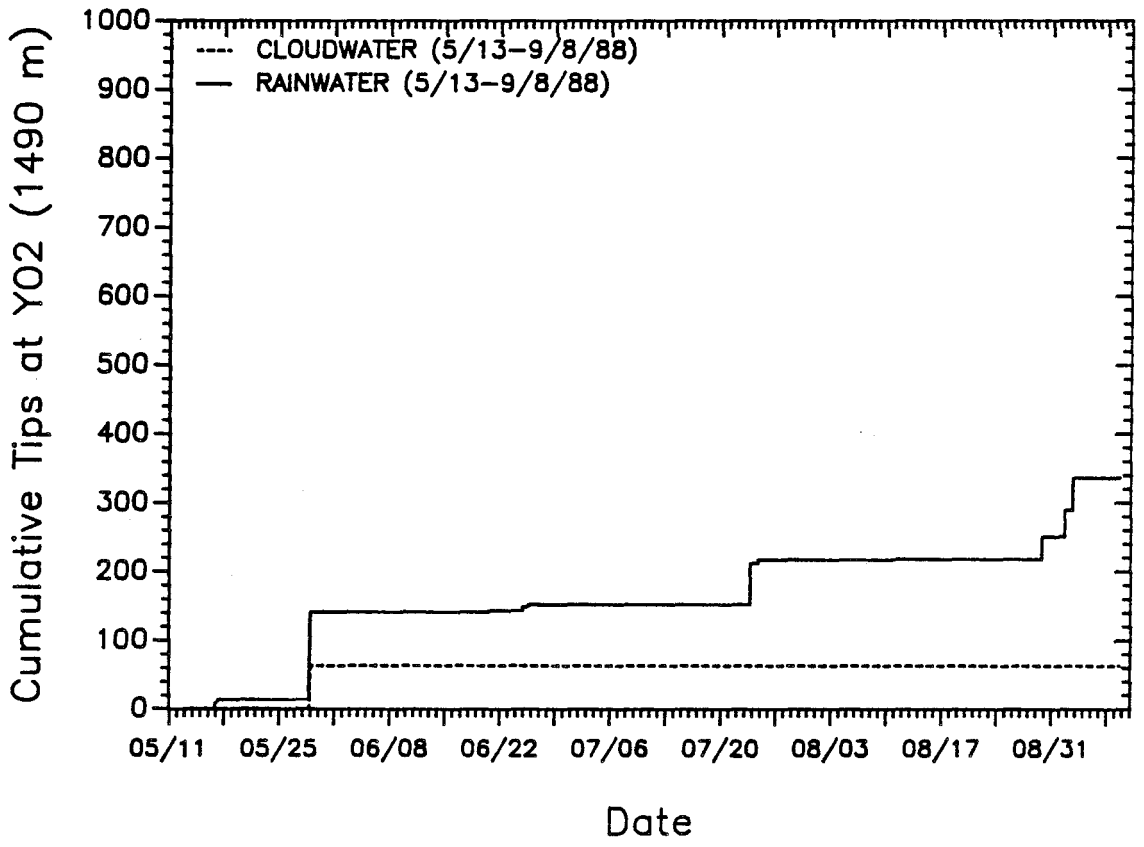

Figure 4.22. Precipitation and cloudwater deposition at YO2 (elev. 1490 m) during the spring and summer of 1988. Each tip of the rain gauge corresponds to 0.26 mm of precipitation; each tip of the cloudwater gauge corresponds to 0.46 mm of deposited cloudwater.

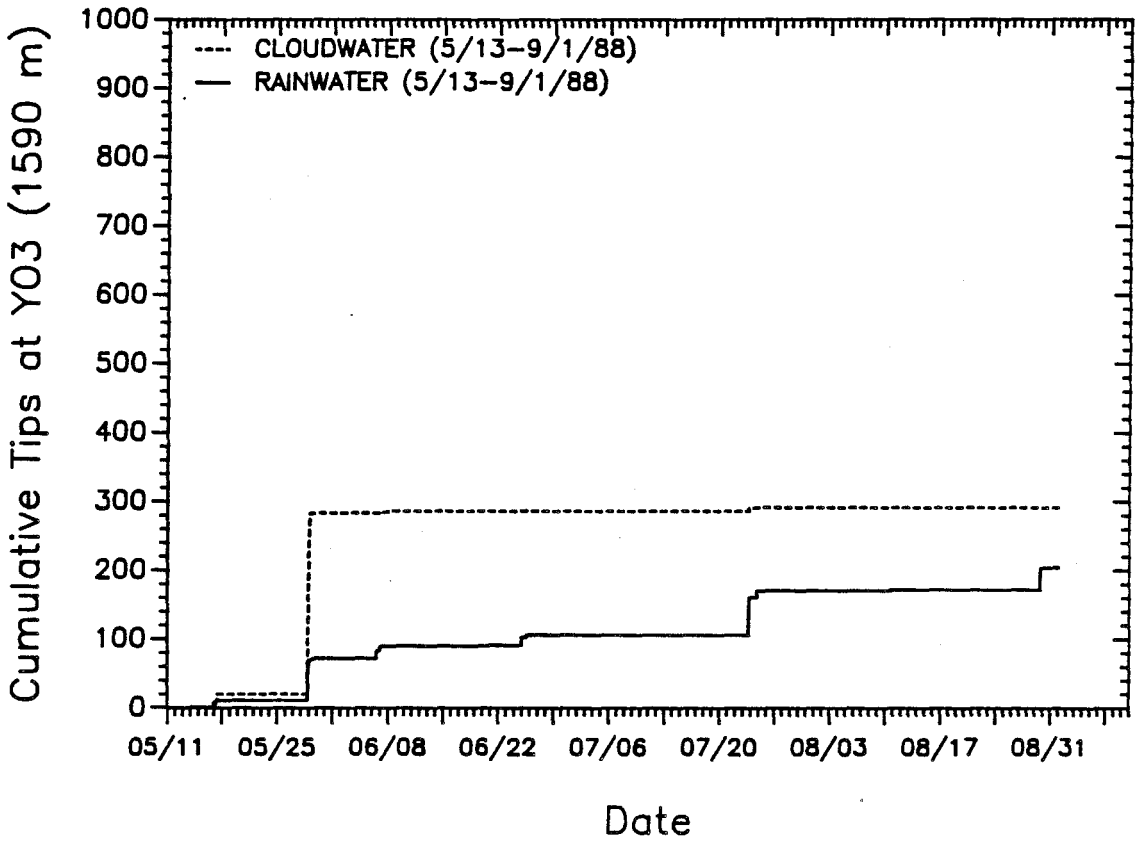

Figure 4.23. Precipitation and cloudwater deposition at YO3 (elev. 1590 m) during the spring and summer of 1988. Each tip of the rain gauge corresponds to 0.26 mm of precipitation; each tip of the cloudwater gauge corresponds to 0.46 mm of deposited cloudwater.

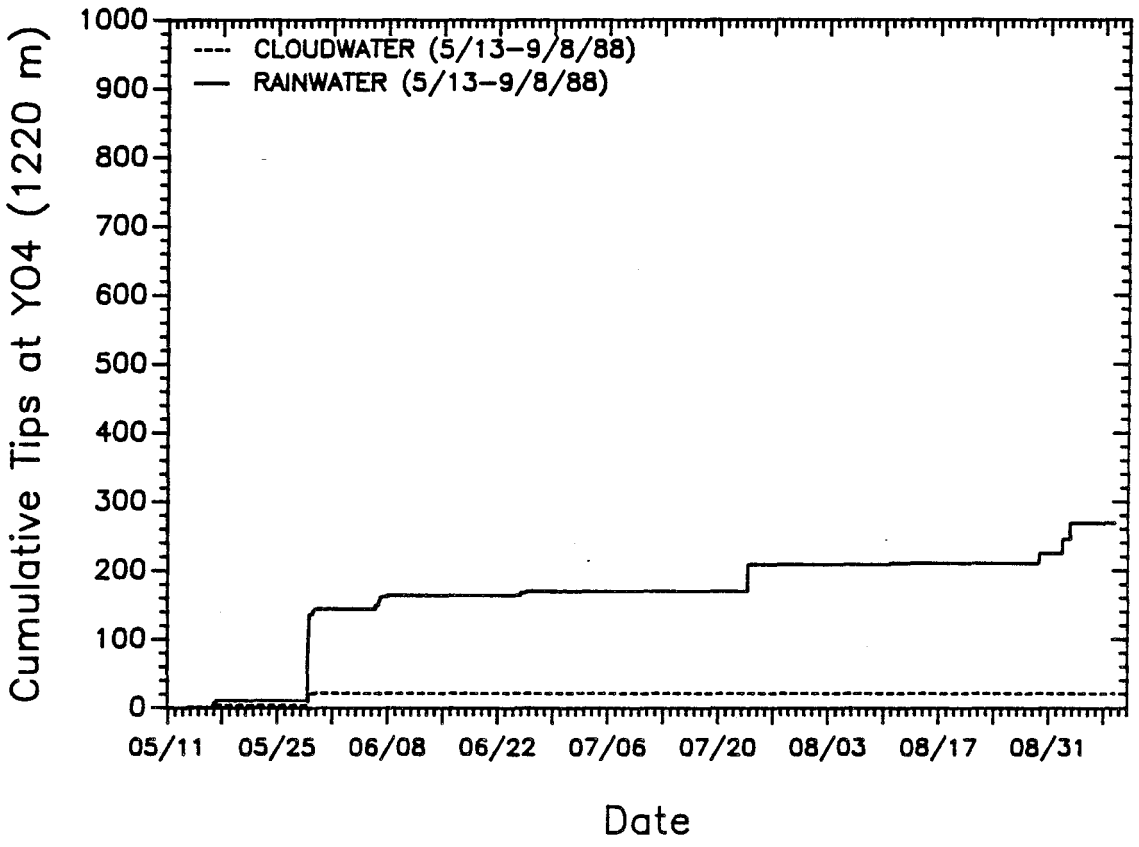

Figure 4.24. Precipitation and cloudwater deposition at YO4 (elev. 1220 m) during the spring and summer of 1988. Each tip of the rain gauge corresponds to 0.26 mm of precipitation; each tip of the cloudwater gauge corresponds to 0.46 mm of deposited cloudwater.

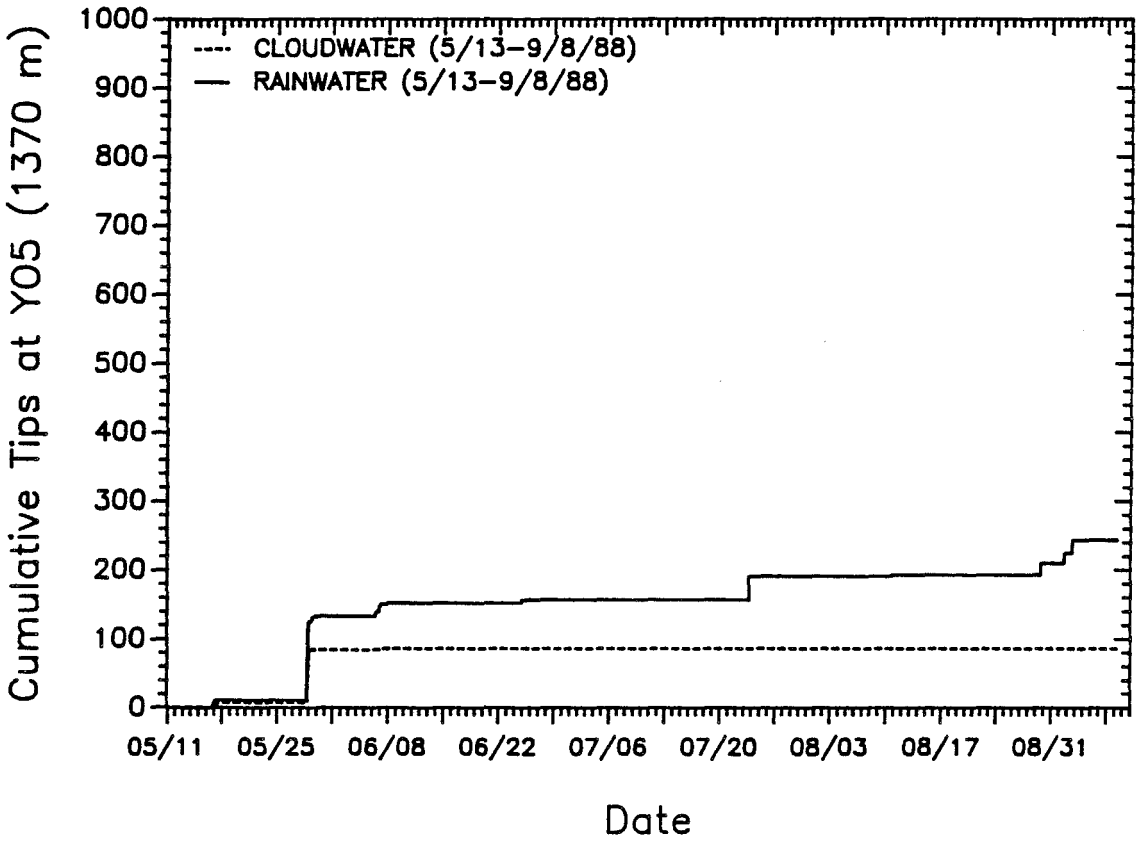

Figure 4.25. Precipitation and cloudwater deposition at YO5 (elev. 1370 m) during the spring and summer of 1988. Each tip of the rain gauge corresponds to 0.26 mm of precipitation; each tip of the cloudwater gauge corresponds to 0.46 mm of deposited cloudwater.

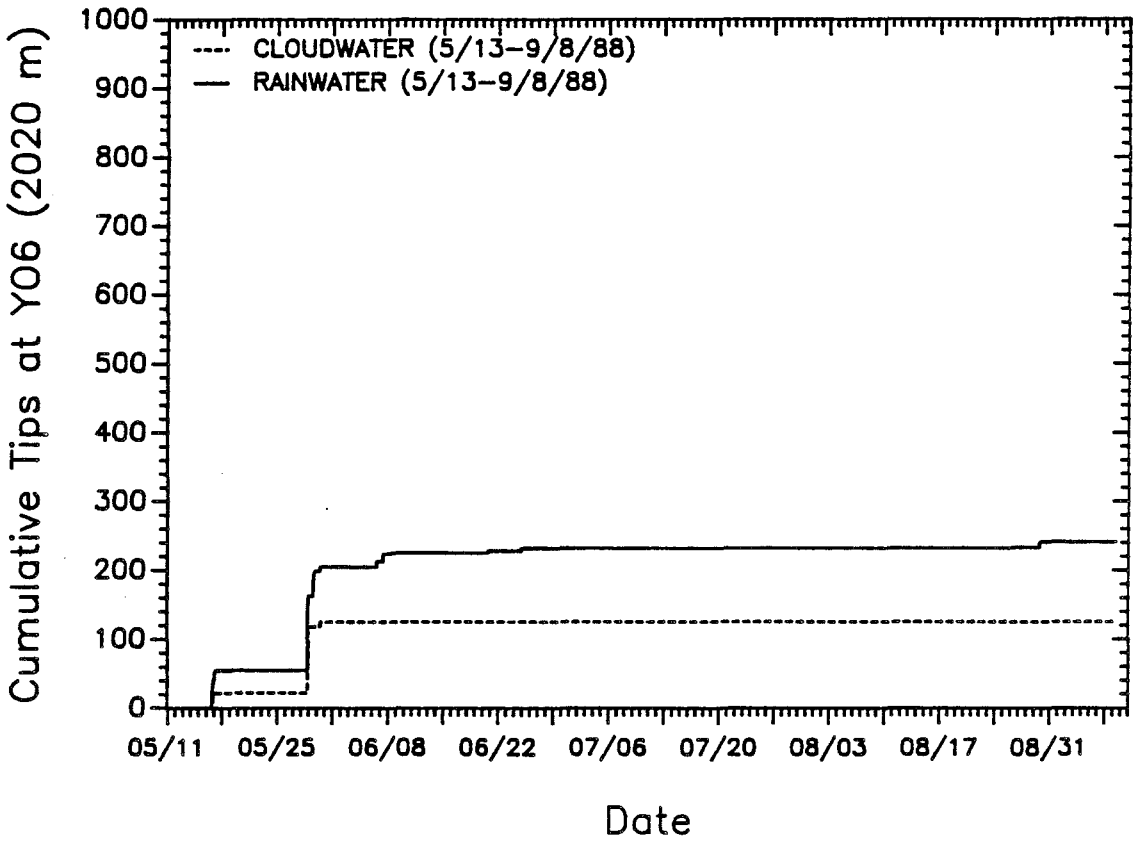

Figure 4.26. Precipitation and cloudwater deposition at YO6 (elev. 2020 m) during the spring and summer of 1988. Each tip of the rain gauge corresponds to 0.26 mm of precipitation; each tip of the cloudwater gauge corresponds to 0.46 mm of deposited cloudwater.

cloudwater deposition rate of 13.4 mm hr^{-1} also was observed at YO6, during an overlapping 3–hour period on the same evening. Wind speeds at YO6 averaged 4–5 m s^{-1} during the period. These cloudwater deposition rates are much higher than have been reported previously.

Data from the cloudwater monitoring stations can also be used to track the progress of an advancing cloud mass. On May 28, for example, a strong Pacific cold front, approaching from the northwest, reached the Sierra. Cloudwater interception began at YO6 approximately half an hour before interception was observed at YO3. This pattern is consistent with the direction of approach of the storm, since YO6 is located several kilometers northwest of YO3. Cloud interception at YO3 was observed to continue for approximately two hours after it had ceased at YO6.

Volume–weighted average YO3 cloudwater concentrations of NO_3^-, SO_4^{2-}, NH_4^+, and H^+ were observed to be 20, 14, 34, and 9.4 μN, respectively, during the May 28 cloud interception event (see Chapter 2); cloudwater deposition to the passive cloudwater collector at YO3 was approximately 118 mm during this period. Chemical deposition to the collector during this event, therefore, can be estimated as 150 mg m^{-2} of NO_3^-, 81 mg m^{-2} of SO_4^{2-}, 72 mg m^{-2} of NH_4^+, and 1.1 mg m^{-2} of H^+. By comparison, the average annual quantities of NO_3^-, SO_4^{2-}, NH_4^+, and H^+ deposited in YNP precipitation in 1983 and 1984 were 550, 495, 145, and 5.3 mg m^{-2}, respectively (NADP/NTN, 1985, 1986), suggesting that cloudwater deposition of these ions to the passive collector, on May 28, 1988 alone, probably contributed significantly to their total annual deposition at the site. Since rates of cloudwater deposition to exposed conifers may be comparable to those measured by the passive cloudwater collector, as discussed above, a significant portion of the total annual deposition of NO_3^-, SO_4^{2-}, NH_4^+, and H^+ to the trees at YO6 may have been delivered

during this single cloud interception event.

Conclusions

The spatial and temporal variations exhibited in patterns of precipitation and cloud interception were investigated at fourteen sites in the Sierra Nevada Mountains of California. The sites, located in Sequoia and Yosemite National Parks, were selected to represent an elevational gradient in each Park, ranging from approximately 800 to 2400 m in elevation. The study began in September, 1987 and continued through October, 1988. A new monitoring system, which incorporated a passive cloudwater collector, was developed and built specifically for this study. The system also included a rain gauge and an anemometer. A data–logger, designed specifically for this program, maintained a time–resolved record of activity by the cloudwater collector, the rain gauge, and the anemometer.

Data collected during the program illustrates that cloud interception contributes significantly to the total deposition budgets of water and pollutants in the Sierra. The contributions are particularly important for exposed conifers, which are subject to direct impaction of ambient clouds. Rates of deposition to the passive cloudwater collectors, which may be comparable to rates for exposed conifers, were observed to frequently exceed 1.0 mm hr^{-1} at several sites, and surpassed 20 mm hr^{-1} at one site in Yosemite National Park during passage of a strong Pacific cold front. Cloudwater deposition of NH_4^+, NO_3^-, SO_4^{2-}, and H^+ to exposed conifers near this site, during this single interception event, is believed to have contributed a significant portion of the total annual atmospheric flux of these species to nearby trees, and the ground beneath them.

Most Sierra cloud interception events are believed to result from the interception of convective clouds, associated with frontal activity; however, there is some evidence to suggest that dense winter "Tule" fogs, formed near the floor of the San Joaquin Valley, may intercept lower elevation sites in Sequoia National Park, when the atmosphere over the valley is destabilized. Interception of convective clouds is observed most frequently at sites above 1500 m elevation. Ridge–top sites, which often experienced the highest wind speeds, usually receive the greatest hydrological deposition fluxes from impacting cloudwater. Correlations of cloudwater deposition between sites in Sequoia National Park and similarly elevated sites in Yosemite National Park are often stronger than those between sites with differing elevations in a single Park. The progress of the leading edge of an incoming storm is illustrated by the time–resolved cloud interception records of the spatially distributed sites.

Acknowledgments

We are grateful to the National Park Service for granting access to the monitoring sites in both Yosemite and Sequoia National Parks. We also would like to acknowledge the assistance of members of the Research staff at Sequoia National Park and the Resource Management staff at Yosemite National Park who helped us to select the sites. John Lee is gratefully acknowledged for his role in the development of the data–loggers used in the study. Finally, we would like to thank our colleagues, J. William Munger and Dieter Gunz, who frequently provided field assistance during the project. This work was funded by the California Air Resources Board (CARB contract #A6–185–32).

References

Azevedo, J. and Morgan, D. L. (1974) Fog precipitation in coastal California forests. *Ecology* **55**, 1135–1141.

Collett, J., Jr., Daube, B., Jr., Munger, J. W. and Hoffmann, M. R. (1989) Cloudwater chemistry in Sequoia National Park. *Atmos. Environ.*, in press.

Dasch, J. M. (1988) Hydrological and chemical inputs to fir trees from rain and clouds during a 1–month study at Clingmans Peak, NC. *Atmos. Environ.* **22**, 2255–2262.

Jacob, D. J., Munger, J. W., Waldman, J. M. and Hoffmann, M. R. (1986) The H_2SO_4–HNO_3–NH_3 system at high humidities and in fogs: I. Spatial and temporal patterns in the San Joaquin Valley of California. *J. Geophys. Res.* **91**, 1073–1088.

Kerfoot, O. (1968) Mist precipitation on vegetation. *For. Abstr.* **29**, 8–20.

Lovett, G. M. (1984) Rates and mechanisms of cloud water deposition to a subalpine balsam fir forest. *Atmos. Environ.* **18**, 361–371.

Lovett, G. M. and Reiners, W. A. (1986) Canopy structure and cloud water deposition in subalpine coniferous forests. *Tellus* **38B**, 319–327.

National Atmospheric Deposition Program / National Trends Network (1985) 1983 NADP/NTN Annual Data Summary, available from the NADP/NTN Coordinator's Office, Colorado State University, Fort Collins, CO, 209 p.

National Atmospheric Deposition Program / National Trends Network (1986) 1984 NADP/NTN Annual Data Summary, available from the NADP/NTN Coordinator's Office, Colorado State University, Fort Collins, CO, 240 p.

National Oceanic and Atmospheric Administration (1987) Local climatological data Bakersfield, CA, December, 1987, available from the National Climatic Data Center, Asheville, NC, 4 p.

Schemenauer, R. S. (1986) Acidic deposition to forests: the 1985 Chemistry of High Elevation Fog (CHEF) project. *Atmos. Ocean* **24**, 303–328.

Schemenauer, R. S., Cereceda, P. and Carvajal, N. (1987) Measurements of fog water deposition and their relationships to terrain features. *J. Climate Appl. Meteorol.* **26**, 1285–1291.

CHAPTER 5

THREE AUTOMATED SYSTEMS FOR THE COLLECTION OF CLOUDWATER

Introduction

In order to initiate an automated cloudwater sampling program in the Sierra Nevada Mountains of California, specialized sampling equipment had to be developed. Cloudwater samples collected during the study discussed in this report were obtained using three different collection systems. Each system utilized a different cloudwater collector. The three collection systems, and their corresponding cloudwater collectors, are described in this chapter.

Equipment

Integrated Cloudwater Monitoring System

The integrated cloudwater monitoring system was used during the spring, summer, and fall to collect samples of cloudwater in Sequoia and Yosemite National Parks (see Chapter 2). The system is composed of three primary pieces of equipment: a cloudwater collector to collect samples, an autosampler to fractionate and store the collected samples, and a cloudwater sensor to monitor for the presence of impacting clouds and activate the collector.

The Caltech Active Strand Cloudwater Collector (CASCC), pictured in Figure 5.1, serves as the cloudwater collector for this sampling system. Operating parameters of the CASCC are listed in Table 5.1. The CASCC (Daube et al., 1987a) has been in use at Caltech since the summer of 1985. It is an improved version of collectors described in detail elsewhere (Jacob et al., 1985; Daube et al., 1987b). The CASCC employs a 14 volt DC fan to draw air across a bank of six angled rows of 510 μm Teflon strands at a velocity of 9 m s^{-1}. Cloudwater droplets

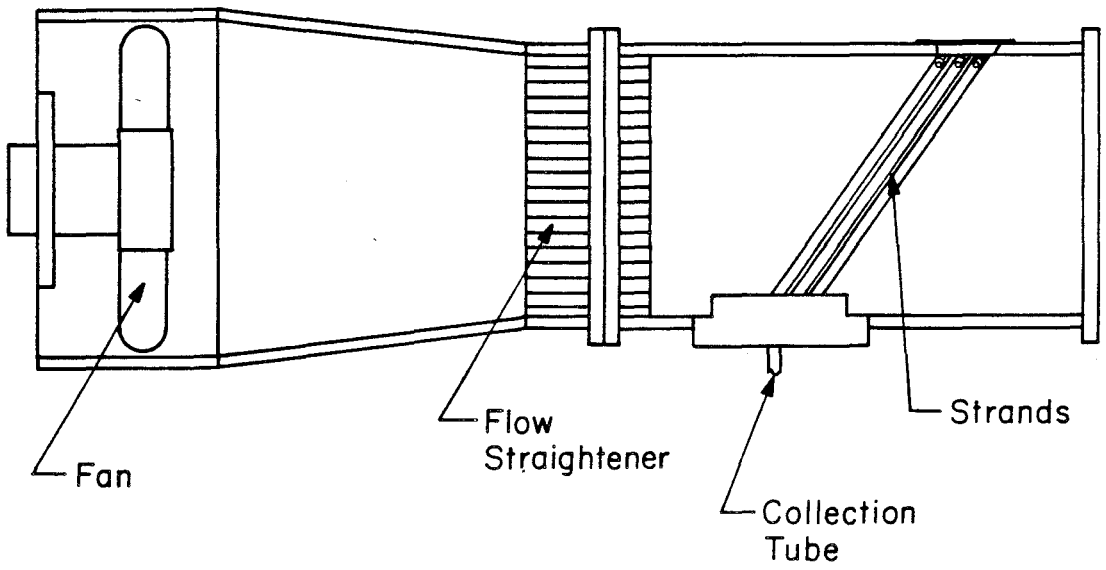

Figure 5.1. Caltech Active Strand Cloudwater Collector (CASCC). Cloudwater droplets are collected by inertial impaction on 510 μm Teflon strands. See the text for details.

Table 5.1. Caltech Active Strand Cloudwater Collector (CASCC) Operating Parameters

Parameter	Value
Strand diameter, μm	510
Total strand length, m	190
No. of rows of strand	6
Strand spacing, mm	1.8
Air flow rate, $m^3\ min^{-1}$	24.5
Percent of air sampled, first row	27.9
Percent of air sampled, total	86.0
Total sampled flow, $m^3\ min^{-1}$	21.1
Droplet diameter size cut (50% efficiency), μm	3.5
Average velocity at strands, $m\ s^{-1}$	8.5
Pressure drop, mm Hg	0.93
Operating voltage, VDC	14.0
Theor. collection rate, (0.5 $g\ m^{-3}$ LWC), $ml\ min^{-1}$	9.0

in the air parcel (typically 2 to 50 μm diameter) are collected on the strands by inertial impaction. These droplets coalesce with others previously collected and flow down into a Teflon sample trough located beneath the bank of strands, aided by gravity and aerodynamic drag.

One of the primary reasons for developing the CASCC was to enable automated sample collection. Prior to the summer of 1985, cloud and fogwater samples collected in Caltech projects were obtained using a Rotating Arm Collector (RAC). The RAC, described in detail elsewhere (Jacob et al., 1984), collects samples by impaction in slots milled in the leading edges of a stainless steel rod rotated at 1700 rpm. The sample is accelerated outward to two 30 ml sample bottles, one located at each end of the rod. The difficulty of automatically changing sample bottles on a rotating arm prohibits the incorporation of the RAC into an automated collection system. The CASCC, which delivers sample to a fixed point, is more easily adapted for this purpose. A side–by–side sampling comparison of the RAC and the CASCC is discussed elsewhere (Collett et al., 1989).

The collection efficiency of the CASCC, η, is a product of the collection efficiency of each strand, η_1, and the percentage of total flow through the collector sampled by the strands, η_2.

(Eq'n. 5.1) $$\eta = \eta_1 \cdot \eta_2$$

The efficiency of collection by impaction on a single cylinder, η_1, is well characterized in the literature (e.g. Bird, Stewart, and Lightfoot, 1960; Friedlander, 1977). The percentage of air sampled by the strands, η_2, is a function of the strand geometry and can be approximated using

(Eq'n. 5.2) $$\eta_2 = \{1-(1-DL^{-1})^n\}$$

where,

D = strand diameter

L = spacing between strands

n = number of rows of strands.

For the CASCC, with six rows of 510 μm strands spaced 1.8 mm apart, 86% of the air passing through the collector is sampled. Figure 5.2 depicts the overall collection efficiency of the CASCC, η, as a function of droplet size. Values of η_1 are taken from Friedlander (1977). The collection efficiency asymptotically approaches 0.86 at large droplet sizes and drops sharply for droplets with diameters less than about 6 μm. The 50% collection efficiency size cut corresponds to a droplet diameter of approximately 3.5 μm. Figure 5.2 indicates that most of the droplets in the activated size region (droplet diameter > 1 μm) are collected efficiently while non-activated sub-micron aerosol particles are not.

The automated CASCC used in this study was equipped with several additional features depicted in Figure 5.3. First, a special inlet was mounted on the front of the collector to exclude the sampling of rain drops. The opening of this inlet faces downward. Trajectory analysis indicates that droplets larger than 3 μm diameter are excluded under most conditions encountered, which enables the CASCC to operate under conditions where cloud and rain are present at the sampling site simultaneously. Second, automated covers were added to the inlet and the rear of the collector. These covers help to prevent the accumulation of dry deposition inside the collector between sampling periods. The covers are opened

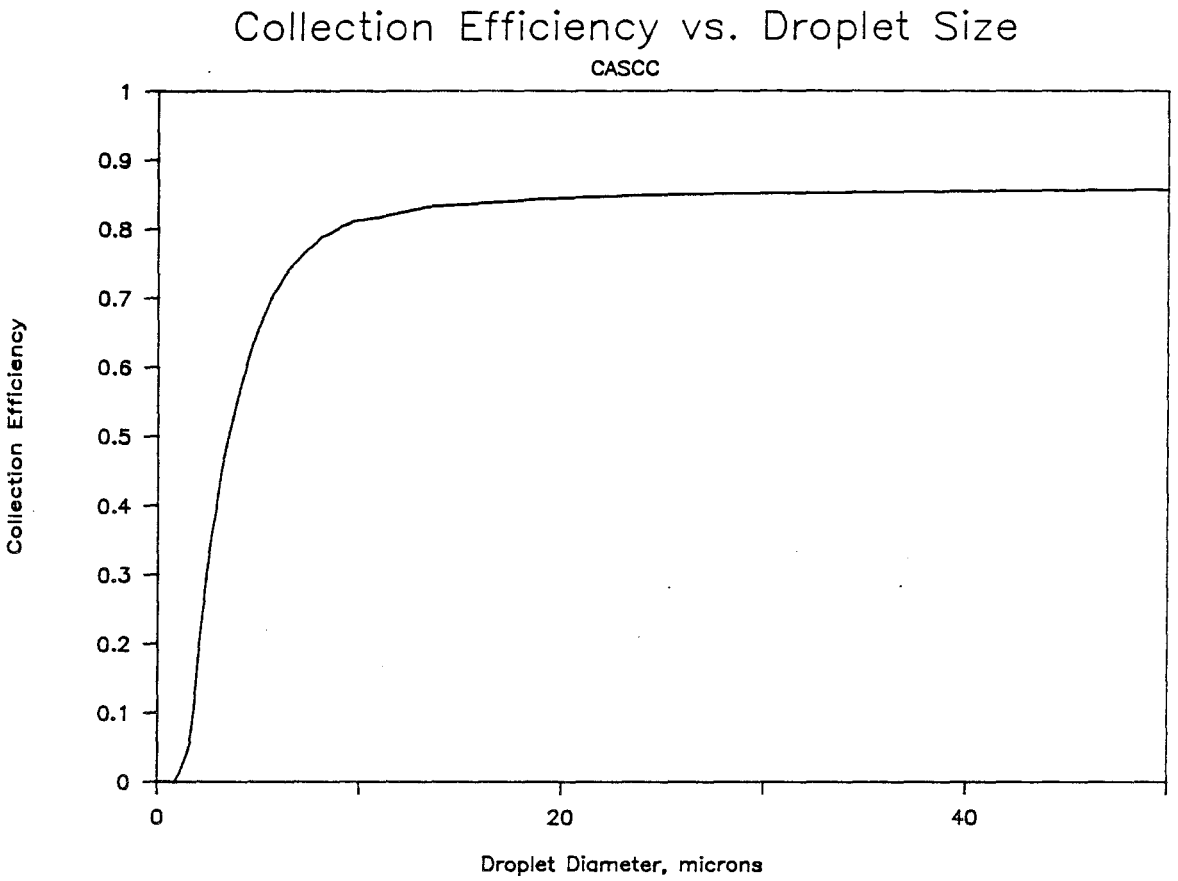

Figure 5.2. Caltech Active Strand Cloudwater Collector (CASCC) collection efficiency as a function of droplet size.

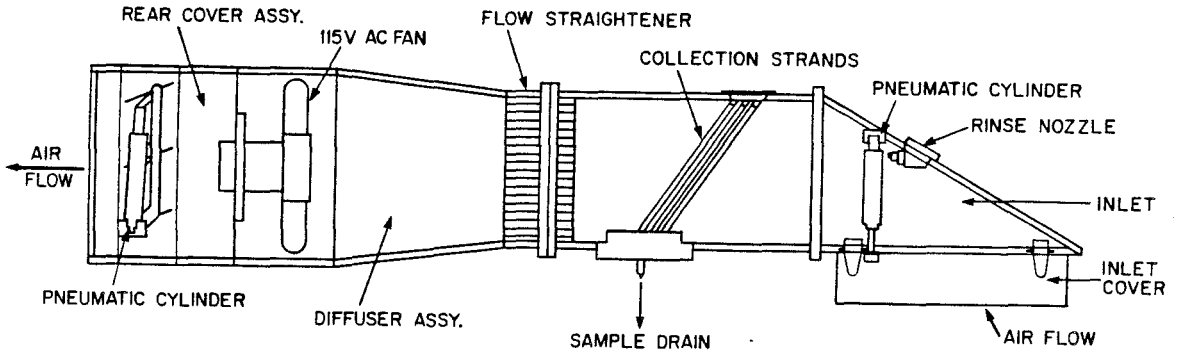

Figure 5.3: The Caltech Active Strand Cloudwater Collector (CASCC) as modified for use in the Integrated Cloudwater Monitoring System. Major modifications include the addition of automated covers and an automated rinsing system.

pneumatically when sampling begins. Last, the CASCC was equipped with an automated rinsing system. Distilled deionized water is pumped from a 15 l reservoir through a polypropylene nozzle (Bete, type WL) mounted inside the sampler inlet. Spray from the nozzle is directed onto the Teflon collection strands in the CASCC. A rinsing cycle is initiated at the beginning and end of each sampling period to ensure the cleanliness of the Teflon collection surfaces. The CASCC is mounted on top of a 3 m anodized aluminum stand.

The automated fractionating sampler, pictured in Figure 5.4, was developed to fractionate and store samples collected by the CASCC. In this study samples were fractionated by volume. The main features of the sampler are (1) a carousel containing 20 sample bottles, (2) a rinsewater diversion valve, (3) a sample reservoir which holds each sample until it is dumped into a sample bottle, (4) a refrigerator which houses the carousel and reservoir to help preserve the chemical integrity of the samples, (5) the electronic circuitry which controls the operation of the autosampler, and (6) a printer which records pertinent data about the collection process.

The rinsewater diversion valve, mounted above the sample entrance to the autosampler, is used to control the flow of sample into the sampler reservoir. During periods when the CASCC is being rinsed, this valve diverts the rinsewater away from the autosampler. Sample collected by the CASCC, during the first 20 minutes of each event, also is diverted to ensure that all rinsewater has been washed from the strands by cloudwater. After 20 minutes the valve is switched to allow sample to flow into the reservoir. Sample is collected in the reservoir assembly, pictured in Figure 5.4, until it is released to a sample bottle. The sample is released either when the level of sample in the connected side tube reaches the level of the

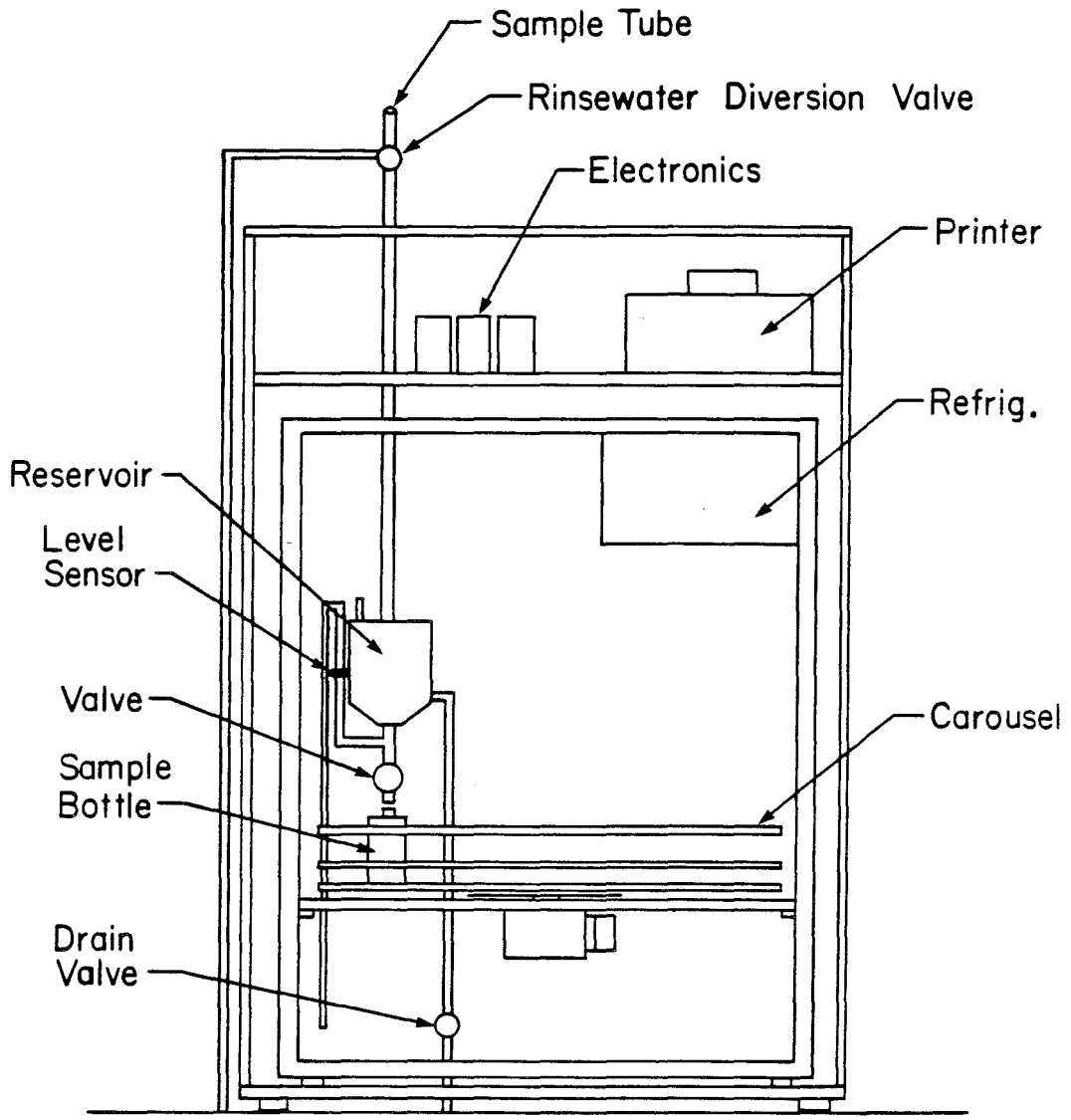

Figure 5.4. Autosampler used in the Integrated Cloudwater Monitoring System. Cloudwater collected by the CASCC is fractionated into sequential samples by this refrigerated unit.

optical liquid level sensor or when the collector is turned off and then back on (signifying a new event). The position of the liquid level sensor can be adjusted so that the volume of sample collected before release to a sample bottle varies from 60 to 500 ml. Any amount in excess of 60 ml is discarded before releasing the sample to a 60 ml bottle.

Up to twenty consecutive samples can be collected by the autosampler. The carousel, holding twenty 60 ml sample bottles, rotates to bring each consecutive bottle beneath the reservoir as needed. A counter is used to keep track of the number of bottles used. When the last bottle is used, power to the liquid level sensor is turned off and subsequent sample accumulates in the reservoir. Filled sample bottles remain in the refrigerated environment (4 C) until they are picked up by a site operator.

An eight channel printer (Hecon model A0544) is used to record the time and sequence of events in the collection process. Four channels are used to record the status of the cloudwater sensor (described in the following section), the rinse pump, the rinsewater diversion valve, and the liquid level sensor. Whenever a channel changes status, the time and the new channel state (high or low) is recorded. Power failure and restoration also are recorded by the printer. A battery provides backup power to the printer's internal clock in the event of power failure.

Automated collection of cloudwater requires the use of a cloudwater sensor to determine when clouds are present at the site in order that sampling may be initiated. The sensor used in this collection system is pictured in Figure 5.5. Operating parameters of the sensor are listed in Table 5.2. Like the CASCC, the sensor relies on a fan to draw air through a rain-excluding inlet and across an

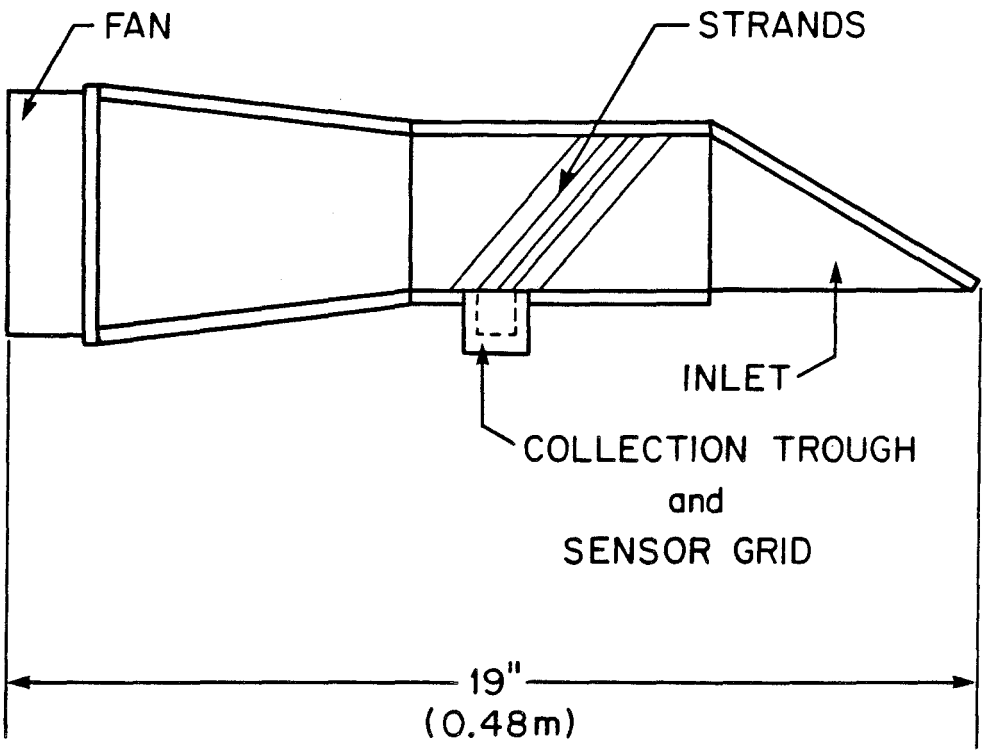

Figure 5.5. Cloudwater sensor used as part of the Integrated Cloudwater Monitoring System. A description of sensor operation is provided in the text.

Table 5.2. Cloudwater Sensor Operating Parameters

Parameter	Value
Strand diameter, μm	280
Total strand length, m	25
No. of rows of strand	6
Strand spacing, mm	1.1
Air flow rate, $m^3\ min^{-1}$	1.7
Percent of flow sampled, first row	26.4
Percent of flow sampled, total	84.0
Total sampled flow, $m^3\ min^{-1}$	1.4
Droplet diameter size cut (50% efficiency), μm	3.5
Average velocity at strands, $m\ s^{-1}$	6.0
Operating voltage, VAC	117
Theor. collection rate (0.5 g m^{-3} LWC), ml min^{-1}	0.5

angled bank of strands. When cloudwater droplets are present in the air parcel, they are collected by inertial impaction upon the strands. Collected droplets coalesce and run down the strands where they drip onto a sensing grid pictured in Figure 5.6. When water bridges the gap between the upper grid and the plate (see Figure 5.6), a circuit is completed, and the CASCC is activated. A heater is mounted under the grid to aid in evaporating the collected water. When water ceases to drip onto the grid, the heater dries it. If the grid remains dry for 20 minutes, the cloudwater impaction event is deemed over, and the CASCC is turned off.

The cloudwater sensor is mounted on a 3 m anodized aluminum stand. A pivot is located at the top of the stand, and a wind vane keeps the sensor pointed into the wind to maximize the efficiency of cloudwater collection. A six channel slip–ring carries the electrical signals through the rotating joint.

The use of the CASCC, the cloudwater sensor, and the autosampler together constitutes an integrated cloudwater sampling system. As indicated above, the sensor serves to turn the system on and off, the CASCC collects the cloudwater, and the autosampler fractionates the samples and maintains them in a refrigerated environment. Operation of the system is outlined schematically in Figure 5.7.

Winter Cloudwater Sampling System

Since the cloudwater monitoring program was designed to sample throughout the year in the central and southern Sierra Nevada Mountains of California, the cloudwater collection system was required to function in freezing conditions. Both the cloudwater sensor described above and the CASCC are not operational in such

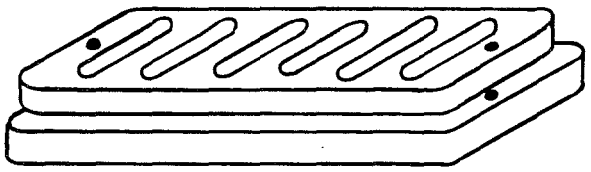

ORTHOGRAPHIC VIEW

Figure 5.6. Detail of the resistance grid incorporated into the cloudwater sensor. Water bridging the gap between the upper grid and the lower plate completes an electrical circuit which sends a signal to activate the collection system.

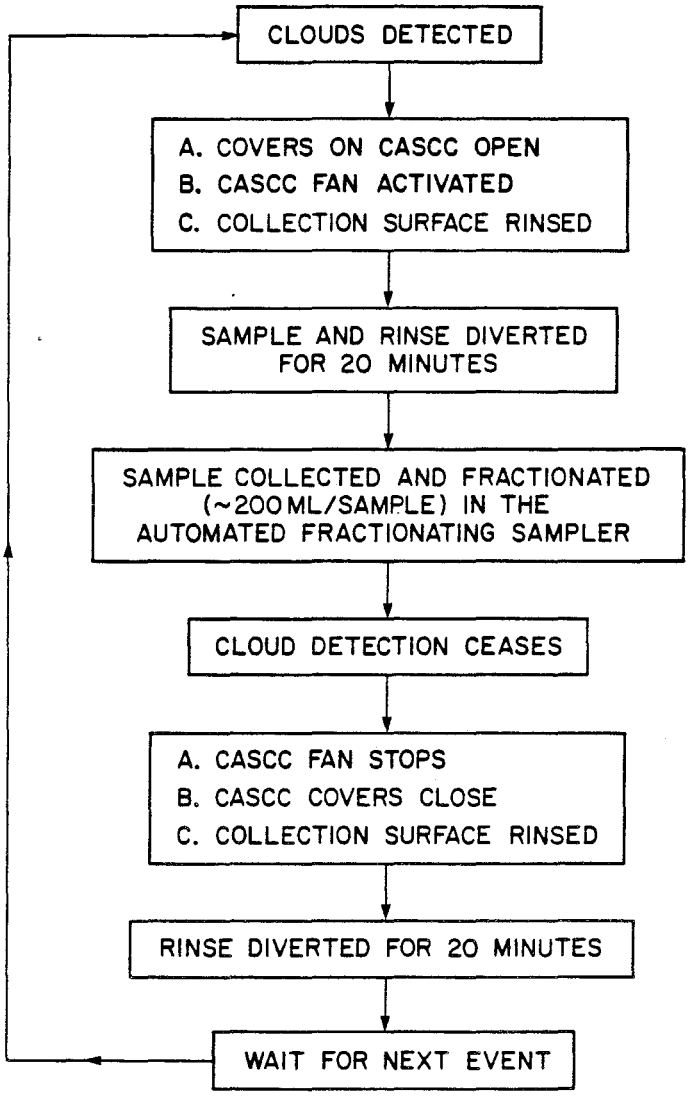

Figure 5.7. Schematic outline of Integrated Cloudwater Monitoring System operation.

an environment. Supercooled cloudwater droplets impacting on the strands freeze almost immediately when temperatures are below freezing. The frozen droplets, or rime, clog both the collector and the sensor, preventing the collection of any samples. A new cloudwater collector and a new sensor were designed and built to cope with this problem.

The collector, referred to as the Caltech Heated Rod Cloudwater Collector (CHRCC), is similar in design to the CASCC (see Figure 5.8 and Table 5.3). Several important differences, however, distinguish the two instruments. First, the CHRCC is a much smaller collector than the CASCC. Second, the amount of air sampled by the CHRCC in a given amount of time is approximately 20% that sampled by the CASCC. Last, the CHRCC has a different collection surface. While the CASCC uses six rows of 0.51 mm teflon strands, the CHRCC utilizes six rows of 3.18 mm stainless steel (passivated, type 304) rods. The collection efficiency of both instruments is similar for all droplet diameters greater than about 15 μm; however, the CHRCC is less efficient at collecting smaller droplets, due to the larger diameter of the collection cylinders (see Figure 5.9). The 50% collection efficiency size cut for the CHRCC corresponds to a droplet diameter of approximately 7.5 μm.

The stainless steel rods in the CHRCC are hollow. A nichrome wire, encased in a teflon sleeve, is threaded through the rods. When current is passed through the wire, heat is dissipated and the rods are warmed. The teflon sleeve serves to electrically insulate the wire from the stainless steel rods. Heat can be dissipated through the rods at rates up to 285 W, utilizing a 117 VAC power source. Originally it was hoped that the collector could be operated continuously with a temperature feedback control system, maintaining the temperature of the rods slightly above freezing. Mass transfer calculations, however, indicated that small

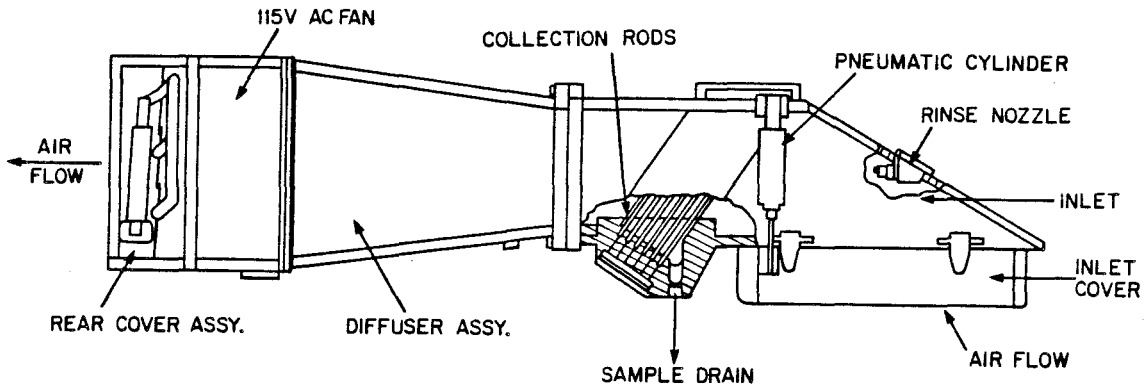

Figure 5.8. The Caltech Heated Rod Cloudwater Collector (CHRCC) utilized by the Winter Cloudwater Sampling System. Heat can be dissipated through the stainless steel rods, which comprise the collection surfaces of this sampler, in order to melt accumulated frozen cloudwater.

Table 5.3. Caltech Heated Rod Cloudwater Collector (CHRCC) Operating Parameters

Parameter	Value
Rod diameter, μm	3175
Total rod length, m	8
No. of rows of rods	6
Rod spacing, mm	9.5
Air flow rate, $m^3\ min^{-1}$	6.3
Percent of air sampled, first row	32.3
Percent of air sampled, total	90.4
Total sampled flow, $m^3\ min^{-1}$	5.7
Droplet diameter size cut (50% efficiency), μm	7.7
Average velocity at strands, $m\ s^{-1}$	9.0
Pressure drop, mm Hg	0.97
Operating voltage, VAC	117
Theor. collection rate, (0.5 g m^{-3} LWC), ml min^{-1}	2.2

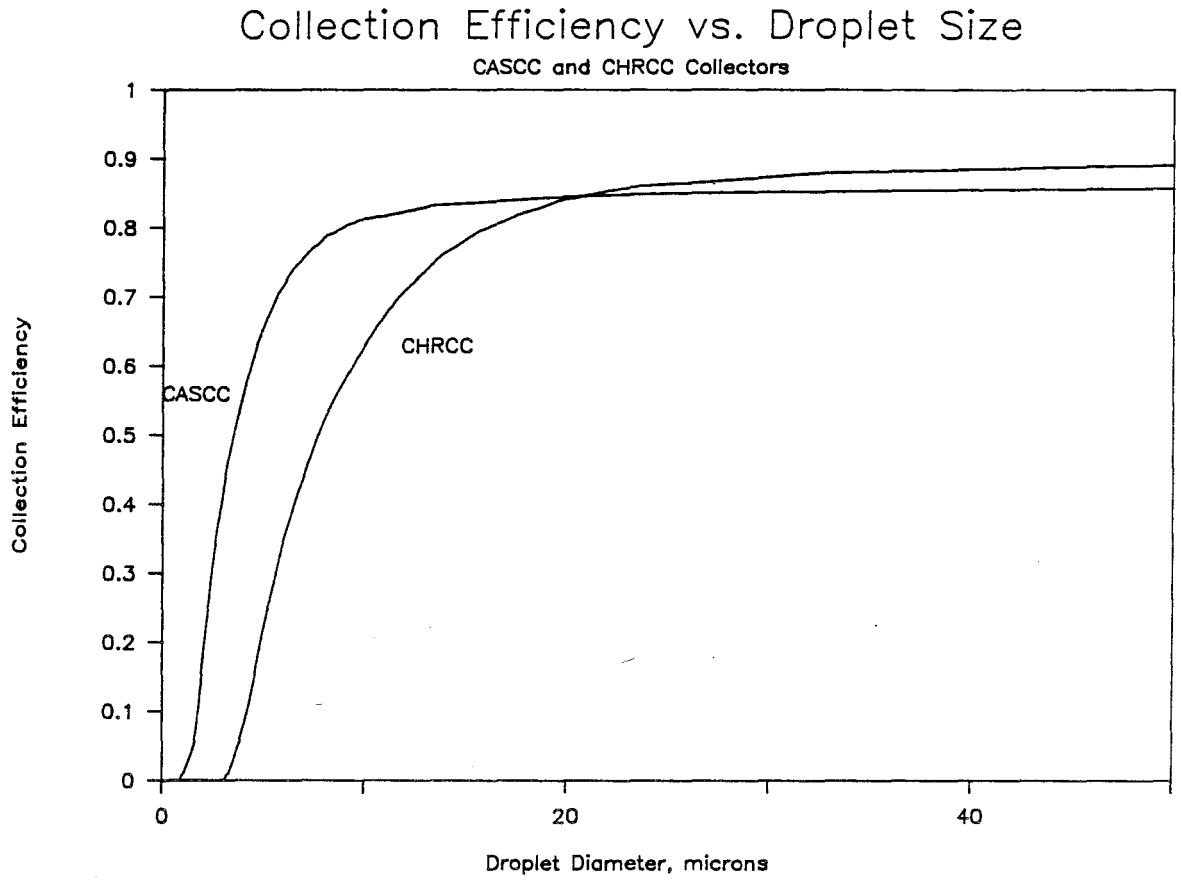

Figure 5.9. A comparison of the collection efficiencies of the Caltech Heated Rod Cloudwater Collector (CHRCC) and the Caltech Active Strand Cloudwater Collector (CASCC).

droplets ($\leq$ 50 μm) would evaporate almost completely under typical conditions ($T_{rod} \simeq 4$ C, $T_{amb} \simeq -1$ C) within a few seconds. For this reason, a cyclical mode of operation was adopted for the CHRCC during cold sampling periods. In this mode, a 15–minute period of collection is followed by a 1–minute heating cycle. During the heating portion of the cycle, the fan on the collector is turned off, and the covers on the collector are closed to help reduce evaporation by eliminating forced convection. More importantly, the 15–minute collection period is intended to allow coalescence of the collected drops to decrease the surface to volume ratio of the collected sample, and thereby greatly reduce rates of evaporation. Assuming a typical collection rate of 0.5 ml min^{-1} for the 15–minute collection period, calculations of free convection mass transfer of sample from the rods to the air indicate that evaporation should be less than 1%. Concentrations of natural background ions (e.g. Ca^{2+} and K^{+}) in cloudwater collected using the CHRCC were comparable to those found in CASC samples collected at other times of the year (see Chapter 2), further suggesting that evaporation was not a serious problem under conditions encountered during this study.

Sample melted off the rods during the heating cycle flows down into a Teflon sample trough, through a heated teflon tube, and into a sample bottle. Only bulk cloudwater samples are collected using the winter collection system. Samples are not refrigerated because the system is used when ambient temperatures are low. Since the system is not equipped with an automated rinsing system to rinse before and after each event, attendance by a site operator is required on an event basis. Both the CHRCC, and the cloudwater sensor described below, are mounted on a 3 m anodized aluminum stand. The CHRCC is mounted on top of the stand, while the sensor is mounted approximately 0.5 m below the top.

The new sensor designed for the winter collection system (see Figure 5.10) relies on an optical system to detect the presence of clouds. An LED light source (Skan–A–Matic, model L43004) emits light with a wavelength of 940 nm. Emitted light, scattered back toward the source by any target, is measured by a photodetector (Skan–A–Matic, model P43004), with peak response at 910 nm. Light emitted from the LED is modulated at 1 kHz. Only light of the proper wavelength and modulation is measured by the photodetector, helping to exclude interference from ambient light. Regular checks of the background reading are performed automatically to further reduce interference. Both the light source and the photodetector are housed by sight tubes, in an anodized aluminum housing, which fix their alignment at five degrees with respect to each other, resulting in a focal length of 0.75 m. The sight tubes are heated to prevent accumulation of ice. Air is pumped through the tubes at a rate of 1 l min^{-1}, reducing the collection of dust and discouraging habitation by insects. The housing also contains the control unit for the sensor.

In the presence of clouds, a significant degree of backscattering is observed by the photodetector, generating an increase in the photodetector output signal. When the signal exceeds a predetermined level for ten minutes, the collector is activated. Figure 5.11 shows a typical set of output data from the backscattering sensor during a period without cloud interception. There is some variation of the signal as a function of the time of day. Four periods of cloud interception are signified in Figure 5.12 by large spikes (up to 250 mV) in the output of the photodetector. A threshold value of 50 mV is used to activate the collector.

Data–logging and system control for the winter collection system is performed by a Campbell CR–10 controller. This unit processes and records

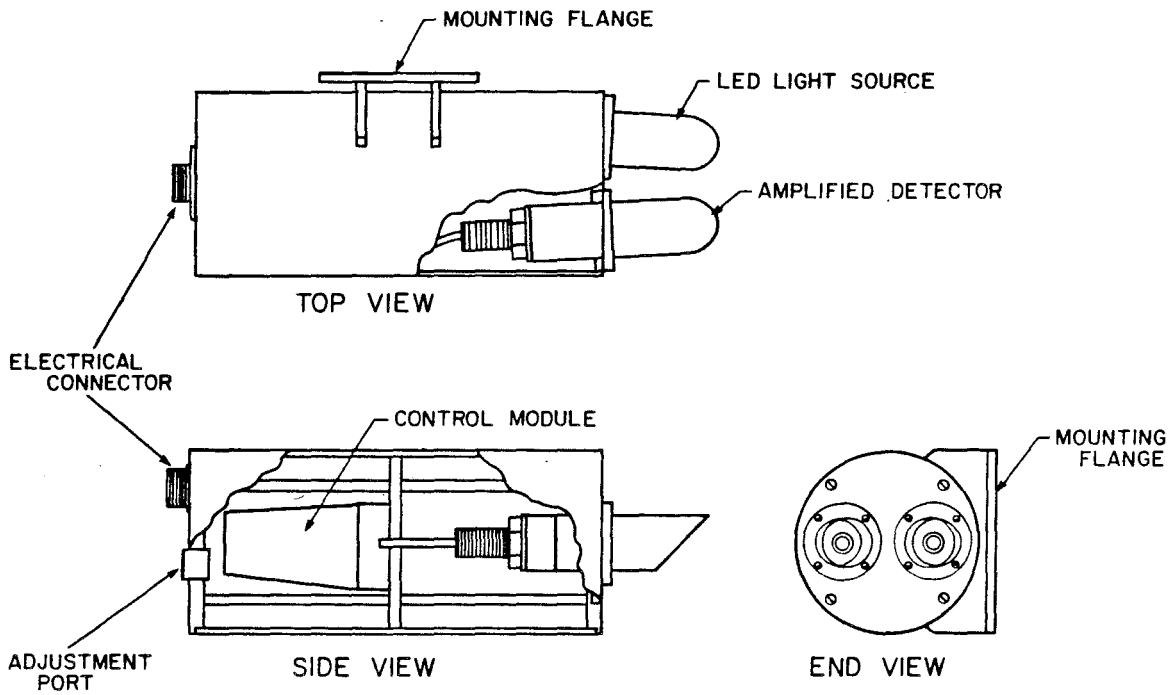

Figure 5.10. The cloudwater sensor used by the Winter Cloudwater Sampling System. The sensor relies on an increase in the level of backscattering of an infrared light beam to detect the presence of clouds.

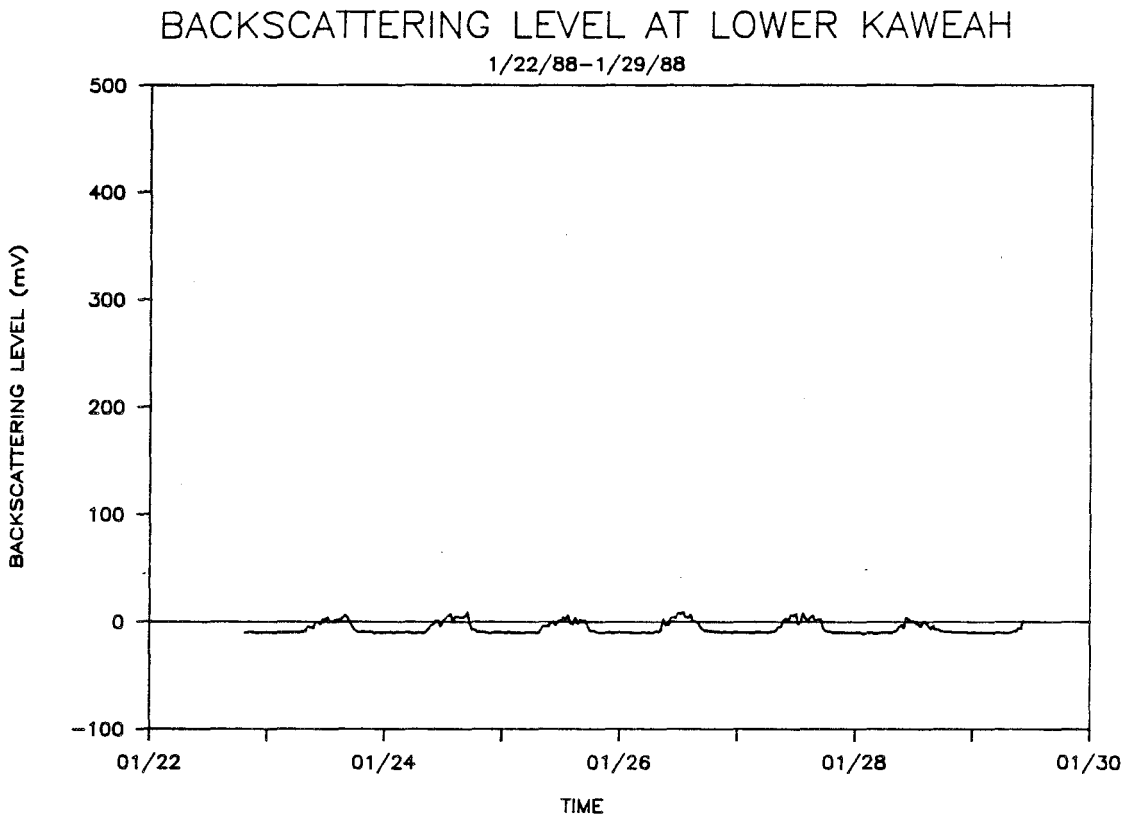

Figure 5.11. Typical output of the backscattering cloudwater sensor during a period without cloud interception.

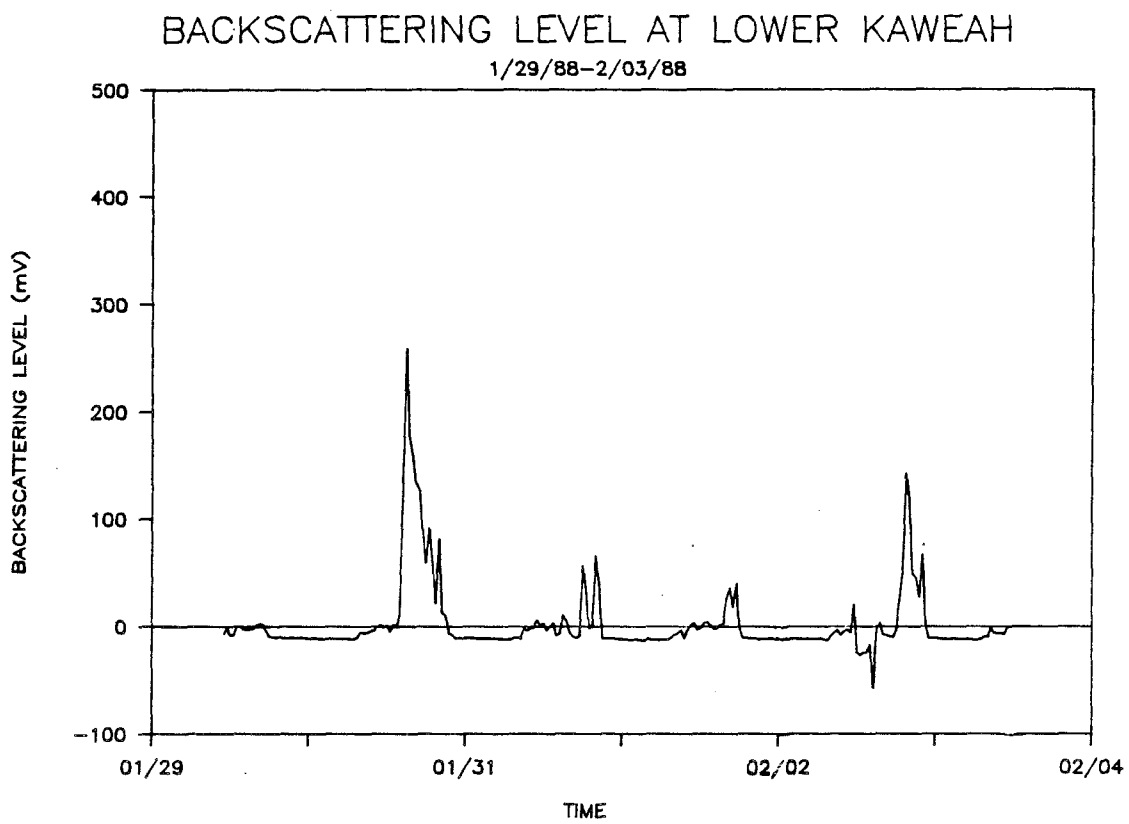

Figure 5.12. Typical response of the backscattering cloudwater sensor during several periods of cloud interception. The presence of clouds is indicated by the large positive response peaks evident in the diagram.

information from the backscattering sensor, a thermistor temperature probe, a barometer, an anemometer and wind vane, and the CHRCC. Half–hour averages of all parameters are recorded during normal operation. When clouds are intercepting the site, minimum and maximum backscattering levels, along with the running average and standard deviation of the backscattering level, are recorded every five minutes. The CR–10 interprets the signal from the backscattering sensor and determines when the collector should be activated. The CR–10 also is programmed to monitor the ambient temperature and to activate the heating cycle in the collector when warranted ($T_{ambient} \leq 4.5$ C).

Passive Cloudwater Monitoring System

Several of the cloudwater monitoring sites selected in the Sierras were located a considerable distance away from any source of electric power. Power requirements at the site therefore had to be limited to what could be supplied by batteries carried in to the sites once per month. This necessitated the development of a cloudwater collector which could collect droplets efficiently by utilizing the ambient winds. The cylindrical collector, depicted in Figure 5.13, is comprised of two concentric rows of 510 μm strands, making its collection efficiency independent of wind direction. The device collects most cloud droplets efficiently when the wind speed exceeds 2 miles per hour (see Figure 5.14). The collector is mounted on a 3 m anodized aluminum stand designed to withstand wind speeds exceeding 100 miles per hour. An anemometer (Weathermeasure #2612) is mounted at the same height as the collector on an arm extending 0.66 m out from the stand. A rain gauge (Weathermeasure #6011–A) is located on the ground a few meters away from the base of the stand.

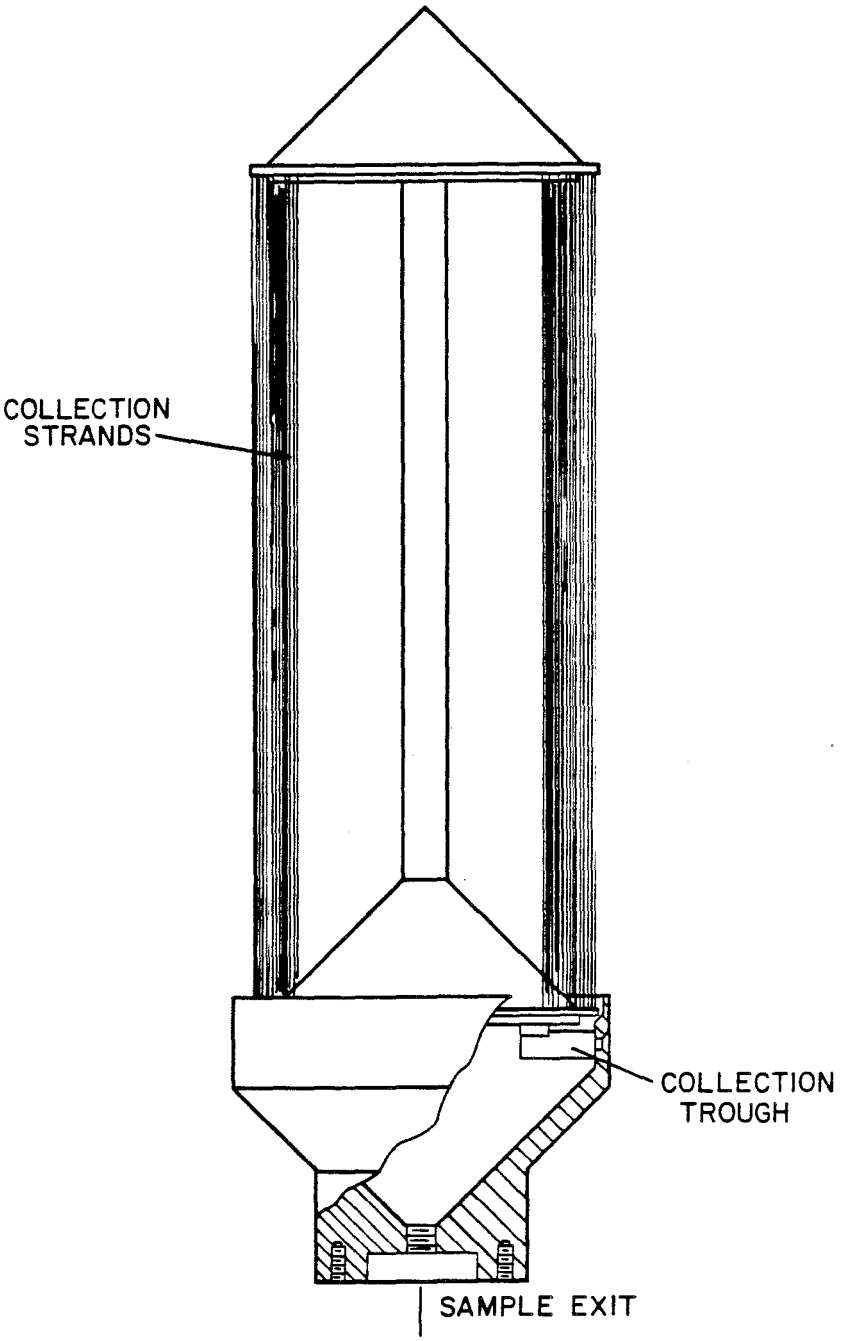

Figure 5.13. The cylindrical passive cloudwater collector utilized in the Passive Cloudwater Monitoring System.

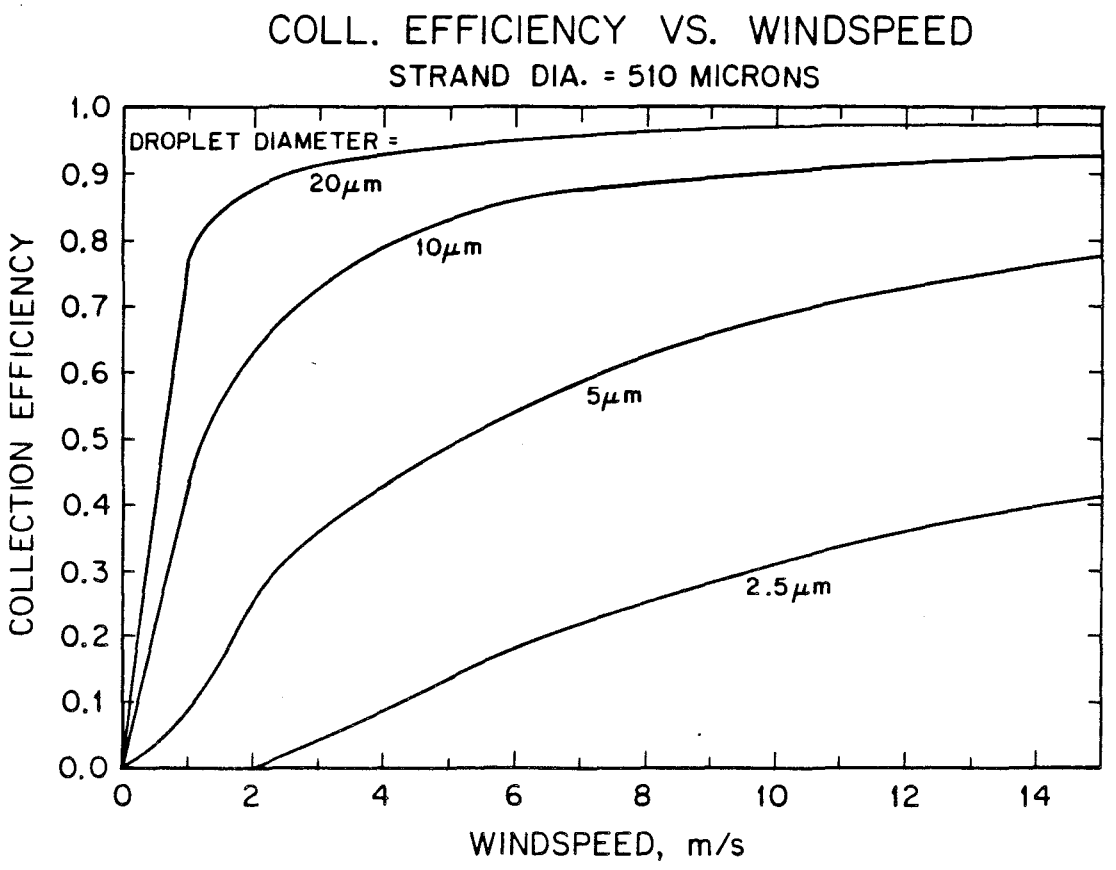

Figure 5.14. Collection efficiency of the passive cloudwater collector, as a function of wind speed, for several different droplet sizes.

Collected cloudwater is gravity fed through a Teflon tube into a tipping cup counter where its volume is measured in 8.7 ml increments. The counter is housed in a waterproof enclosure attached to the collector stand. A data collection system also is housed in this enclosure. Data is recorded from the counter mentioned above, a tipping cup rain gauge, and an anemometer. The data is stored on a Tandy 102 portable computer. The digital circuitry required to interface the computer to these three instruments was designed specifically for this project. Power consumed by the data-logging system is minimized by supplying power to the computer only during periods of cloud impaction or rainfall.

The key objective in software design for the system was compact data storage, since only 22 kbytes of memory were available. Most data from the tipping cups is stored as a two byte representation indicating the time and which cup tipped. Only two bytes are required per data point, since the time at which the tip occurs is recorded as elapsed time from the start of an event, rather than as real time. During periods of rainfall or cloud impaction, 5-minute average wind speeds are measured and recorded, also as a two byte representation. Compacting the stored information in this way allows a record of over 100 inches of rain and an equivalent amount of impacted cloudwater to be compiled before the available memory is fully depleted.

The design of the passive cloudwater collector allows rain as well as cloudwater to be collected. Determining which data points represent rainfall and which represent cloudwater impaction would be impossible without the simultaneous collection of data from the rain gauge. Figure 5.15 presents data describing the relative efficiency of rain collection by these two instruments as a function of ambient wind speed. Figure 5.16 depicts the same collection efficiency

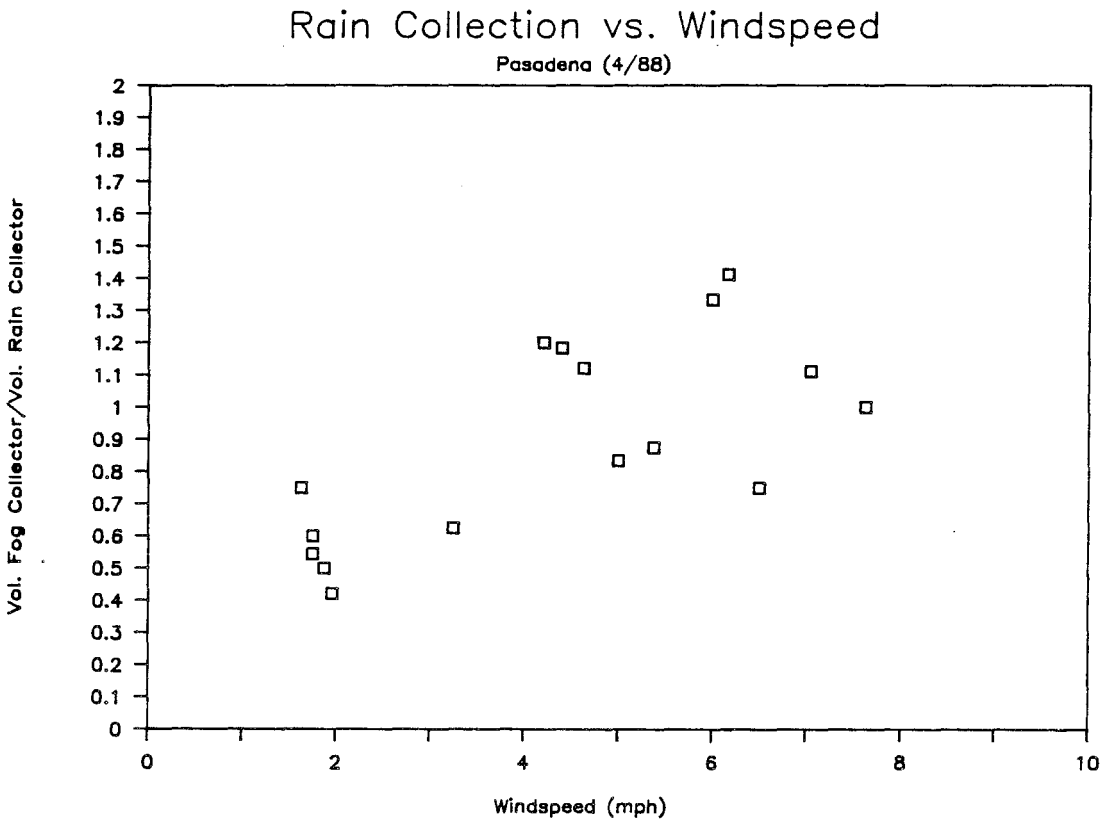

Figure 5.15. Comparison of the rainfall collection rates, exhibited by the rain gauge and the passive cloudwater collector, as a function of ambient wind speed.

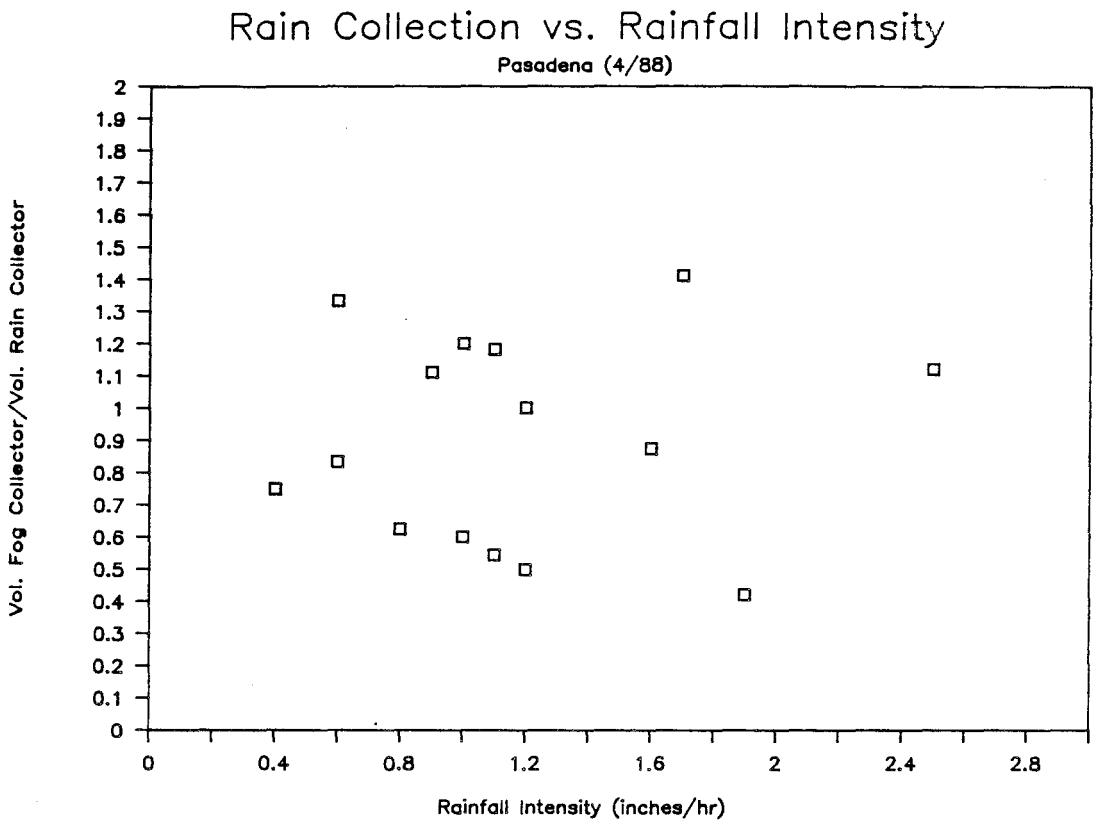

Figure 5.16. Comparison of the rainfall collection rates, exhibited by the rain gauge and the passive cloudwater collector, as a function of rainfall intensity.

data as a function of rainfall intensity. This data was collected in a side–by–side comparison of the two instruments during a number of rain storms occurring in Pasadena in early 1988. At low wind speeds (< 4 miles per hour), the rain gauge collected rainfall more efficiently than the cloudwater collector. This was expected since the cross–sectional area of the rain gauge is nearly 60% greater than the cross–sectional area of the passive cloudwater collector. At moderate wind speeds (4–8 miles per hour), however, impaction of droplets with a horizontal component to their motion, on the strands of the cloudwater collector, became more important, and the two instruments exhibited comparable collection efficiencies. At higher wind speeds than were observed in this intercomparison, droplets are likely to begin to blow off the strands of the cloudwater collector, resulting in a decrease in the collector's rainfall collection efficiency.

Conclusions

Three separate automated cloudwater collection systems were developed for use in a study of cloud interception frequency and cloudwater chemistry in the Sierra Nevada Mountains of central California. The first system utilized an active cloudwater collector, a sample–fractionating autosampler to divide and store the collected sample, and a cloudwater sensor to activate and deactivate the system. The cloudwater collector was equipped with automated covers and an automated rinsing system. This system was used to collect cloudwater samples, on a sub–event basis, during the spring, summer, and fall periods of the study. Collected samples were analyzed to determine their chemical composition.

The second system, also utilizing an active cloudwater collector, was used to collect Sierra cloudwater samples during the winter sampling period. The collector

used in this system incorporated a heating system, enabling frozen cloudwater (rime ice) to be melted and drained off of the collection surfaces during freezing conditions. An optical cloudwater sensor was used to detect the presence of clouds. Collected cloudwater was stored as a single bulk sample, which was chemically analyzed to determine the concentration levels of major ions.

Samples collected by the first two systems provided information about spatial and temporal variations in the chemical composition of Sierra cloudwater. The third system, utilizing a passive cloudwater collector in order to minimize power requirements, recorded the volume of cloudwater collected as a function of time, but samples were not chemically analyzed. The system also incorporated a rain gauge, and recorded precipitation as a function of time. This system was used to collect information on spatial and temporal variations in precipitation and cloud interception in the Sierra.

References

Bird, R. B., Stewart, W. E. and Lightfoot, E. N. (1960) *Transport Phenomena.* John Wiley and Sons, New York, 780 p.

Collett, J., Jr., Daube, B., Jr., Munger, J. W. and Hoffmann, M. R. (1989) A comparison of two cloudwater/fogwater collectors: The Rotating Arm Collector and The Caltech Active Strand Collector. submitted to *Atmos. Environ.*

Daube, B. C., Jr., Flagan, R. C. and Hoffmann, M. R. (1987a) Active cloudwater collector. United States Patent No. 4,697,462.

Daube, B. C., Jr., Kimball, K. D., Lamar, P. A. and Weathers, K. C. (1987b) Two new ground–level cloud water sampler designs which reduce rain contamination. *Atmos. Environ.* **21**, 893–900.

Friedlander, S. K. (1977) *Smoke, Dust, and Haze.* John Wiley and Sons, New York, 317 p.

Jacob, D. J., Wang, R. F. T. and Flagan, R. C. (1984) Fogwater collector design and characterization. *Envir. Sci. Technol.* **18**, 827–833.

Jacob, D. J., Waldman, J. M., Haghi, M., Hoffmann, M. R. and Flagan, R. C. (1985a) Instrument to collect fogwater for chemical analysis. *Rev. Sci. Instrum.* **56**, 1291–1293.

CHAPTER 6

A COMPARISON OF TWO CLOUDWATER/FOGWATER COLLECTORS: THE ROTATING ARM COLLECTOR AND THE CALTECH ACTIVE STRAND COLLECTOR

Atmospheric Environment

(submitted)

Abstract

A side–by–side comparison of the Rotating Arm Collector (RAC) and the Caltech Active Strand Collector (CASC) was conducted at an elevated coastal site near the eastern end of the Santa Barbara Channel. The CASC was observed to collect cloudwater at rates of up to 8.5 ml min^{-1}. The ratio of cloudwater collection rates was found to be close to the theoretical prediction of 4.2:1 (CASC:RAC) over a wide range of liquid water contents (LWC). At low LWC, however, this ratio climbed rapidly, possibly reflecting a predominance of small droplets under these conditions, coupled with a greater collection efficiency of small droplets by the CASC. The RAC collected cloudwater samples with significantly higher concentrations of Na^+, Ca^{2+}, Mg^{2+}, and Cl^- than were collected by the CASC. These higher concentrations may be due to differences in the chemical composition of large vs. small droplets. No significant differences were observed in concentrations of NO_3^-, SO_4^{2-}, or NH_4^+ in samples collected by the two instruments.

Introduction

The development of the Caltech Active Strand Collector (Daube et al., 1987) led to a need to compare the performance of this collector with the Rotating Arm Collector (Jacob et al., 1984) used in previous studies of fog and cloudwater chemistry in California. Of particular interest were the rate of sample collection by each instrument and the comparability of the chemical composition of the samples collected by the two instruments. In order to make these comparisons we needed a location at which we could sample several fog events with widely varying liquid water contents and chemical compositions. Side–by–side comparison of the collectors under these conditions would provide a good test of the relative performance of the two instruments.

Site Description and Measurement Techniques

Sampling Site

The site selected for the collector comparison was the roof of a one–story building located at 475 m, just below the summit of La Jolla Peak. La Jolla Peak is situated 3 km NNE of Pt. Mugu at the eastern end of the Santa Barbara Channel. The collectors were placed approximately 15 m apart with the exhaust from each directed away from the other collector.

This site was selected because of its elevation, its proximity to the ocean, and its location away from major anthropogenic sources. The combination of elevation and proximity to the ocean were expected to result in frequent impaction of coastal stratus moving inland with the nighttime sea breeze during the summer

period we planned to sample. The location away from any immediately neighboring anthropogenic sources was expected to provide a variety of cloudwater compositions, these varying with the mesoscale transport conditions associated with each event. Previous work had suggested that the site might be subjected to pollutant laden air masses originating in the Los Angeles Basin (Shair et al., 1982) or from oil platforms located in the coastal waters to the west (California Air Resources Board, 1982). These types of air masses, if associated with periods of coastal stratus, could result in the presence of highly polluted cloudwater at the site. Alternatively, it was expected that periods of air movement from the southwest (not associated with offshore flow from the South Coast Air Basin) during periods of coastal stratus would result in the presence of much cleaner cloudwater at the site.

Measurement Techniques

Cloudwater samples were collected simultaneously with the Rotating Arm Collector (RAC) and the Caltech Active Strand Collector (CASC) depicted in Figures 6.1 and 6.2, respectively. The RAC (Jacob et al., 1984) utilizes a 1.5 HP motor to drive a 63 cm long solid stainless steel rod at 1700 rpm. Each end of the rod has a slot milled into its leading edge to collect the impacting fogwater droplets. High density polyethylene (HDPE) bottles mounted on each end of the rod catch the fogwater sample as it is accelerated outward from each slot. Collection rates of up to 2 ml min^{-1} have been obtained in the field with this instrument. A scale model calibration of the RAC indicated a 50% lower size cut, based on droplet diameter, of 20 μm for the RAC.

The CASC (Daube et al., 1987) employs a fan to draw air across six angled banks of 510 μm teflon strands at a velocity of 9 m s^{-1}. Cloudwater droplets in the

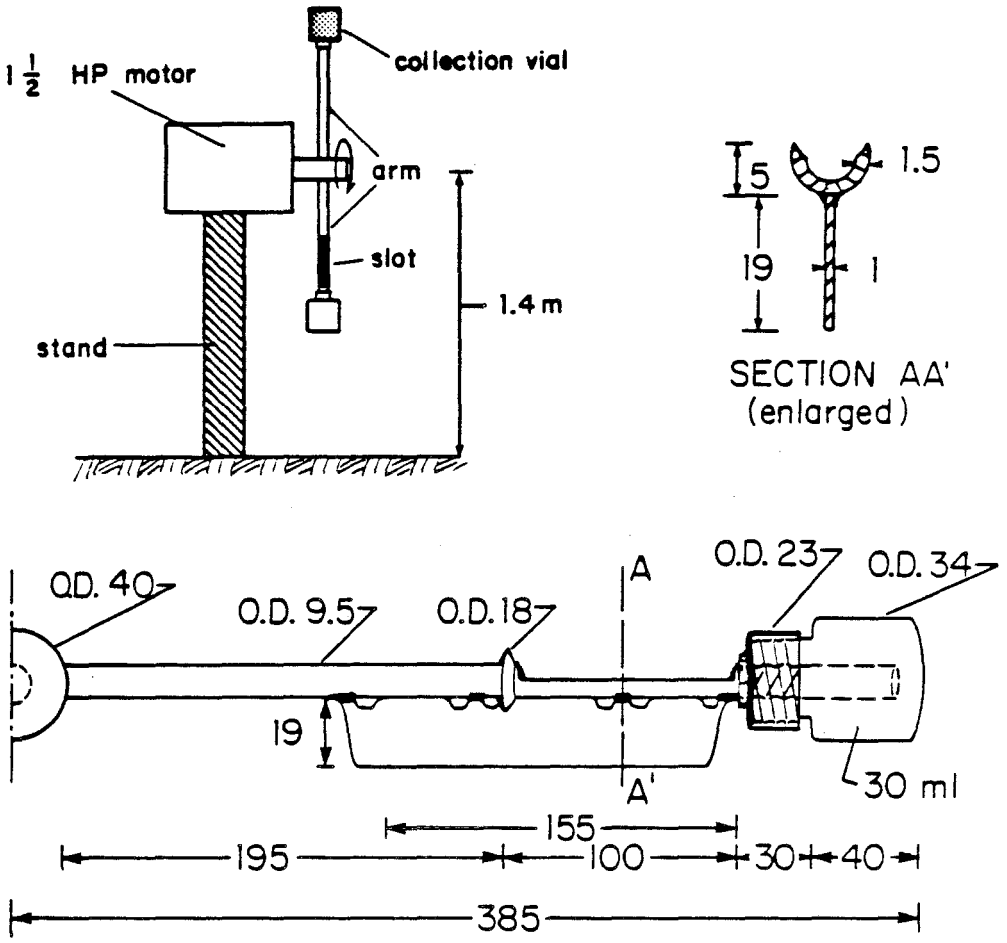

Figure 6.1. Caltech Rotating Arm Collector.

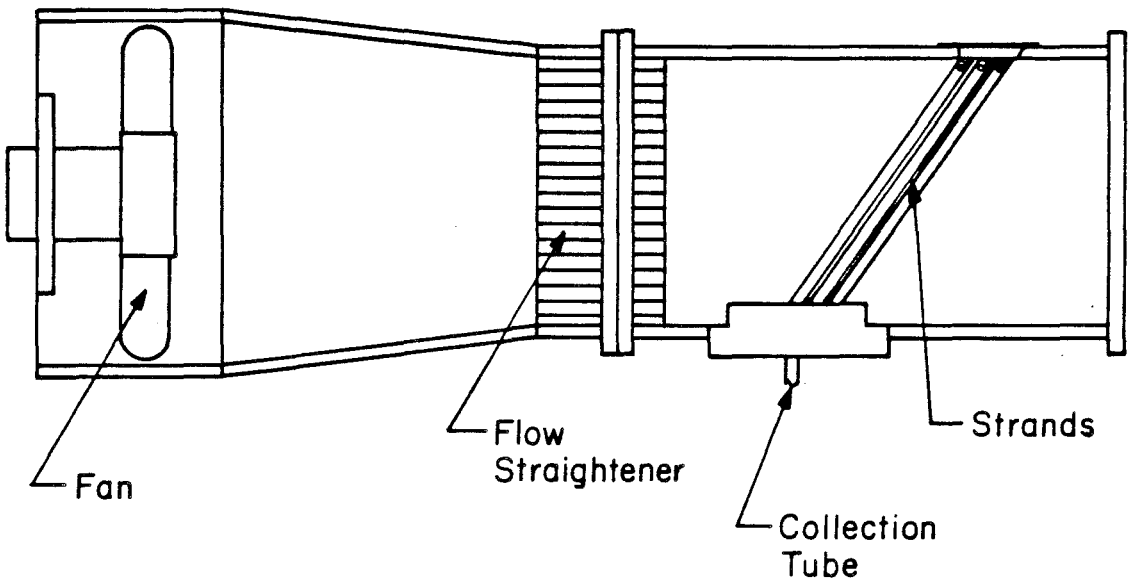

Figure 6.2. Caltech Active Strand Collector. Air flow is from right to left through the collector as viewed in the figure.

air parcel are collected on the strands by inertial impaction. The collected droplets run down the strands, aided by gravity and aerodynamic drag, through a teflon sample trough into a HDPE collection bottle. This instrument has a theoretical lower size cut of 3.5 μm, based on droplet diameter, and has collected cloudwater at rates of up to 8.5 ml min^{-1} in the field.

The major ions, Cl^-, SO_4^{2-}, and NO_3^-, were measured in our laboratory using a Dionex 2020i ion chromatograph with a Dionex AS−4 column and a bicarbonate−carbonate eluent. Na^+, Ca^{2+}, and Mg^{2+} concentrations were determined using a Varian Techtron AA6 atomic absorption spectrophotometer. NH_4^+ was measured by the phenol−hypochlorite method (Solorzano, 1967) using an Alpkem flow injection analyzer.

Sample Comparison Results

Collection Rate

The rates of cloudwater collection by the two instruments were compared for 22 periods during which samples were collected simultaneously. The theoretical ratio of collection rates between the two instruments is 4.2:1 (CASC:RAC). This figure is based on the expected air sampling rates of each instrument. In Figure 6.3 the actual collection rate data from this study are depicted along with this theoretical line. The data are plotted as the ratio of CASC to RAC collection rates vs. CASC collection rate. Most of the data points are scattered closely about the theoretical line. Several points at low CASC collection rate, however, fall well above this line, indicating that under these conditions the performance of the CASC relative to the RAC is much better than expected.

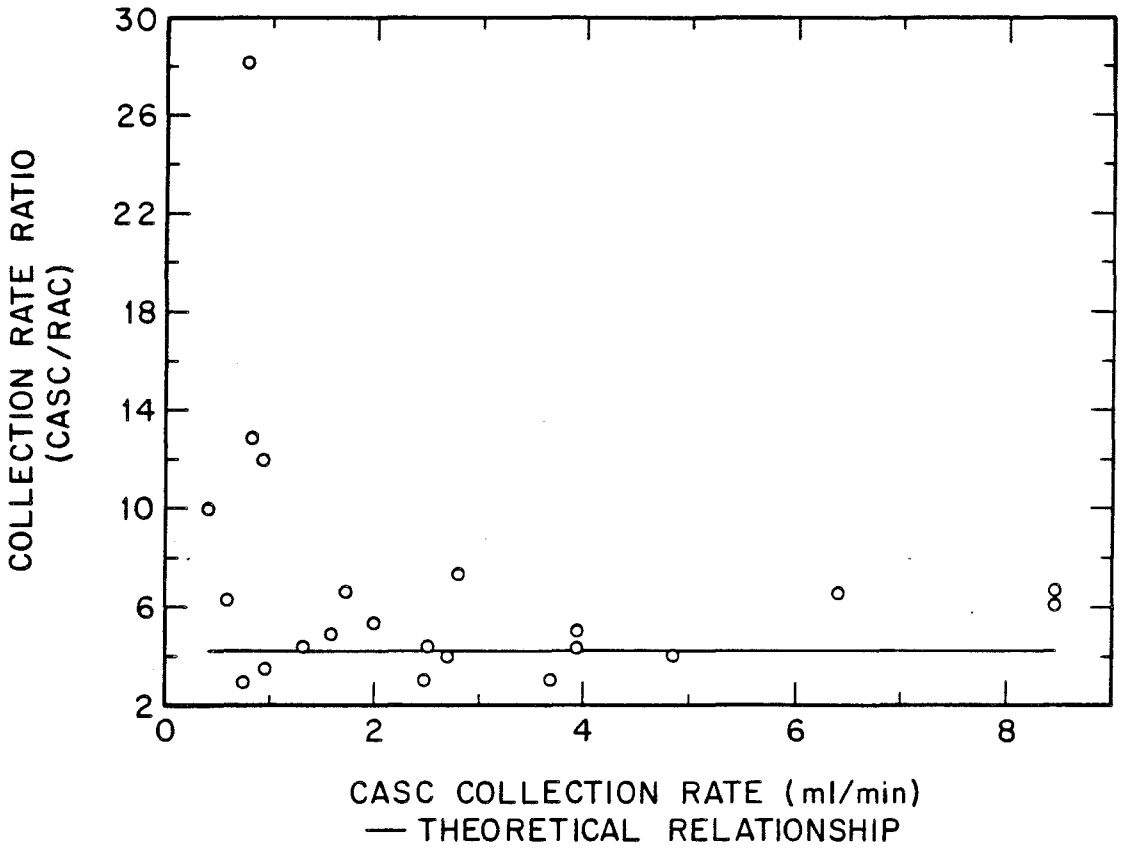

Figure 6.3. Comparison of CASC and RAC cloudwater collection rates.

Since the collection rate of the CASC is proportional to the liquid water content (LWC) of the cloud, these particular samples indicate that under low LWC conditions the collection efficiency of the RAC declines to a greater extent than that of the CASC. This may be due to the differing lower sizecuts of the two instruments. Typically low LWC clouds have a greater proportion of liquid water residing in smaller droplets (Best, 1951a). Since the RAC collects only those droplets above 20 μm efficiently, it may be sampling less than half of the droplet spectrum under these conditions. The 3.5 μm lower size cut of the CASC, however, allows it to sample the bulk of the available liquid water.

Chemical Composition

Of the 22 samples collected simultaneously by the CASC and the RAC, 11 were chosen for a comparison of major ion composition. These 11 samples were collected on three different nights in July and August of 1985. The other 11 samples were relatively small in volume. Since small volume samples are more likely to show signs of contamination than large ones, these samples were not used for this portion of the collector comparison. Trends exhibited by those samples used in the comparison, however, were generally observed in the low volume samples as well.

Seven ions were used for comparison of the samples: NO_3^-, SO_4^{2-}, Cl^-, NH_4^+, Mg^{2+}, Ca^{2+}, and Na^+. Along with H^+, these ions form the bulk of the ionic composition for all 11 samples. Figures 6.4 through 6.10 depict the sample comparison for each ion. Data is plotted as concentration in the CASC sample vs. concentration in the RAC sample. The eleven samples exhibited a wide range of concentrations for each of these ions. Also plotted on each graph is a 1:1 line. If the

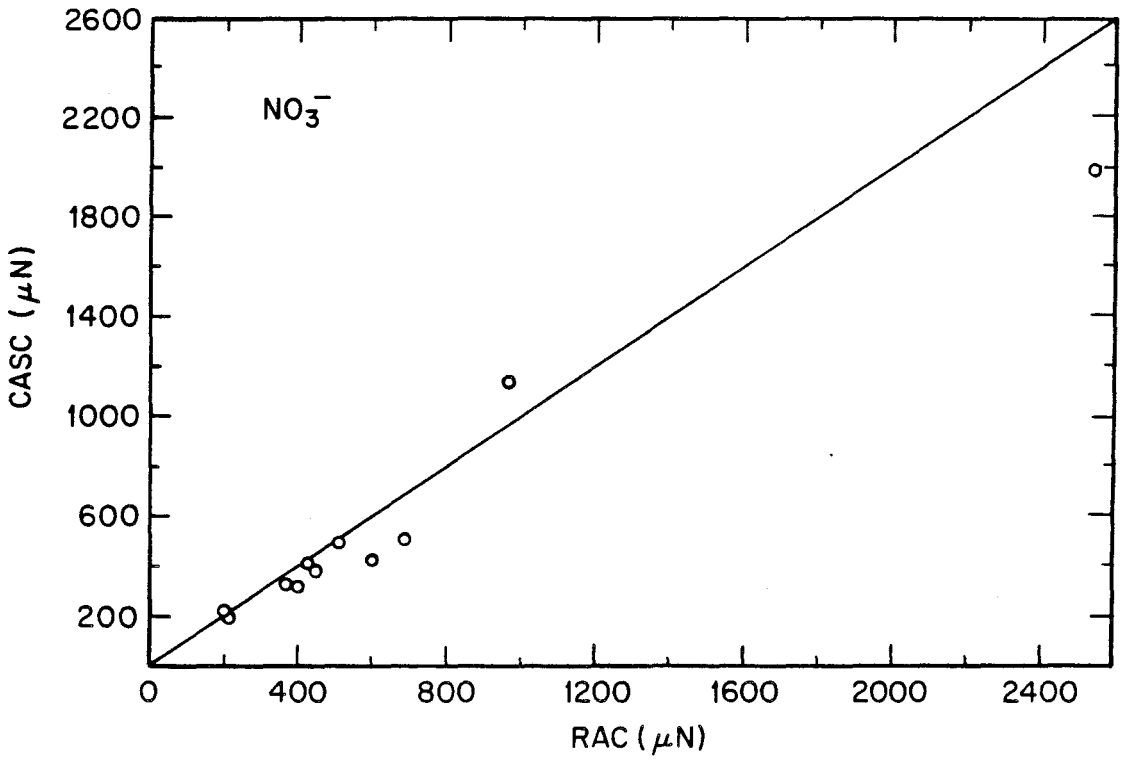

Figure 6.4. Comparison of NO_3^- concentrations in CASC and RAC samples. A line of perfect correlation is included for reference.

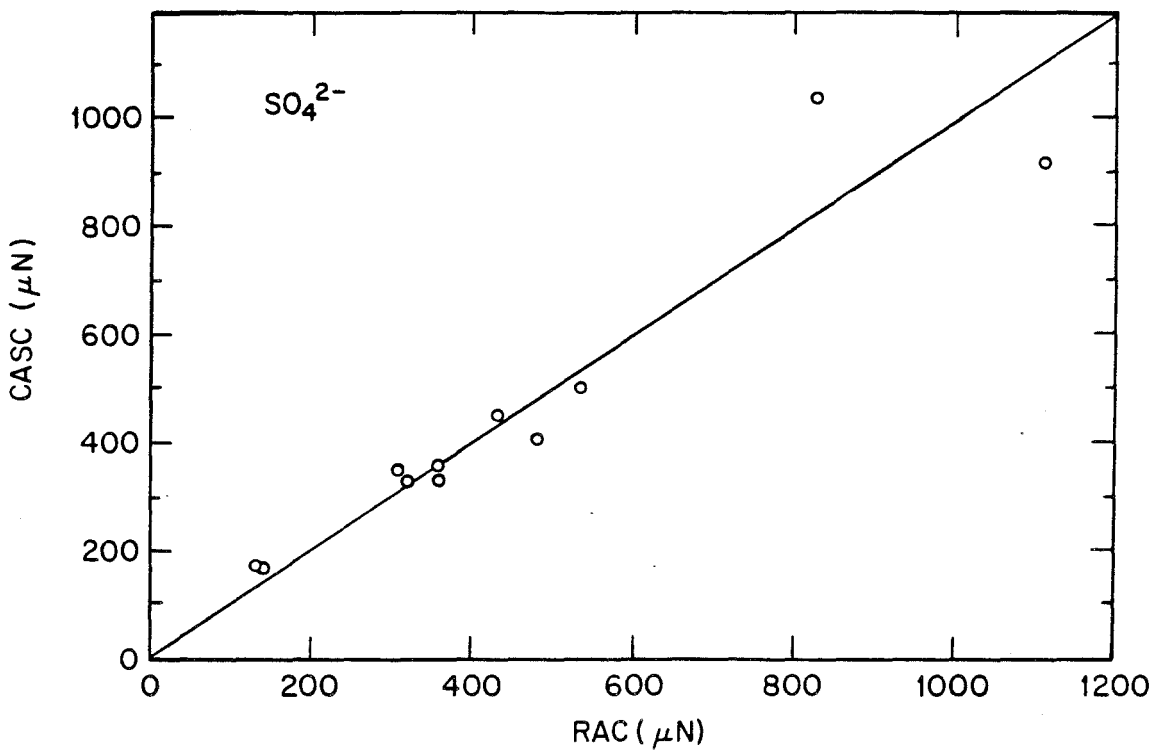

Figure 6.5. Comparison of SO_4^{2-} concentrations in CASC and RAC samples. A line of perfect correlation is included for reference.

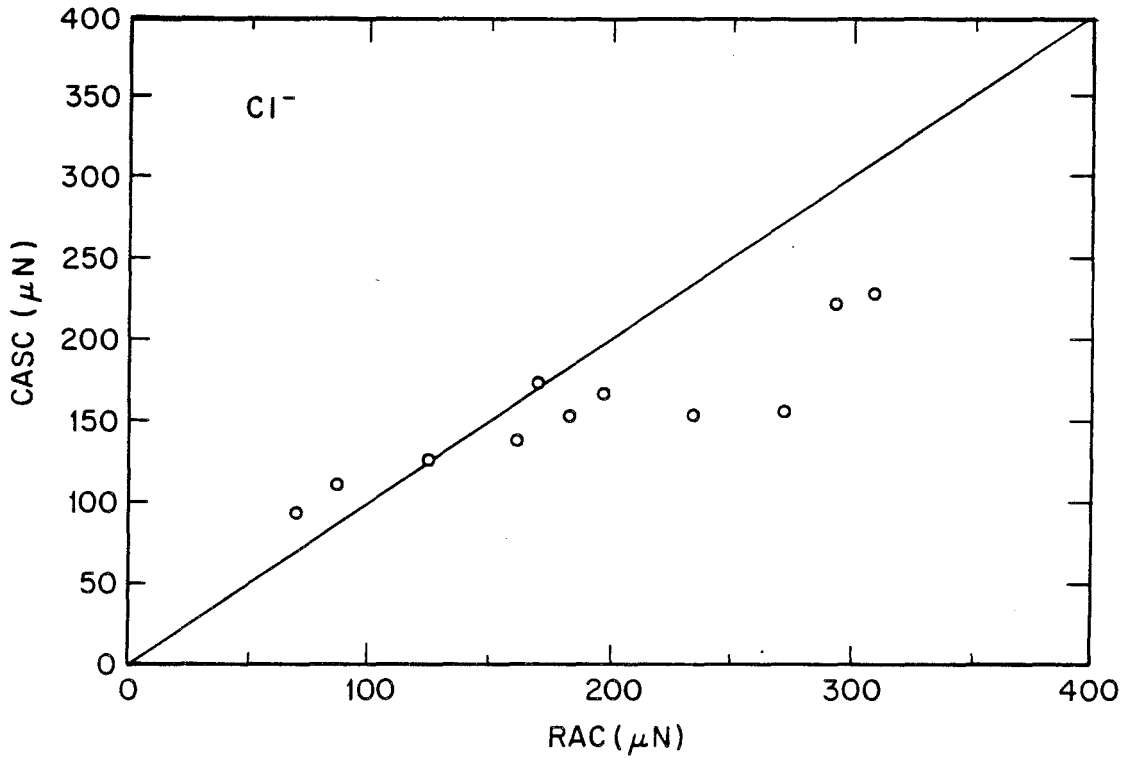

Figure 6.6. Comparison of Cl^- concentrations in CASC and RAC samples. A line of perfect correlation is included for reference.

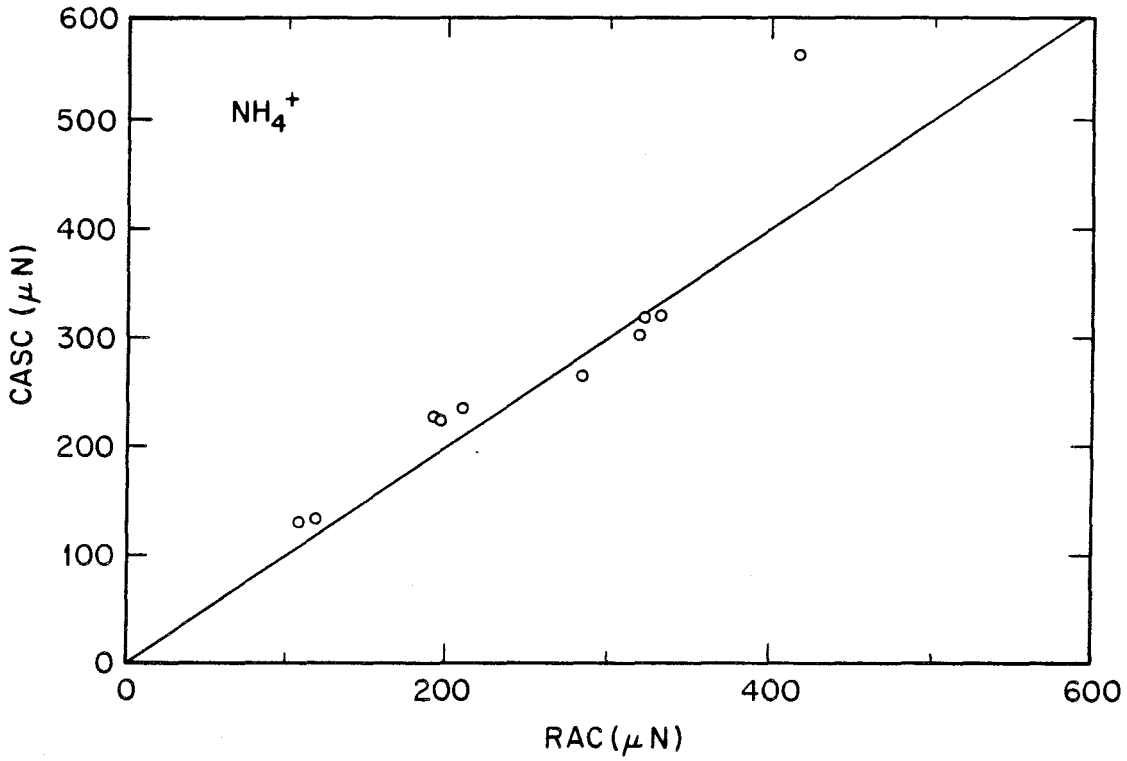

Figure 6.7. Comparison of NH_4^+ concentrations in CASC and RAC samples. A line of perfect correlation is included for reference.

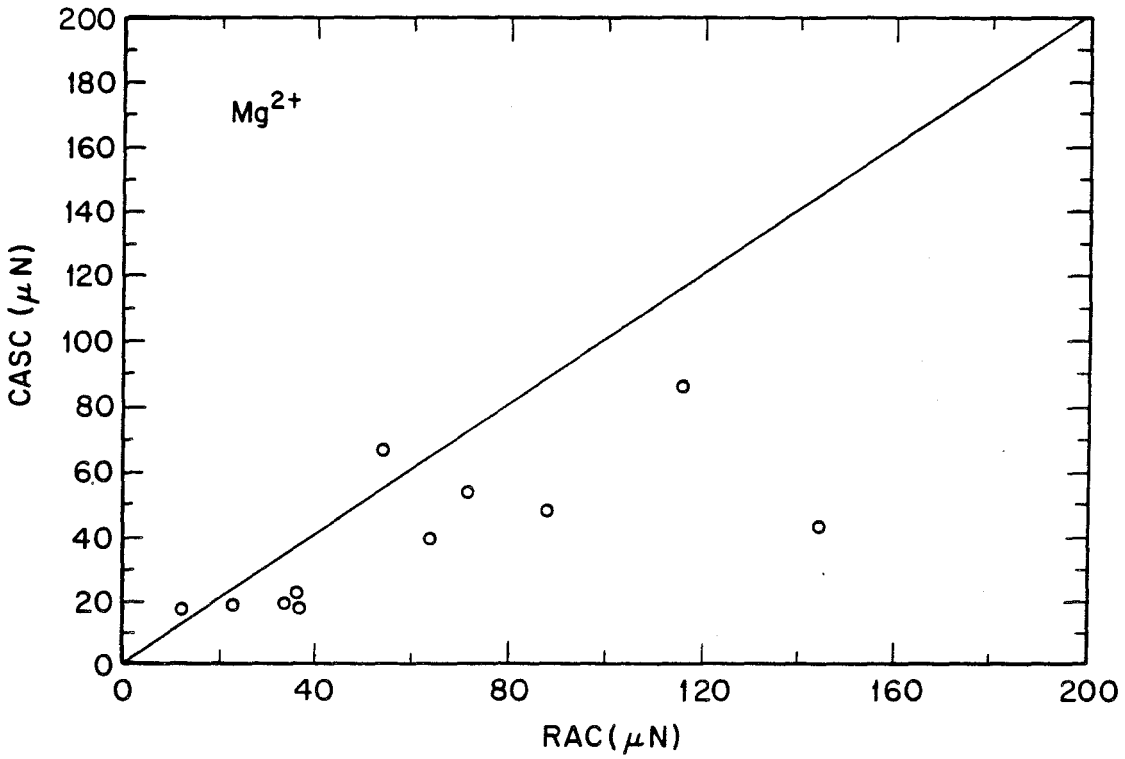

Figure 6.8. Comparison of Mg^{2+} concentrations in CASC and RAC samples. A line of perfect correlation is included for reference.

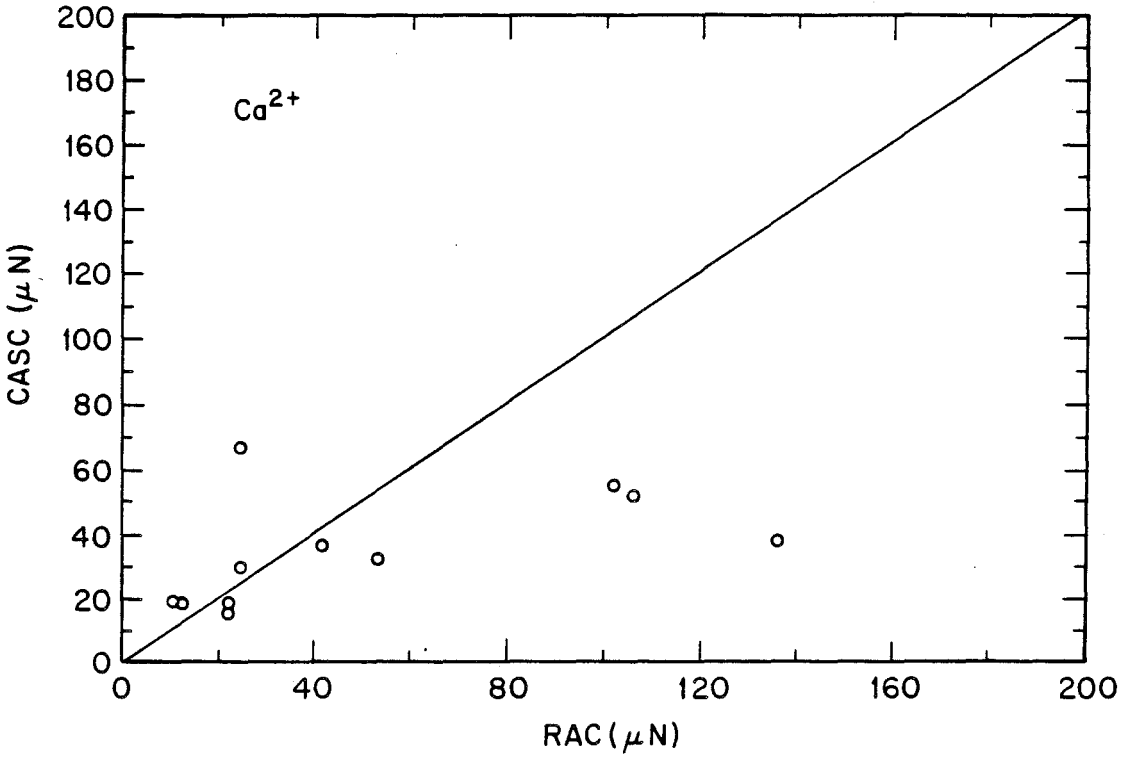

Figure 6.9. Comparison of Ca^{2+} concentrations in CASC and RAC samples. A line of perfect correlation is included for reference.

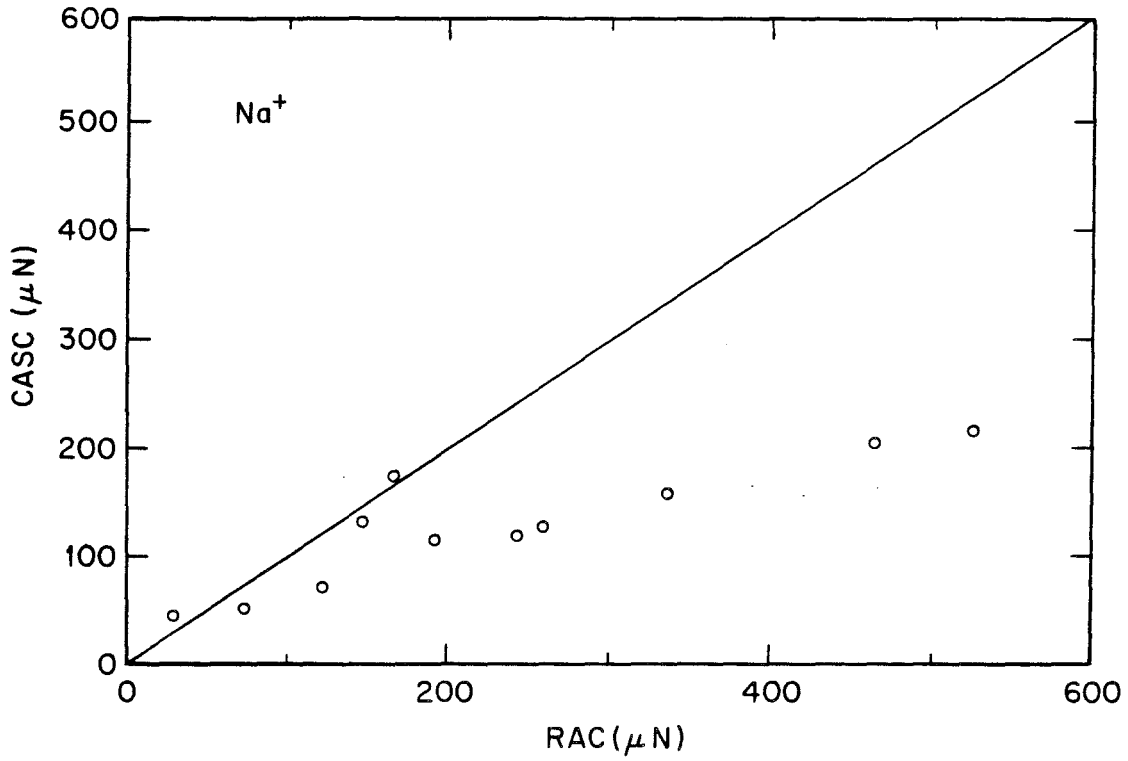

Figure 6.10. Comparison of Na^+ concentrations in CASC and RAC samples. A line of perfect correlation is included for reference.

collected sample pairs were identical in composition, the data points should deviate from this line only due to random errors in analysis.

In the case of NO_3^- , SO_4^{2-} , and NH_4^+ the data points seem fairly well matched with the 1:1 line. Deviation is more evident amongst the Cl^-, Na^+, Mg^{2+}, and Ca^{2+} compositions. In all four cases it appears that the RAC collects these ions preferentially, particularly when the ions are present at higher concentrations.

A statistical analysis was performed to determine whether the deviations suggested above were significant. A linear relationship of the form given by equation 6.1

(Eq'n. 6.1) $$Y_i = \alpha + \beta X_i + \mu$$

may be hypothesized where Y_i and X_i are the matrices of CASC and RAC concentrations of ion "i", respectively, and "μ" represents the error in the equation. Typically, the values of α and β, the intercept and the slope, are estimated using the method of ordinary least squares (OLS). When there are errors in the measurement of both the dependent and independent variables, however, OLS provides a biased estimate of the slope (Johnston, 1984; Maddala, 1977).

Two estimation methods are commonly used to remedy this problem of bias. One requires a fairly accurate knowledge of the magnitudes of the errors. In order to utilize this approach, simultaneous data is needed on side-by-side CASC and side-by-side RAC sampling. Since this was not available, the second estimation method was utilized. This method, known as the Instrumental Variable (IV) method (Johnston, 1984), provides a consistent estimate of both the slope and

intercept. The method requires a matrix of variables correlated with the X variables but uncorrelated with the errors in the X variables.

The particular method utilized for this comparison has been described in detail by Bartlett (1949), and is a modification of earlier work by Wald (1940). The mean of the coordinates ($\bar{x}$,$\bar{y}$) is used to define one point of the fitted line. To determine the slope, the n data points are divided into three groups which are nonoverlapping in either the x or the y direction. The groups should be chosen so that the two extreme groups are as near n/3 as possible. The slope of the fitted line is then defined by the slope of the join of the mean coordinates, ($\bar{x}_1$,$\bar{y}_1$) and ($\bar{x}_3$,$\bar{y}_3$), for the two extreme groups.

While Bartlett's method provides a consistent estimate for the slope and intercept of the relationship (1) it is not as efficient as OLS. A decrease in efficiency results in an increase in the size of the confidence limits placed on these estimates. When faced with a situation where there are errors in the independent variables, however, it becomes necessary to sacrifice some efficiency to gain an unbiased estimator. Table 6.1 lists the results of applying this method to the Na^+, Cl^-, Ca^{2+}, and Mg^{2+} data. The slope and the corresponding 95% confidence limits are given for the CASC vs. RAC comparison for each ion. A slope greater than one indicates preferential collection of that ion by the RAC (i.e., RAC sample concentrations of the ion are significantly higher than CASC sample concentrations of the same ion), while a slope less than one indicates that the CASC collects the ion preferentially. A slope of one indicates no preferential collection. The results in Table 6.1 indicate that at the 95% confidence level the RAC collects Na^+, Cl^-, and Ca^{2+} preferentially. Preferential collection of Mg^{2+} by the RAC is indicated at the 90% confidence level. Data for NH_4^+, NO_3^-, and SO_4^{2-} indicated no preferential

Table 6.1. Slopes Different from One for CASC vs. RAC Sample Ionic Composition Comparison

Ion	*Slope*	*95% Confidence Limits*
Na^+	0.34	(0.18, 0.50)
Cl^-	0.42	(0.22, 0.61)
Ca^{2+}	0.37	(0.08, 0.66)
Mg^{2+}	0.58	(0.14, 1.03)

collection of these ions by either collector.

Typically, larger condensation nuclei lead to the formation of larger cloud droplets in the lower portions of a cloud not subjected to significant horizontal entrainment of dry air (Best, 1951b, Mason and Chien, 1962, Hudson, 1984). Since sea salt and soil dust are found to reside in the larger end of the aerosol size spectrum (Seinfeld, 1986), the elements found predominantly in these types of particles (e.g. Cl^-, Na^+, Mg^{2+}, and Ca^{2+}) will reside there as well. Therefore, as cloud droplets form on the available aerosol nuclei and grow by condensation, it should be expected that these elements would be found predominantly in the upper end of the droplet size spectrum. In the more mature portions of a cloud this trend may be obscured somewhat as droplet coalescence becomes increasingly important (Mason, 1971).

The fact that the RAC preferentially collected Na^+, Cl^-, Mg^{2+}, and Ca^{2+} is consistent with its lower collection efficiency for small droplets. Since these droplets should come predominantly from condensation on smaller aerosol nuclei, they are likely to contain much lower concentrations of Na^+, Cl^-, Mg^{2+}, and Ca^{2+}. The smaller droplets, collected efficiently by the CASC, act to dilute the concentrations of these four ions in the CASC samples.

In an intercomparison of fogwater collectors conducted at Henninger Flats in (Hering et al., 1987), some of the devices collected samples with higher concentrations of soil dust cations, notably Ca^{2+} and Mg^{2+}, and Na^+. Data from a comparison of a Desert Research Institute linear–jet impactor and a RAC exhibited trends very comparable to those seen in the current study for Na^+, Ca^{2+}, and Mg^{2+}: preferential collection by the RAC (Hering et al., 1987). A lower size cut of

between 2 and 5 μm has been reported for the DRI jet impactor (Katz, 1980), comparable to the lower size cut for the CASC. Some speculation was made about whether the preferential collection by the RAC was due to differences in the lower size cuts of the collectors or due to some other factor. The final conclusion was that this difference was due to intense research activity at the site which probably led to soil dust particles being kicked up. These dense particles would be sampled more efficiently by the RAC than by the DRI jet impactor due to differences in the sampler inlets (Waldman, 1985). No explanation was offered for the preferential collection of Na^+, which is primarily derived from sea spray.

In the CASC vs. RAC comparison both samplers were located on a rooftop away from possible sources of soil dust contamination. During sampling periods the rooftop was heavily wetted by deposition from the dense fog, providing further protection from soil dust contamination. There was also very little activity at the site. The combination of these factors in the current study suggests that perhaps the differences seen are due to differences between the collectors in the collection efficiency of small droplets.

During the CASC vs. RAC comparison no significant collection preferences for any ion were exhibited by the CASC. This happened despite the fact that aerosol NO_3^-, SO_4^{2-}, and NH_4^+, resulting primarily from gas-to-particle conversion processes, are found predominantly in the fine particle fraction (Seinfeld, 1986). Since smaller cloud droplets should tend to have smaller condensation nuclei, it might be expected that these ions would reside mostly in the smaller droplets and therefore be collected preferentially by the CASC. The situation is not so simple, however, since cloudwater concentrations of all three of these ions may be altered by absorption of precursor gas phase species followed by chemical reaction. $NH_3(g)$ can

be absorbed by the droplets and protonated to form NH_4^+; $HNO_3(g)$ can be absorbed, followed by deprotonation to yield NO_3^-; $SO_2(g)$ can be absorbed and oxidized to SO_4^{2-}. The first two processes are extremely rapid. The oxidation of S(IV) to S(VI) in cloudwater is also rapid in the presence H_2O_2 or a metal catalyst (Hoffmann and Jacob, 1984). All three of these processes occur throughout the droplet size spectrum making them likely candidates for masking the signature of aerosol NO_3^-, NH_4^+, and SO_4^{2-}.

Summary

A comparison of cloudwater collection characteristics of the Caltech Active Strand Collector (CASC) and the Rotating Arm Collector (RAC) was conducted at an elevated coastal site near the eastern end of the Santa Barbara Channel during the summer of 1985. Of particular interest were the rates of collection and the chemical comparability of the samples obtained using each instrument.

Collection rates as high as 8.5 ml min^{-1} were obtained using the CASC in this study. Collection rates for the RAC have been seen to go as high as 2 ml min^{-1} in past studies. During this intercomparison the ratio of CASC to RAC collection rates was found to be close to the theoretical prediction of 4.2:1 over a wide range of LWC. At low LWC, however, this ratio climbed rapidly. This may be attributable to the differing lower size cuts of the two instruments: since the CASC collects small droplets more efficiently than the RAC, its performance relative to the RAC should increase in thinner fogs and clouds where the mass median droplet diameter decreases.

Concentrations of Na^+, Cl^-, NO_3^-, SO_4^{2-}, NH_4^+, Ca^{2+}, and Mg^{2+} in simultaneous

samples collected by the two instruments were compared. Preferential collection of Na^+, Cl^-, and Ca^{2+} by the RAC was observed to occur with a confidence level greater than 95%. Preferential collection of Mg^{2+} by the RAC was observed to occur with a confidence level greater than 90%. This preferential collection may also be attributable to the differing lower size cuts of the two samplers since these ions, derived primarily from soil dust and sea spray, may be expected to reside primarily in larger cloud droplets which make up a larger fraction of each RAC sample. No significant preferential collection by either collector was observed for NO_3^-, SO_4^{2-}, or NH_4^+.

References

Bartlett, M. S. (1949) Fitting a straight line when both variables are subject to error. *Biometrics* **5**, 207–212.

Best, A. C. (1951a) Drop–size distribution in cloud and fog. *Q. Jl. R. met. Soc.* **77**, 418–426.

Best, A. C. (1951b) The size of cloud droplets in layer–type cloud. *Q. Jl. R. met. Soc.* **77**, 241–248.

California Air Resources Board (1982) Air quality aspects of the development of offshore oil and gas resources, a staff report available from the CARB, 1800 15th St., Sacramento, CA.

Daube, B. C., Jr., Flagan, R. C. and Hoffmann, M. R. (1987) *Active cloudwater collector.* United States Patent No. 4,697,462.

Hering, S. V., Blumenthal, D. L., Brewer, R. L., Gertler, A., Hoffmann, M., Kadlecek, J. A. and Pettus, K. (1987) Field intercomparison of five types of fogwater collectors. *Environ. Sci. Technol.* **21**, 654–663.

Hoffmann, M. R. and Jacob, D. J. (1984) Kinetics and mechanisms of the catalytic oxidation of dissolved sulfur dioxide in aqueous solution: an application to nighttime fogwater chemistry, in *Acid Precipitation: SO_2, NO, and NO_x Oxidation Mechanisms: Atmospheric Considerations*, J. G. Calvert, ed., Butterworth Publishers, Boston, 101–172.

Hudson, J. G. (1984) Ambient CCN and FCN measurements, in *Hygroscopic Aerosols*, L. H. Ruhnke and A. Deepak, eds., A. Deepak Publishing, Hampton, VA.

Jacob, D. J., Wang, R. F. T. and Flagan, R. C. (1984) Fogwater collector design and characterization. *Environ. Sci. Technol.* **18**, 827–833.

Johnston, J. (1984) *Econometric Methods*, 3rd Ed., McGraw–Hill, New York.

Katz, U. (1980) A droplet impactor to collect liquid water from laboratory clouds for chemical analysis, in *Communications à la VII Conference Internationale sur la Physique des Nuages*, Laboratoire Associe de Meteorologie Physique, Aubiere France, 697–700.

Maddala, G. S. (1977) *Econometrics*, McGraw–Hill, New York.

Mason, B. J. (1971) *The Physics of Clouds*, 2nd Ed., Oxford University Press, London.

Mason, B. J. and Chien, C. W. (1962) Cloud–droplet growth by condensation in cumulus. Q. *Jl. R. met. Soc.* 88, 133–138.

Seinfeld, J. H. (1986) *Atmospheric Chemistry and Physics of Air Pollution*, Wiley Interscience, New York.

Shair, F. H., Sasaki, E. J., Carlan, D. E., Cass, G. R., Goodin, W. R., Edinger, J. G. and Schacher, G. E. (1982) Transport and dispersion of airborne pollutants associated with the land breeze–sea breeze system. *Atmos. Environ.* **16**, 2043–2053.

Solorzano, L. (1967) Determination of ammonia in natural waters by the phenol–hypochlorite method. *Limnol. Oceanogr.* 14, 799–801.

Wald, A. (1940) The fitting of straight lines if both variables are subject to error. *Ann. Math. Stat.* **11**, 284–300.

Waldman, J. M. (1985) Depositional aspects of pollutant behavior in fog, Ph.D. thesis, California Institute of Technology, Pasadena, CA.

CHAPTER 7

SHORT-TERM TRENDS AND SPATIAL VARIABILITY IN PRECIPITATION CHEMISTRY IN THE SOUTH COAST AIR BASIN

Introduction

Storm systems passing through Los Angeles normally originate over the Pacific Ocean and have little or no contact with polluted air masses until they reach the South Coast Air Basin. Once over Los Angeles, the storm serves both to cleanse pollutants from the atmosphere and to deposit them at the ground. Several processes are important in determining the efficiency of atmospheric cleansing and the total deposition of each species of interest. Important processes within the cloud include scavenging of aerosol by nucleation, diffusion, and impaction, scavenging of gases, and aqueous phase reaction. Below the cloud, raindrops continue to scavenge gases and aerosol, and reaction may continue within the droplets as they fall to the ground. The relative importance of in-cloud vs. below-cloud processes can be evaluated by examining vertical profiles of rainwater concentrations and deposition rates for each species of interest.

The amount of wet deposition of each species during the course of the storm, relative to the quantity of that species present in the air mass over the basin prior to the onset of rain (referred to here as the pre-storm atmospheric burden of that species), is also of interest. If the deposition of a given species is greater than its pre-storm atmospheric burden, then some inferences about the emission rate of the species, or its production rate in the atmosphere, may be drawn, giving proper consideration to the potential for transport of the species from other locations. Questions about transport are related further to local emissions influences, which affect the composition of rainfall on a distance scale much smaller than the size of the South Coast Air Basin.

In order to properly investigate the issues discussed above, simultaneous

measurements of rainfall rate and composition are needed, as a function of time, at several sites throughout the basin. Compositional measurements of the aerosol and gas phases as a function of time also are needed at the same sites. The development of both an automated sub–event precipitation sampler and an automated aerosol collector enabled us to meet these requirements and proceed to address these issues.

Site Description and Measurement Techniques

Sampling Sites

Five sites were selected for use in the study. These sites, depicted in Figure 7.1, were located at West Los Angeles, Pasadena, Henninger Flats, Mount Wilson, and Riverside. West Los Angeles, Pasadena, and Riverside were selected to provide a sampling transect from east to west in the South Coast Air Basin (SoCAB). Pasadena, Henninger Flats, and Mount Wilson were chosen to represent a "vertical" profile. The floor of the basin rises from just over 200 m elevation at Pasadena to approximately 1700 m at Mount Wilson, 12 km farther inland. Henninger Flats is located at an elevation of approximately 700 m.

The site at Mt. Wilson is located on the grounds of the Mt. Wilson Observatory. The site at Henninger Flats is in a tree nursery operated by the Los Angeles County Fire Department. Both the Mount Wilson site and the Henninger Flats site are situated in areas away from regular vehicle travel. The Pasadena site is located on the roof of the three–story W. M. Keck Laboratories building on the Caltech campus. A paved parking lot is located 75 m to the north of the building. The West Los Angeles site is located on the grounds of the Veterans Administration Hospital. The 405 freeway is located approximately 1 km to the east. The

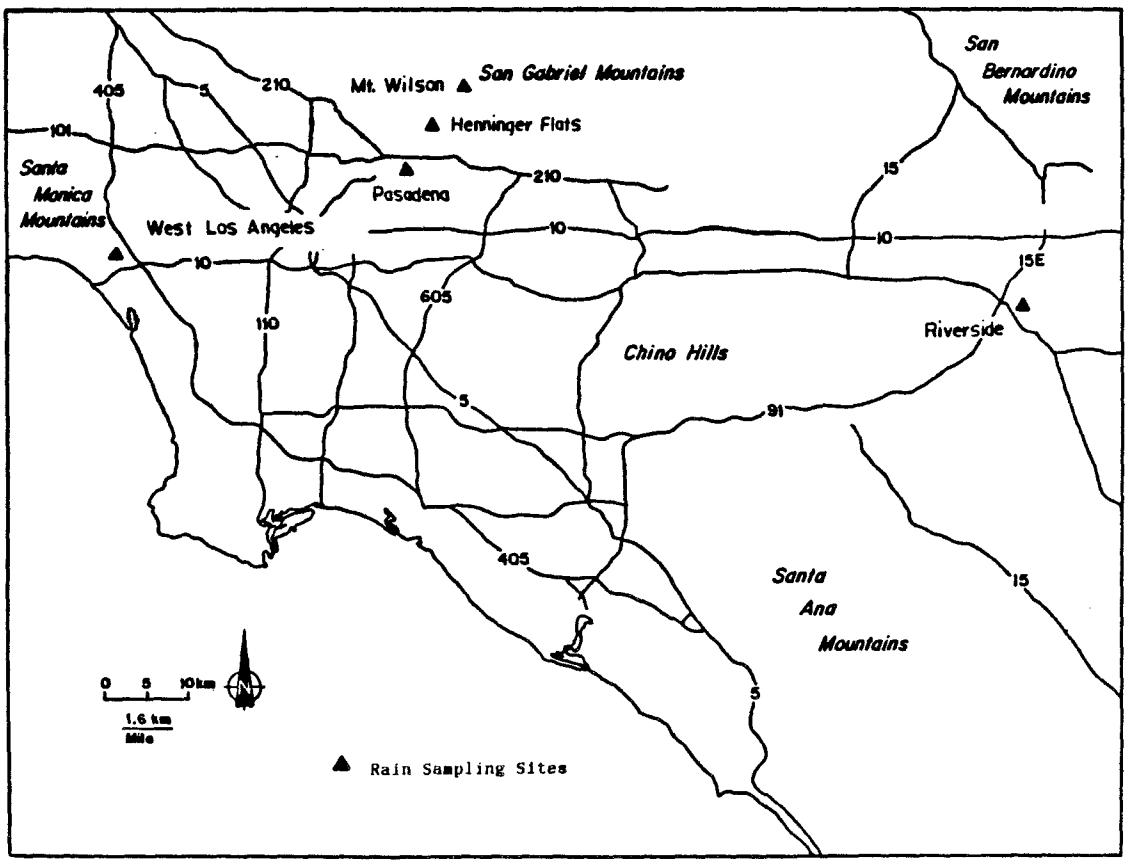

Figure 7.1. Map of the Los Angeles area showing the five sites used for sampling rain, aerosol, and selected gases during the winter of 1987.

sampling equipment was situated near a lightly used corner of the hospital's paved parking lot. The Riverside site is on the roof of a one–story trailer on the eastern edge of the campus of the University of California at Riverside. A small dirt parking lot, used by three or four vehicles, is situated on one side of the trailer and a lightly used, paved campus road is located on the opposing side.

Sampling Techniques

Rain samples were collected at each of the five sites using a 195 mm polyethylene funnel mounted on a Caltech Automated Fractionating Sampler (Figure 7.2), described in detail elsewhere (Hoffmann, 1989). The sampler is equipped with a plexiglas cover which closes over the funnel when it is not raining. A resistance grid sensor, similar to the one described in Chapter 5, is used to detect the presence of rain. When rain is detected the cover is opened so that sample can be collected. The rain sensor is continuously heated to evaporate sedimenting rain drops. The heating level is set so that the sensor dries within 10 to 15 minutes after the rain stops. When the sensor is dry the funnel cover is closed.

The sampler is equipped with a carousel which holds twenty 60 ml sample bottles. Rain collected by the funnel is stored in a reservoir either until enough is collected to trigger an optical level sensor or until a break occurs in the rain. A rain break is defined as a period when the sensor dries off and the cover is closed over the funnel. The level sensor is set to activate the reservoir drain valve when the reservoir contains 60 ml of precipitation (60 ml of collected rain corresponds to just under 20 mm of rainfall). When the level sensor is triggered or rain is sensed following a rain break, the sample collected in the reservoir is dumped to a bottle. The carousel then indexes, bringing the next bottle into position under the reservoir

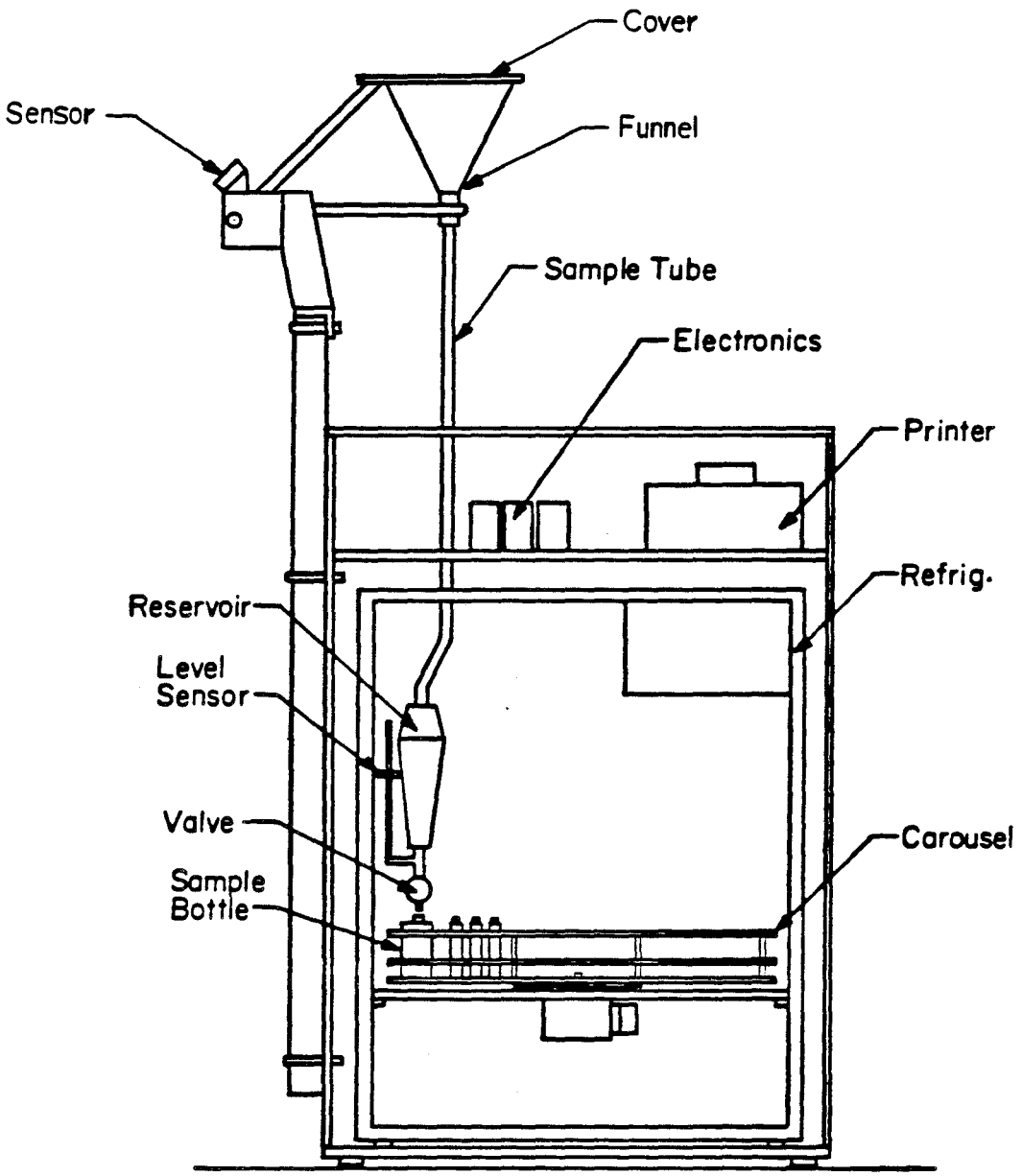

Figure 7.2. Automated fractionating sampling system for rainwater.

to receive the subsequent sample. Once the carousel has indexed twenty times, indicating that all of the sample bottles have been used, no more sample is released from the reservoir. This prevents contamination of samples already collected. Samples are stored refrigerated in the autosampler until picked up by a research staff member. Samples were normally picked up within 12 hours after an event. During extended events it was necessary to pick up collected samples and reload the carousel with empty bottles while the event was in progress.

Each of the five sampling sites also was equipped with an automated aerosol sampler (see Chapter 5). This sampler can be programmed to collect individual samples over three different time periods. We employed a filter pack method to obtain samples of aerosol and gas phase species. Teflon filters (Zefluor, 1 μm pore size) were used to collect the aerosol for the determination of major ion concentrations. Two oxalic acid impregnated glass fiber back-up filters were used in series to collect $NH_{3(g)}$. A nylon back-up filter was used to collect $HNO_{3(g)}$. A flow rate of 10.8 liters per minute through each filter pack was maintained by a critical orifice. Filter samples normally were collected over four hour periods with two hour intervals between samples. Samples usually were picked up within a few hours after the last set was run.

Upon return to the laboratory each rain sample was weighed to determine its volume. An aliquot of each sample was used to determine the pH. pH measurements were made using a Radiometer PHM82 Standard pH meter and a GK2320C semi-micro combination electrode, calibrated with pH 4 and 7 buffers. Following the pH measurements, the samples were refrigerated until further analyses could be made. The major ions, Cl^-, SO_4^{2-}, and NO_3^-, were measured with a Dionex 2020i ion chromatograph, equipped with a Dionex AS-4 column, using a

carbonate–bicarbonate eluent. NH_4^+ was measured by the phenol–hypochlorite method (Solorzano, 1967) using an Alpkem flow injection analyzer. Na^+, Ca^{2+}, and Mg^{2+} concentrations were measured using a Varian Techtron AA6 atomic absorption spectrophotometer. Filters were extracted in a known volume of liquid on a reciprocating shaker. The extracting liquid was carbonate–bicarbonate IC eluent for the nylon filters, water for the oxalic acid impregnated glass fiber filters, and water with 2% EtOH (to help wet the surface) for the Teflon filters. The extracts were analyzed by the same methods used for the rain samples.

Results

Six rain events were sampled during the period from January 1, 1987 to April 30, 1987. During this period nearly 300 samples were collected at the five sampling sites and analyzed in our laboratory. Tables 7.1 through 7.5 list the data obtained for those samples. Included in these five tables are the date and collection period for each sample, the amount of rainfall each sample represents, the sample pH, concentrations of major inorganic ions in each sample, and the ion charge balance for the inorganic species measured. The volume of each sample (in ml) is equal to 32.4 times the rainfall amount (in mm). A few entries in the tables are marked "NA" for not available. These represent times when (1) the sample volume was too small to allow all of the measurements to be made, (2) no sample was collected for a period during which it was raining at the site because the capacity of the sampling carousel had been exceeded, or (3) the sample was contaminated during handling. In a few cases, two or more small samples were combined in order to provide a sufficient volume for analysis. These samples have been labeled.

Table 7.6 provides a brief summary of the data. Listed here are the number

Table 7.1. Chemical Composition of West Los Angeles Rain Samples–1987

Time	Rain (mm)	pH	NH_4^+	Na^+	Ca^{2+}	Mg^{2+}	Cl^-	NO_3^-	SO_4^{2-}	−/+
			←			μN			→	
02/13/87										
1112–1153	1.8	5.36	36.5	32.1	7.0	7.2	42.1	12.3	24.4	0.90
1153–1300	2.1	5.45	16.5	11.7	2.0	2.6	17.1	4.5	11.2	0.90
1300–1322	2.1	5.66	10.5	3.2	0.0	0.4	3.5	1.5	4.7	0.59
1322–1338	1.8	5.61	6.8	0.7	0.0	0.0	1.0	1.6	3.3	0.58
1338–1348	0.9	5.53	6.8	0.9	0.0	0.0	1.0	1.6	3.6	0.59
1348–1407	1.8	5.45	7.3	2.2	0.0	0.4	0.7	1.6	3.3	0.41
1407–1500	1.8	5.60	18.3	23.5	0.0	4.9	35.8	5.7	12.5	1.10
1502–1549	1.8	5.73	12.7	12.0	0.0	2.6	16.1	2.5	7.0	0.88
1549–1623	0.8	5.85	22.2	20.5	2.7	4.4	29.2	5.9	12.2	0.93
1721–1810	1.0	6.10	32.4	24.9	3.3	5.5	34.1	5.8	14.4	0.81
02/15/87										
0713–0852	1.1	4.68	47.3	46.6	6.4	10.4	61.4	27.8	41.1	0.99
0915–0953	0.2	4.19	105.6	NA	NA	NA	67.1	69.4	73.0	NA
03/05–03/06/87										
1111–1442*	0.2	4.10	68.5	55.6	25.0	0.7	49.6	80.5	98.0	1.00
1442–1529	2.1	4.67	25.9	3.9	8.5	2.4	4.9	15.9	22.1	0.69
1534–1645	0.2	5.10	42.4	13.2	11.0	0.7	5.4	18.9	22.7	0.62
1701–1938	1.1	5.62	67.3	4.5	9.3	2.6	7.1	17.4	28.6	0.62
1938–2017	2.2	5.33	58.6	7.1	6.2	2.7	9.2	17.4	28.6	0.70
2017–2041	1.9	5.03	26.4	4.2	5.7	1.9	5.3	13.2	19.5	0.80
2041–2044	1.2	5.69	28.8	4.7	4.6	2.2	5.3	12.9	13.5	0.75
2044–2108	<0.1	5.45	NA	NA	NA	NA	NA	NA	NA	NA
2224–0026	1.7	5.01	52.3	7.0	4.3	2.1	14.6	18.2	33.1	0.87
0033–0044	0.1	5.33	86.9	NA	NA	NA	6.7	20.0	37.0	NA
0305–0508	1.4	4.65	38.7	1.7	3.7	1.2	3.9	23.5	25.5	0.78
0521–0612	0.4	4.66	38.7	2.3	4.2	2.1	4.2	24.5	23.9	0.76
0622–0748	0.7	4.76	46.8	5.9	5.1	2.6	5.9	20.7	30.1	0.73

−/+ indicates the charge balance (anions/cations) for all measured species.
* Rain was not continuous over this period. Two or more small samples were combined.
NA denotes not available.

Table 7.1 (Cont'd). Chemical Composition of West Los Angeles Rain Samples–1987

Time	Rain (mm)	pH	NH_4^+	Na^+	Ca^{2+}	Mg^{2+}	Cl^-	NO_3^-	SO_4^{2-}	−/+
			←			μN			→	
03/14/87										
2213–2232	2.1	5.47	8.0	13.1	4.8	3.9	16.0	9.9	7.4	1.00
2332–0014	0.2	5.67	12.4	6.8	8.0	3.3	6.4	6.8	9.4	0.69
03/21/87										
0858–1004	2.1	4.72	65.0	86.6	15.5	21.0	86.0	42.2	55.8	0.89
1004–1041	2.0	5.36	11.4	20.8	5.0	5.4	27.7	4.8	12.7	0.96
1041–1105	2.1	5.19	14.0	8.4	5.0	5.4	11.5	3.9	14.3	0.75
1105–1122	2.0	5.09	17.6	8.8	2.3	2.5	11.6	6.9	15.1	0.86
1122–1237	1.5	4.88	22.6	31.5	4.2	7.8	39.6	12.2	26.2	0.98
1320–1414	0.4	5.00	14.2	24.5	5.3	6.6	31.5	11.1	15.6	0.96

−/+ indicates the charge balance (anions/cations) for all measured species.

Table 7.2. Chemical Composition of Pasadena Rain Samples–1987

Time	Rain (mm)	pH	NH_4^+	Na^+	Ca^{2+}	Mg^{2+}	Cl^-	NO_3^-	SO_4^{2-}	−/+
			←			μN			→	
01/04–01/05/87										
0533–0543	NA	NA	NA	NA	NA	NA	NA	NA	NA	NA
0543–0630	1.8	4.30	91.2	12.1	4.5	2.4	12.3	96.4	42.7	0.94
0630–0717	2.0	4.78	92.1	3.6	2.0	0.6	12.4	65.6	26.9	0.91
0717–0727	0.5	4.87	44.2	1.6	2.0	0.0	7.5	33.2	15.0	0.91
0727–0746	2.1	5.04	33.1	1.9	1.7	0.1	7.5	24.5	14.1	1.00
0746–0755	1.8	5.02	18.0	5.1	2.7	0.4	7.8	17.5	10.7	1.01
0755–0802	1.3	5.03	14.5	2.4	1.1	0.0	5.0	13.3	8.3	0.97
0802–0814	1.3	4.99	17.6	1.6	0.8	0.0	4.0	14.0	11.5	0.97
0814–0823	0.9	5.06	10.6	2.7	0.8	0.1	4.8	10.4	11.1	1.15
0823–0836	1.5	5.20	9.9	1.6	0.8	0.0	4.9	9.7	7.5	1.18
0836–0838	1.6	5.07	5.7	0.1	0.8	0.0	2.3	6.4	9.2	1.18
0838–0846	1.4	5.35	3.2	0.3	0.8	0.0	5.1	5.2	3.5	1.58
0846–0919	0.6	5.36	6.6	0.9	0.8	0.0	3.1	7.1	3.5	1.08
0919–0920	0.5	5.34	9.3	1.9	2.0	0.1	3.8	7.7	4.7	0.90
0928–1000	1.1	5.36	6.4	0.5	0.8	0.0	2.6	5.8	3.5	0.99
1332–1343	0.3	5.35	0.9	0.1	0.8	0.0	2.7	2.9	2.5	1.30
1408–1446	NA	NA	NA	NA	NA	NA	NA	NA	NA	NA
1520–1554	NA	NA	NA	NA	NA	NA	NA	NA	NA	NA
1632–1656	NA	NA	NA	NA	NA	NA	NA	NA	NA	NA
2033–2108	NA	NA	NA	NA	NA	NA	NA	NA	NA	NA
2157–2213	1.5	4.71	28.8	29.8	3.0	6.2	41.0	18.6	22.8	0.94
2213–2231	2.1	4.81	18.0	8.6	2.0	1.6	14.1	12.5	12.4	0.85
2231–2246	1.5	4.97	2.4	2.0	0.8	0.1	4.4	8.0	2.7	0.94
2246–2254	0.2	5.06	1.7	5.4	NA	NA	5.5	8.1	2.7	NA
0200–0242	1.5	4.80	2.7	8.7	2.0	1.5	13.6	13.2	8.5	1.15
0242–0254	0.3	4.78	2.6	9.3	2.7	1.5	11.3	11.8	10.2	1.02
0331–0351	NA	NA	NA	NA	NA	NA	NA	NA	NA	NA
02/08/87										
1737–1825	1.2	5.29	74.5	31.6	49.5	11.1	33.6	90.9	70.1	1.13
1840–1907	1.3	5.21	43.4	16.8	32.1	6.2	17.3	51.0	39.4	1.03
1907–1914	1.4	5.43	12.5	4.8	9.5	1.5	0.5	14.4	9.2	0.75
1914–1927	2.1	5.54	8.4	3.2	5.5	0.9	0.9	11.7	6.6	0.92
1927–1937	0.9	5.40	6.8	1.8	4.5	0.4	1.0	8.2	6.3	0.88
1937–1950	0.2	5.21	13.7	0.1	6.7	1.2	4.3	13.0	11.4	1.03
2014–2021	0.1	5.40	51.8	NA	NA	NA	22.0	59.0	43.7	NA

−/+ indicates the charge balance (anions/cations) for all measured species.
NA denotes not available.

Table 7.2 (Cont'd). Chemical Composition of Pasadena Rain Samples-1987

Time	Rain (mm)	pH	NH_4^+	Na^+	Ca^{2+}	Mg^{2+}	Cl^-	NO_3^-	SO_4^{2-}	−/+
			←			μN			→	
02/13/87										
1205–1308	1.4	3.95	134.2	14.8	13.2	4.4	28.1	129.0	118.0	0.99
1308–1341	2.1	4.29	62.4	7.4	8.9	2.3	10.1	60.0	51.1	0.92
1341–1351	1.3	4.60	39.2	2.8	4.5	0.7	3.0	30.2	26.7	0.83
1351–1405	1.5	4.94	22.1	5.0	13.2	2.0	5.9	27.8	21.6	1.03
1405–1415	1.5	5.18	12.9	1.9	7.6	0.7	1.1	12.5	13.0	0.89
1415–1433	1.5	5.34	13.5	1.3	5.5	0.3	1.0	8.6	8.7	0.73
1433–1505	1.4	5.24	10.2	0.9	5.1	0.3	1.0	9.0	7.2	0.77
1505–1519	1.5	5.13	10.4	0.8	3.9	0.0	1.0	9.3	9.1	0.86
1519–1544	1.5	4.94	9.6	0.5	2.4	0.0	1.0	8.4	10.9	0.85
1544–1557	1.5	5.03	8.8	0.6	2.7	0.0	1.0	6.8	9.4	0.80
1557–1604	1.5	5.09	6.1	0.7	3.3	0.0	1.0	5.2	7.7	0.76
1604–1608	0.9	NA	NA	NA	NA	NA	NA	NA	NA	NA
1608–1623	1.1	5.13	6.7	1.0	3.9	0.0	1.0	6.4	9.1	0.87
1634–1659	0.5	4.88	15.9	1.5	7.0	0.4	1.4	15.0	17.3	0.89
1659–1659	0.1	4.90	NA	NA	NA	NA	10.6	16.4	18.3	NA
1714–1727	1.5	4.88	18.4	1.5	3.3	0.1	1.0	11.8	20.2	0.91
1727–1747	1.3	5.03	10.8	0.6	3.3	0.0	0.5	7.1	12.1	0.82
1747–1810	1.4	5.03	7.1	0.1	2.4	0.0	1.0	5.1	7.8	0.74
1810–1834	1.2	4.96	5.7	0.1	1.1	0.0	1.0	4.8	8.0	0.77
2012–2026	0.2	5.07	19.1	NA	NA	NA	0.4	13.9	17.8	NA
03/05/87										
1207–1256*	0.7	4.44	101.8	20.8	23.3	7.8	24.8	66.9	83.8	0.92
1545–1712*	0.7	4.76	44.7	1.0	6.8	2.4	6.0	25.4	29.7	0.85
1736–0811	NA	NA	NA	NA	NA	NA	NA	NA	NA	NA
03/21/87										
0946–1054	1.4	4.35	84.5	77.0	22.8	20.7	81.5	87.6	72.0	0.97
1054–1113	1.4	4.49	34.7	16.9	6.1	4.7	19.7	30.2	32.9	0.87
1113–1141	2.0	4.64	25.0	10.7	3.4	2.9	12.9	22.2	21.2	0.87
1141–1209	2.0	4.87	6.1	3.1	2.3	1.4	4.6	6.5	7.8	0.71
1209–1221	2.1	4.95	6.2	0.9	2.6	1.3	2.5	5.7	7.8	0.72
1221–1305*	1.4	4.81	10.8	1.5	2.3	0.8	4.1	11.2	12.6	0.90
1335–1351	1.2	4.38	31.1	8.1	3.4	2.6	13.2	35.9	31.1	0.92
1351–1453*	1.6	4.54	19.8	2.7	2.6	1.3	4.7	23.8	19.2	0.86

−/+ indicates the charge balance (anions/cations) for all measured species.
* Rain was not continuous over this period. Two or more small samples were combined.
NA denotes not available.

Table 7.3. Chemical Composition of Henninger Flats Rain Samples–1987

Time	Rain (mm)	pH	NH_4^+	Na^+	Ca^{2+}	Mg^{2+}	Cl^-	NO_3^-	SO_4^{2-}	–/+
			←			μN			→	
01/04–01/05/87										
0329–0343	0.1	4.10	NA	NA	NA	NA	NA	NA	NA	NA
0531–0608	2.0	4.22	53.1	15.5	8.9	3.9	10.3	94.4	30.2	0.95
0608–0626	1.0	4.50	10.0	2.2	2.0	0.7	4.2	23.9	14.5	0.92
0626–0642	0.7	4.75	4.0	1.0	1.7	0.0	2.9	11.3	7.2	0.87
0648–0717	2.0	4.98	3.6	0.2	0.8	0.0	3.6	8.6	4.1	1.08
0717–0743	1.9	5.07	1.4	0.1	0.8	0.0	2.5	5.9	2.8	1.04
0743–0749	1.8	5.27	0.6	0.0	0.8	0.0	2.2	4.3	3.0	1.40
0749–0807	2.1	5.13	0.4	0.6	0.8	0.0	2.8	3.2	5.6	1.27
0807–0821	1.6	5.21	0.1	1.2	0.8	0.0	3.2	3.4	5.2	1.43
0821–0839	2.0	5.34	0.0	0.8	0.8	0.0	3.7	2.8	4.8	1.83
0839–0845	1.7	5.30	0.0	0.2	0.8	0.0	0.0	0.0	3.9	0.65
0845–0859	0.9	5.42	0.0	0.6	0.8	0.0	3.1	3.2	2.5	1.71
0902–0920	0.7	5.27	2.2	1.3	0.8	0.0	3.2	4.2	2.9	1.06
0928–0955	1.7	4.93	1.8	5.7	2.0	0.0	8.8	5.3	13.3	1.29
1009–1650	NA	NA	NA	NA	NA	NA	NA	NA	NA	NA
1936–1955	0.7	4.77	7.1	29.1	1.7	6.2	35.0	13.4	13.0	1.00
2042–2108	0.7	4.85	2.8	24.3	1.1	5.3	31.4	9.9	10.9	1.10
2158–2233	2.1	4.86	5.3	11.9	0.8	2.6	15.9	12.8	9.3	1.11
2233–2235	0.7	5.00	4.6	3.4	0.8	0.7	5.8	8.4	4.7	0.97
2235–2241	2.0	5.04	4.4	1.9	0.8	0.4	4.4	8.7	3.7	1.01
2241–2252	2.1	5.04	2.8	0.8	0.8	0.1	3.2	7.1	4.0	1.05
2252–2253	0.2	5.00	3.8	NA	NA	NA	4.2	8.2	3.9	NA
2253–2306	1.2	5.11	1.2	0.7	0.8	0.0	2.7	7.6	3.2	1.29
0155–0223	0.7	4.87	0.9	14.8	0.8	2.3	15.6	10.6	7.4	1.04
0402–0403	1.3	4.85	0.3	12.8	0.8	2.4	17.0	10.1	7.5	1.14
0403–0404	0.1	4.84	NA	NA	NA	NA	15.6	9.7	7.2	NA
02/13/87										
1141–1304	2.1	4.20	64.9	4.0	3.6	0.9	6.3	80.7	39.1	0.92
1304–1340	2.1	4.38	19.4	2.8	3.0	0.1	2.4	38.4	25.3	0.99
1340–1403	1.9	4.69	8.2	1.0	2.7	0.0	1.0	15.6	9.5	0.81
1403–1419	1.4	4.97	3.8	0.3	1.1	0.0	1.0	8.0	4.4	0.84
1419–1434	1.5	5.09	3.1	0.2	0.8	0.0	1.0	6.0	2.9	0.81
1434–1508	1.5	5.12	2.8	0.0	0.8	0.0	1.0	4.7	2.4	0.72
1508–1525	1.6	5.18	3.4	0.5	0.8	0.0	1.0	5.8	1.9	0.77
1525–1543	1.5	4.95	3.1	0.3	0.8	0.0	1.0	5.8	2.8	0.62

–/+ indicates the charge balance (anions/cations) for all measured species.
NA denotes not available.

Table 7.3 (Cont'd). Chemical Composition of Henninger Flats Rain Samples–1987

Time	Rain (mm)	pH	NH_4^+	Na^+	Ca^{2+}	Mg^{2+}	Cl^-	NO_3^-	SO_4^{2-}	−/+
			←			μN			→	
02/13/87 (cont'd).										
1543–1558	1.6	5.05	2.5	0.0	0.8	0.0	1.0	4.1	3.0	0.66
1558–1608	1.5	5.15	0.0	0.0	0.8	0.0	1.0	3.0	4.3	0.93
1608–1729	2.1	4.98	4.4	0.5	0.8	0.0	1.0	6.2	5.7	0.80
1729–1832	1.6	5.01	3.0	0.0	0.8	0.0	1.0	5.9	3.6	0.78
1832–1925	1.2	4.96	3.3	0.4	0.8	0.0	1.0	9.5	3.4	0.90
1941–2023	1.1	4.82	3.9	0.6	2.4	0.0	1.0	13.9	4.0	0.86
03/05–03/06/87										
0908–0936	0.1	4.34	57.9	NA	NA	NA	10.1	50.5	63.5	NA
1113–1155	0.5	4.80	128.2	17.4	26.4	7.3	22.3	89.3	108.0	1.13
1203–1245	1.4	4.70	102.8	17.6	16.3	5.8	16.4	50.2	66.0	0.82
1245–1323	0.4	5.37	72.2	4.9	8.5	2.2	6.3	21.8	37.0	0.71
1350–1414	0.1	4.99	64.0	7.9	1.2	0.7	5.1	25.8	31.2	0.74
1513–1614	1.3	4.65	15.7	1.6	4.3	1.0	5.6	16.2	15.3	0.83
1614–1715	2.1	4.86	7.0	0.0	0.0	0.0	2.0	9.6	8.4	0.96
1715–1819	1.4	5.09	5.6	0.0	0.0	0.0	0.8	6.1	4.2	0.81
1819–1920	2.1	5.02	8.5	0.0	0.0	0.0	0.3	6.4	7.2	0.77
1920–1953	1.3	5.07	6.2	0.3	0.0	1.0	2.0	6.2	6.4	0.92
1953–2057	1.4	5.18	5.8	0.8	2.6	0.0	1.6	6.3	4.1	0.76
2144–2228	1.4	4.79	19.5	0.0	0.0	0.0	1.7	16.0	12.1	0.83
2228–2332	1.5	4.82	12.9	0.0	2.3	0.0	0.5	12.8	9.0	0.73
2332–0016	1.4	4.76	8.8	0.0	2.3	0.0	0.3	9.2	9.7	0.67
0016–0101	0.4	4.72	13.9	0.8	2.3	0.0	1.9	14.8	16.7	0.93
0135–0224	0.3	4.65	11.4	0.0	2.0	0.0	1.7	12.8	15.9	0.85
0248–0350	1.4	4.77	7.8	0.0	0.0	0.0	1.7	7.9	10.4	0.81
0350–0448	1.4	4.95	7.0	0.0	0.0	0.0	0.8	6.2	8.4	0.85
0448–0522	1.4	5.10	7.0	0.0	0.0	0.0	0.3	4.0	8.2	0.83
0522–0537	1.3	5.10	7.8	0.0	0.0	0.0	1.7	3.5	8.5	0.87
0537–0617	1.4	5.10	7.3	0.0	0.0	0.0	0.3	3.6	8.1	0.79
0617–0726	1.4	5.03	6.0	0.0	0.0	0.0	0.5	4.0	6.0	0.68
0726–0822	1.3	5.20	7.3	0.0	0.0	0.0	1.1	4.0	6.0	0.82
0822–0859	0.4	5.39	8.3	0.0	0.0	0.0	0.1	5.3	4.2	0.78
1303–1409	0.9	4.52	34.8	0.0	3.6	0.0	1.8	35.4	15.8	0.77
1446–1501	0.6	4.89	97.2	0.2	4.8	1.5	3.4	53.8	26.5	0.72
1501–1542	0.7	5.87	140.2	0.3	4.3	1.0	3.4	54.9	24.9	0.57
1708–1733	<0.1	5.97	NA	NA	NA	NA	NA	NA	NA	NA
2111–2153	0.3	4.40	100.0	1.1	8.8	2.6	3.8	97.2	22.5	0.81

−/+ indicates the charge balance (anions/cations) for all measured species.
NA denotes not available.

Table 7.3 (Cont'd). Chemical Composition of Henninger Flats Rain Samples–1987

Time	Rain (mm)	pH	NH_4^+	Na^+	Ca^{2+}	Mg^{2+}	Cl^-	NO_3^-	SO_4^{2-}	−/+
			←			μN			→	
03/14/87										
2138–2225	0.1	NA	NA	NA	NA	NA	NA	NA	NA	NA
2230–2250	1.4	4.49	55.0	92.4	16.9	28.1	107.8	90.0	66.6	1.18
2250–2256	1.5	4.78	12.6	42.4	4.5	9.9	52.5	18.7	20.2	1.06
2256–2304	1.5	4.85	6.8	20.2	2.6	5.4	26.3	10.2	10.4	0.95
2304–2307	1.3	4.87	7.4	13.3	2.1	3.6	18.1	10.1	8.3	0.91
2307–2321	1.7	5.00	7.4	9.8	4.0	3.2	10.0	15.0	7.6	0.95
2321–2344	1.5	NA	NA	NA	NA	NA	NA	NA	NA	NA
2344–0037	1.3	5.16	3.9	3.6	5.0	2.3	3.1	9.4	6.9	0.89
03/21/87										
1027–1109	1.7	4.62	53.3	70.3	14.7	18.3	63.6	68.4	46.1	0.99
1109–1130	2.1	4.70	16.6	12.2	4.8	3.9	13.0	20.9	18.0	0.90
1130–1205	2.1	4.97	7.8	4.6	2.6	1.6	6.6	10.8	8.9	0.96
1205–1316	>3.5	NA	NA	NA	NA	NA	NA	NA	NA	NA

−/+ indicates the charge balance (anions/cations) for all measured species.
NA denotes not available.

Table 7.4. Chemical Composition of Mt. Wilson Rain Samples–1987

Time	Rain (mm)	pH	NH_4^+	Na^+	Ca^{2+}	Mg^{2+}	Cl^-	NO_3^-	SO_4^{2-}	−/+
			←			μN			→	
02/13/87										
1146–1327	2.1	4.73	6.6	3.5	10.7	0.6	3.8	19.3	8.7	0.79
1327–1405	2.1	4.88	3.1	0.3	2.0	0.0	1.5	8.0	8.4	0.96
1405–1421	1.7	5.19	2.4	0.7	2.7	0.0	1.0	5.2	3.4	0.79
1421–1445	2.1	5.71	2.5	0.0	1.1	0.0	1.0	1.9	1.2	0.73
1445–1513	2.1	5.61	0.0	0.0	0.0	0.0	1.0	1.7	1.3	1.62
1513–1538	2.2	5.53	0.0	0.0	0.0	0.0	1.0	1.4	2.2	1.54
1538–1556	2.1	5.43	0.0	0.0	0.0	0.0	1.0	1.2	1.0	0.86
1556–1609	2.2	5.45	0.0	0.0	0.0	0.0	1.0	1.4	1.4	1.06
1609–1701	2.2	5.34	0.0	0.1	0.0	0.0	1.0	2.8	2.8	1.42
1701–1734	2.1	5.31	2.5	0.0	0.0	0.0	1.0	2.1	2.3	0.73
1734–1942	1.0	5.13	2.8	2.4	4.2	0.0	4.4	9.8	3.2	1.03
02/15/87										
0745–0949	0.5	4.90	7.2	2.1	2.4	0.3	1.0	12.8	6.1	0.81
03/05/87										
0514–0607	0.3	4.39	6.4	5.5	9.9	4.6	7.1	34.5	25.4	1.00
0731–0833*	0.2	4.31	14.6	5.5	11.9	5.3	9.1	38.8	32.6	0.93
0839–0954	0.7	4.37	20.5	5.6	10.7	4.4	7.3	35.1	32.7	0.90
1014–1226	2.1	4.62	53.6	9.2	11.6	3.8	10.4	38.3	40.0	0.87
1226–1329	1.2	5.39	59.8	3.4	4.9	2.2	4.7	22.5	26.4	0.72
1349–1418	0.2	4.90	27.2	1.4	7.4	2.4	4.5	22.4	18.4	0.89
1421–1431	<0.1	4.76	24.7	NA	NA	NA	NA	NA	NA	NA
1515–1633	2.1	4.80	7.2	0.8	3.6	1.0	2.3	11.6	9.8	0.83
1633–1652	1.3	4.83	7.5	0.0	2.9	0.9	1.3	10.5	8.5	0.78
1652–1744	1.6	4.95	5.6	0.0	0.0	0.0	0.7	7.4	6.7	0.88
1744–1827	1.4	4.94	6.4	0.0	0.0	0.0	1.2	6.3	5.8	0.75
1824–1854	2.0	4.90	9.2	0.0	2.3	0.0	0.7	8.1	10.1	0.78
1854–1924	2.1	4.84	7.6	0.0	0.0	0.0	0.5	6.4	9.2	0.73
1924–1957	2.0	5.01	4.7	0.0	0.0	0.0	0.2	3.5	5.7	0.65
1957–2020	1.4	5.19	7.5	0.0	0.0	0.0	0.3	3.4	4.4	0.58
2020–2130	1.5	4.70	18.7	0.0	2.3	0.0	2.0	16.7	12.4	0.76
2138–2208	1.5	4.92	8.7	0.0	0.0	0.0	1.3	8.9	6.6	0.81
2208–2218	1.7	4.92	7.7	0.0	0.0	0.0	0.4	9.2	7.0	0.84
2218–2242	1.7	4.88	7.3	0.0	0.0	0.0	1.2	8.3	7.6	0.83
2242–2334	1.9	4.99	4.4	0.0	0.0	0.0	0.0	4.0	5.4	0.64
2334–0011	1.3	5.08	4.4	0.0	0.0	0.0	0.1	2.9	4.8	0.61

−/+ indicates the charge balance (anions/cations) for all measured species.

* Rain was not continuous over this period. Two or more small samples were combined.

NA denotes not available.

Table 7.4 (Cont'd). Chemical Composition of Mt. Wilson Rain Samples–1987

Time	Rain (mm)	pH	NH_4^+	Na^+	Ca^{2+}	Mg^{2+}	Cl^-	NO_3^-	SO_4^{2-}	−/+
			←			μN			→	
03/06/87										
0011–0018	2.1	4.81	7.7	0.0	0.0	0.0	0.5	6.7	10.3	0.75
0134–0240	2.1	4.89	6.7	0.0	0.0	0.0	0.2	5.1	8.9	0.73
0240–0342	1.1	5.12	4.2	0.0	0.0	0.0	0.3	3.7	4.4	0.71
0342–0408	1.7	5.06	6.5	0.0	1.5	0.0	0.8	3.9	9.0	0.82
0408–0532	2.1	5.2	4.8	0.0	0.0	0.7	0.3	2.3	5.3	0.67
0532–0543	1.5	5.34	3.0	0.0	0.0	0.0	0.0	0.9	3.0	0.52
0543–0703	1.5	5.33	2.8	0.0	0.0	0.0	2.4	1.6	3.0	0.94
0703–0802	2.1	5.29	3.3	0.0	1.5	0.0	0.1	2.0	2.8	0.50
0802–0914	1.4	5.39	4.2	0.0	1.5	0.0	2.6	3.2	3.0	0.90
1514–1610	0.9	4.96	18.5	0.0	1.2	0.0	2.9	13.9	4.5	0.70
1635–1745	0.1	5.06	37.5	NA	NA	NA	1.5	23.7	10.4	NA
2035–2200	0.9	4.68	23.1	0.0	2.3	0.2	0.6	33.7	7.3	0.90

−/+ indicates the charge balance (anions/cations) for all measured species.
NA denotes not available.

Table 7.5. Chemical Composition of Riverside Rain Samples–1987

Time	Rain (mm)	pH	NH_4^+	Na^+	Ca^{2+}	Mg^{2+}	Cl^-	NO_3^-	SO_4^{2-}	−/+
			←			μN			→	
01/04–01/05/87										
2033–2053	1.6	5.71	26.9	25.1	2.7	4.6	40.0	8.1	14.3	1.02
2053–2059	1.5	5.75	22.9	10.6	1.4	1.6	17.8	7.7	8.3	0.88
2059–2121	1.9	6.00	20.7	5.0	1.3	0.4	11.2	7.2	3.9	0.79
2121–2130	0.3	6.00	37.0	NA	NA	NA	32.4	15.3	10.5	NA
2139–2202	2.0	5.73	28.5	4.3	1.4	0.3	9.4	8.5	7.9	0.71
2202–2224	0.8	6.00	9.2	2.8	0.8	0.0	6.6	4.6	3.8	1.09
2228–2233	0.1	5.53	NA	NA	NA	NA	5.6	5.3	5.6	NA
0049–0124	1.6	5.82	8.4	3.8	0.8	0.3	7.1	3.0	4.8	1.01
0159–0222	1.6	5.63	29.5	5.2	0.8	0.7	10.7	5.3	5.5	0.57
0222–0239	1.6	5.87	4.8	1.5	2.7	0.0	5.0	17.1	5.2	2.65
0239–0248	0.2	5.93	17.6	NA	NA	NA	5.4	10.6	3.8	NA
02/13/87										
1447–1511	0.2	6.33	219.5	NA	NA	NA	15.2	82.6	92.8	NA
1621–1630	0.3	6.65	174.9	NA	NA	NA	6.1	47.9	44.1	NA
1638–1707	1.1	6.72	52.1	0.7	1.1	0.0	1.4	10.0	9.9	0.39
1708–1733	1.1	6.47	32.8	0.0	1.7	0.0	1.0	5.4	5.0	0.33
1835–1919	1.3	6.60	62.8	0.1	0.0	0.0	0.7	21.3	10.2	0.51
2034–2045	0.2	6.26	80.4	NA	NA	NA	0.2	33.4	12.4	NA
03/05/87										
0904–1101*	0.2	5.01	42.1	16.2	24.5	6.3	20.2	34.3	33.4	0.89
1154–1345*	0.2	4.55	84.9	14.5	0.0	6.1	19.6	60.4	60.6	1.05
1720–1750	0.1	5.45	64.0	NA	NA	NA	14.0	25.3	27.4	NA
1806–1851	0.4	5.32	61.9	6.4	19.4	2.8	8.7	29.7	33.6	0.76
2037–2135	0.6	5.10	28.9	9.6	13.0	3.1	11.8	16.2	20.2	0.77
2144–2156	0.0	5.10	48.5	NA	NA	NA	NA	NA	NA	NA
2159–2233	0.3	4.91	26.3	NA	10.2	2.1	10.1	16.2	20.8	NA
2240–2313	0.3	4.99	30.6	6.0	8.5	1.9	7.0	15.6	22.5	0.79
2314–2319	0.1	5.15	49.3	NA	NA	NA	11.4	15.5	24.6	NA
2322–2354	0.3	5.13	33.6	10.4	8.8	2.4	11.3	14.7	22.0	0.77

−/+ indicates the charge balance (anions/cations) for all measured species.

* Rain was not continuous over this period. Two or more small samples were combined.

NA denotes not available.

Table 7.5 (Cont'd). Chemical Composition of Riverside Rain Samples–1987

Time	Rain (mm)	pH	NH_4^+	Na^+	Ca^{2+}	Mg^{2+}	Cl^-	NO_3^-	SO_4^{2-}	−/+
			←			μN			→	
03/06/87										
0021–0138	1.5	5.15	16.2	1.0	4.0	1.2	2.1	6.3	11.9	0.69
0138–0315	1.3	5.02	10.6	0.6	2.9	1.7	3.1	6.4	7.9	0.69
0317–0358	0.4	4.95	25.3	13.1	16.1	4.6	10.6	26.3	24.0	0.87
0400–0605	1.5	5.44	23.6	4.8	8.2	2.7	11.1	12.1	15.3	0.90
0638–0717	0.4	5.42	17.7	2.0	6.0	1.4	3.9	9.8	9.1	0.74
0727–0924	1.6	5.50	13.4	0.3	4.0	1.0	2.9	7.1	5.5	0.71
0935–1237	0.4	5.04	18.6	0.6	4.8	1.2	5.2	19.2	5.8	0.88
1626–1743	0.8	5.80	59.2	0.0	2.6	0.9	3.3	17.1	12.9	0.52
1746–1859*	0.2	5.81	60.9	0.0	1.5	1.0	3.8	19.1	12.3	0.54
2018–2209*	0.1	6.73	134.8	NA	NA	NA	4.1	45.1	18.6	NA

−/+ indicates the charge balance (anions/cations) for all measured species.
* Rain was not continuous over this period. Two or more small samples were combined.
NA denotes not available.

Table 7.6. Summary of LA Basin Rain Composition - 1987

Parameter	West Los Angeles	Pasadena	Henninger Flats	Mt. Wilson	Riverside
pH	4.10–6.10	3.95–5.54	4.10–5.97	4.31–5.71	4.55–6.73
H^+ (μN)	0.8–79.4	2.9–112.2	79.4–1.1	2.0–49.0	0.2–28.2
NH_4^+ (μN)	6.8–105.6	0.9–134.2	0.0–140.2	0.0–59.8	4.8–219.5
Na^+ (μN)	0.7–86.6	0.1–77.0	0.0–92.4	0.0–9.2	0.0–25.1
Ca^{2+} (μN)	0.0–25.0	0.8–49.5	0.0–26.4	0.0–11.9	0.0–24.5
Mg^{2+} (μN)	0.0–21.0	0.0–20.7	0.0–28.1	0.0–5.3	0.0–6.3
Cl^- (μN)	0.7–86.0	0.4–81.5	0.0–107.8	0.0–10.4	0.2–40.0
NO_3^- (μN)	1.5–80.5	2.9–129.0	0.0–94.4	0.9–38.8	3.0–82.6
SO_4^{2-} (μN)	3.3–98.0	2.5–118.0	1.9–108.0	1.0–40.1	3.8–92.8
# samples	35	70	81	46	44
# events	5	5	5	3	3

of events sampled and samples obtained, the range of pH observed, and the range of concentrations measured for each ion at each site. pH values at West Los Angeles and Henninger Flats ranged from 4.1 to approximately 6. At Pasadena the range extended from slightly below 4 to about 5.5. Mount Wilson rainwater pH values varied from 4.3 to 5.7, while values at Riverside were observed to fall between 4.5 and 6.8. The highest concentrations of Na^+ and Cl^-, derivatives of sea salt, were measured in the early part of a storm at Henninger Flats. Concentrations of these species on average, however, were highest at the West Los Angeles site, which is closest to the ocean. By far the highest concentrations of NH_4^+ were seen at Riverside. This is not surprising since nearby dairy operations in Chino are the dominant source of $NH_{3(g)}$ emissions in the SoCAB (Russell et al., 1983). The highest NO_3^- and SO_4^{2-} concentrations were observed in samples collected in Pasadena, although concentrations nearly as high were measured in samples from West Los Angeles, Henninger Flats, and Riverside. Maximum concentrations of Ca^{2+} and Mg^{2+} were measured at Pasadena and Henninger Flats, respectively. In most samples the dominant inorganic ions were H^+, NO_3^-, SO_4^{2-}, and NH_4^+. In some samples Na^+ and Cl^- also were important contributors.

Ratios of nitrate to sulfate varied considerably between sites, from storm to storm, and even within a single storm at a given site. In Figure 7.3 the concentration of nitrate has been plotted vs. the sulfate concentration for each sample collected at the West Los Angeles site. The different symbols represent samples collected in different rain events. Also plotted here is a linear regression line fitted to the data using the method of ordinary least squares. The data, which fit closely to the regression line (slope = 0.86, 95% confidence limits of 0.79 and 0.92) indicate that a slight excess of sulfate over nitrate is typical of West Los Angeles rainwater. Figures 7.4 through 7.7 present similar plots for the other four

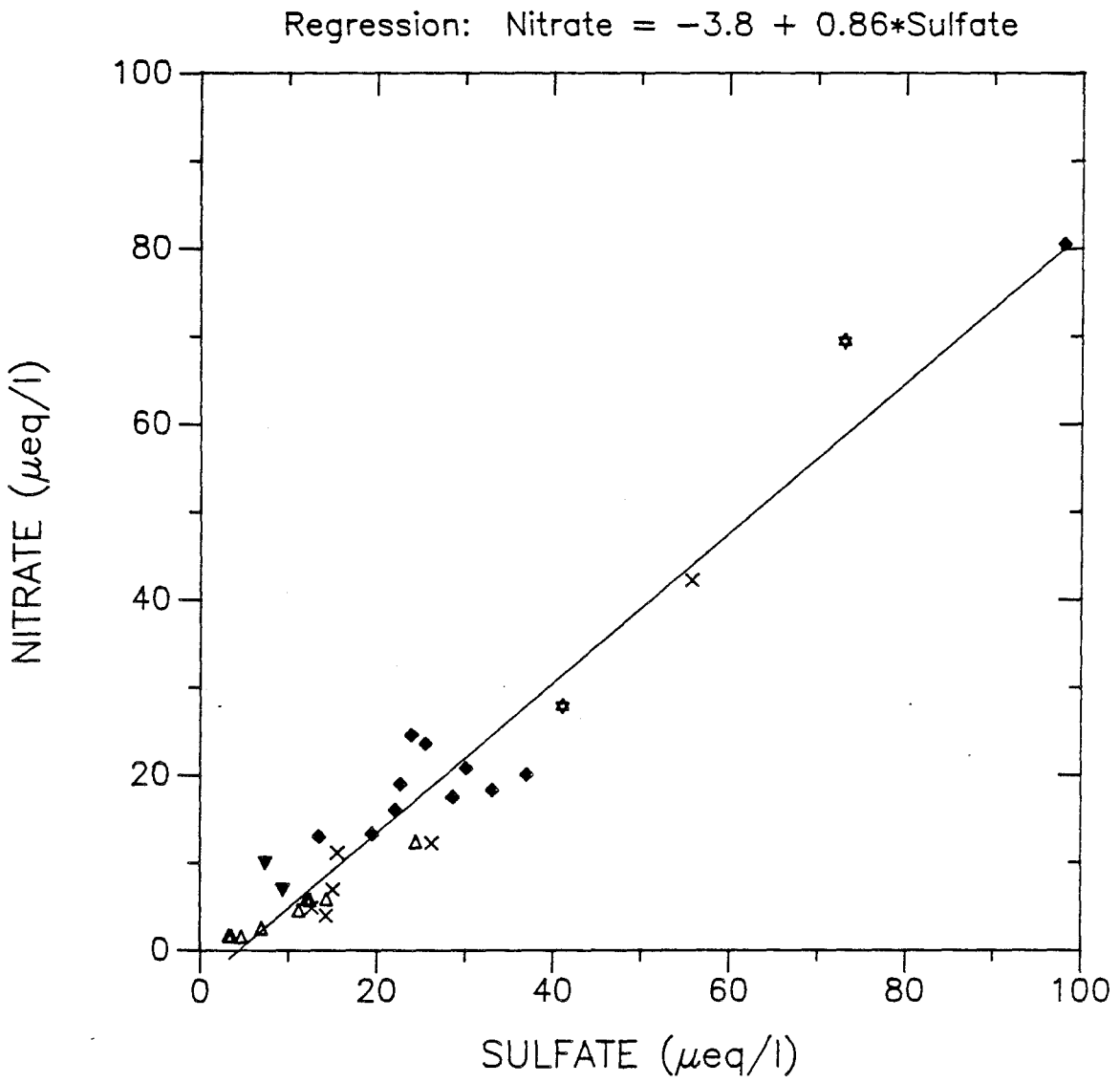

Figure 7.3. Comparison of nitrate and sulfate concentrations in rain samples collected at West Los Angeles during the winter of 1987. The different symbols represent samples from different storms. The least–squares regression line is included for reference.

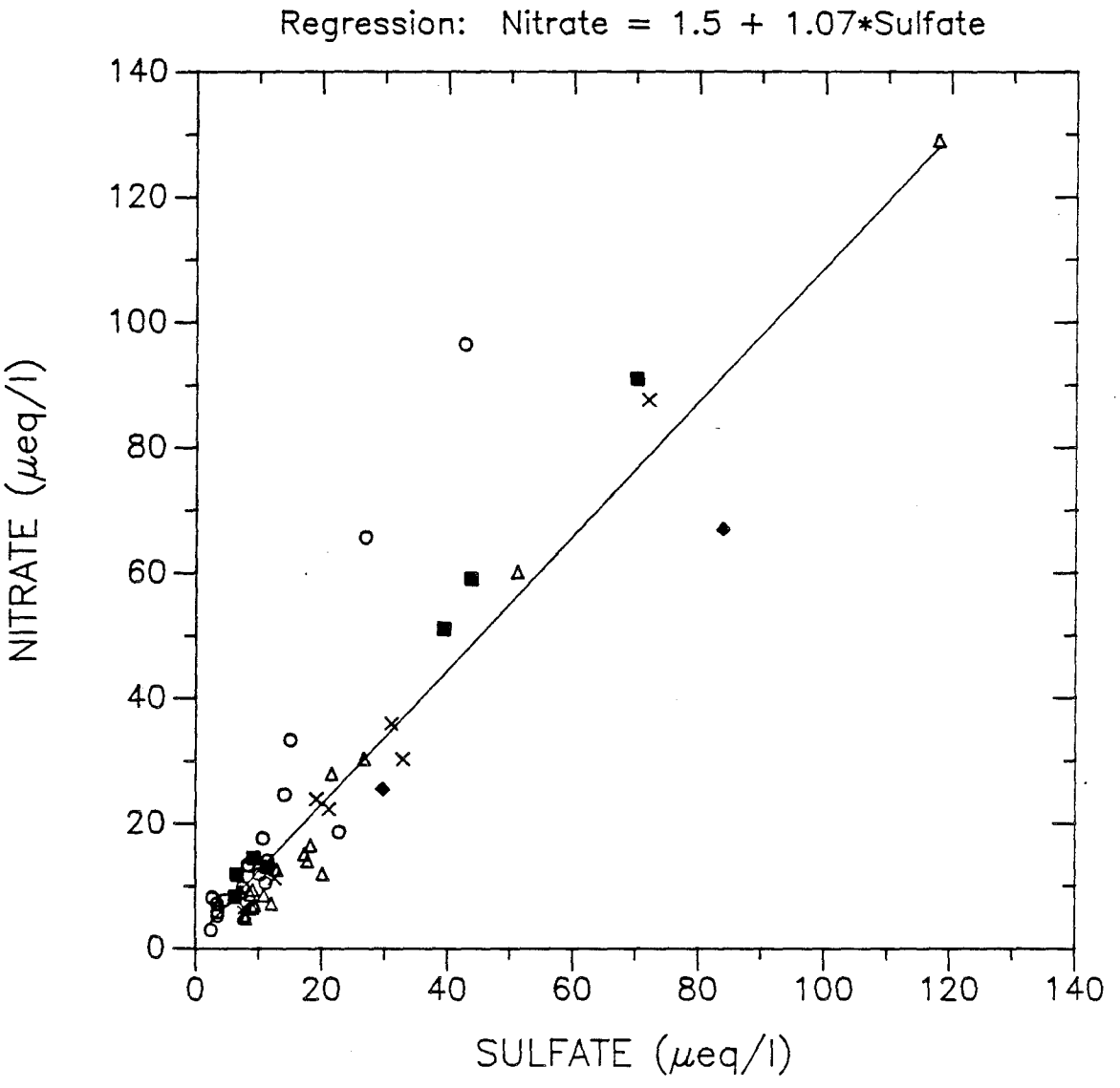

Figure 7.4. Comparison of nitrate and sulfate concentrations in rain samples collected at Pasadena during the winter of 1987. The different symbols represent samples from different storms. The least-squares regression line is included for reference.

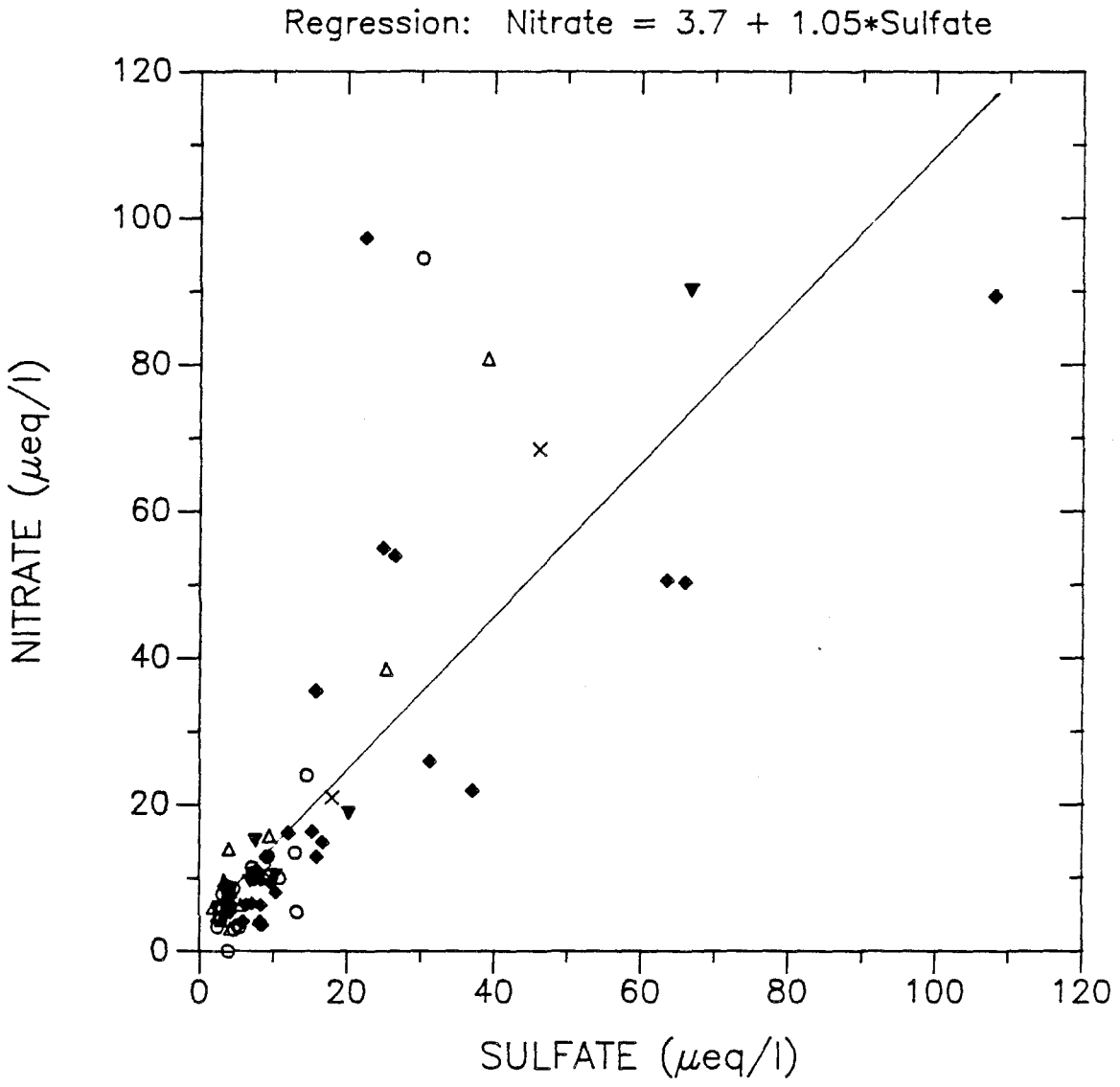

Figure 7.5. Comparison of nitrate and sulfate concentrations in rain samples collected at Henninger Flats during the winter of 1987. The different symbols represent samples from different storms. The least–squares regression line is included for reference.

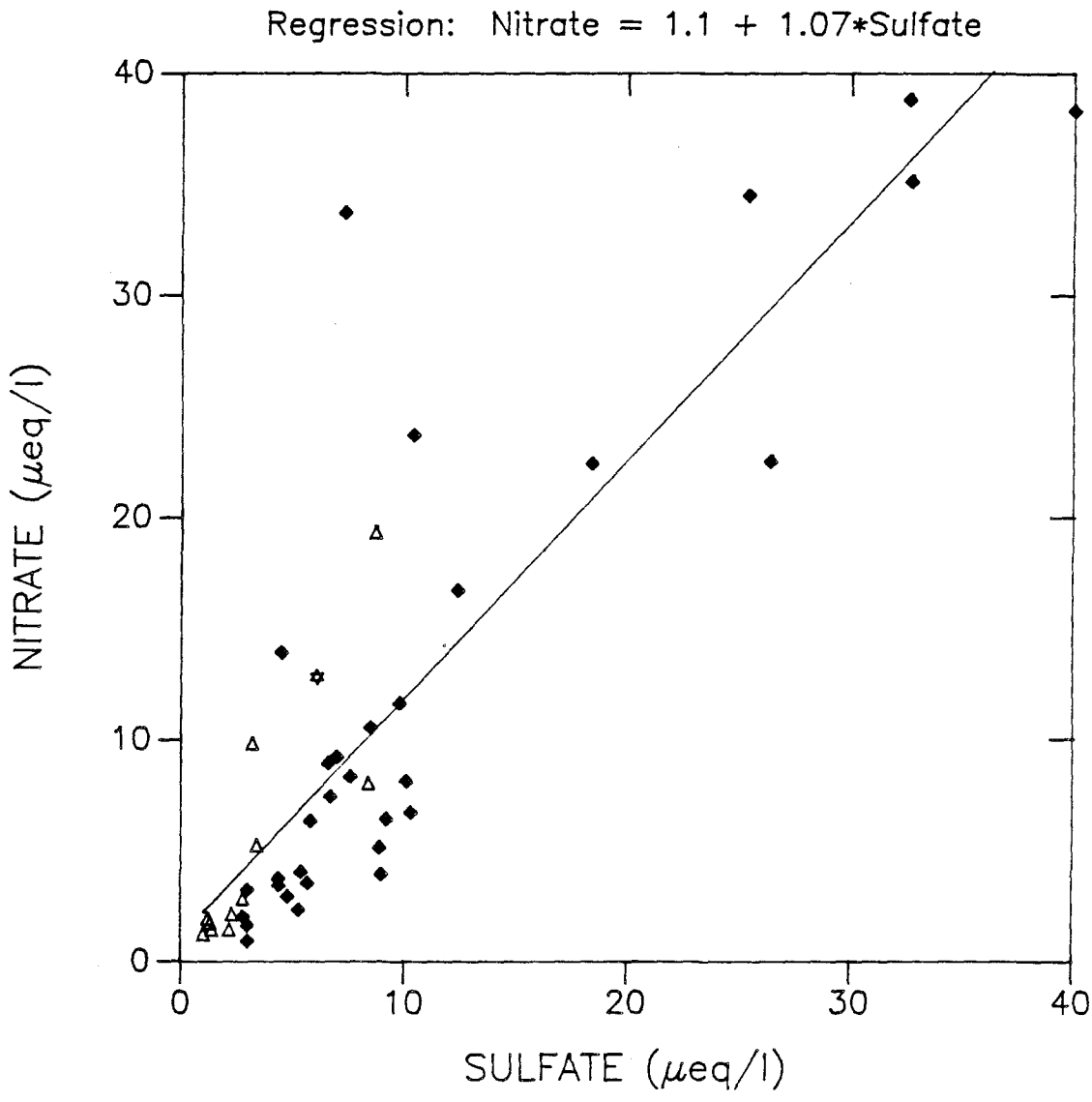

Figure 7.6. Comparison of nitrate and sulfate concentrations in rain samples collected at Mt. Wilson during the winter of 1987. The different symbols represent samples from different storms. The least-squares regression line is included for reference.

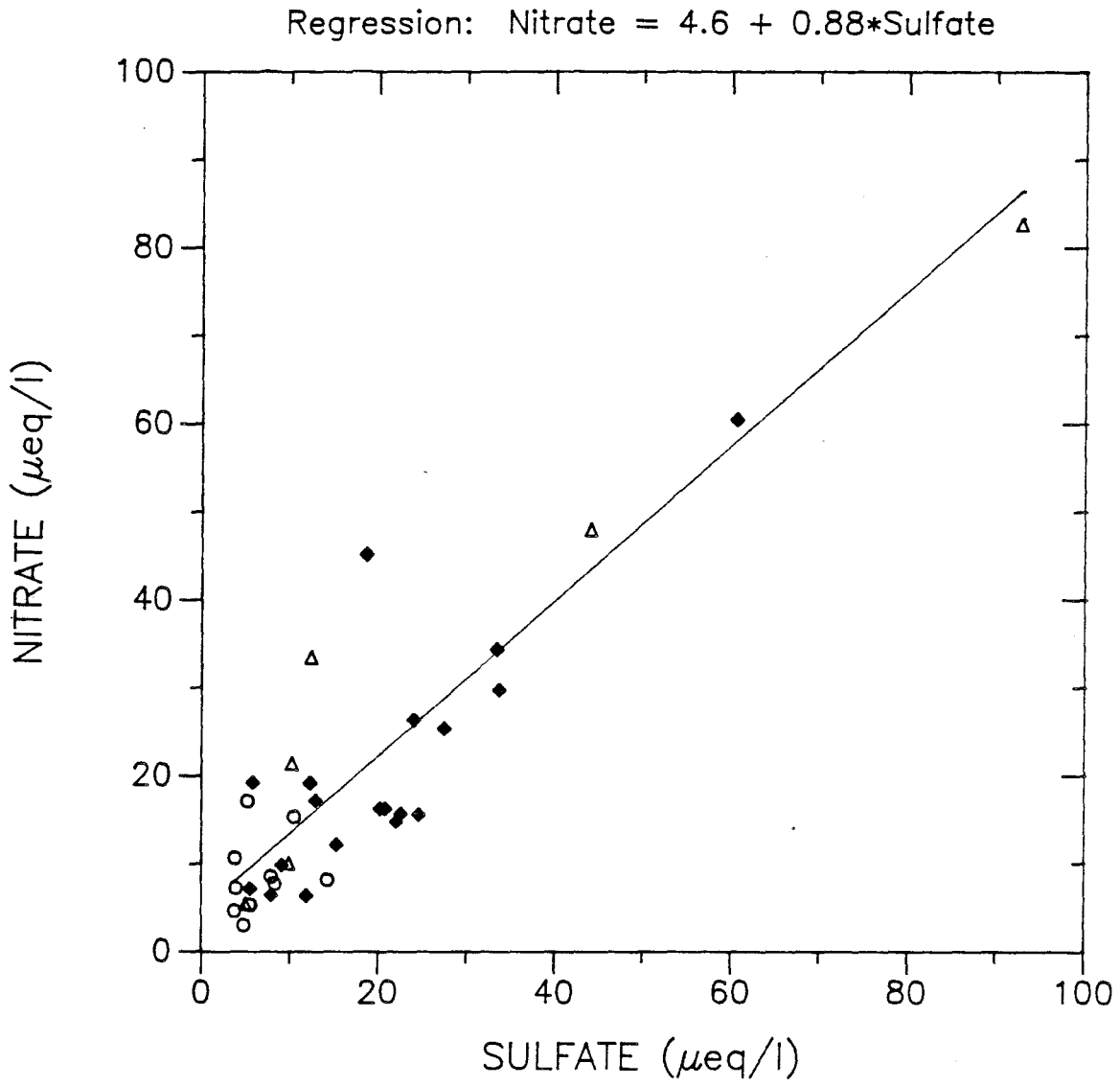

Figure 7.7. Comparison of nitrate and sulfate concentrations in rain samples collected at Riverside during the winter of 1987. The different symbols represent samples from different storms. The least-squares regression line is included for reference.

sites. The data for Pasadena indicate considerably more variation in the ratio of these two species in the rainfall there. Looking closely at Figure 7.4, it is evident that much of the variation occurs between storms. Two of the sampled storms show considerably higher nitrate to sulfate ratios than the 1.07 suggested by the regression line. One storm shows considerably less. Samples within a given storm, however, seem to maintain a fairly constant ratio.

The nitrate to sulfate ratios at Henninger Flats, depicted in Figure 7.5, are even more variable than those at Pasadena. The ratio not only varies from one event to another, considerable variation is observed within a single event. Figure 7.8 illustrates the variations observed during a storm on March 5 and 6, 1987. Data points connected by lines represent samples that were collected over periods of fairly continuous rain. Breaks in a line indicate breaks in the rainfall. Several dramatic changes were observed in the ratio of nitrate to sulfate over the course of this storm, with the range of ratios stretching from less than one–half to nearly five. The largest changes generally followed a break in the rain. Ratios of the two species at Mount Wilson were similarly variable as illustrated by Figure 7.6.

Riverside rain samples, on average, had a slight excess of sulfate over nitrate as seen in Figure 7.7. This is somewhat surprising since past work has indicated that fogwater sampled at the site generally has a large excess of nitrate (Munger et al., 1989). The result is consistent, however, with the work of Liljestrand and Morgan (1981) who observed equal inputs of nitrate and sulfate in Riverside precipitation.

Electroneutrality requires that the sum of negative charges in the rainwater equals the sum of positive charges. Clearly the data listed in Tables 7.1 through 7.5

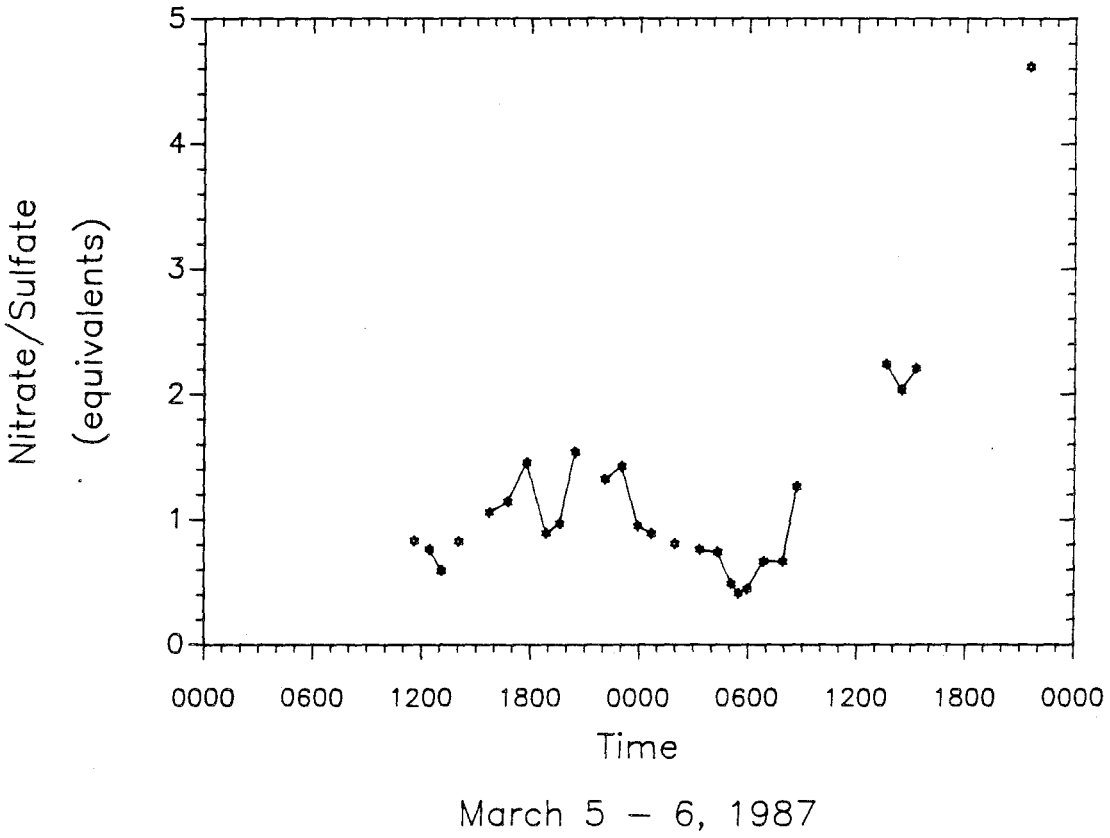

Figure 7.8. Variations in the nitrate to sulfate ratio observed in rain samples collected at Henninger Flats over the course of a single storm on March 5 and 6, 1987.

do not always conform to this requirement as indicated by the preponderance of $-/+$ ratios (representing the ratio of total measured negative charge concentration to total measured positive charge concentration) considerably different from one. Two reasons may be hypothesized to explain this discrepancy: (1) errors in analytical measurements of ion concentrations and (2) failure to include important species in the ion balance. For several of the samples, concentrations of most species are near our detection limit (approximately 2 μN for most measured species). For these samples it is not surprising to see the ion balance differ significantly from 1.0 since relative error in concentration measurements increases near the detection limit. Removing these dilute samples from consideration, however, leaves a number of samples with ion balances considerably less than one. This anion deficit suggests that lower molecular weight organic acids may be important contributors to the composition of the samples. Formic and acetic acid have been shown to be important components in rainwater collected in remote as well as urban areas, including Los Angeles (Galloway et al., 1982; Keene and Galloway, 1984; Kawamura and Kaplan, 1984). At the pH levels found in many of the rain samples, both formic and acetic acid will exist largely in their deprotonated form (pK_a^{298} of 3.74 and 4.76, respectively, Martell and Smith, 1977). Samples with the highest pH values also tended to exhibit the largest anion deficits, consistent with the hypothesis that formate and acetate are the missing anions. Since no one was present at each site to immediately preserve unstable species such as acetic and formic acid which undergo biodegradation, we cannot positively confirm that acetate and formate were present at the levels necessary to correct the calculated anion deficits. During the ion chromatographic analysis of NO_3^-, SO_4^{2-}, and Cl^-, however, we did observe significant concentrations of "formate + acetate", which elute in a peak before chloride, despite the fact that the samples had not been preserved. These concentrations have not been reported here because of the instability of the species. They are indicators,

however, of the presence of significant levels of low molecular weight organic acids in the collected samples.

During the study 100 filter sets were run in an attempt to define aerosol and gas phase concentrations prior to, during, and following rain events. Approximately one-half of these were used in an intensive monitoring effort during the period from March 4 to March 8. Results of the filter analyses are listed in Table 7.7. Highest concentrations of $NH_{3(g)}$ and $HNO_{3(g)}$ were seen at Riverside and Pasadena, respectively. Na^+ and Cl^- aerosol concentrations were highest at West Los Angeles, followed by Pasadena. The ratio of Na^+ to Cl^- frequently was observed to significantly exceed the sea-salt ratio of 0.86. This suggests that much of the original Cl^- in the aerosol may have been volatilized as HCl via acid exchange with nitric acid. The highest concentrations of aerosol NO_3^- and SO_4^{2-} were observed at Pasadena. NH_4^+ concentrations in the aerosol were highest at Riverside and Pasadena. Occasional high NH_4^+ aerosol concentrations were also observed at West Los Angeles. During all periods sampled, ammonia was found predominantly in the aerosol phase at Pasadena and West Los Angeles; at Riverside, it was located predominantly in the gas phase. Concentrations of $HNO_{3(g)}$ at Riverside were small during the periods sampled, due to the high levels of $NH_{3(g)}$ and the tendency of these two species to form ammonium nitrate aerosol.

Discussion

Two storms were selected for more detailed consideration: February 13, 1987 and March 5-6, 1987. The February 13 event was selected because it provided the most complete data set for the "vertical" profile from Pasadena to Mt. Wilson. This event also provided a significant number of samples for the horizontal transect

Table 7.7. South Coast Air Basin Aerosol and Gas Data–1987

Date	Time	Na^+	NH_4^+	Ca^{2+}	Mg^{2+}	Cl^-	NO_3^-	SO_4^{2-}	NH_3	HNO_3
		←———			neq/m^3		——→		←nmole/m^3→	
Henninger Flats										
01/03	2200–0200	52.0	135.6	13.5	12.8	6.9	109.2	87.6	0.8	53.3
01/04	0700–1100	3.9	11.7	2.8	2.6	8.5	9.5	8.1	7.7	10.0
01/04	1101–1501	3.7	8.2	3.4	2.2	12.3	6.4	7.5	12.3	9.1
01/27	2000–0000	18.5	434.6	15.7	6.3	10.6	349.3	61.3	40.9	70.3
01/28	0200–0600	0.6	7.5	2.5	1.0	7.7	12.5	3.8	23.1	4.5
01/28	0800–1200	11.6	131.8	15.3	4.1	4.8	115.2	26.8	48.6	61.2
02/10	1500–1800	19.3	198.8	16.2	7.0	0.5	155.9	52.0	159.5	27.0
02/10	2000–0000	8.9	124.0	10.5	3.6	0.0	33.0	105.3	27.8	11.2
02/11	0200–0600	11.8	161.1	8.1	3.9	0.0	61.3	101.3	29.3	8.7
03/04	2000–0000	5.3	45.3	10.5	3.8	3.1	10.2	31.6	34.0	39.7
03/05	0200–0600	9.5	61.8	10.7	5.1	1.5	9.1	47.8	34.7	39.7
03/05	0800–1200	9.0	67.1	11.3	8.9	3.5	31.4	33.8	51.7	20.4
03/05	2000–0000	0.0	18.8	3.2	2.0	1.9	7.1	14.3	6.9	8.5
03/06	0200–0600	2.0	20.4	2.5	2.3	0.0	4.4	16.4	0.0	5.7
03/06	0800–1200	2.7	22.2	3.7	1.0	1.9	10.8	12.3	14.7	6.6
03/06	1515–1800	5.1	123.7	6.7	2.6	0.0	80.2	22.4	3.4	8.2
03/06	2000–0000	3.7	142.5	11.9	2.7	2.7	98.4	33.2	2.3	6.0
03/07	0800–1200	10.2	279.4	5.9	1.8	9.3	189.8	93.6	0.0	39.5
Mount Wilson										
01/27	2000–0000	5.7	19.2	10.5	2.0	8.5	14.7	8.9	3.1	9.6
01/28	0200–0600	1.6	12.6	4.8	2.0	7.1	7.3	5.6	0.8	10.2
01/28	0800–1100	2.8	24.7	2.6	2.7	14.9	47.8	8.7	14.4	8.3
02/10	1400–1800	4.3	186.8	7.2	2.4	2.3	134.1	47.8	44.0	9.8
02/10	2000–0000	2.4	90.7	4.2	2.4	0.0	45.5	44.8	0.0	14.4
02/11	0200–0600	0.0	6.9	2.3	2.0	0.0	3.8	8.3	13.9	5.7
03/04	2000–0000	4.0	50.9	7.9	3.4	0.8	17.9	32.2	12.3	43.7
03/05	0200–0600	0.0	50.1	5.8	2.2	6.6	7.7	40.7	5.4	19.1
03/05	0800–1200	0.5	48.6	3.6	2.4	1.4	20.8	24.1	5.4	7.4
03/05	2000–0000	0.0	7.7	2.5	2.0	8.5	3.2	2.1	0.0	3.8
03/06	0200–0600	1.0	9.6	2.3	2.0	3.9	3.9	2.5	0.0	3.8
03/06	0800–1200	1.7	12.1	2.5	1.0	1.9	4.8	4.2	0.0	3.4
03/06	1400–1800	0.0	17.2	0.5	1.0	0.0	10.6	6.4	1.5	4.5
03/07	0200–0600	0.0	11.3	2.5	1.0	0.0	5.6	6.0	0.0	8.9
03/07	0800–1115	2.3	19.6	5.0	0.8	0.6	10.2	10.2	0.0	10.0

Table 7.7 (Cont'd). South Coast Air Basin Aerosol and Gas Data–1987

Date	Time	Na^+	NH_4^+	Ca^{2+}	Mg^{2+}	Cl^-	NO_3^-	SO_4^{2-}	NH_3	HNO_3
		←———			neq/m^3		——→		←nmole/m^3→	
Riverside										
01/04	0001–0301	45.2	245.4	21.7	14.5	14.9	203.2	78.4	324.1	17.9
01/04	0700–1100	33.1	124.6	5.9	9.3	8.7	79.1	58.1	102.6	14.0
01/04	1101–1501	10.3	27.2	10.9	3.5	0.0	13.3	20.8	145.1	8.1
01/27	1515–1815	24.3	795.1	87.3	22.7	14.9	706.0	59.9	3074.1	35.5
01/28	0200–0500	14.3	291.2	48.0	8.4	30.1	289.1	54.5	410.5	12.6
01/28	0800–1100	29.5	729.0	36.4	9.1	30.9	540.6	204.7	495.9	27.5
02/10	1500–1800	15.8	138.0	20.5	7.3	14.7	99.8	44.0	2259.3	13.9
02/10	2000–0000	12.4	125.0	12.4	7.1	11.6	91.6	38.2	1958.3	7.6
02/11	0200–0600	13.5	118.5	15.7	5.5	3.5	79.5	40.9	589.5	3.6
03/04	2000–0000	23.1	112.8	81.0	22.6	17.0	33.8	83.3	345.7	36.9
03/05	0200–0600	10.8	145.8	110.7	19.0	6.9	53.8	76.2	546.3	14.7
03/05	0800–1200	27.5	79.7	41.2	9.8	2.1	22.0	49.2	474.5	24.2
03/05	2000–0000	8.8	115.9	6.7	1.4	0.0	12.3	24.7	104.2	8.5
03/06	0200–0600	2.8	49.4	7.5	2.7	0.0	16.8	28.2	58.6	7.8
03/06	0800–1200	1.1	47.2	7.3	1.8	0.0	22.4	22.2	100.3	10.0
03/06	1400–1800	5.4	101.2	11.2	3.3	4.0	70.0	28.5	131.2	18.9
03/06	2000–0000	9.4	294.4	14.0	7.0	4.6	195.4	53.8	1134.3	6.8
03/07	0800–1200	9.8	689.0	11.6	5.0	13.7	430.7	148.7	434.4	11.7
West Los Angeles										
01/27	1500–1800	118.3	421.7	71.2	42.0	70.2	423.4	75.9	297.3	35.8
01/27	2000–0000	95.0	524.6	29.6	27.4	80.8	425.5	92.6	280.1	18.7
01/28	0200–0600	47.1	154.4	12.2	4.1	14.3	110.3	69.3	88.7	9.1
02/10	1400–1800	33.7	262.2	15.1	10.2	11.8	206.4	63.7	298.6	51.2
02/10	2000–0000	61.4	156.2	6.0	15.2	35.1	122.1	76.4	137.3	13.4
02/14	1230–1800	76.3	46.6	11.2	18.1	45.0	67.3	31.0	185.2	35.7
02/14	1900–0000	97.8	75.3	11.9	25.2	63.0	71.8	36.6	145.7	5.3
02/15	1230–1800	68.4	70.1	12.6	17.3	17.6	61.6	51.5	107.7	26.1
02/15	1900–0000	31.3	26.9	11.5	9.1	7.5	17.1	22.5	119.8	12.6
03/04	2000–0000	185.0	122.6	31.7	50.3	157.4	125.2	84.5	208.3	37.8
03/05	0800–1200	54.7	113.4	32.2	18.0	35.5	82.4	64.2	205.2	24.0
03/05	1400–1800	28.6	154.0	24.2	15.4	25.3	106.9	49.0	356.5	14.9
03/05	2040–0000	4.7	70.6	8.0	5.1	6.5	32.9	30.1	144.4	5.9
03/06	0200–0600	0.8	46.8	4.3	1.8	0.6	17.0	28.7	107.3	8.9
03/06	0800–1200	2.2	101.3	9.1	3.3	2.3	64.4	36.1	206.0	31.2
03/06	1400–1800	80.9	68.7	20.1	21.9	58.4	58.3	42.2	96.5	24.0
03/06	2000–0000	142.5	178.5	18.5	37.1	119.2	161.5	65.8	125.0	7.8
03/07	0800–1200	126.2	139.3	20.1	30.5	89.5	132.9	68.7	160.5	21.7

Table 7.7 (Cont'd). South Coast Air Basin Aerosol and Gas Data–1987

Date	Time	Na^+	NH_4^+	Ca^{2+}	Mg^{2+}	Cl^-	NO_3^-	SO_4^{2-}	NH_3	HNO_3
		←———			neq/m^3		——→		←nmole/m^3→	
Pasadena										
01/04	1101–1501	19.2	45.9	15.8	2.0	0.0	34.5	15.4	31.6	12.3
01/05	1100–1500	23.6	112.2	15.3	7.4	0.6	109.0	30.9	67.1	95.5
01/27	1300–1700	45.5	984.8	93.3	24.5	20.8	794.8	93.7	296.3	102.1
01/27	2000–0000	61.4	981.7	77.0	28.4	68.7	791.7	142.6	371.1	43.5
01/28	0200–0600	22.1	630.4	34.4	6.2	43.2	478.0	76.0	339.5	17.2
01/28	1000–1400	31.4	298.6	21.4	9.2	19.7	255.6	88.0	120.4	132.5
01/28	1400–1650	35.2	76.0	14.2	11.0	13.8	70.3	31.2	123.1	58.7
02/10	1400–1800	22.0	155.3	19.4	7.9	6.2	114.0	58.3	183.6	84.3
02/10	2000–0000	27.7	176.8	11.7	8.2	16.6	97.6	42.4	159.0	15.3
02/11	0200–0600	25.8	197.0	12.9	7.3	26.0	89.5	108.6	217.6	8.3
02/14	1200–1800	20.2	354.4	9.4	8.3	11.2	314.3	59.9	187.2	98.9
02/14	1800–0000	55.5	74.9	12.8	15.9	20.6	77.0	30.1	193.4	21.8
02/15	0100–0600	55.2	126.8	13.0	18.8	31.8	112.0	42.7	212.3	8.5
02/15	1200–1800	37.6	159.8	9.0	9.9	2.1	86.5	73.0	42.2	42.0
02/15	1800–0000	21.9	29.1	8.4	7.0	1.4	11.8	25.8	73.6	59.6
02/16	0100–0600	23.8	24.7	9.3	7.6	9.1	11.6	28.4	41.4	17.8
02/22	1200–1600	12.8	18.1	5.7	0.9	0.0	9.6	2.2	9.3	3.6
02/22	2000–0000	59.8	110.3	17.5	14.7	17.7	54.8	42.2	125.0	11.3
02/23	0200–0600	53.5	130.5	24.6	9.5	26.0	93.4	44.8	81.8	9.5
03/04	2000–0000	36.6	117.8	47.8	15.6	17.2	72.5	61.0	331.8	34.2
03/05	0200–0600	29.2	108.4	31.6	12.7	7.7	50.9	54.8	216.0	37.4
03/05	0800–1200	32.6	125.0	42.4	13.5	18.9	90.3	62.5	293.2	26.8
03/05	1400–1800	3.4	34.0	4.3	2.0	3.7	15.2	24.3	141.2	19.1
03/05	2000–0000	0.6	42.9	4.6	3.2	2.7	23.9	21.0	56.3	10.0
03/06	0800–1200	0.9	69.4	4.9	3.1	0.0	40.1	23.7	91.0	21.7
03/06	1420–1800	12.9	151.0	15.5	5.2	7.6	114.7	43.4	262.6	16.3
03/07	0200–0600	31.6	268.7	17.0	10.7	33.8	195.2	85.5	133.5	5.9
03/07	0800–1200	55.2	538.2	20.6	16.8	36.7	374.0	138.1	65.6	56.5
03/07	2000–0000	94.7	197.4	11.1	23.2	38.2	141.4	112.5	24.7	33.6
03/08	0800–1200	94.3	159.3	10.5	22.5	40.7	149.5	71.0	81.8	42.5
03/08	1400–1800	75.3	115.2	13.3	19.8	28.7	104.0	48.2	71.8	86.3

from West Los Angeles to Riverside. The discussion in the following section will consider the patterns of deposition and rainfall for these two transects. The second storm, March 5–6, will be addressed in the subsequent section. Here the discussion will focus on the relationship between the aerosol and gas phase compositions and the composition of the rainfall.

The Storm of February 13, 1987

The storm of February 13 was the second wettest event at Pasadena during the period studied. 25.1 mm of rainfall were recorded by the Los Angeles County Flood Control District rain gauge on the Caltech campus. This rain gauge is located on top of a three–story building approximately 100 m south of the study site. The Pasadena study site recorded 24 mm of rainfall during the storm. Cumulative rainfall as a function of time at Pasadena, Henninger Flats, and Mount Wilson, is depicted in Figure 7.9. Both the total hydrological deposition and the pattern in which it occurred are remarkably similar for the three sites. For most of the storm the rain fell at all three sites at a rate of approximately 4 mm hr^{-1}.

The similarity in hydrological deposition patterns at the three sites facilitates an intersite comparison of deposition rates of the major ionic species. Plots of the deposition patterns of NO_3^-, NH_4^+, SO_4^{2-}, H^+, Na^+, Cl^-, Mg^{2+}, and Ca^{2+} are presented in Figures 7.10 through 7.13, respectively. Deposition of nitrate was 530 μeq m^{-2} at Pasadena, 40% higher than at Henninger Flats and 380% higher than at Mt. Wilson (see Figure 7.10). Deposition of most species at these three sites was in fact observed to be highest at Pasadena and lowest at Mt. Wilson. Deposition of NH_4^+ was approximately 580 μeq m^{-2} at Pasadena, 130% higher than at Henninger Flats and more than 1000% higher than at Mt. Wilson (see Figure 7.10); for SO_4^{2-} the

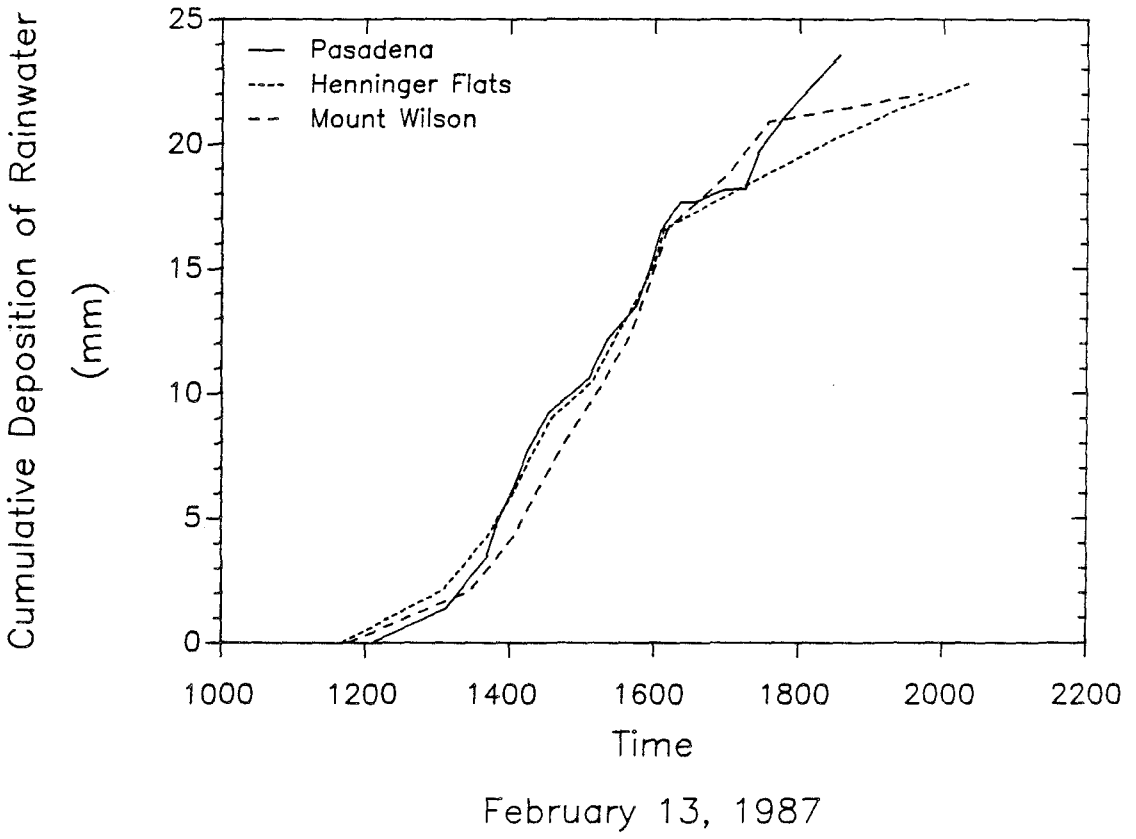

Figure 7.9. Cumulative rainfall measured at Pasadena, Henninger Flats, and Mt. Wilson on February 13, 1987.

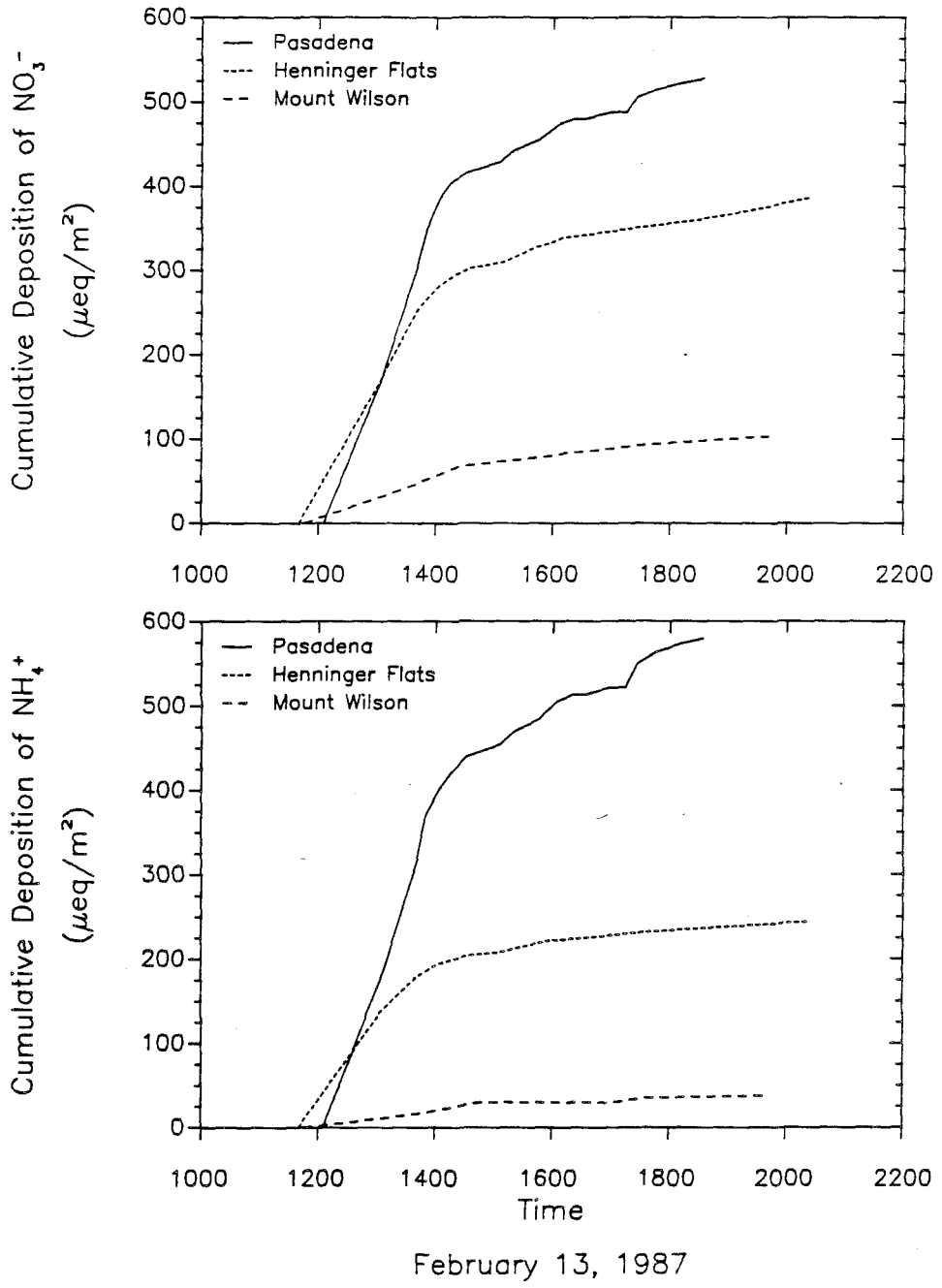

Figure 7.10. Cumulative deposition of NO_3^- and NH_4^+ measured at Pasadena, Henninger Flats, and Mt. Wilson on February 13, 1987.

enhancement at Pasadena was 150% compared to Henninger Flats and 600% compared to Mt. Wilson (see Figure 7.11). Since the rainfall patterns were essentially identical at all three sites, and the sites are located within 12 km of one another, these differences in deposition indicate that much of the loading of these species in the rain collected at Pasadena was picked up in the lowest 500 m of the atmosphere. Likewise, much of the loading in the rain collected at Henninger Flats was picked up in the 1000 m elevation between there and Mt. Wilson.

Deposition of H^+ was only slightly higher at Pasadena than at Henninger Flats (approximately 475 vs. 425 μeq m^{-2}, see Figure 7.11), suggesting that the net acidity of the rain droplets was not affected significantly as they fell through the lowest portion of the atmosphere; however, a substantial increase in deposition of H^+ was observed between Mt. Wilson and Henninger Flats. Na^+ deposition was highest at Pasadena and lowest at Mt. Wilson. Na^+ deposition at each site was substantially less than Cl^- deposition (Figure 7.12), suggesting that $HCl_{(g)}$ was probably scavenged by the cloud and/or rain droplets. Deposition of Mg^{2+} was relatively small at all three sites, but was still significantly higher at Pasadena than at the other two sites (Figure 7.13), while Ca^{2+} deposition was somewhat higher, contributing 130 μeq m^{-2} at Pasadena and 30 to 40 μeq m^{-2} at both Henninger Flats and Mt. Wilson.

For most species, at least 75% of the deposition occurred during the first two hours of the storm. After this time, deposition rates dropped off considerably, despite the fact that average rainfall rates increased over the subsequent two hours of the storm. Mg^{2+}, Cl^-, and Na^+ were seemingly almost completely washed out of the air column by this point. Deposition of NO_3^-, SO_4^{2-}, and NH_4^+ continued at reduced, but roughly constant, rates during the remainder of the storm. Ca^{2+} was

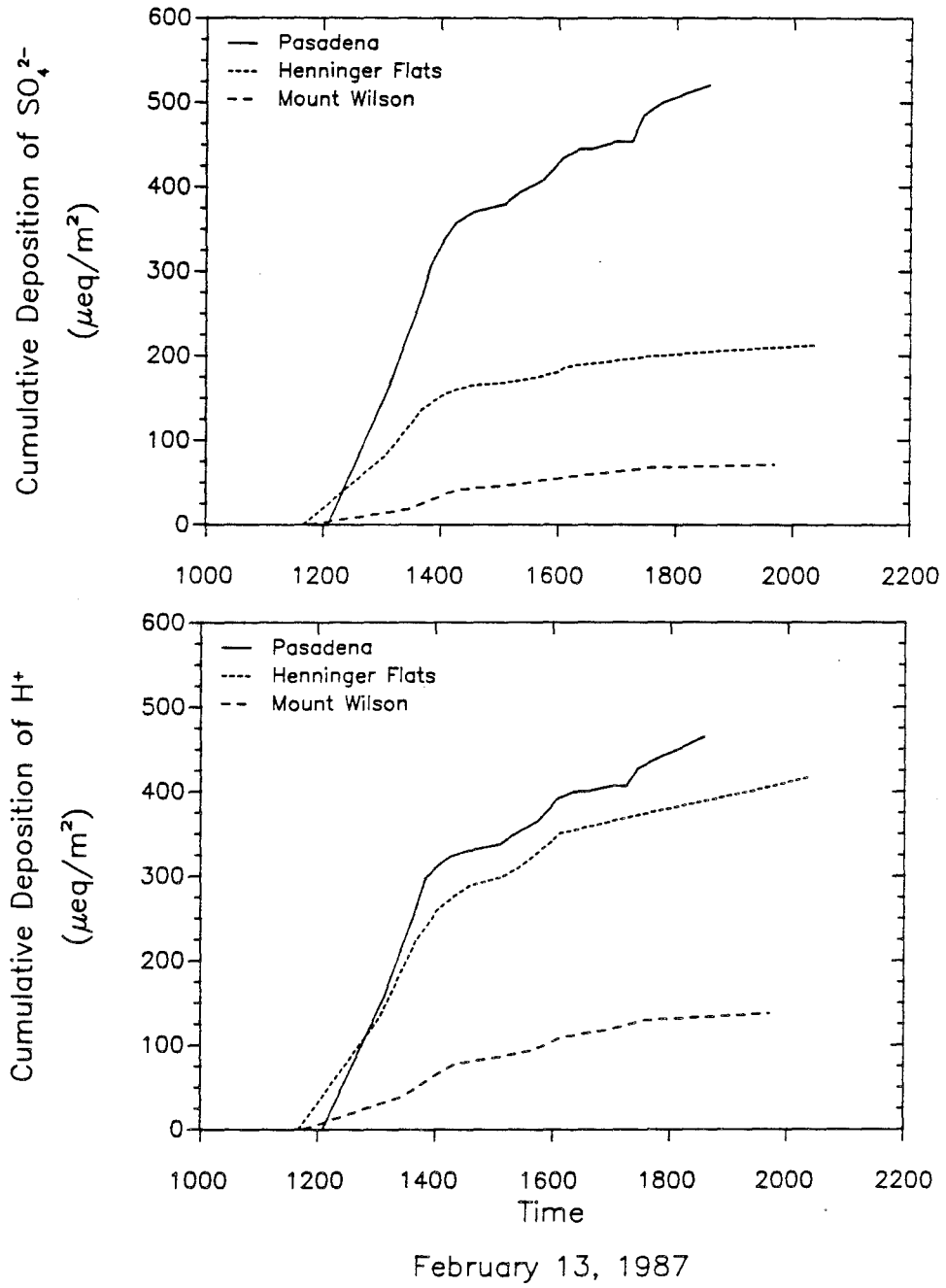

Figure 7.11. Cumulative deposition of SO_4^{2-} and H^+ measured at Pasadena, Henninger Flats, and Mt. Wilson on February 13, 1987.

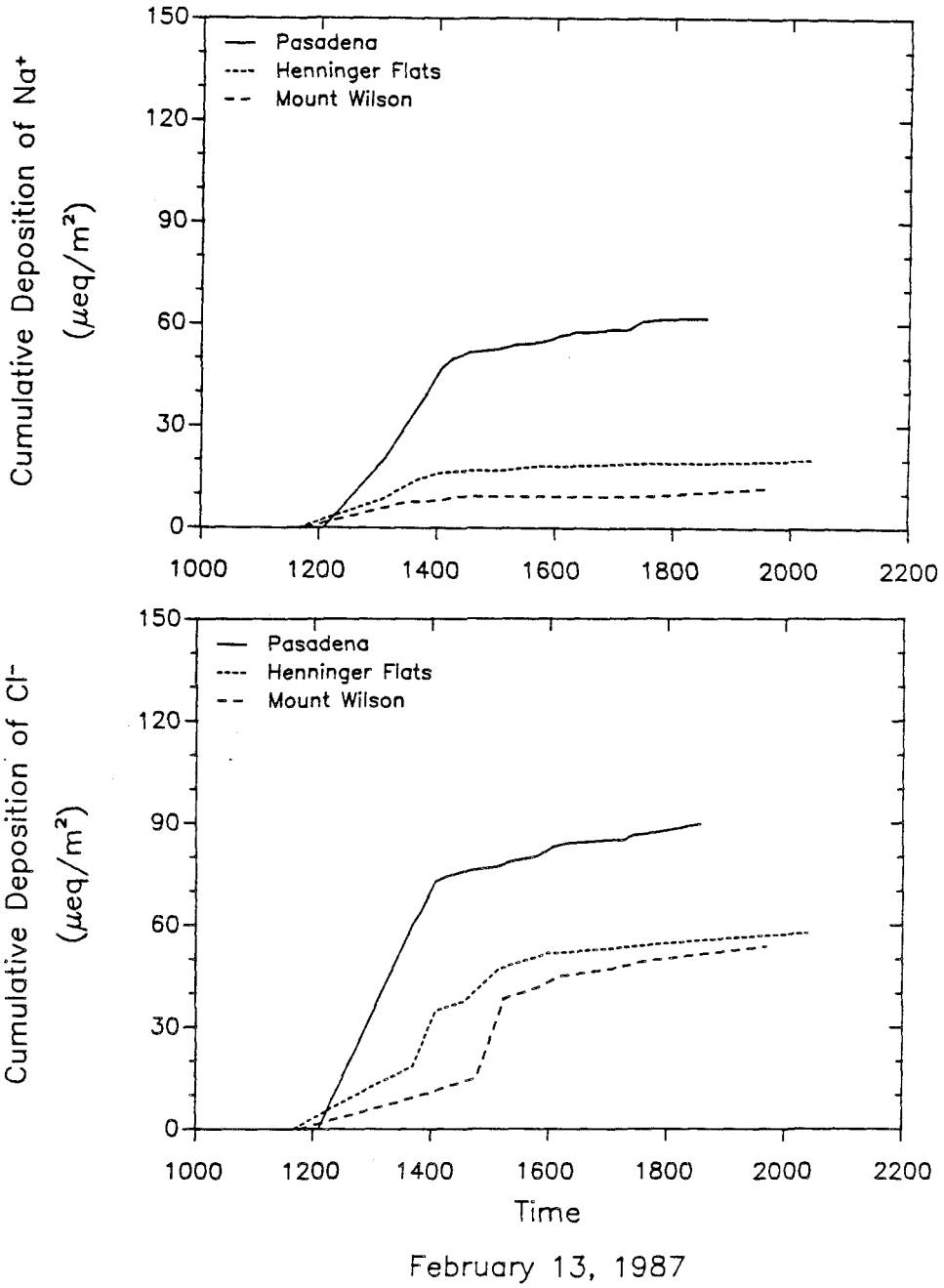

Figure 7.12. Cumulative deposition of Na^+ and Cl^- measured at Pasadena, Henninger Flats, and Mt. Wilson on February 13, 1987.

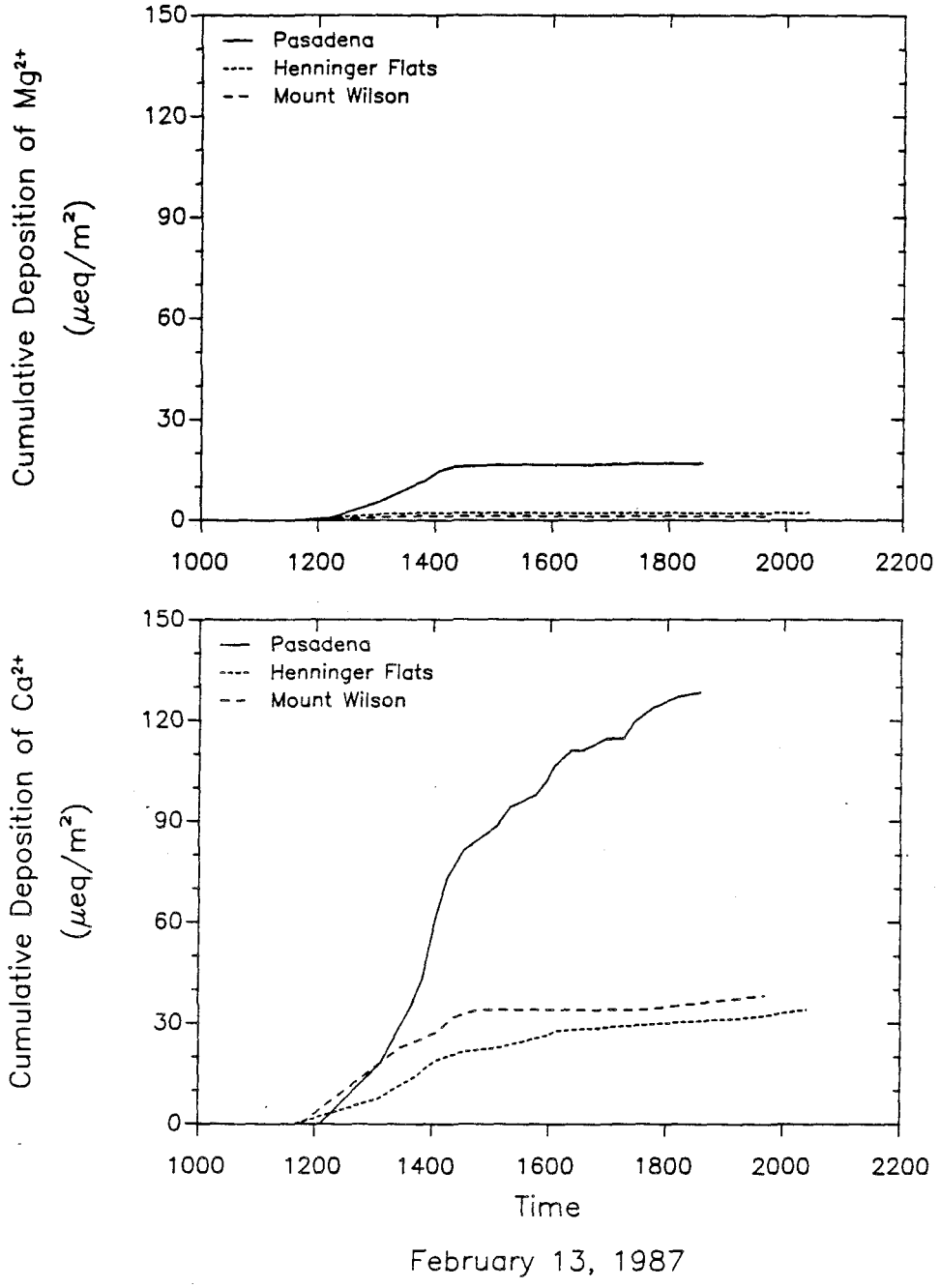

Figure 7.13. Cumulative deposition of Mg^{2+} and Ca^{2+} measured at Pasadena, Henninger Flats, and Mt. Wilson on February 13, 1987.

the only ion which continued to be deposited at a rate even close to its initial deposition rate, and this occurred only at Pasadena. At Henninger Flats and Mt. Wilson, deposition of Ca^{2+} was essentially complete after the first three hours.

The rainfall deposition patterns at West Los Angeles and Riverside were somewhat different than those observed at Pasadena, Henninger Flats, and Mt. Wilson (see Figure 7.14). The rain began an hour earlier at West Los Angeles than at Pasadena, while at Riverside the rain began three hours later. Total rainfall at West Los Angeles was approximately 16 mm, while Riverside received less than 5 mm, predominantly in two short rainy periods. Figure 7.15 presents the deposition of NO_3^- and NH_4^+ vs. time at the three sites. Deposition of NO_3^- at both West Los Angeles and Riverside was considerably less than at Pasadena. The amount of nitrate deposition at Riverside was roughly equivalent to that at Pasadena, when normalized by rainfall amounts at the two sites. Normalized nitrate deposition at West Los Angeles, however, was much less, despite the fact that the rain began there earlier than at any of the other sites. Normalized NH_4^+ deposition at Riverside was more than twice that at Pasadena, while at West Los Angeles it was considerably less (see Figure 7.15). It is interesting to note that the deposition patterns of both species at West Los Angeles and Riverside closely paralleled the rainfall patterns at the same sites. Unlike Pasadena, neither site experienced a dramatic drop in the deposition rate as the storm progressed, aside from periods of reduced rainfall intensity.

The patterns of cumulative deposition of SO_4^{2-} and H^+ are shown in Figure 7.16. Deposited amounts of both species, normalized by the amount of rainfall, were considerably less at both West Los Angeles and Riverside than they were at Pasadena. The high level of $NH_{3(g)}$ at Riverside essentially neutralized all of the

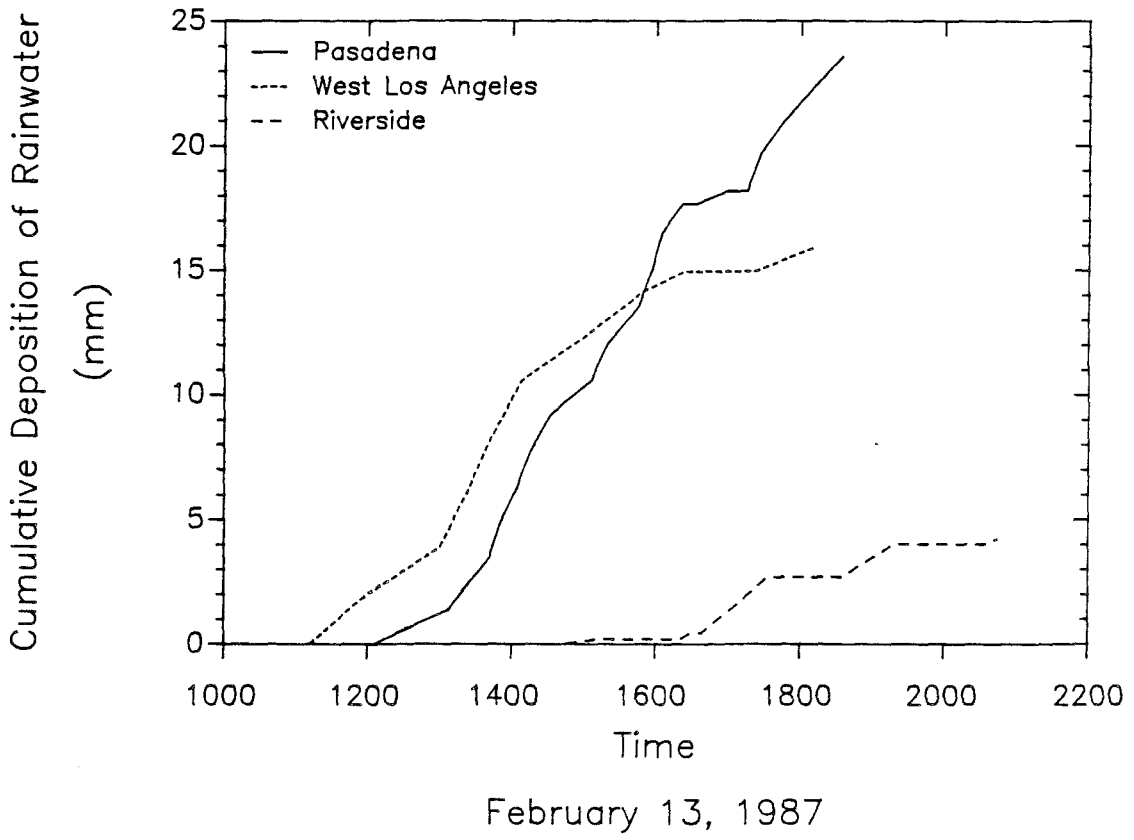

Figure 7.14. Cumulative rainfall measured at Pasadena, West Los Angeles, and Riverside on February 13, 1987.

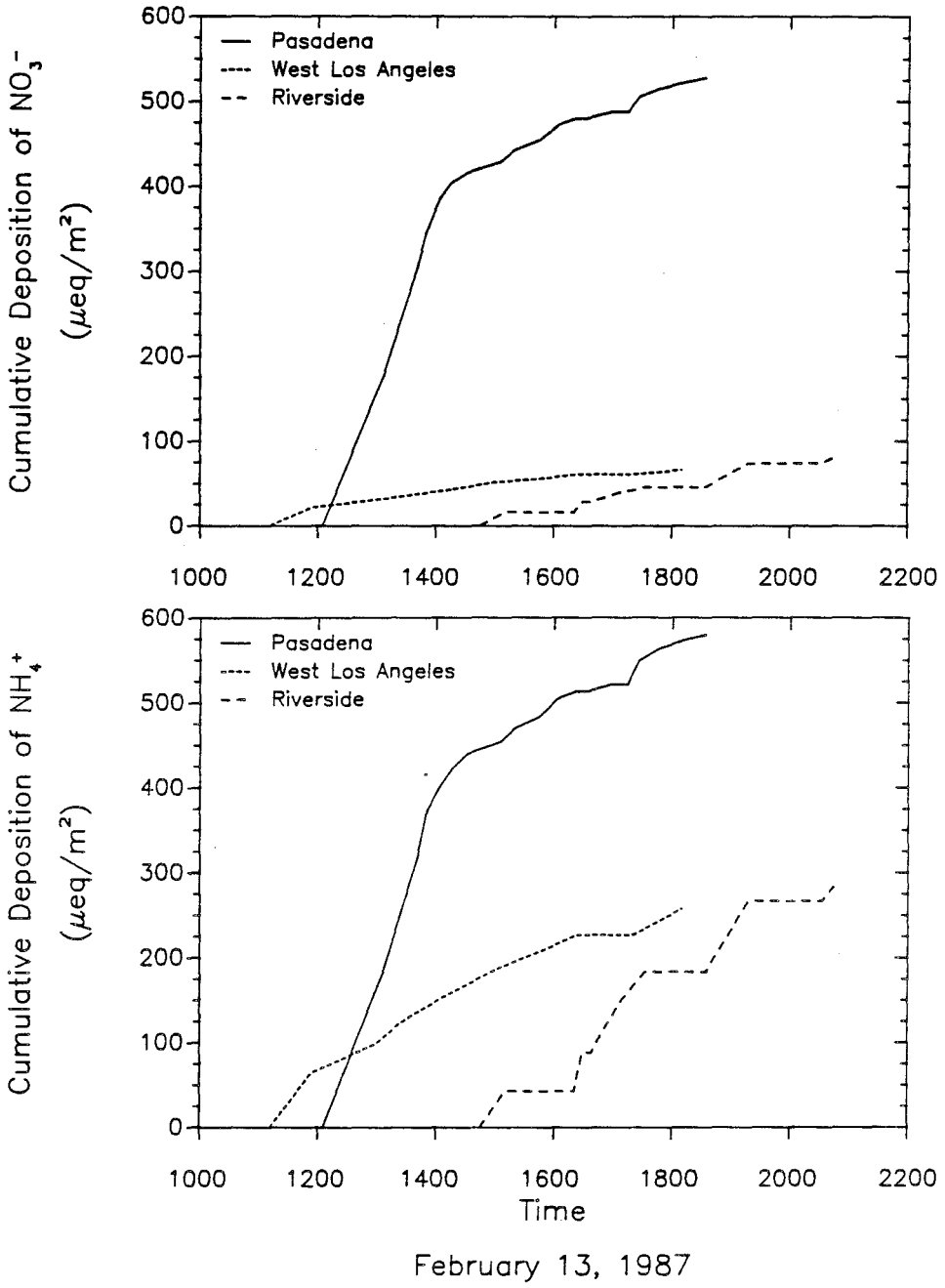

Figure 7.15. Cumulative deposition of NO_3^- and NH_4^+ measured at Pasadena, West Los Angeles, and Riverside on February 13, 1987.

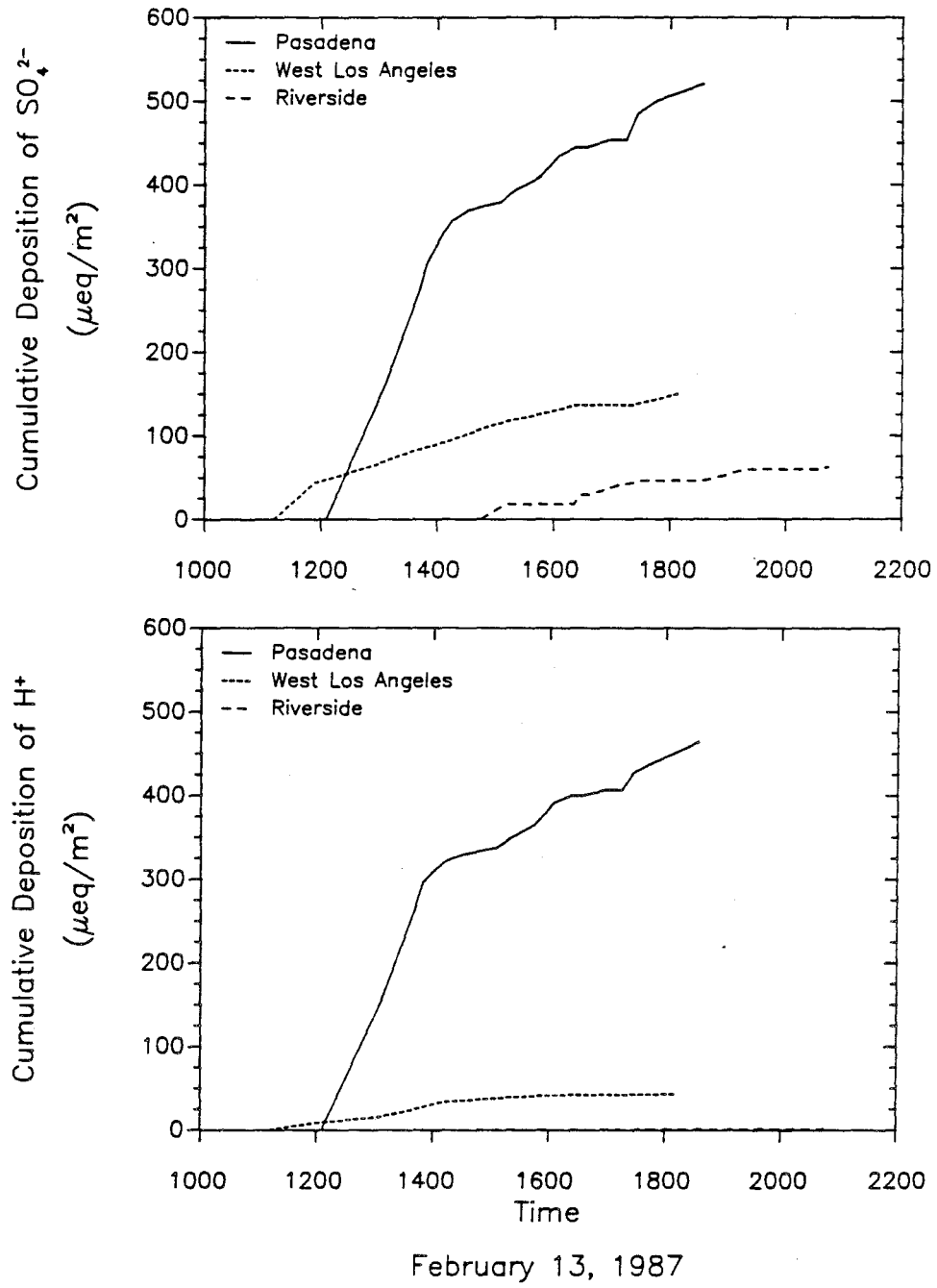

Figure 7.16. Cumulative deposition of SO_4^{2-} and H^+ measured at Pasadena, West Los Angeles, and Riverside on February 13, 1987.

acidity in the rain there, leaving rain with pH > 6 and almost no H^+ deposition.

Deposition of Na^+ and Cl^- were, as expected, highest at West Los Angeles (see Figure 7.17). An increase in the deposition rate of each of these species occurred at this site shortly after 1400, despite a decrease in rainfall intensity, and seems more closely correlated with a change in the wind direction at the site from southerly to southwesterly at about the same time (SCAQMD, 1987). This shift in wind direction shortened the transport path from the ocean to the sampling site; therefore, it is not surprising to see levels of Na^+ and Cl^- increase in the rain samples.

Figures 7.18, 7.19, and 7.20 depict the washout of the major ionic species from the atmosphere above Pasadena, Henninger Flats, and West Los Angeles, respectively. Also plotted here are the rainfall intensities as a function of time for each site. Lines drawn between data points indicate periods of fairly continuous rain. Concentrations of all measured species dropped rapidly in the first part of the storm, although somewhat less rapidly at West Los Angeles than at the other two sites. The concentrations of H^+, NO_3^-, SO_4^{2-}, and NH_4^+ are remarkably similar during all phases of the storm at Pasadena. A decrease in the Pasadena rainfall rate after 1600 coincided with an increase in the rainwater concentrations of these four species and Ca^{2+}. Little change was observed in the concentrations of Na^+, Cl^-, or Mg^{2+} at Pasadena during the same period. At West Los Angeles, a drop in the rainfall intensity at approximately 1400 coincided with an increase of all species concentrations except Ca^{2+}. Most of these species concentrations climbed to 50% or more of their initial rain sample levels during this period. A similar drop in rainfall intensity at Henninger Flats in the late stages of the event was accompanied by only slight increases in rainwater concentrations of the major species.

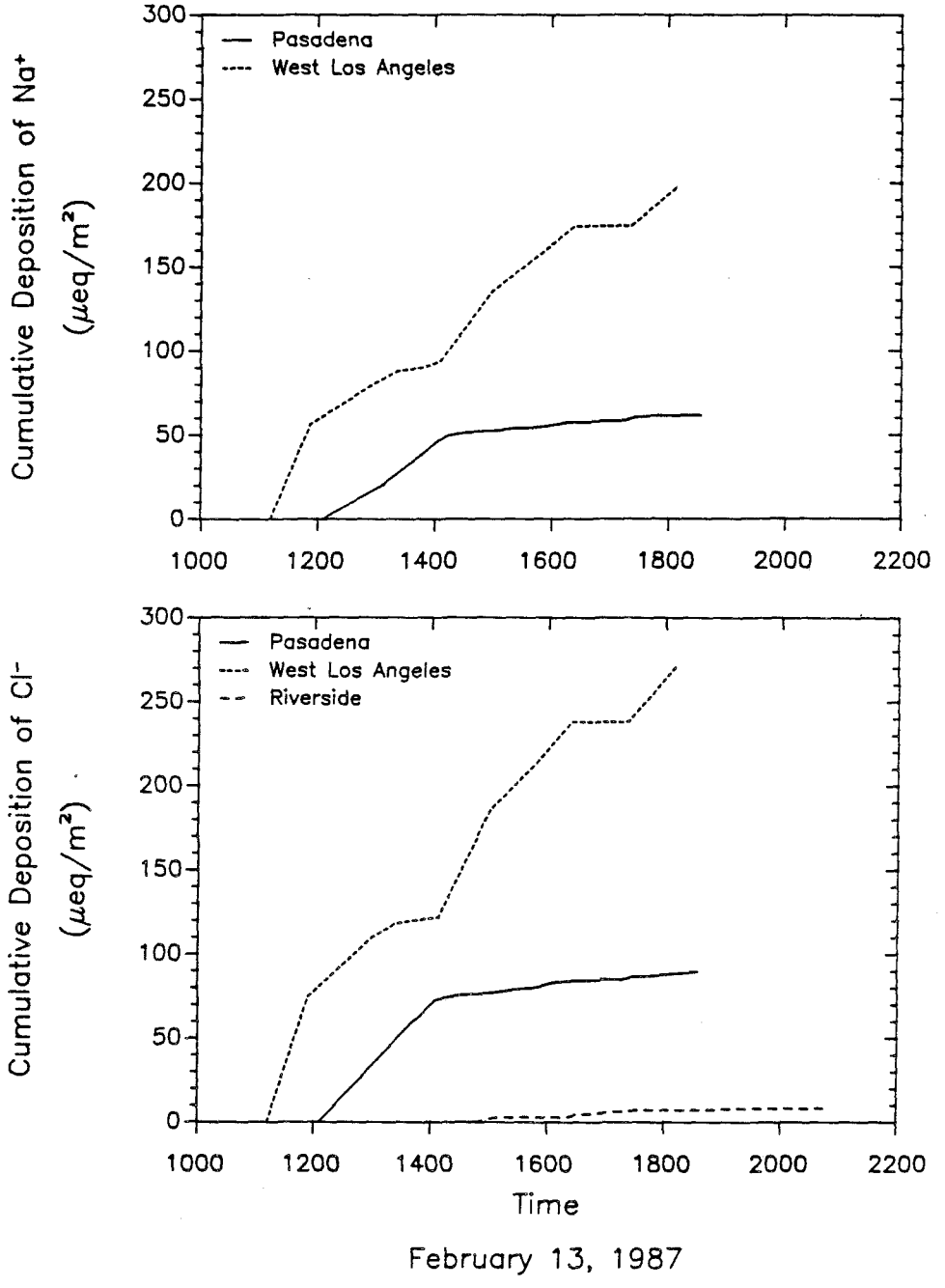

Figure 7.17. Cumulative deposition of Na^+ and Cl^- measured at Pasadena, West Los Angeles, and Riverside on February 13, 1987.

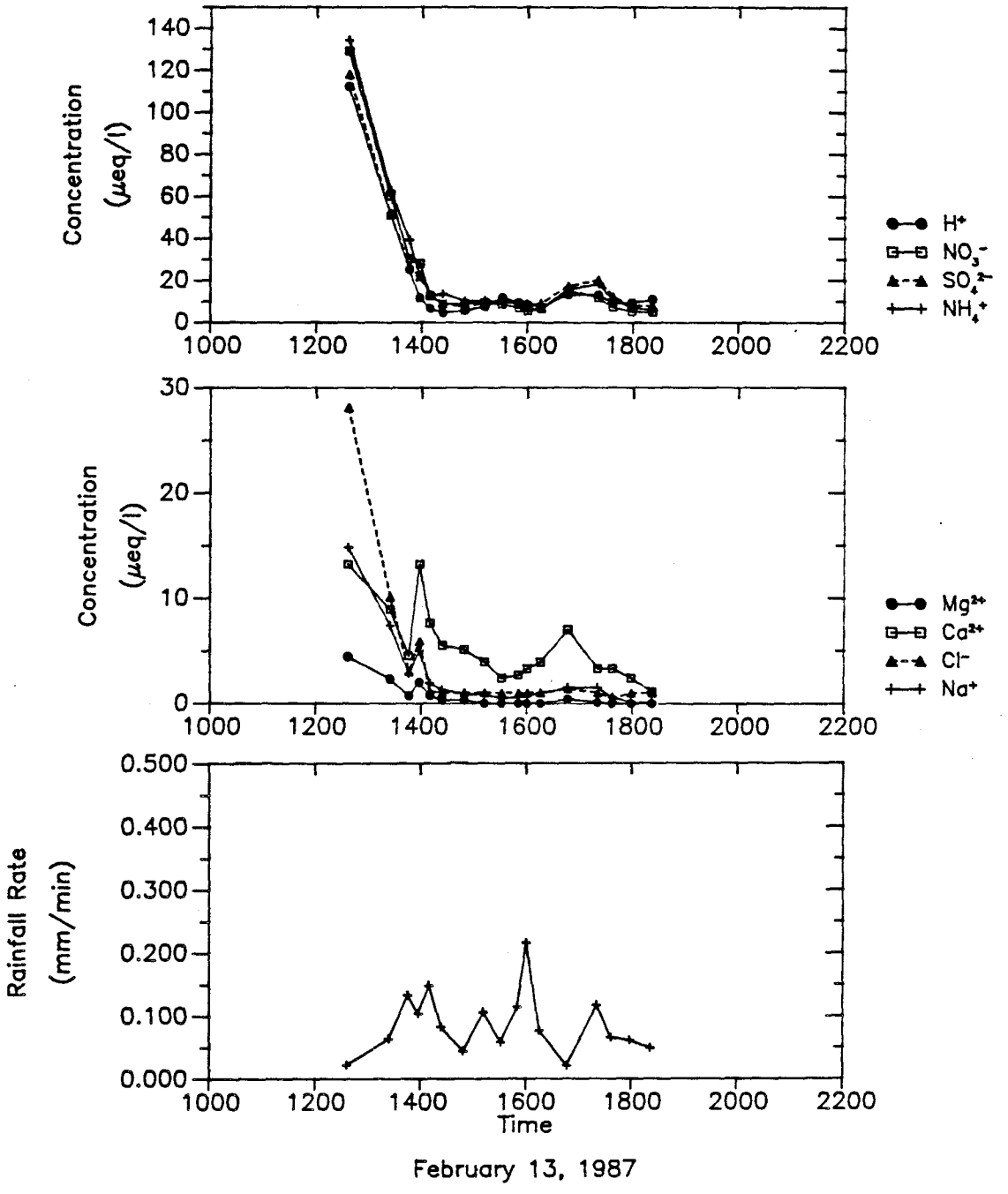

Figure 7.18. Concentrations of major species measured in rain samples collected at Pasadena as a function of time. Samples were collected on February 13, 1987. Also shown is a plot of the rainfall rate as a function of time (averaged over the collection period of each sample) for the same storm. No significant breaks in the continuity of the rainfall were observed during this period.

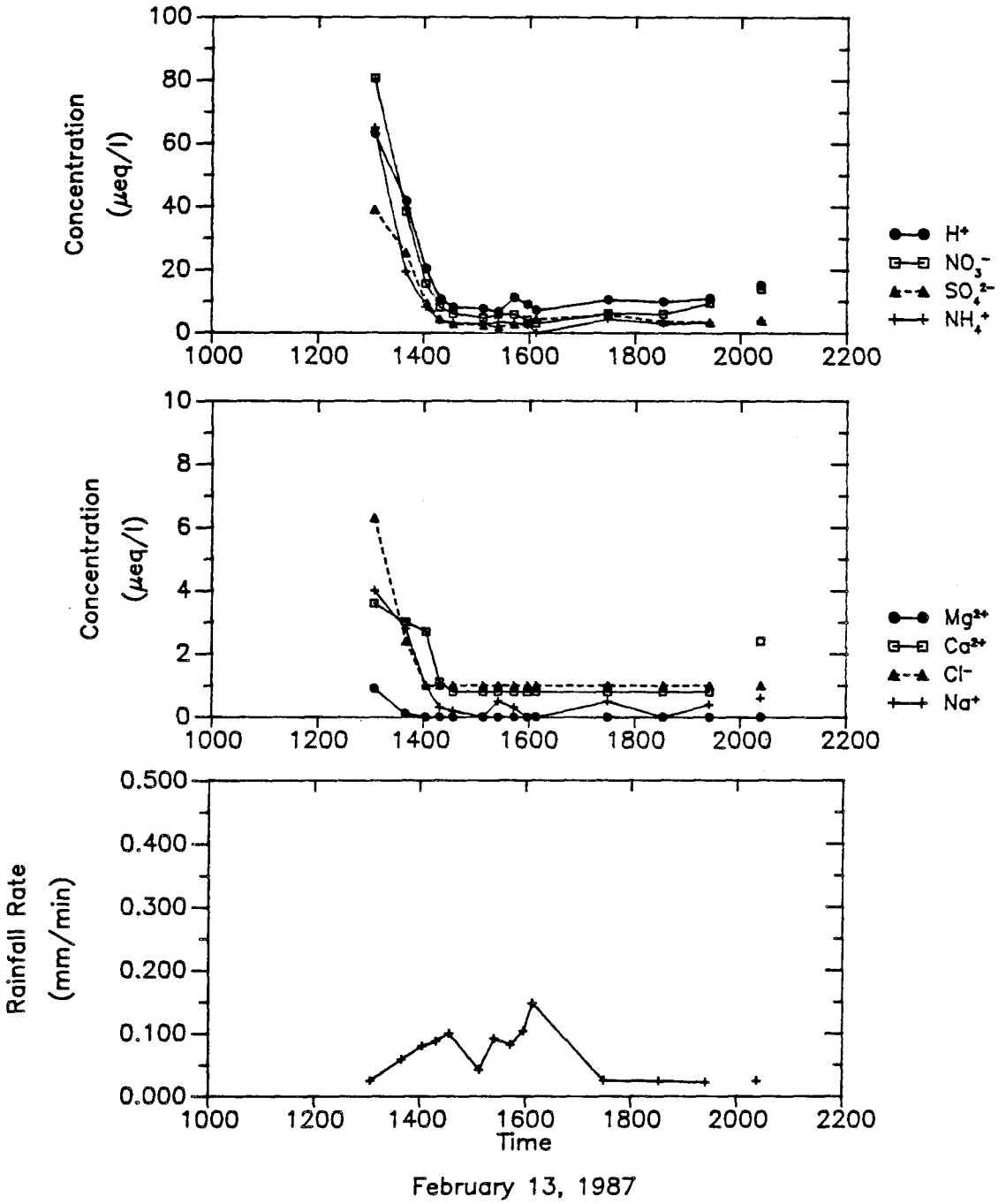

Figure 7.19. Concentrations of major species measured in rain samples collected at Henninger Flats as a function of time. Samples were collected on February 13, 1987. Also shown is a plot of the rainfall rate as a function of time (averaged over the collection period of each sample) for the same storm. Breaks in a line indicate breaks in the rain.

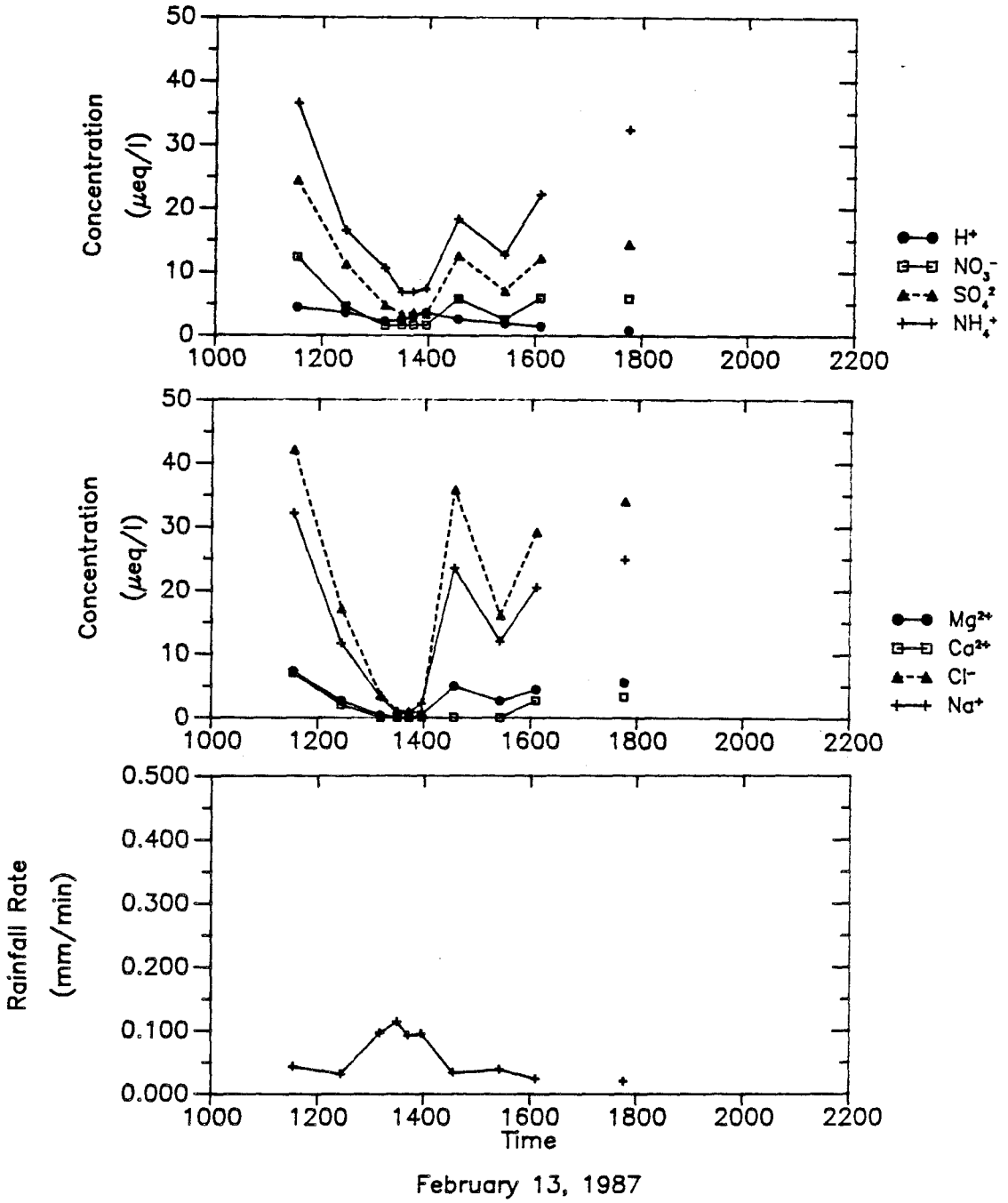

Figure 7.20. Concentrations of major species measured in rain samples collected at Mt. Wilson. Samples were collected on February 13, 1987. Also shown is a plot of the rainfall rate as a function of time (averaged over the collection period of each sample) for the same storm. Breaks in a line indicate breaks in the rain.

The Storm of March 5 and 6, 1987

Upon forecast that a rainstorm was headed for the Los Angeles area, an intensive aerosol and gas phase monitoring program was begun on March 4 to characterize pre–storm conditions throughout the SoCAB. The monitoring was continued during and after the storm as well. Plots of the observed concentrations of aerosol NH_4^+, NO_3^-, and SO_4^{2-}, and of $NH_{3(g)}$ and $HNO_{3(g)}$ as a function of time at the five sites are presented in Figures 7.21 through 7.25 (note the different scales used for the different sites). Also shown in each figure is a plot of the cumulative rainfall deposition at the site as a function of time. Most of the rain event was not sampled at Pasadena due to an unusually long period of intermittent showers which used up the twenty bottles in the carousel before most of the rainfall occurred. Data on rainfall deposition for Pasadena was taken from the Los Angeles County Flood Control District (LACFCD) recording rain gauge also located on the Caltech campus. During other events the rainfall observed by this gauge and the study rain sampler were closely correlated.

Concentrations of all measured species were observed to drop at all of the sites except West Los Angeles following the onset of the rain. At West Los Angeles, the aerosol SO_4^{2-} concentration dropped immediately, as did the concentration of $HNO_{3(g)}$. Concentrations of $NH_{3(g)}$ and aerosol NO_3^- and NH_4^+, however, were observed to increase at West Los Angeles during the early part of the storm. These increases are most likely due to a change in wind direction that coincided roughly with the time the rain began. During the morning the wind primarily had been blowing lightly from the west. After noon, however, the wind shifted to the east and began to blow more strongly (SCAQMD, 1987). Since the production of NO_3^-

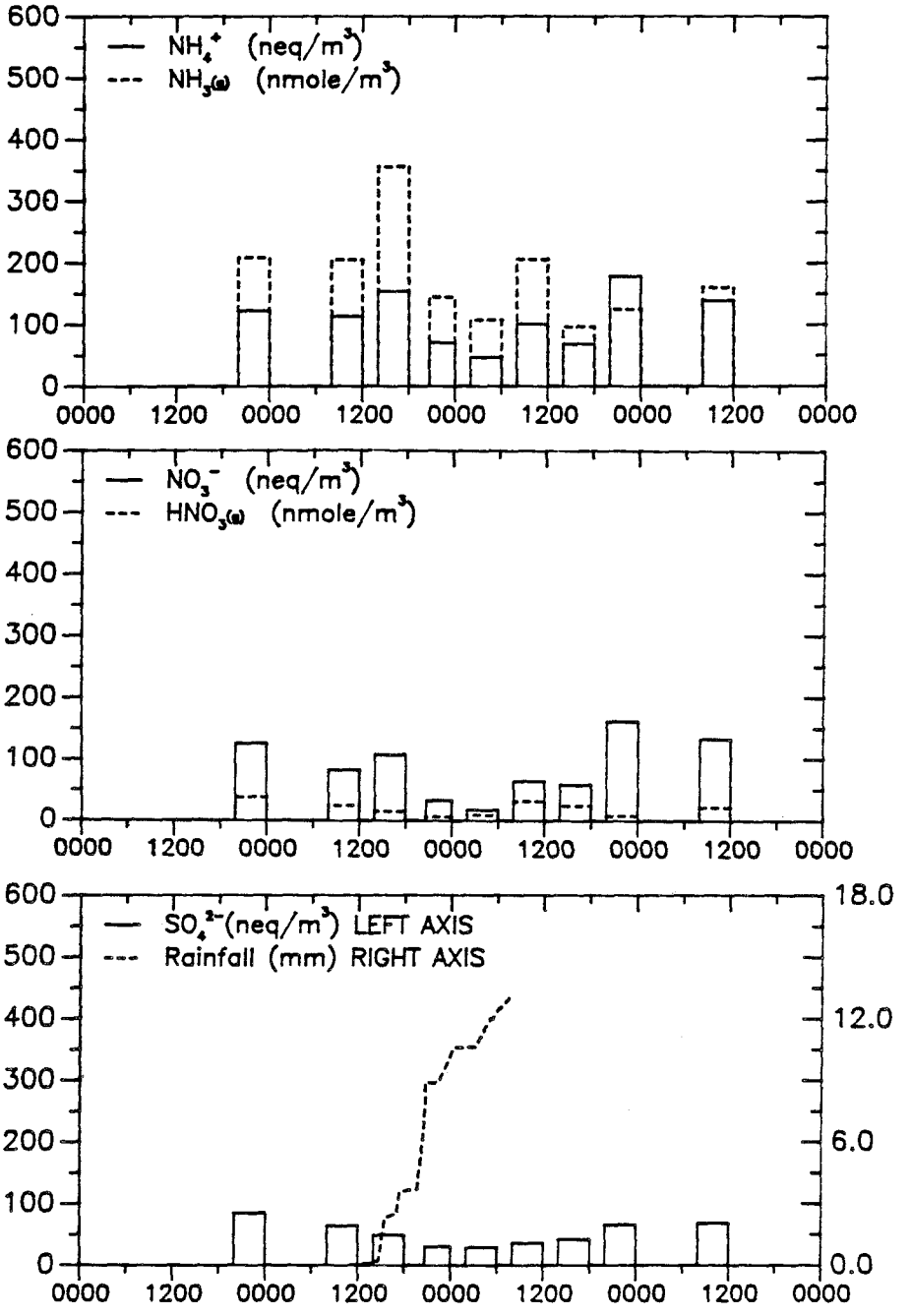

Figure 7.21. Concentrations of selected aerosol and gas phase species measured at West Los Angeles from March 4 through March 7, 1987. Also shown is the cumulative rainfall measured at the same site during this period.

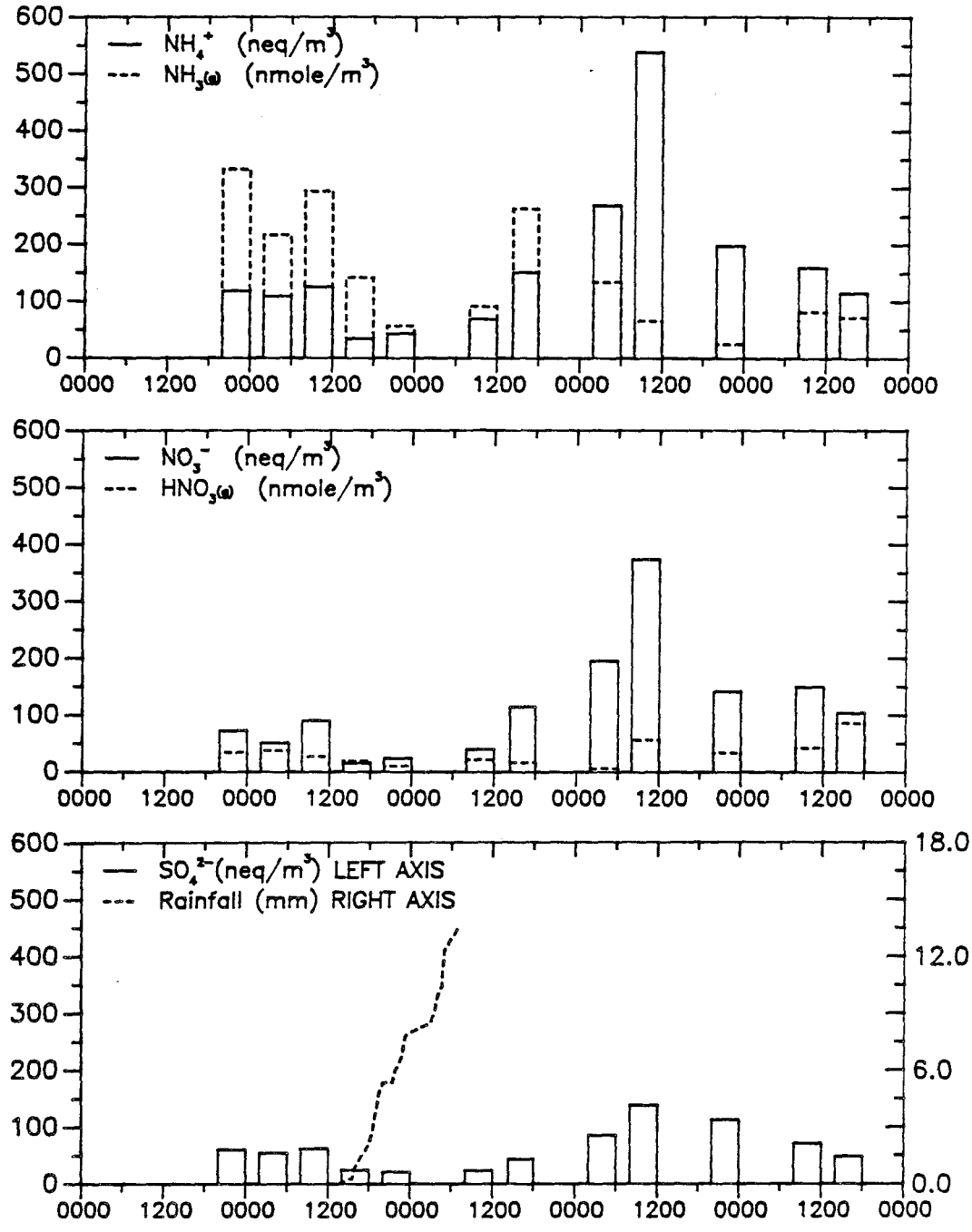

Figure 7.22. Concentrations of selected aerosol and gas phase species measured at Pasadena from March 4 through March 8, 1987. Also shown is the cumulative rainfall measured at the same site during this period.

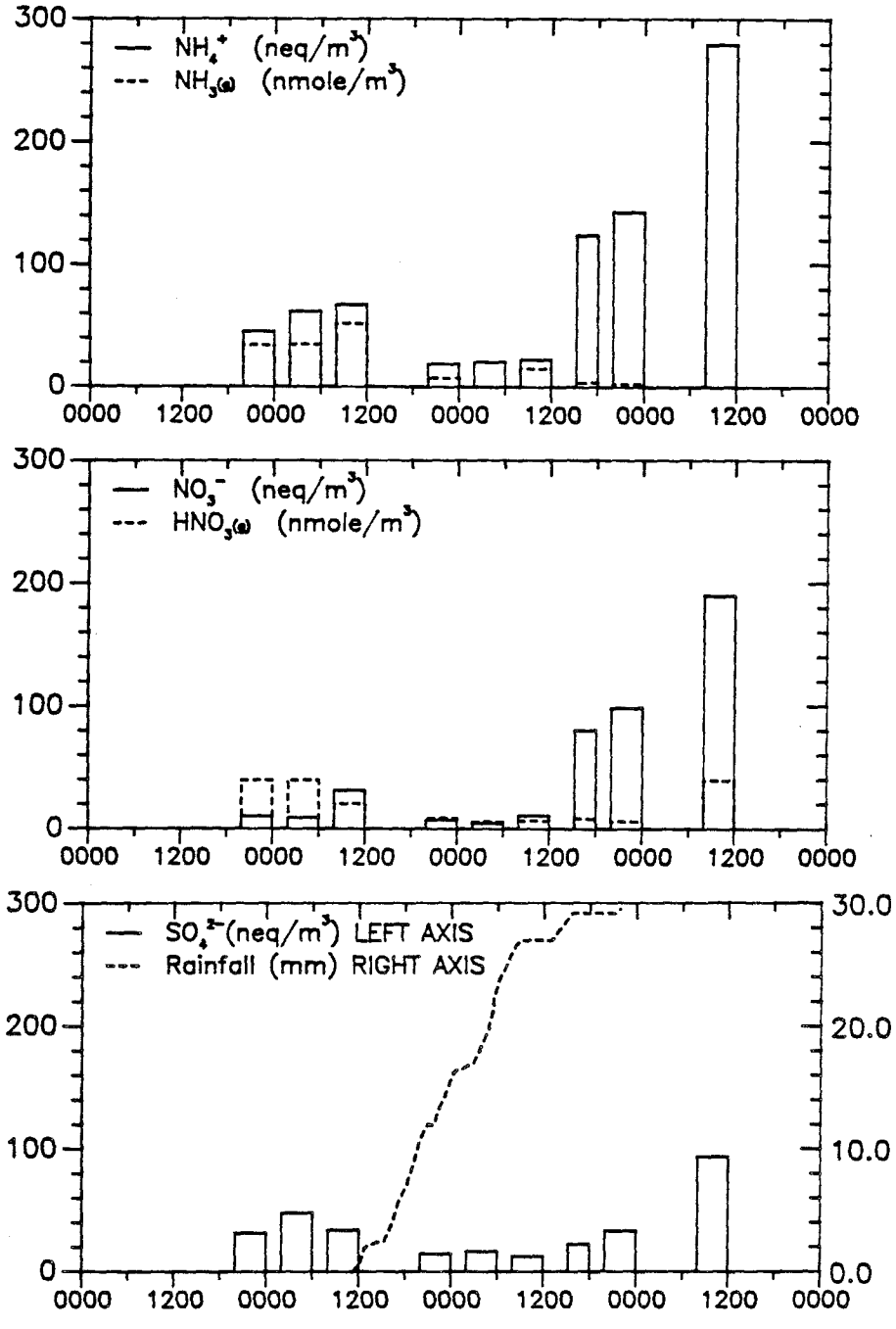

Figure 7.23. Concentrations of selected aerosol and gas phase species measured at Henninger Flats from March 4 through March 7, 1987. Also shown is the cumulative rainfall measured at the same site during this period.

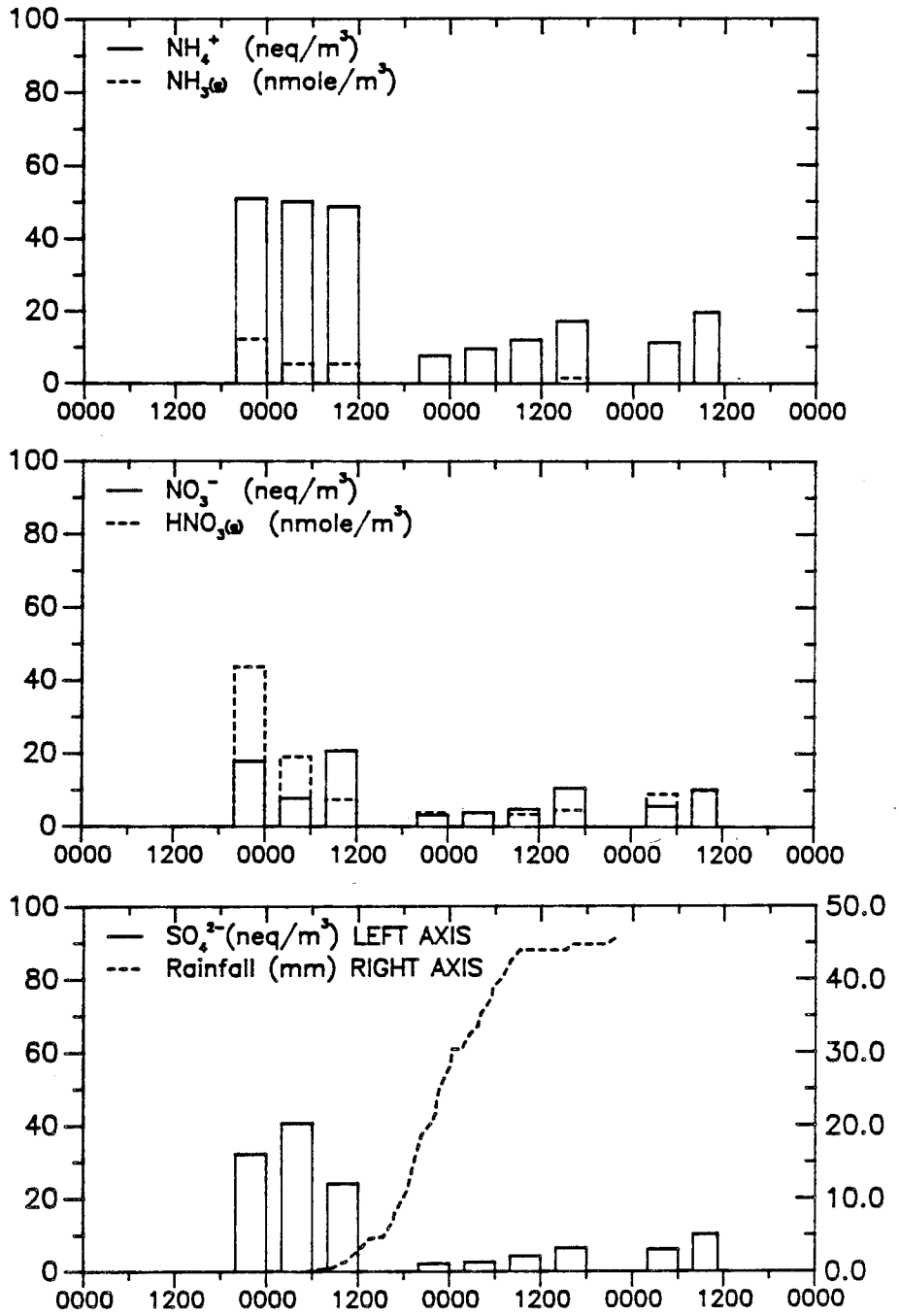

Figure 7.24. Concentrations of selected aerosol and gas phase species measured at Mt. Wilson from March 4 through March 7, 1987. Also shown is the cumulative rainfall measured at the same site during this period.

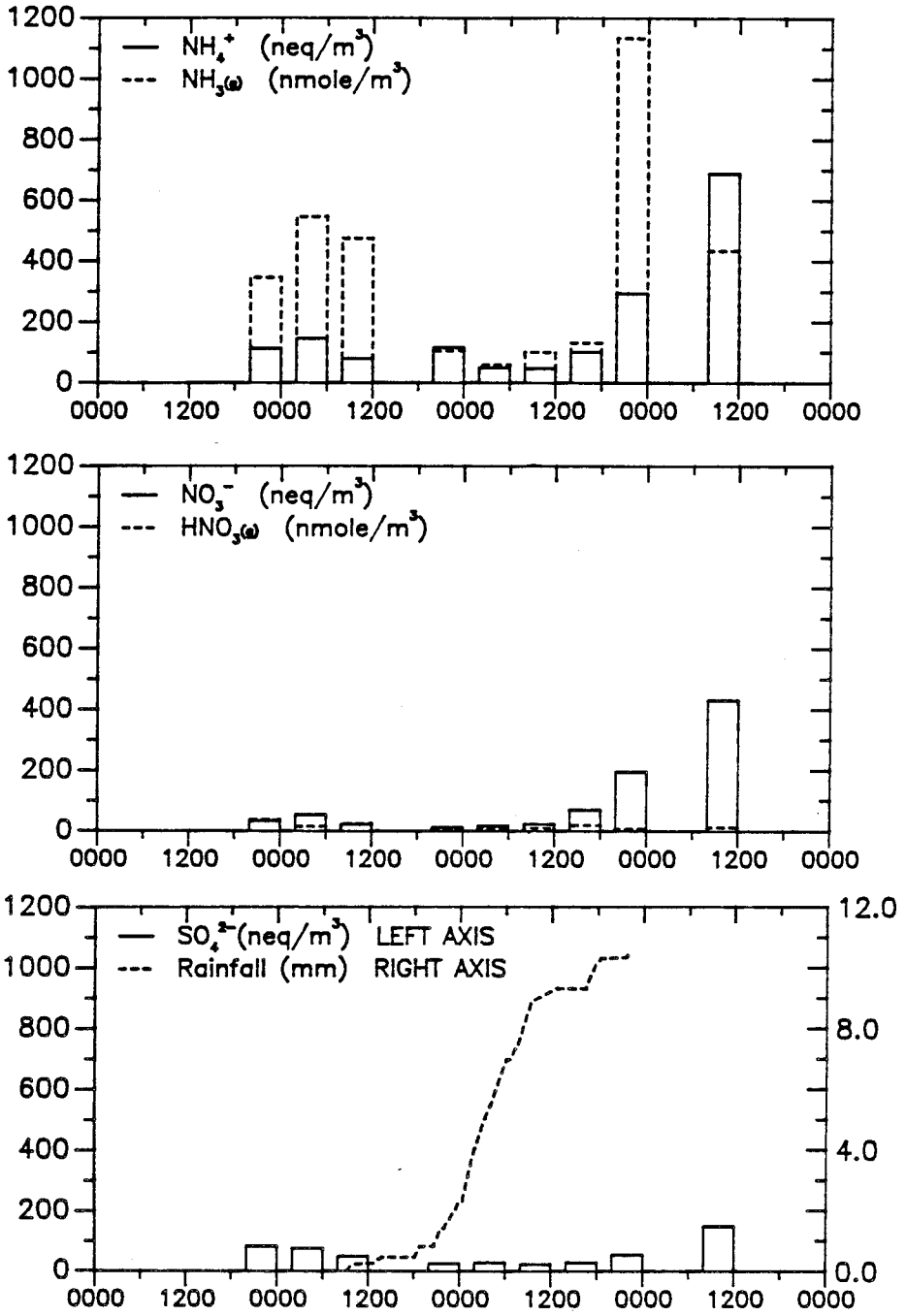

Figure 7.25. Concentrations of selected aerosol and gas phase species measured at Riverside from March 4 through March 7, 1987. Also shown is the cumulative rainfall measured at the same site during this period.

and NH_4^+ occurs predominantly in the central and eastern portions of the SoCAB, the rise in concentrations of these species in the air mass at West Los Angeles is consistent with the change in wind direction.

With the rain essentially over by mid–morning on March 6, concentrations of aerosol NO_3^-, SO_4^{2-}, and NH_4^+ began to increase at Pasadena, Henninger Flats, and Riverside. By early morning on March 7, NO_3^- and NH_4^+ concentrations had achieved their pre–storm levels at all three sites. Concentrations of aerosol SO_4^{2-} also achieved pre–storm levels by this time at Pasadena and Henninger Flats, but required a few extra hours at Riverside. Concentrations continued to rise through noon of March 7 when monitoring was discontinued at all of the sites except Pasadena, where concentrations were observed to drop off substantially on March 8. Aerosol concentrations were seen to rise following the end of the rain event at West Los Angeles as well, however, during the period sampled, they never significantly exceeded their pre–storm levels. SO_4^{2-} did not quite even reach that level. Concentrations at Mt. Wilson were observed to increase slightly following the storm, but never came close to reaching their pre–storm levels by noon of March 7.

Rainfall deposition amounts during the storm were highest at Mt. Wilson, followed by Henninger Flats, West Los Angeles, and Riverside, in that order (see Figure 7.26). Data from the LACFCD rain gauge in Pasadena place that site closely behind West Los Angeles in rainfall for this storm. Compared to the storm of February 13, rainfall was much higher at Mt. Wilson and Riverside, slightly higher at Henninger Flats, slightly lower at West Los Angeles, and substantially lower at Pasadena during this event.

The deposition patterns of the major ionic species in the rainwater are shown

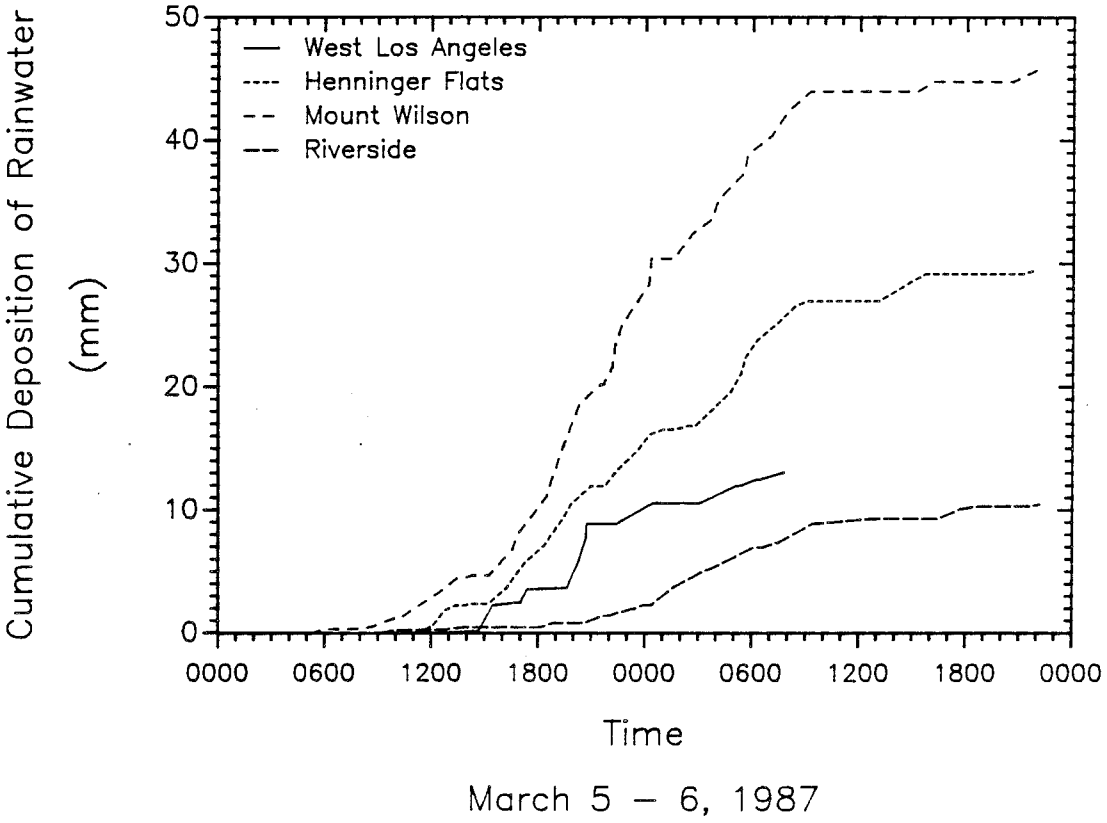

Figure 7.26. Cumulative rainfall measured at West Los Angeles, Henninger Flats, Mt. Wilson, and Riverside on March 5 and 6, 1987.

for West Los Angeles, Henninger Flats, Mt. Wilson, and Riverside in Figures 7.27 through 7.30. Despite somewhat lower concentrations of nitrate and sulfate in the Mt. Wilson samples than in those from other sites, deposition of these species was highest at Mt. Wilson through the bulk of the storm, due to higher rainfall amounts there (see Figures 7.27 and 7.28). A late spurt of rain at Henninger Flats brought the total nitrate deposition there slightly above that at Mt. Wilson around noon on March 6. H^+ concentrations, which were nearly equal at all four sites, led to deposition patterns that closely resembled those for rainfall (Figure 7.28). NH_4^+ concentrations were substantially lower at Mt. Wilson than at the other sites; consequently, deposition of NH_4^+ at Mt. Wilson was exceeded by the levels observed at two other sites. The highest NH_4^+ deposition was observed at Henninger Flats, followed by West Los Angeles (see Figure 7.27). Deposition of Na^+ and Cl^-, not surprisingly, was highest at West Los Angeles (Figure 7.29). Like the event of February 13, the ratio of Cl^- to Na^+ deposition at Henninger Flats and Mt. Wilson was observed to significantly exceed the sea salt ratio, suggesting that $HCl_{(g)}$ had been incorporated into the rain droplets. Deposition of Ca^{2+} and Mg^{2+} was comparable at all four sites (see Figure 7.30).

By comparing the measured wet deposition of the different species to their pre–storm concentrations in the aerosol and gas phases, we can determine whether wet deposition during the storm was more or less than the atmospheric burden over the basin prior to the storm's onset. The concentrations of the nine species measured in the gas and aerosol phases prior to the storm at Pasadena, Henninger Flats, and Mt. Wilson are depicted in Figure 7.31. The data chosen for this plot are those collected from 0200–0600 on March 5. The data for the period 0800–1200 are similar. The former period was chosen because some precipitation fell at Mt. Wilson and Henninger Flats during the latter period. The general trend observed

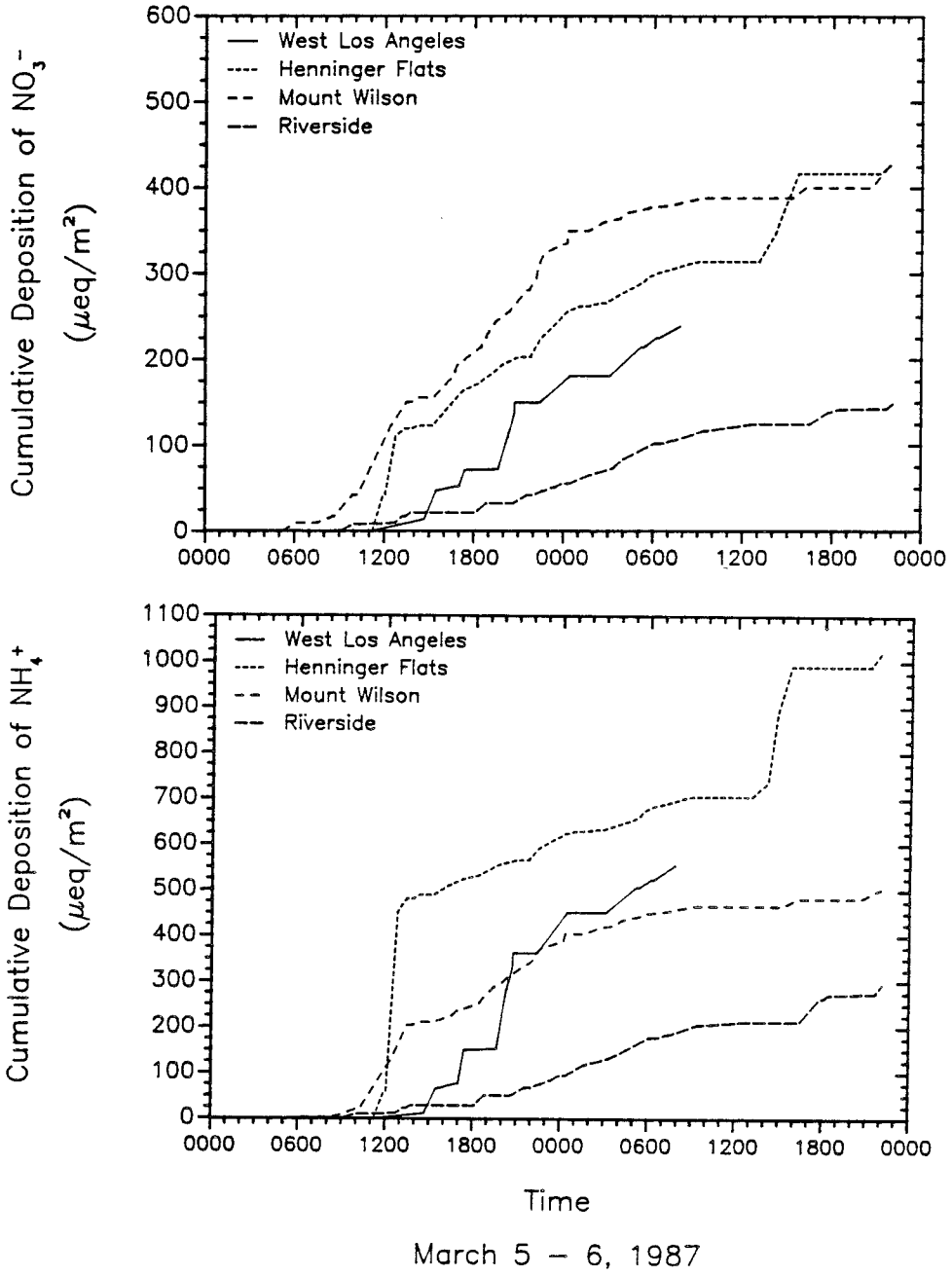

Figure 7.27. Cumulative deposition of NO_3^- and NH_4^+ measured at West Los Angeles, Henninger Flats, Mt. Wilson, and Riverside on March 5 and 6, 1987.

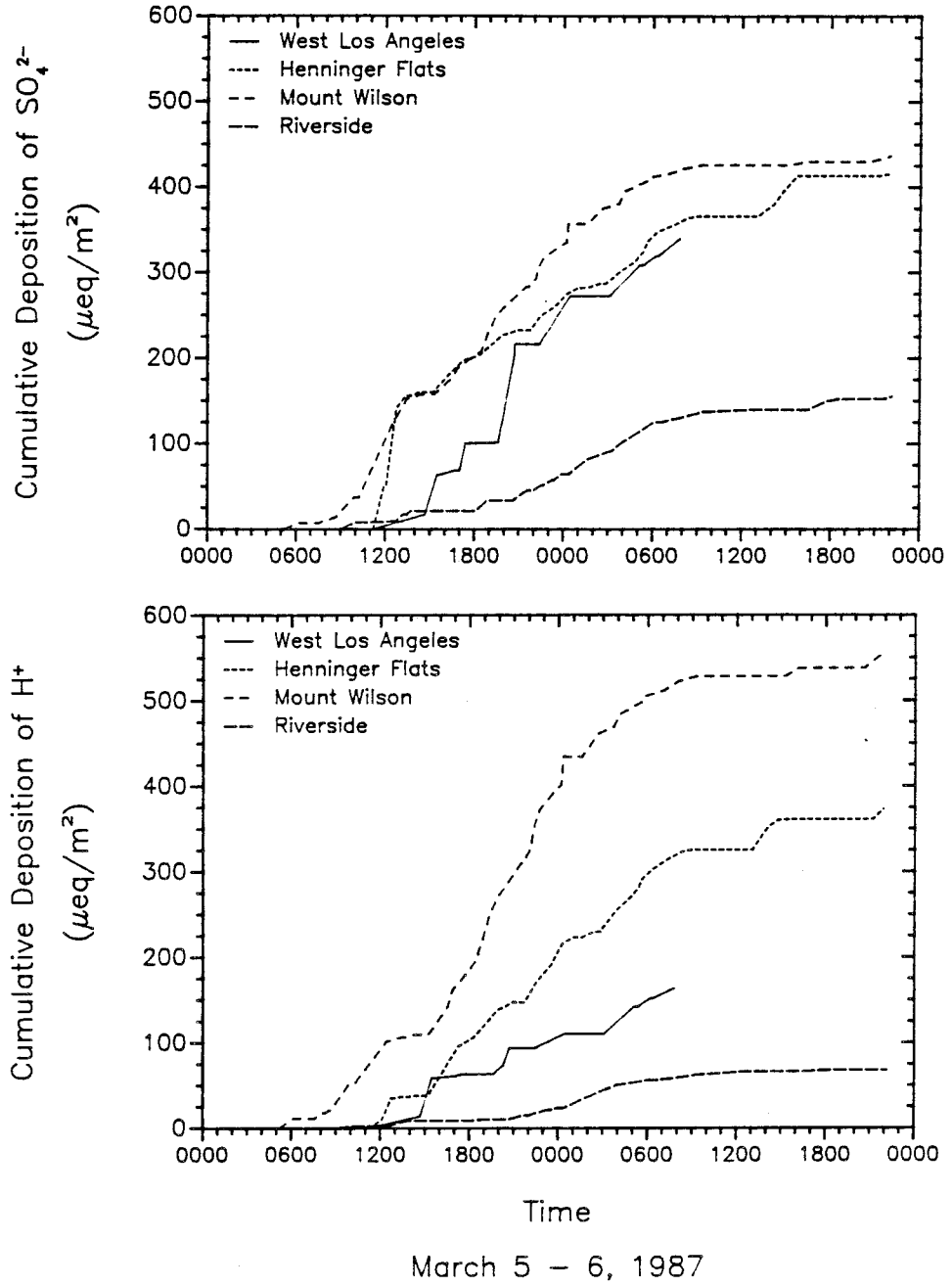

Figure 7.28. Cumulative deposition of SO_4^{2-} and H^+ measured at West Los Angeles, Henninger Flats, Mt. Wilson, and Riverside on March 5 and 6, 1987.

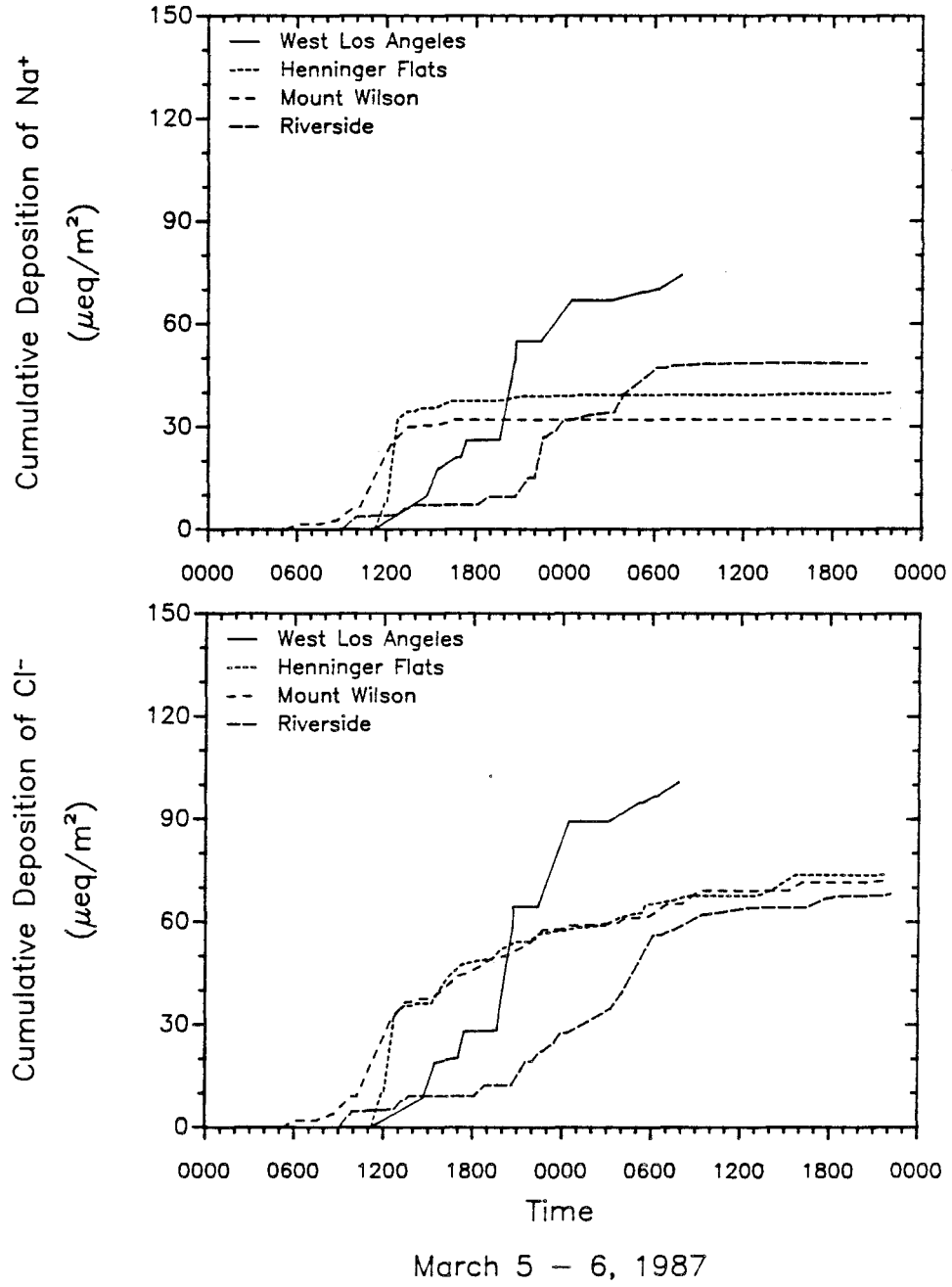

Figure 7.29. Cumulative deposition of Na^+ and Cl^- measured at West Los Angeles, Henninger Flats, Mt. Wilson, and Riverside on March 5 and 6, 1987.

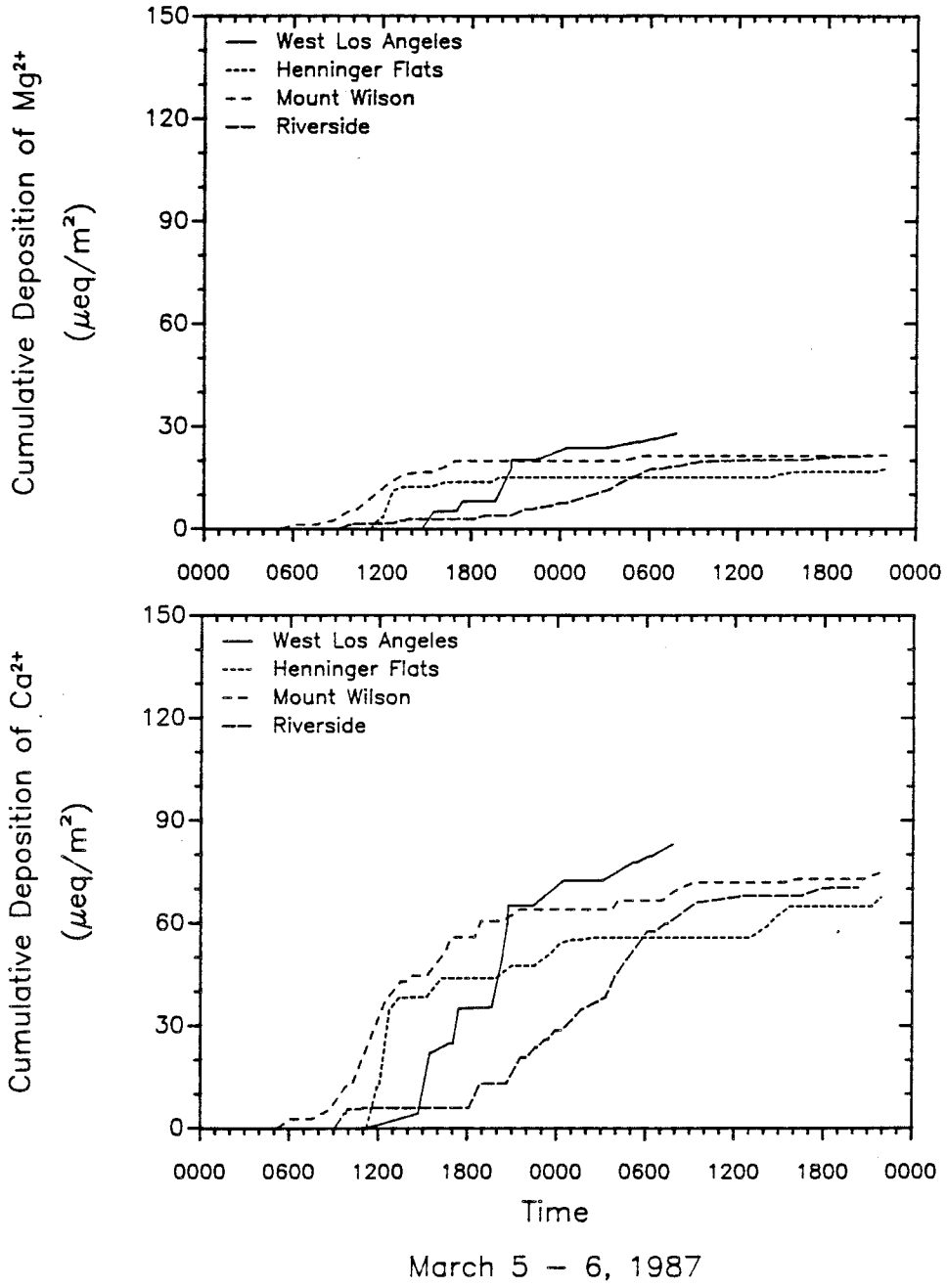

Figure 7.30. Cumulative deposition of Mg^{2+} and Ca^{2+} measured at West Los Angeles, Henninger Flats, Mt. Wilson, and Riverside on March 5 and 6, 1987.

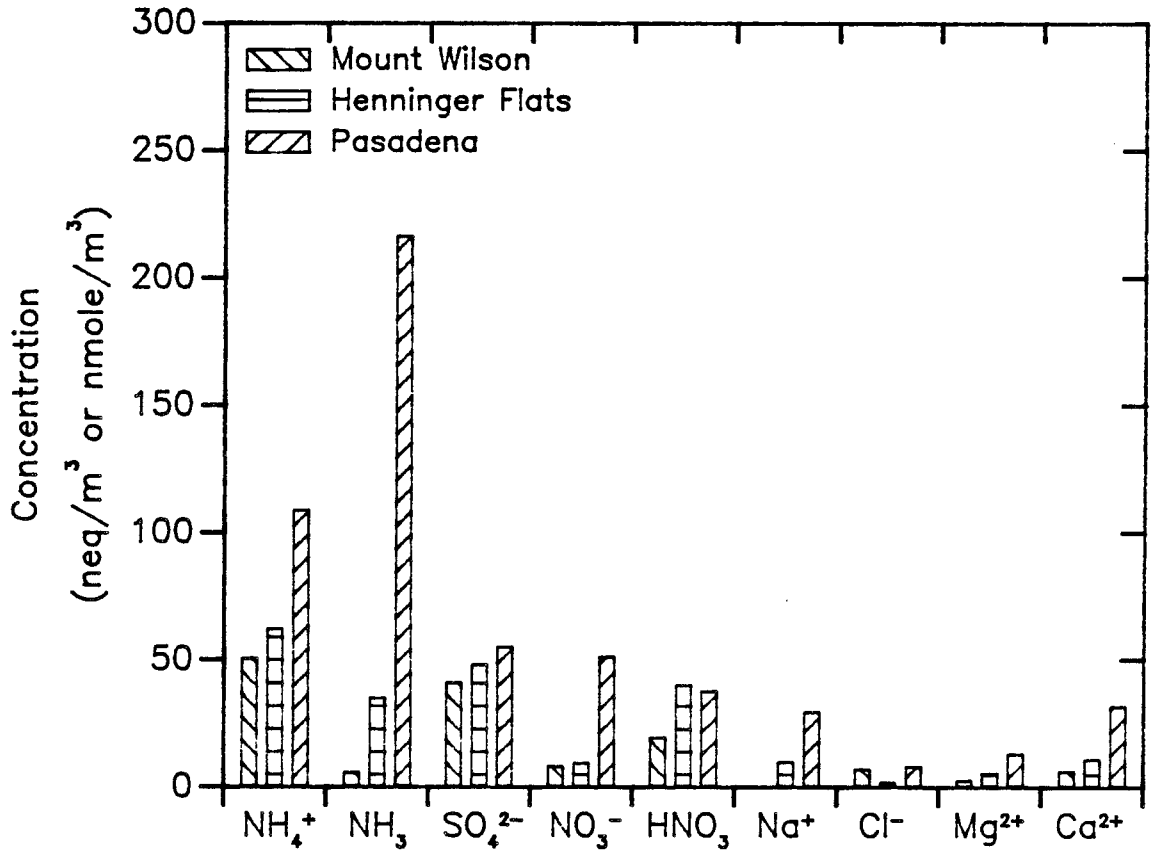

Figure 7.31. Concentrations of selected aerosol and gas phase species measured at Pasadena, Henninger Flats, and Mt. Wilson on the morning of March 5, 1987. Samples were collected from 0200 to 0600 PST.

for most species is that concentrations are highest at Pasadena (elev. 200 m) and lowest at Mt. Wilson (elev. 1700 m), with concentrations at Henninger Flats (elev. 700 m) falling in between. Using the observed concentrations at these three elevations, we can estimate the atmospheric burden of the measured species over the Pasadena area.

Since no information is available on the gradient of each species between sites we choose to assume that the concentration in each portion of the air column is equivalent to that measured at the closest site with a lower elevation. For example, between 200 and 700 m we assume the concentration of available N(V), which represents $NO_3^- + HNO_{3(g)}$, is equal to that measured at Pasadena: approximately 88 neq m^{-3}. Between 700 and 1700 m the N(V) concentration measured at Henninger Flats (49 neq m^{-3}) is used. From 1700 m, the elevation of the Mt. Wilson site, up to the top boundary of the air column of interest, the N(V) concentration is assumed to be equivalent to that measured at Mt. Wilson: approximately 27 neq m^{-3}. Since the concentrations really drop more gradually with elevation, this procedure should tend to overestimate the atmospheric burden somewhat.

At 0800 on the morning of March 5, the cloud base was observed to lie at approximately 3000 m elevation. Assuming the cloud extends 1000 m upward from its base, we can estimate the upper boundary of the air column accessible to processing by the cloud droplets and rain droplets to be approximately 4000 m. Given the preceding observations and assumptions, the atmospheric burdens of N(V), S(VI), and N(–III) over the Pasadena area can be calculated to be 160, 170, and 390 μeq m^{-2}, respectively. Estimates of the burdens of N(V) and N(–III) include not only contributions from aerosol NO_3^- and NH_4^+, but also from $HNO_{3(g)}$

and $NH_{3(g)}$. Similar estimates for Na^+, Ca^{2+}, and Mg^{2+} yield burdens of 24, 40, and 21 μeq m^{-2}, respectively, in the air column above Pasadena.

The important processes that govern concentration changes of a species, i, in the air column are advection, diffusion, emission, deposition, and chemical reaction. These may be represented for each phase, φ (i.e. aqueous, gas, or aerosol), by equation 7.1:

(Eq'n. 7.1)
$$\frac{dC_i^{\varphi}}{dt} - u\cdot\nabla C_i^{\varphi} = \nabla\cdot K\cdot\nabla C_i^{\varphi} + \frac{E_i^{\varphi}}{H} - \frac{C_i^{\varphi} V_{d,i}^{\varphi}}{H} + R_i^{\varphi} + T_i^{\varphi}$$

where C_i^{φ} is the concentration of species i in phase φ (C_i^{φ} is a function of time and the spatial coordinates x, y, and z), u is the three-dimensional wind vector, K is the diffusion coefficient tensor, E_i^{φ} is the emission flux of species i in phase φ, H is the height of the air column, $V_{d,i}^{\varphi}$ is the deposition velocity of species i in phase φ, R_i^{φ} is the net reaction rate of species i in phase φ, and T_i^{φ} is the net rate of transformation of species i into phase φ. All the phases that a species can exist in must be considered together, implying that three coupled partial differential equations of the form of equation 7.1, for each species i, must be solved simultaneously.

During a rainstorm, the diffusion term will be relatively unimportant for soluble species; dry deposition of soluble species will also be relatively unimportant. The remaining important terms to balance are those representing emission, wet deposition, chemical reaction, advection, and phase transformation. This implies that if (1) all available i is removed from the air column in precipitation during the rainstorm (by some combination of in-cloud and below-cloud scavenging), (2) no

chemical production or destruction of i occurs in the air column, (3) no emission of i into the air column occurs, and (4) there is no net advection of i into or out of the air column during the storm, then the wet deposition of i in the rain at the base of the air column should be equal to the calculated atmospheric burden of i prior to the onset of the storm. Looking at the data from Henninger Flats and Mt. Wilson (since no deposition data is available for this storm at the base of the column in Pasadena) we can compare the observed deposition to the calculated burdens for each species of interest. Neglecting the last portion of rain that occurred around noon on March 6, deposition amounts of N(V) at Henninger Flats and Mt. Wilson were 310 and 380 μeq m^{-2}, respectively. For N(–III) the amounts were 700 and 450 μeq m^{-2}; for S(VI) they were 360 and 425 μeq m^{-2}; and for Na^+ they were 40 and 30 μeq m^{-2}.

The cumulative quantities of Mg^{2+} deposited at Henninger Flats and Mt. Wilson during the storm were 15 and 22 μeq m^{-2}, respectively. These quantities are in good agreement with the calculated pre–storm atmospheric burden of Mg^{2+}: 21 μeq m^{-2}. The cumulative deposition of Ca^{2+} observed at Henninger Flats was 55 μeq m^{-2}, while 70 μeq m^{-2} were measured at Mt. Wilson. These values are somewhat higher than the calculated Ca^{2+} burden of 41 μeq m^{-2}, possibly indicating that some dust was introduced into the air in the vicinity of the sampler during the storm. Cumulative Na^+ deposition was also somewhat higher than its calculated pre–storm atmospheric burden, suggesting that some Na^+ continued to be transported inland from over the ocean during the storm.

N(–III) deposition at Mt. Wilson was approximately equal to the calculated pre–storm atmospheric burden of N(–III), however, deposition of N(–III) at Henninger Flats showed an 80% excess over the pre–storm burden. The most

dramatic differences between the amount of wet deposition and the pre–storm atmospheric burden, however, were observed for N(V) and S(VI). Cumulative deposition of both of these species at Mt. Wilson equaled approximately 2.5 times their pre–storm atmospheric burdens. Surface level winds at Pasadena generally blew from the east during the afternoon of March 5. Since the rain did not begin in earnest until somewhat later in the eastern portions of the SoCAB, as evidenced by the rain record from Riverside, it is possible that some contributions to the deposition were made by transport of species from the east which were incorporated into the clouds or rainwater over Pasadena, Henninger Flats, and Mt. Wilson and rained out on these sites. This is a plausible explanation for the excess N(–III) deposition, since most of the basin's NH_3 emissions occur to the east of Pasadena; however, it is unlikely that this explains all of the excess S(VI) and N(V) deposition, since the excesses for these species were much larger than the N(–III) excess. In addition N(–III) was observed at much higher concentrations in the eastern part of the SoCAB than were either S(VI) or N(V), during the entire period monitored. Upper level winds may, in fact, have been coming from some other direction where the relative concentrations of atmospheric S(VI) and N(V) were higher. Even in the western part of the basin, however, atmospheric loadings of N(–III) during this storm exceeded those of S(VI) and N(V) by several hundred percent.

Since both SO_4^{2-} and NO_3^- are secondary pollutants, no direct emissions from ground level sources could contribute to their presence in the atmosphere. Emissions of their primary pollutant precursors, $NO_{x(g)}$ and $SO_{2(g)}$, followed by oxidation in the atmosphere during the storm, may have played some role. While the heavy cloud cover over the basin should have reduced the gas phase production of S(VI) and N(V), we should not discard these pathways entirely as possible

contributors to production of these species during the rain event; however, aqueous phase production mechanisms, either in the cloud droplets, or in the falling rain drops, are probably more likely contributors, at least for S(VI). We can estimate whether in–cloud oxidation is important by looking at the fluxes of these species into the bottom of the cloud vs. the return fluxes in the rain drops as they emerge from the base of the cloud.

Over the period from 1500 on March 5 to 0200 on March 6, the rainfall rate and the deposition rates of SO_4^{2-}, NO_3^-, and NH_4^+ were observed to be fairly constant at both Henninger Flats and Mt. Wilson. Data from the period 2000 to 0600 indicate that the concentrations of aerosol NO_3^-, SO_4^{2-}, and NH_4^+, and of $NH_{3(g)}$ and $HNO_{3(g)}$ were constant at Mount Wilson. An observation at 1700 on March 5 placed the cloud base at the same elevation as the Mount Wilson site. Using the data for rainfall deposition at Mt. Wilson, along with the rate of transport into the base of the cloud and the observed Mt. Wilson gas and aerosol concentrations, we can investigate whether any production of SO_4^{2-} or NO_3^- took place in the cloud. Since no data on the vertical air velocity through the cloud is available, we will have to estimate it. Using N(–III) as a conservative tracer, we can determine what flux of aerosol and gas phase N(–III) into the base of the cloud is necessary to account for the return flux of N(–III) out of the base of the cloud in the rain. The vertical velocity will be given by the quotient of the flux into the cloud and the total N(–III) concentration in the gas and aerosol. Performing this calculation yields an average velocity of 0.7 m s^{-1}. This value, which is reasonable for a convective cloud, is calculated assuming 100% scavenging of the N(–III) by the cloud. Using this updraft velocity for transport of the measured concentrations of aerosol and gas phase S(VI) and N(V) into the cloud base indicates that 92% of the N(V) flux out of the cloud in the rain is accounted for, but slightly less than 40% of the S(VI) rain

flux is accounted for.

The apparent net flux of S(VI) out of the base of the cloud suggests that there is probably substantial production of S(VI) taking place in the cloud. With assumptions about cloud depth and liquid water content, we can estimate the S(VI) production rate needed to account for this efflux. During the eleven-hour period from 1500 to 0200, 200 μeq m^{-2} of S(VI) were deposited in the rainfall at Mt. Wilson. With the calculated updraft of 0.7 m s^{-1}, only 39%, or approximately 80 μeq m^{-2}, of this flux could be accounted for by in-cloud scavenging of aerosol SO_4^{2-}. This leaves approximately 120 μeq m^{-2} to account for. If we assume that the cloud was 1000 m deep with a liquid water content of 0.5 g m^{-3}, then a production rate of 3.0×10^{-9} **M** sec^{-1} of S(VI) is required. The pH of the rain falling at Mt. Wilson at this time was approximately 5. Typically cloudwater has been observed to have a pH approximately 0.5 units lower than the pH of simultaneously collected rainwater. For only moderate levels of $SO_{2(g)}$ and $O_{3(g)}$ (5 ppb and 50 ppb, respectively), the aqueous phase oxidation rate of S(IV) to S(VI) is on the order of 10^{-8} **M** sec^{-1} at pH 4.5 (Seinfeld, 1986), making the required S(VI) production rate calculated for the Mt. Wilson cloud seem quite reasonable. Aqueous phase oxidation of S(IV) by H_2O_2 may also have contributed to S(VI) production in this environment.

It should be noted that S(VI) production attributed to in-cloud processes may also be due partially to oxidation of S(IV) within the rain samples after collection. Since concentrations of SO_4^{2-} in precipitation at Mt. Wilson were comparable to, or slightly higher than, those at Henninger Flats (even though the rainfall intensity was higher at Mt. Wilson than at Henninger Flats), however, it seems clear that below-cloud scavenging of $SO_{2(g)}$, followed by oxidation to SO_4^{2-},

was not important during this period.

Summary

Automated sub–event sequential rain samplers were used to sample rain during the winter and spring of 1987 in the South Coast Air Basin. The five sites used in the study were located at West Los Angeles, Pasadena, Henninger Flats, Mount Wilson, and Riverside. These sites were specifically chosen to represent a "vertical" profile in the basin (Pasadena to Henninger Flats to Mt. Wilson) and an east–west profile (Riverside to Pasadena to West Los Angeles). Measurements of aerosol and gas phase species also were made at the five sites using filter pack methods and an automated sampler.

The highest rainwater concentrations of NO_3^- and SO_4^{2-} were observed at Pasadena; highest NH_4^+ levels were measured at Riverside; highest average levels of rainwater Na^+ and Cl^- were found at West Los Angeles. Rainwater pH levels varied from 4 to 6 at West Los Angeles and Henninger Flats, from 4 to 5.5 at Pasadena, from 4.3 to 5.7 at Mt. Wilson, and from 4.5 to 6.8 at Riverside. Rainwater concentrations at all five sites generally were dominated by NH_4^+, SO_4^{2-}, NO_3^-, and H^+. Na^+ and Cl^- were important contributors in some samples, particularly those collected near the coast. The highest deposition rates of some species were often observed at the site with the lowest rainwater concentrations, Mt. Wilson, due to heavier rainfall there.

Rainfall concentration data from the "vertical" profile indicate that much of of the ionic loading in the rain at Henninger Flats (elev. 700 m) was picked up between there and Mt. Wilson (1700 m), while much of the ionic loading in the rain

at Pasadena (200 m) was picked up between there and Henninger Flats. Measurements of the atmospheric burdens of aerosol and gas phase species prior to a storm indicated that considerably more N(V) and S(VI) were deposited in rainfall than could be accounted for by pre–storm atmospheric burdens of these species. Pre–storm burdens of Ca^{2+}, Mg^{2+}, Na^{+} , and N(–III) were closer to the measured deposition of these species in the rainfall. In–cloud production of SO_4^{2-} may account for at least a portion of the additional SO_4^{2-} deposition; no evidence was seen for in–cloud production of NO_3^-.

References

Galloway, J. N., Likens, G. E., Keene, W. C., and Miller, J. M. (1982) The composition of precipitation in remote areas of the world. *J. Geophys. Res.* **87**, 8771–8786.

Hoffmann, M. R. (1989) Short–term trends and spatial variability in precipitation chemistry in the South Coast Air Basin. Final report to the California Air Resources Board, Sacramento, CA.

Kawamura, K. and Kaplan, I. R. (1984) Capillary gas chromatography determination of volatile organic acids in rain and fog samples. *Anal. Chem.* **19**, 175–188.

Keene, W. C. and Galloway, J. N. (1984) Organic acidity in precipitation of North America. *Atmos. Environ.* **18**, 2491–2497.

Liljestrand, H. M. and Morgan, J. J. (1981) Spatial variations of acid precipitation in southern California. *Environ. Sci. Technol.* **15**, 333–339.

Martell, A. E., and Smith, R. M. (1977) *Critical Stability Constants*, Vol. 3, Plenum, New York.

Munger, J. W., Collett, J. L., Daube, B. D., Jr., and Hoffmann, M. R. (1989) Fogwater chemistry at Riverside California. *Atmos. Environ.* in press.

Russell, A. G., McRae, G. J. and Cass, G. R. (1983) Mathematical modeling of the formation and transport of ammonium nitrate aerosol. *Atmos. Environ.* **17**, 949–964.

SCAQMD (1987) Meteorological data obtained from the South Coast Air Quality Management District, Los Angeles, California.

Seinfeld, J. H. (1986) *Atmospheric Chemistry and Physics of Air Pollution*, Wiley–Interscience, New York.

Solorzano, L. (1967) Determination of ammonia in natural waters by the phenol–hypochlorite method. *Limnol. Oceanogr.* 14, 799–801.

CHAPTER 8

CONCLUSIONS

Several important conclusions may be drawn from the results of the research described in this thesis. Major conclusions of the Sierra Nevada cloud interception study (Chapters 1 through 5) are described first, followed by those of the cloudwater collector comparison study (Chapter 6) and the South Coast Air Basin precipitation study (Chapter 7).

Sierra Nevada Cloud Interception

In order to formulate a model of cloudwater chemistry, interception, and deposition for elevated sites in the Sierra Nevada, four key issues must be addressed. First, it is necessary to define which meteorological processes dominate the production of clouds which are intercepted by the slopes of the Sierra Nevada. Second, an understanding of regional pollutant transport mechanisms must be developed. In particular, it is crucial to examine how these mechanisms function during the periods immediately preceding cloud formation and interception. Third, the importance of aerosol and gas scavenging by the cloudwater droplets, relative to the significance of aqueous–phase reactions within the droplets, must be understood. Last, values of those parameters which govern the actual rate of cloudwater deposition to the forest canopy must be measured, modeled, or estimated. These parameters include the canopy structure, the cloud liquid water content, and ambient wind speeds during cloud interception.

The results of the Sierra Nevada cloud interception study have enabled us to examine these four issues. Cloud interception at mid–elevation sites (800–2500 m elevation) in the region appears to be associated primarily with frontal activity. The passage of cold fronts, approaching from the north or northwest was observed to produce the bulk of total cloud interception. Frontal activity was particularly

important in producing interception during the fall and spring study periods. Both cloud interception frequency and total cloudwater deposition were observed to increase significantly with elevation. Many of the interception events were observed only at elevations above 1500 m, reflecting the predominance of cloud base elevations above this height.

The chemical composition of Sierra cloudwater typically is dominated by inputs of NO_3^-, SO_4^{2-}, and NH_4^+. Cloudwater pH, which was observed to range from 3.8 to 6.5, largely is controlled by the relative inputs of base (represented by NH_4^+) and acid (represented by NO_3^- and SO_4^{2-}), although in the absence of large anthropogenic inputs, the cloudwater pH appears to be controlled by local inputs of formic and acetic acid. While differences in total cloudwater pollutant concentrations between Sequoia and Yosemite National Parks were not substantial, significant differences in cloudwater pH were observed, with Yosemite cloudwater typically a few tenths of a pH unit more acidic than Sequoia cloudwater. These pH differences reflect relatively small differences in the balance of acids and bases at the two sites.

Results of intensive monitoring efforts in Sequoia National Park suggest that the chemical composition of cloudwater in the region is determined primarily by the concentrations of precursor aerosol and soluble gases. Concentrations of aerosol pollutants were observed to increase substantially in Sequoia National Park immediately preceding the arrival of a cold front. This increase appears to be related to both a breakdown in the vertical stability of the atmosphere above the San Joaquin Valley and an increase in southerly flow aloft. Since the timing of peak aerosol pollutant concentrations coincides with the prime period for cloud formation and interception, Sierra cloudwater is often more polluted than would be predicted

based on average Sierra aerosol and gas concentrations.

Relative rates of cloudwater deposition to passive cloudwater collectors indicate that cloudwater deposition in the Sierra is most important at elevations above 1500 m, where interception occurs most frequently and wind speeds during frontal passage may be substantial. Deposition rates to vegetative surfaces also are likely to reflect this trend since conifers, which serve as efficient natural cloudwater collectors, are found predominantly above 1500 m elevation as well. Ridge–top sites, which often experience the highest wind speeds, usually receive the greatest hydrological deposition fluxes from impacting cloudwater. At some of these sites, the hydrological cloudwater flux to exposed conifers actually may exceed hydrological inputs from precipitation.

Although the volume of water deposited to most regions of the forest canopy over the course of a year due to cloudwater interception is smaller than that due to precipitation, concentrations of NO_3^-, SO_4^{2-}, and NH_4^+ in Sequoia cloudwater are much higher than those typically observed in precipitation collected at the same site. Average concentrations of NH_4^+ and NO_3^- in cloudwater are more than ten times those observed in precipitation; cloudwater SO_4^{2-} concentrations are more than three times those observed in precipitation. Since the cloudwater concentrations are so much higher, even small inputs of cloudwater can contribute relatively large quantities of these species to the ecosystem.

Estimates of annual deposition rates of major ions via cloudwater interception to the forest canopy were calculated. The rates for NO_3^-, SO_4^{2-}, and NH_4^+ are significant with regard to measured contributions from precipitation and estimated contributions from dry deposition. Cloudwater interception may, in fact,

be the dominant deposition mechanism for NO_3^- and NH_4^+, particularly for isolated trees or ridge–top canopies where wind speeds are higher and cloudy air parcels can impact directly on foliar surfaces.

In summary, a common mechanism for pollutant deposition by cloudwater interception in the Sierra may be described conceptually as follows. The advance of a Pacific cold front from the north or northwest leads to a change in the predominant wind direction in the central valley of California from northwesterly to southerly, at least at some elevations. As the front crosses the valley, the atmosphere over the valley is destabilized, allowing pollutants previously trapped near the valley floor to mix up to higher elevations. These two meteorological changes act in combination to increase pollutant concentrations at elevations above 500 m in the region of Sequoia National Park. Ambient aerosol and soluble gases are scavenged efficiently by convective clouds associated with the frontal system, which begin to intercept the slopes of the Sierra, predominantly at elevations above 1500 m. Increased winds accompanying the convective activity enhance the deposition of cloudwater to the vegetative canopy. Deposition of water and pollutants is most important for exposed conifers which serve as efficient natural cloudwater collectors; however, wet deposition of pollutants due to cloud interception is significant even for closed conifer canopies, also found predominantly at elevations above 1500 m.

Cloudwater Collector Comparison

A side–by–side sampling comparison of the Caltech Active Strand Collector (CASC) and the Rotating Arm Collector (RAC) illustrated the sampling versatility of the CASC. The CASC was observed to collect cloudwater much more efficiently

than did the RAC. The difference in sampling efficiencies is important particularly during low liquid water content events, which typically have a small median droplet diameter. The CASC, which collects droplets down to 3.5 μm diameter efficiently, performed much better during low liquid content events than did the RAC, which fails to collect droplets with diameters less than 15 μm efficiently.

A comparison of major ion concentrations in samples from the two instruments indicated that Na^+, Cl^-, Ca^{2+}, and Mg^{2+} were present at significantly higher concentrations in the RAC samples. The enrichment of these ions in the RAC samples is believed to be due to the differing collection efficiencies of the two samplers for small droplets. At coastal sites, these four ions are associated primarily with coarse aerosol such as soil dust and sea salt. During droplet nucleation and growth, large aerosol nuclei tend to produce large cloudwater droplets, in comparison to droplets growing on smaller secondary aerosol nuclei. Since the portion of each RAC sample comprised of large droplets is greater than the portion of each corresponding CASC sample comprised of these droplets, it is reasonable to expect that ions associated primarily with large aerosol will be found at higher concentrations in the RAC samples.

Our observations indicate that a difference does exist between the chemical composition of small and large cloudwater droplets, at least in some situations. This finding has important implications for cloudwater chemistry modeling efforts, which usually assume a uniform droplet composition, and for studies examining the health effects associated with inhaling polluted fogwater, since deposition of droplets in the respiratory tract is a highly size–selective process. In a highly turbulent or aged cloud mass, differences in droplet composition are likely to diminish as droplet collision and coalescence becomes more important.

South Coast Air Basin Precipitation

The chemical composition of precipitation collected during several events in the South Coast Air Basin (SoCAB) was dominated by inputs from basin emissions of SO_2, NO_x, and NH_3. These inputs typically are introduced in the form of aerosol containing NO_3^-, SO_4^{2-}, and NH_4^+, as well as gas phase inputs of HNO_3 and NH_3. Na^+ and Cl^- often contribute significantly to the composition of samples collected near the coast, reflecting their origin in marine aerosol. The strong dominance of NO_3^- over SO_4^{2-} normally observed in fog and cloudwater samples collected in the SoCAB generally was not observed in the precipitation samples. Higher precipitation amounts at elevated sites in the basin appear to lead frequently to greater wet deposition fluxes of pollutants there than are observed at sites on the basin floor, despite the fact that precipitation pollutant concentrations normally are much higher near the basin floor.

Both in-cloud and below-cloud scavenging of aerosol and gases were shown to play an important role in determining precipitation composition. In-cloud production of SO_4^{2-} was indicated by the results of a mass balance completed around the precipitating clouds in one event. The SO_2 oxidation rate required to complete the mass balance was consistent with the expected rate of oxidation by O_3 for the conditions observed. No evidence was observed for in-cloud production of NO_3^-.

CHAPTER 9

TOPICS FOR FUTURE RESEARCH

The results of the research described in this thesis have added to the base of information regarding cloudwater and precipitation chemistry, constructed through previous investigations at Caltech and elsewhere. Considerable progress has been made in developing an understanding of the important processes controlling the chemistry and deposition of these atmospheric water droplets; however, several topics, which should prove to be fruitful areas for further investigation, still remain. Some of these are outlined below.

1. Continued monitoring of the chemical composition of cloudwater in the Sierra in conjunction with dry deposition measurements. Recent additions of wet and dry deposition monitoring stations in Sequoia and Yosemite National Parks provide the opportunity for constructing a complete picture of regional atmospheric deposition. This may be particularly interesting since amounts of dry deposition depend to a large extent on the frequency of both cloud interception and precipitation.

2. The interaction of deposited pollutants on foliar surfaces. Aerosols, gases, rain drops, and cloudwater droplets are all deposited on foliar surfaces. Increasing attention is being paid to the effects that chemical species, particularly acids, deposited via these mechanisms can have upon the plant serving as the deposition surface. While these different forms of deposition may have important effects when considered individually, the combined effects of two or more forms are likely to lead to even more dramatic plant responses. Concentration levels of deposited cloudwater, for example, may be increased significantly by dissolution of aerosol deposited previously. These levels will increase even further as the droplets evaporate following an event. Deposition of soluble gases, like nitric acid or sulfur dioxide, is also

enhanced when the plant surface is wetted with rain, cloudwater, or dew. This topic provides the possibility for field and laboratory research, as well as modeling. This line of research would also provide further insight regarding the effects of atmospheric pollutants on building materials and paints.

3. Variability of cloudwater composition as a function of droplet size. Preliminary field evidence suggests that there are significant differences in the chemical composition of small vs. large droplets in a single cloud or fog. These differences appear to be related to the size–composition relationship of the precursor aerosol. Understanding how fogwater composition varies with droplet size is particularly important for examining the health effects associated with inhaling polluted fogwater, since deposition of the droplets in the respiratory tract is a highly size–selective process. The deposition of cloudwater to a forest canopy is also a size–dependent process and should be examined in the context of droplet size–composition relationships. Variations of composition with droplet size may also significantly affect estimates of aqueous phase atmospheric reaction rates based on bulk properties of the cloudwater. Possible research topics include the development of sampling equipment to collect size–fractionated samples of cloud/fogwater, using these samplers to investigate the size–composition relationship under varying conditions for different cloud types, and modeling the growth of the cloud/fog droplets on the precursor aerosol.

4. Routine monitoring of the concentrations of organic acids in cloudwater in Sequoia and Yosemite National Parks. By modifying the sample delivery mechanism in the autosampler, it could be adapted to automatically preserve

separate aliquots of sample for later determination of organic acids. These preserved aliquots could also be used for measuring the sample pH, which can change rapidly in unpreserved samples with large concentrations of organic acids. The result will be a better characterization of the cloudwater acidity at the time it intercepts the forest canopy. Regular measurements of organic acid concentrations would help to determine their contribution to total acid deposition in the two Parks. These measurements would also enable seasonal variations in organic acid levels, which may be indicators of the strength of biogenic vs. anthropogenic sources, to be examined.

5. Monitoring of the chemical composition of cloudwater during the winter at lower elevation (~ 800 m) sites in the Sierra Nevada Mountains where winter "Tule" fogs may be intercepted, as they rise above the floor of the San Joaquin Valley following destabilization of the atmosphere over the valley. Previous Caltech studies have revealed that these fogs are highly polluted; thus, their interception by Sierra vegetation may have important ecological consequences.